Mengjia Zhang

Reliability of Dielectric Elastomers

Dissertation

BOSCH

Reliability of Dielectric Elastomers

Von der Fakultät Chemie der Universität Stuttgart

zur Erlangung der Würde eines Doktors der

Naturwissenschaften (Dr. rer. nat) genehmigte Abhandlung

vorgelegt von

M.Sc. Mengjia Zhang

aus China

Hauptberichter: Prof. Dr. Michael R. Buchmeiser

Mitberichter: Prof. Dr. Frank Gießelmann

Vorsitzende des Prüfungsausschusses: Prof. Dr. Bernhard Hauer

Tag der mündlichen Prüfung: 19.12.2016

Institut für Polymerchemie

der Universität Stuttgart

2017

Acknowledgement

Abstract

Silicone-based dielectric elastomers have excellent mechanical and electrical properties in a broad operation temperature range. Over the past decade various potential applications were assessed for this novel transducer concept, however, the lack of information on the reliability is currently considered as one of the main barriers for the commercialization of this technology.

With the aims of investigating the long-term behavior of silicone-based dielectric elastomers and clarifying the underlying ageing mechanisms, a systematic approach has been developed in this study, which is organized into four main work packages, namely the preparation of silicone formulations, structure-property relationships, mechanical ageing, and electromechanical ageing.

Firstly, a benchmark silicone material with chemical structures and material properties similar to those of a commercial material Elastosil® P7670 was developed. It was synthesized via a cross-linking reaction between linear vinyl-terminated PDMS and tetrafunctional methylhydrosiloxane-dimethylsiloxane copolymer. Silicone oil and silica were also added to adjust the mechanical properties.

In the second part, a series of thin silicone films with different cross-linking densities was prepared by varying the stoichiometric imbalance between the hydrosilane and vinyl groups. The prepared thin silicone films were characterized in terms of elastic modulus, relative permittivity and breakdown strength; these values were then correlated with the network characteristics in terms of cross-linking density and degree of crystallization.

In the third part, thin silicone films were fatigued under mechanical cyclic deformation until rupture. The fatigued specimens showed increased cross-linking density due to the mechanically-induced secondary cross-linking of excessive hydrosilane groups. This was found responsible for changes in the elastic modulus, relative permittivity, and breakdown strength of the material. Variations of these properties were also found most significant in specimens fatigued under the so-called *critical load conditions*, depending on excess hydrosilane contents.

In the final part, thin silicone films were coated with self-prepared compliant silver nanowire electrodes and electromechanically aged under alternating high voltage. With increasing number of load cycles, a significant electrically-induced cross-linking of the hydrosilane groups occurred, which led to an increase in the cross-linking density of the material. Concurrently, an increase in the elastic modulus and a decrease in the relative permittivity were observed, resulting in a significant deterioration of actuation performance.

Kurzfassung

Silikonbasierte dielektrische Elastomere sind vielversprechende elektroaktive Polymere für aktorische Anwendungen. Trotz vieler herausragender Eigenschaften verhindert jedoch das fehlende Wissen über ihre Zuverlässigkeit eine kommerzielle Verwertung. Das Ziel dieser Arbeit war es, das Langzeitverhalten von silikonbasierten dielektrischen Elastomeren aufzuzeigen und die der Alterung zugrundeliegenden Mechanismen aufzuklären.

Dazu wurde zunächst eine Formulierungsbasis für ein Materialsystem realisiert, das eine ähnliche Zusammensetzung und ähnliche Eigenschaften wie das kommerzielle Elastosil® P7670 besaß. Die Materialsynthese erfolgte durch Additionsvernetzung zwischen vinylterminiertem Polydimethylsiloxan und tetrafunktionellem Methylhydrogensiloxan-Dimethylsiloxan-Copolymer. Zur Modifizierung wurden Kieselsäure und Silikonöle zugesetzt.

Durch Variation des stöchiometrischen Verhältnisses zwischen Si-H und Vinyl Gruppen wurde eine Reihe von Silikonmaterialien mit verschiedenen Netzpunktdichten hergestellt. Anschließend wurden sowohl ihre Netzwerkstrukturen als auch ihre mechanischen und elektrischen Eigenschaften detailliert charakterisiert. Aus diesen Ergebnissen wurde eine Struktur-Eigenschafts-Beziehung abgeleitet, die die Grundlage für nachfolgenden mechanischen und elektromechanischen Ermüdungsuntersuchungen lieferte.

Mittels Wöhlerversuchen wurden dünne Silikonfolien bis zum Bruch mechanisch ermüdet und anschließend charakterisiert. Es konnte festgestellt werden, dass eine mechanisch-induzierte Nachvernetzung der Si-H Gruppen im Material hervorgerufen wurde, die zu einem höheren Elastizitätsmodul und zu einer geringeren Permittivität führte. Diese Nachvernetzung trat nur ab einer bestimmten *kritischen Last* auf, die abhängig von der Menge von nicht abreagierten überschüssigen Si-H Gruppen im Material war.

Aufbauend auf den gewonnenen Erkenntnissen bezüglich der mechanischen Ermüdung wurde zudem auch die elektromechanische Ermüdung untersucht. Dafür wurden dünne Silikonfolien mit flexiblen Elektroden bestehend aus Silber-Nanodraht beidseitig beschichtet. Beim Anlegen einer elektrischen Spannung (V_{PP} = 2 kV, V_{DC} = 1 kV) wurde eine mechanische Verformung von ca. 5% erzeugt. Es konnte festgestellt werden, dass eine derartige elektromechanische Last eine signifikant höhere Nachvernetzung im Material verursachte, die auf eine elektrisch-induzierte Nachvernetzung schließen ließ. Mit zunehmenden Lastzyklen wurde eine signifikante Erhöhung des Elastizitätsmoduls festgestellt, die sowohl mit einer Absenkung der Permittivität als auch einer Abnahme der Durchschlagsfestigkeit und einer Verschlechterung der Aktorverformung einherging.

Table of Contents

1   Introduction

1.1   Motivation and objectives

Dielectric elastomers (DEs), belonging to the group of electroactive polymers (EAPs), are rubber-like materials that can be used as transducers converting electrical energy to mechanical energy and vice versa.

The DE transducer technology is especially attractive for future applications for its relatively large stroke (actuation strain up to 10-20%), silent function, and the possibility of energy recuperation and self-sensing during the operation. Currently, silicone elastomers formed by cross-linked polydimethylsiloxane (PDMS) are considered as the most promising types of DEs. Their low stiffness (elastic modulus as low as 0.1 MPa), and low dielectric loss (as low as 10^{-3}) clearly outperform their counterparts such as polyurethane and acrylics.[1-3] Due to the low glass transition temperature these silicone-based dielectric elastomers also possess a broad range of application temperatures (-100 to 250°C), which is especially advantageous in case of automotive and industrial applications.

Since the 1990s, the use of silicone as DE has drawn increasing interest and has become an important topic. Numerous studies have been carried out to explore the potential of silicone-based DEs for a wide range of applications such as actuators, generators and sensors. Especially as actuators, they have been proposed for diverse applications, including miniaturized pumps, valves, optical lenses, haptic features, active vibrators, loudspeakers and soft robotics.[4-9]

A silicone-based DE actuator in a single-layer configuration can be considered as a flexible capacitor, consisting of thin silicone film coated with compliant electrodes on both sides. By applying voltage to the electrodes, the electrostatic pressure deforms the thin elastomer film. Due to the incompressibility of the elastomer, parallel to the contraction in the thickness direction, an expansion in the lateral direction occurs simultaneously (Figure 1). Membrane configurations use this lateral elongation to generate an actuation stroke. Multi-layer configurations can be realized by stacking or rolling coated elastomers. For such application as actuators, the elastomer films are exposed to a combined electrical-mechanical load, which is termed *electromechanical* load in the present work.

With the state-of-the-art processing technologies it is possible to manufacture singly-layer elastomer film with a thickness as low as 20 μm. The breakdown strength of commercially available silicones is about 25-30 V/μm. For large-stroke applications, the driving voltage of the actuators are usually

close to the limit of the breakdown voltage of the elastomer, which thus ranges from several hundred volts to several kilovolts.

The deformation of the DE structure mainly depends on the structural stiffness, the relative permittivity of the dielectric and the applied electric field. A further limitation on the deformation exists through the so-called *electromechanical instability* (EMI, Section 2.3.2.2). In the direction of thickness, the maximum possible deformation can range from several percent to several tens of percent. In case of single-layer configuration with pre-strained silicone elastomers, actuated area strains up to 117% have been reported.[10]
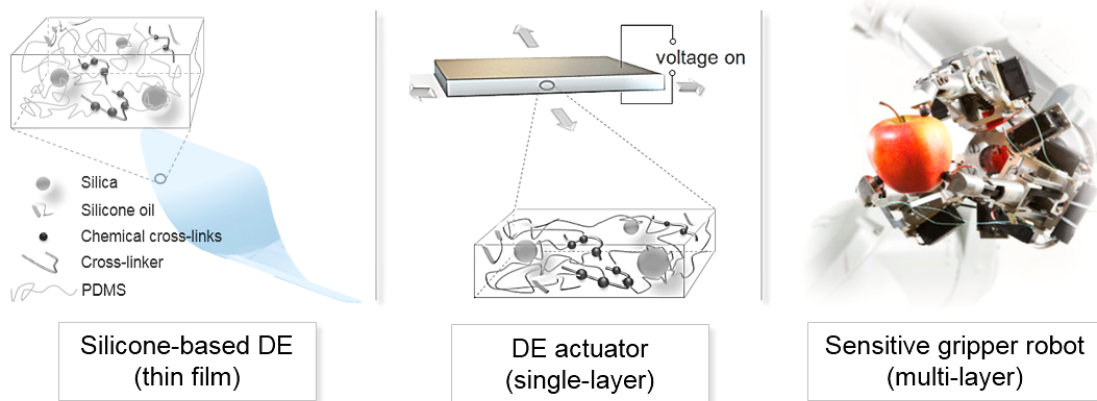
Figure 1. From thin silicone films to dielectric elastomer actuator applications. Right: sensitive gripper robot from FAPS, 2013.[1]

---

[1]   FAPS: Institute for Factory Automation and Production Systems (Erlangen, Germany).

Although silicone-based DEs hold great potential in a number of applications, the lack of knowledge concerning their reliability and long-term behavior is still one of the main barriers for the commercialization of this technology. Besides the lack of thorough experimental investigations, there is currently also no comprehensive understanding about the long-term changes in the network structure of these materials from a molecular point of view.

Some preliminary studies in this field were performed by the research group of Prof. Schlaak,[11, 12] albeit mostly at the system level. They reported[12] that during long-term electromechanical loading (> 1.5x10^6 cycles) the deformation of DE actuators degraded significantly.

It has been demonstrated in previous research that large mechanical deformations can physically,[13, 14] or even chemically alter a polymer's network structure and therefore change its properties.[15] Some phenomena, such as the Mullins-type softening, are known to occur rapidly, typically in only a few single load cycles of sufficiently large deformation. Other phenomena are observed after several load cycles. Those phenomena can have different origins. On the one hand, some of them originate from chemical processes triggered by mechanical stress. For example, mechanical stress may change the density of cross-links and entanglements, which in turn alters the state of stress localization on particular polymer chains.[16, 17] Therefore, the deformed polymer networks may undergo chain scissions,[18] cross-linking reactions,[19] or chemical degradation.[20, 21] On the other hand, it was demonstrated by Kausch[22, 23] that for non-oriented polymers chemical phenomena may not be the predominant cause of ageing. Instead, physical phenomena like disentanglement, chain slip, and void formation were found to be responsible for the weakening of a material during loading. All of these material changes may be related to changes in properties such as relative permittivity and breakdown strength. In a work by Zakaria et al.[24] on ageing behaviors of silicone-based DE materials, it was found that static mechanical stretching (60-120%) can decrease breakdown strength but increase relative permittivity over a long time period. Madsen et al.[25] also observed significantly deteriorated breakdown strength in silicone-based DE materials after long-term static stretching.

Besides mechanical loads, electrical loads can be another cause of damage in silicone-based DEs. For instance, the electrical breakdown, pull-in instability,[26] and degradation of actuator deformation[12] have been suggested as possible failure modes of DE actuators working in high-voltage conditions. From a molecular point of view, it has been suggested that the exerted high voltage can accelerate the generation of free radicals in the polymer, which may react further with absorbed oxygen or moisture, causing chain scissions or cross-linking reactions.[27-29] Oxidative cross-linking, in particular, has been detected for polymers exposed to electrical discharges,[30] corona treatment,[31] high-voltage polarization,[32] or irradiation.[33] In addition, possible damage mechanisms such as hydrophobicity recovery have also been observed under corona treatment.[34] In a work by Andjelkovic and Rajakovic on polyethylene-based insulation materials,[35] it was reported

that tensile strength, tensile elongation, and the degree of crystallization of the material decreased over time under coupled electrical-thermal conditions. In the analysis of the *electrical tree ageing* of silicones by Zhou et al.,[29] similar ageing phenomena such as a lowered melting point and crystallinity were observed by differential scanning calorimetry (DSC).

Depending on the applied load conditions, the chemical nature of the material, and the specimen configurations, different ageing mechanisms may take places, which sometimes even occur in combined form. As a result, the reliability study on silicone-based DE materials requires both constitutive investigations of their individual effects and thorough comprehensions of their interactions.

To shed light on these issues, the present thesis therefore focuses on both investigating the long-term behavior of silicone-based DE materials and clarifying the underlying ageing mechanisms on the molecular level.

1.2 Approach and overview

There are three major challenges when investigating the reliability of silicone-based DEs. Firstly, the chemical formulation of commonly used commercial silicone elastomers is unknown, which hinders the detailed analysis of their ageing behavior on a chemical basis. Secondly, there is still no well-established understanding about the fundamental structure-property relationships of silicone-based DEs. Furthermore, DE actuators undergo a coupled electromechanical load, which complicates the interpretation of possible ageing phenomena.

The approach of this work, towards a comprehensive understanding of silicone-based DEs, is structured as follows. In a first step, a benchmark material with properties similar to those of a commercial DE material was developed. To obtain information about the fundamental structure-property relationships, materials with systematically varied formulation parameters were then prepared and characterized with respect to their electrical and mechanical properties. In the last part, in order to separate mechanically-induced and electrically-induced ageing effects, sole mechanical ageing was firstly studied. Subsequently, electromechanical ageing was investigated and compared with mechanical ageing.

Accordingly, four major work packages were arranged into: *preparation of silicone formulations*, *structure-property relationships*, *mechanical ageing* and *electromechanical ageing* (Figure 2).
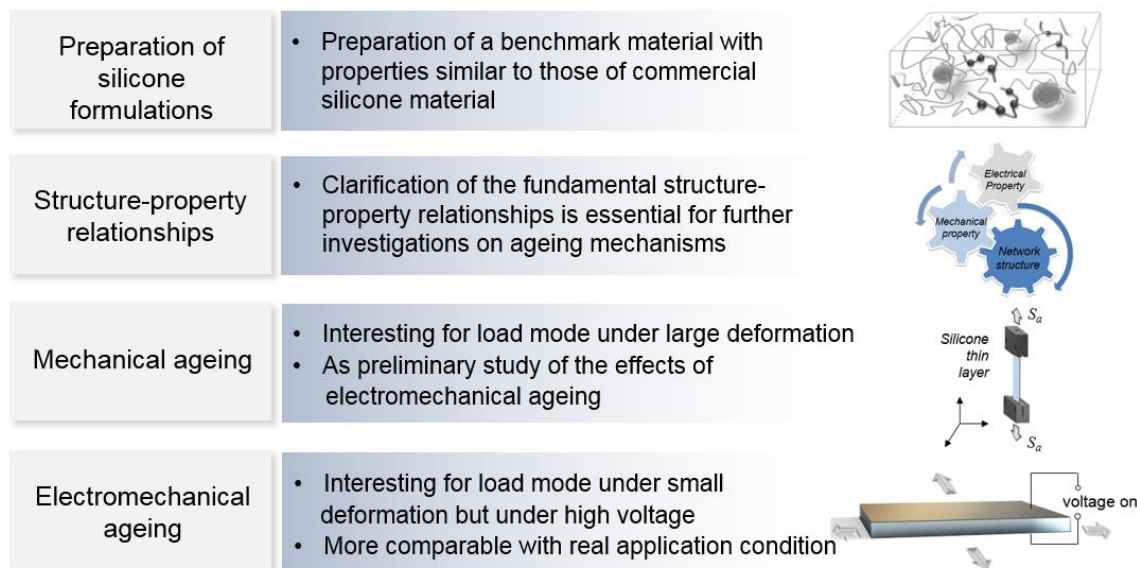
Figure 2. Approach and main work packages within this work.

The goal of the first work package, *preparation of silicone formulations*, was the preparation of a benchmark material with properties similar to those of a commercial silicone Elastosil® P7670 (Wacker Chemie AG, Germany). To clarify the chemical structure of the commercial material, diverse analytical techniques, such as NMR[2], FT-IR[3], GPC[4], ICP-OES[5], and MALDI-TOF[6], were employed. Based on the obtained information, a benchmark material with similar network structures, mechanical, and electrical properties was developed successfully.

In the second work package, *structure-property relationships*, the correlations between the parameters of the network structure and the mechanical and electrical properties of silicone DE materials were studied. For this purpose, mechanical and electrical tests were performed on a series of silicone elastomer films with different cross-linking densities, prepared by changing stoichiometric imbalance based on the formulation of the benchmark material.

In the work package *mechanical ageing*, the prepared thin silicone films were subjected to sinusoidal uniaxial mechanical loading. The series of thin silicone films prepared with different stoichiometric imbalances was fatigued till rupture under various load amplitudes based on a strain amplitude-controlled Wöhler approach and by using a self-developed test facility. The applied strain amplitudes ranged from 60 up to 140%. The corresponding cycle number to rupture ranged from 10^6 cycles

---

[2]   NMR: Nuclear Magnetic Resonance Spectroscopy.
[3]   FT-IR: Fourier-Transform Infrared Spectroscopy.
[4]   GPC: Gel Permeation Chromatography.
[5]   ICP-OES: Inductively-Coupled Plasma Optical Emission Spectrometry.
[6]   MALDI-TOF: Matrix-Assisted Laser Desorption/Ionization with Time-of-flight (ToF) Mass Analysis.

down to only a few tens of cycles. After fatigue tests, changes in elastic modulus, relative permittivity, and breakdown strength were examined with respect to their changes in network structure.

In the fourth work package, *electromechanical ageing*, thin silicone films prepared with varied stoichiometric imbalances were firstly coated with self-prepared compliant silver nanowire electrodes. Then they were electromechanically fatigued under alternating high voltage (V_{pp} = 2 kV, V_{DC} = 1 kV) up to a maximum 10^5 cycles. After ageing, changes in cross-linking density, elastic modulus, relative permittivity, and breakdown strength were examined.

The following chapters of this thesis start with an extensive overview of fundamental and elementary aspects in Chapter 2. The subsequent four chapters are devoted to results obtained from the above-outlined four major work packages (Chapter 3-6).

Based on the obtained results, a comparison between a self-prepared silicone material and the same material treated with thermal post-curing was additionally performed. Preliminary results are outlined in Chapter 7. In Chapter 8 and Chapter 9 the key knowledge gained in this work is summarized. Several promising aspects for future work are addressed as well. Experimental details are compiled in Chapter 10.

2 State of the Art

2.1 Dielectric elastomers

2.1.1 General introduction to electroactive polymers

Electroactive polymers (EAPs) are polymers capable of producing changes in size or shape upon electrical stimulation. The search for polymeric materials that respond to electrical stimulation has lasted for several decades. It can be dated back to 1880, when Röntgen[36] designed an experiment to test the effect of an electric field on the mechanical properties of a natural rubber band. The bare rubber band was fixed at one end while the other end was connected to a scale. As it was subjected to electric discharge, which was applied to its surface via corona treatment, the rubber band was observed to elongate in length and to shrink in thickness. Inspired by this experiment, research was proceeded with the aims of understanding this mechanical response,[37] and identifying more materials with such behavior. Later, in 1925, the first piezoelectric polymer was found by Eguchi.[38] In 1977, Hideki Shirakawa et al.[39] found the first electrically conducting polymers. Especially since 1990s extensive progress has been made both in the area of ionic and field-activated EAPs.

Ionic and field-activated EAPs are two main categories of EAPs. This classification is based on their activation principles. In ionic EAPs, shape change of the polymer is generated through the displacement of ions inside the polymers. Upon electric voltage, which is usually as low as 1-2 V, the movement of ions leads to an unbalanced ion concentration within the polymer. The enrichment of ions causes swelling, while the depletion of ions results in a shrinkage of the polymer. Due to the diffusion process of ions, the ionic EAPs exhibit generally slow responses (fraction of a second).[2, 40] For the transfer of the ions within the polymer an electrolyte in liquid or gel form is used to encapsulate the polymer. Ionic EAPs can be further classified into ionic polymer gels (IPGs), ionic polymer-metal composites (IPMCs), conductive polymers (CPs), and carbon nanotubes (CNTs).

Field-activated EAPs are activated by charge transfer through electrons inside the polymers. They can be hard, thermoplastic/thermoset-like polymers (elastic modulus ca. 100 MPa-1 GPa) or very soft, rubber-like elastomers (elastic modulus ca. 0.1-2 MPa). Compared to ionic EAPs, the field-activated EAPs generally have quick responses (in the millisecond region)[41] during operation. However they require rather high voltages (100 V-3 kV) for activation. According to the polarization characteristics under the applied electric field, the field-activated EAPs can be further classified into

dielectric elastomers (DEs), piezoelectric polymers, electrostrictive graft polymers and liquid-crystalline elastomers (LCEs). Figure 3 shows a general overview of these EAP materials.
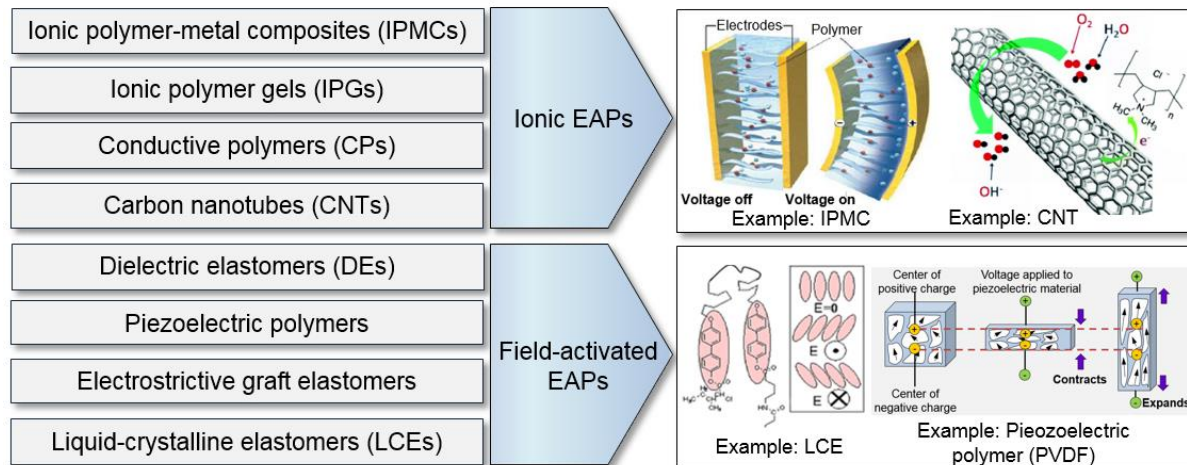
Figure 3. General overview of electroactive polymers (EAPs) (according to references[2, 40, 42, 43]).

Among these EAP materials, dielectric elastomers are isotropic, nearly incompressible rubber-like materials (Poisson's ratio ca. 0.5). They are also generally lightweight and comparatively low in cost. Furthermore, compared to other EAPs they work on a simple electromechanical principle: Upon electric field, they undergo a mechanical deformation induced by the so-called Maxwell stress.

The exploitation of such Maxwell stress effect in soft elastomers has gained first commercial attention since early 1990s, when such soft elastomers were considered as artificial muscle materials.[44-47] In 1999, Dr. Yoseph Bar-Cohen from JPL[7] has proposed an arm wrestling challenge against a dielectric elastomer driven robotic arm. The first attempt to industrialize DE technology was made in 2003 by the company Artificial Muscle Inc.[8] Although the first dielectric elastomers were made of commercially available acrylic-based adhesive films (from the company 3M), further material supplier companies, such as Bayer MaterialScience (now Covestro)[9] and Wacker Chemie AG, started their own research programs on the development of polyurethane- and silicone-based

---

[7] JPL: Jet Propulsion Laboratory of NASA (National Aeronautics and Space Administration).

[8] Artificial Muscle Inc., which was founded as a spin-off of Stanford Research Institute (SRI), was acquired by Bayer MaterialScience (now Convestro) in 2010 and sold to Parker Hannifin Corporation in 2014.

[9] Bayer MaterialScience (now Convestro) stopped the production of polyurethane-based dielectric elastomers in 2014.

elastomers, especially for DE purposes. Danfoss PolyPower [10] and CTS [11] have carried out outstanding work on the processing of such materials into DE-based units for actuators and generators. Start-up companies such as StretchSence and LEAP Technology are also garnering attention through their activities regarding EAP-based sensor solutions. So far, a commercial DE actuator product is for example the so-called laser speckle reducers from Optotune Company.

Triggered by the growing industrial interest, scientific research on EAP is also blooming since the last few years. The main research topics range from material optimization, through modelling, to the development of novel applications. Pioneering work in these areas was done, to name only a few, at Stanford Research Institute (SRI),[10, 40-41, 44-46] Swiss Federal Laboratories for Materials Science and Technology (EMPA),[66] University of British Columbia (UBC),[2] Queen Mary University of London (QMUL),[62] Harvard University,[26] Technical University of Denmark,[2, 24-25] Technical University of Darmstadt,[7, 12] and Fraunhofer Society [12].[82]

Motivated by both the scientific achievements and the high application potentials, in Germany several publicly funded projects regarding the DE technology have been performed. Examples are EPoSil [13] (energy harvesting), DIELASTAR (actuator applications) and PlanDE (multi-layer actuator applications).

The present PhD work focuses exclusively on dielectric elastomers (DE) for actuator applications. The following sections will now provide a brief overview of the functional principles, configurations, applications and materials applied in DE actuator technology.

---

[10] Danfoss Polypower stopped the manufacture of EAP in 2014. In 2013 several co-workers from Danfoss PolyPower founded the LEAP Technology.

[11] CTS: Compliant Transducer Systems.

[12] Fraunhofer Society is a German research organization. Some of the Fraunhofer Institutes, which are currently active in the EAP-field, are the ISC (Silicate Research), LBF (Structural Durability and System Reliability), IWU (Machine Tools and Forming Technology), IFAM (Manufacturing Engineering and Applied Materials Research), IPA (Manufacturing Engineering and Automation), IST (Surface Engineering and Thin Films), to name just a few.

[13] EPosil was a project funded by the German Ministry of Research (BMBF). The consortium consisted of Robert Bosch GmbH (project leader), Wacker Chemie AG, Ingenieurbüro Brinkmeyer & Partner, Technical University of Darmstadt and Technical University of Hamburg.

2.1.2 Dielectric elastomers

2.1.2.1 Functional principles

An actuator is a mechanical device, which is responsible for moving or controlling a system. The basic unit of dielectric elastomer actuators is essentially a stretchable capacitor, comprising of a dielectric elastomer thin film (typically 20-200 µm) sandwiched between two compliant electrodes. The dielectric elastomer is manufactured from incompressible, rubber-like material with good dielectric properties and low stiffness. The electrodes need to be sufficiently compliant so that actuation deformation is not restricted.

When an electrical voltage is applied to both electrodes, the opposite charges induce electrostatic pressure in the dielectric elastomer film, which is also known as *Maxwell stress*.[48] This electrostatic pressure confronts the material's inherent tensile strength and leads to compression in the film's thickness. Due to the incompressibility of elastomer, a simultaneous expansion in the film is then generated. This working principle is illustrated in Figure 4, where it is seen that electrical energy is thus converted into mechanical deformation. When the external voltage is switched off, the elastomer film returns to its original shape. In case of alternating electrical voltage, cyclic deformation is generated and the DE actuator undergoes a coupled electric-mechanical load, which is also referred to in the present work as an *electromechanical* load.
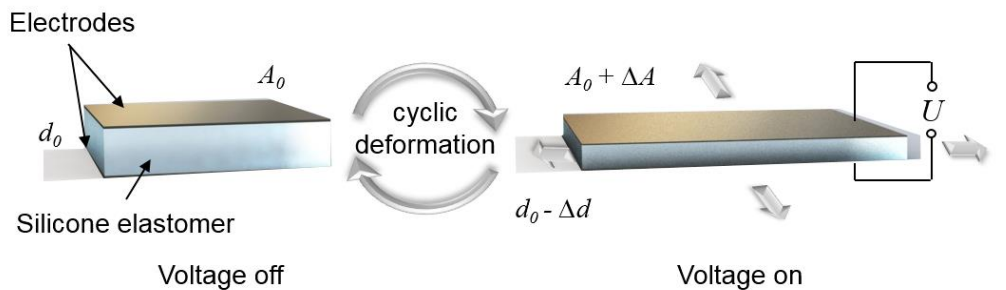
Figure 4. Basic operation principle of a dielectric elastomer.

The electrostatic pressure, P, is related to the permittivity of the material ε, which is the product of relative permittivity of material ε_r multiplied by the permittivity of vacuum ($\varepsilon_0 = 8.85 \times 10^{-12}$ F/m); and to the electrical field E across the dielectric film, which is the quotient of the voltage on the dielectric film U divided by film thickness d.

$$P_{el} = \varepsilon E^2 = \varepsilon_0 \varepsilon_r \left(\frac{U}{d}\right)^2 \qquad\qquad \text{Equation 1}$$

The resulting actuation deformation along thickness direction S_z, also known as electromechanical deformation, is then given by:

$$S_z = \frac{P_{el}}{Y} = \frac{\varepsilon}{Y}E^2 = \frac{\varepsilon_r \varepsilon_0}{Y}\left(\frac{U}{d}\right)^2$$
<div align="right">Equation 2</div>

where Y is the elastic modulus of the dielectric elastomer.

From Equation 2 it is clear that three major material properties, namely relative permittivity, the elastic modulus and the maximum applicable voltage (breakdown strength, $E_B = (U/d)_{max}$), govern the performance of a DE actuator.

Besides the electrostatic pressure described by Equation 2, there are further mechanisms influencing the performance of dielectric elastomers, such as the viscous and viscoelastic characteristic of the components or even property changes caused by the ageing of DEs.

Such DE transducer structures can be used for energy harvesting as well. A harvesting cycle is described as follows:[49] the DE film is stretched and then electrically charged. After the charging phase the power supply is decoupled from the DE, leaving the electric charges constant on the electrode surfaces. During the relaxation the DE film is released, the thickness of the elastomer increases, causing the separation of the electric charges. The excess energy caused by the charge separation is transferred to the grid or to an intermediate energy storage during the discharging phase.

DE structures can be used as capacitive sensors to measure strain or pressure. For example, Pinter et al. [50] have proposed an electric circuitry enabling a DE capacitance sensor array with an accuracy of 100 ppm and with a sampling frequency of 2 kHz. Mannsfeld et al.[51] have demonstrated flexible, sensitive pressure sensors made of micro-structured thin silicone films.

The following sections will present common configurations and applications as well as the fundamental components of a DE actuator, namely the electrode and elastomer materials.

2.1.2.2 Configurations and applications

Dielectric elastomer actuators can be configured into many different shapes. The most fundamental design is the so-called *single-layer actuator*, consisting of one elastomer film coated with compliant electrodes on both sides. It can be found in applications such as planar actuators, where a significant amount of deformation is desired.[10] Based on these planar actuators, pre-straining can be applied, whereby the coated DE film is inserted onto a rigid frame. Pre-straining is also suggested to enhance breakdown strength.[52, 53]

In order to amplify the stroke caused by the change of the elastomer film thickness several hundreds or thousands of coated DE films can be piled on the top of each other. This configuration is referred as stack configuration.

Several other configurations are such as roll (with a spring core or core free), tube, unimorph, bimorph, planar, diaphragm, bowtie, spider, extender and inch worm.[4, 45, 54-57] In Figure 5 several representative configurations are given as examples. On the subject of currently existing DE configurations an extensive review by Carpi[40] is available.
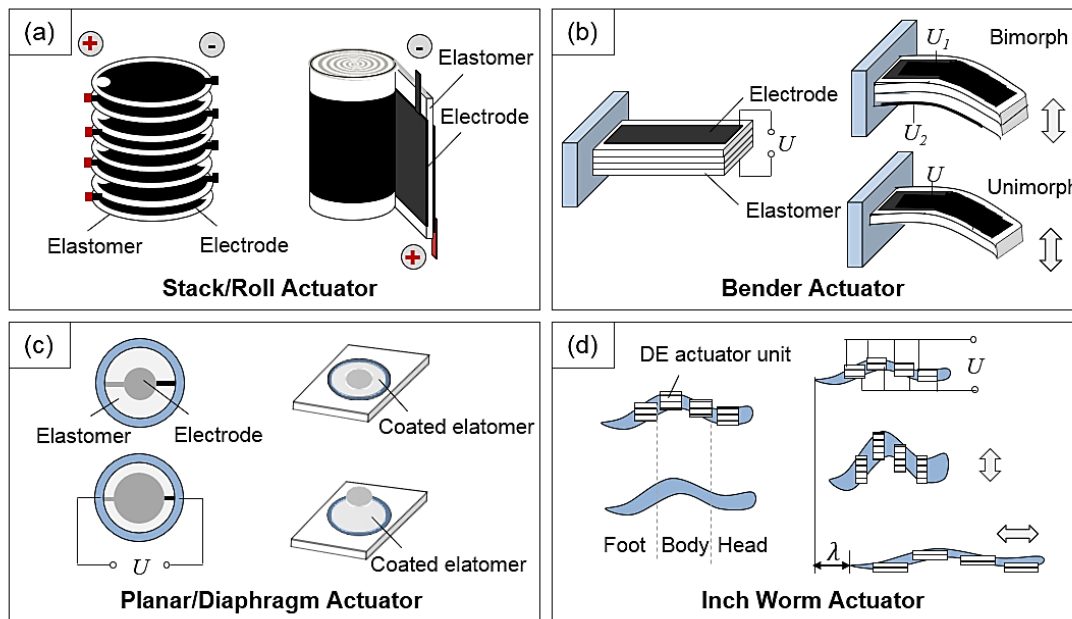
Figure 5. Examples of dielectric elastomer actuator configurations (according to references[4, 40, 56, 57]).

The variety of configuration possibilities for DE actuators gives them the ability to be formed into complex shapes, in order to provide actuation. Together with the superior properties of DE as well as their lightweight properties, DE actuators are feasible for a wide range of novel applications. A planar actuator or stack actuator with low thickness, for example, can be implemented in flat screen speakers,[58] 4D headphones (ViviTouch®) or tactile displays.[7] Stack actuators or roll actuators have been designed to mimic biological systems, such as human muscle motion, in prosthetic or orthotic devices and in biological robotics.[5, 45, 59-61] Research has also been inspired to explore the possibilities of DE actuators for use as pumps and valves,[9] and they have also shown great promise for a variety of applications in optical devices such as optical lenses.[6, 62]

In Figure 6, several examples are presented. The advantageous behavior of dielectric elastomers, such as their low weight, is well-reflected by the application of a flying fish (Figure 6a) as well as the

flexibility, which is preferred for soft robotics, as shown in Figures 6b. In Figure 6c, a chromophore skin is demonstrated, which, by controlling the loading voltage and by using different colors of electrode materials, makes it possible to change surface colors. In Figure 6d a vibrotactile feature based on DE stack actuator is presented. Actuator-driven optical lenses can also be built, as shown in Figure 6e.
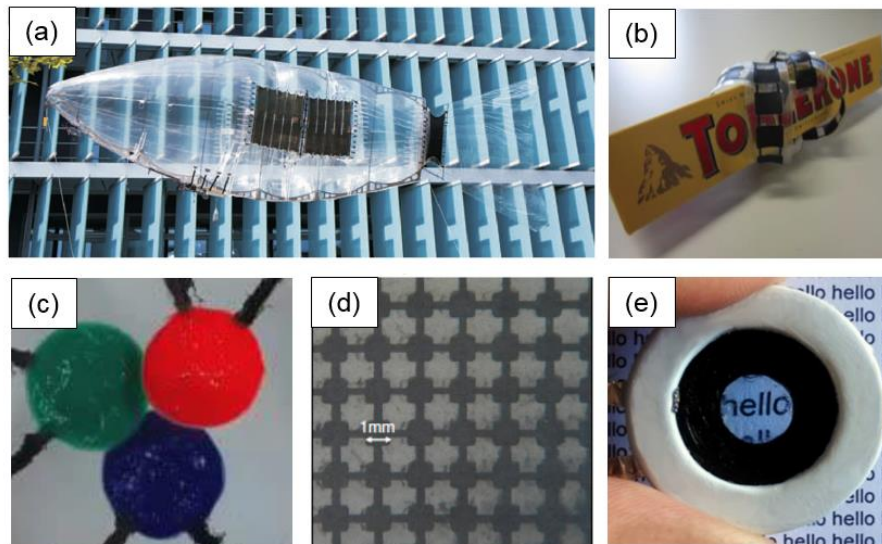
Figure 6. Configurations and representative applications of dielectric elastomer actuators (a) biomimetic model airship driven by DE actuators (EMPA),[63] (b) soft gripper (EPFL[14]),[59] (c) chromophore skin (BRL[15]),[64] (d) vibrotactile display (TUD[16]),[65] (e) electrically tunable optical lenses (QMUL[17]).[62]

2.1.2.3 Electrodes

The performance of a DE actuator depends in part on the electrode material used. Electrodes for use in this application should ideally satisfy the following criteria: high compliance, high conductivity and low thickness.

Electrodes can be made from diverse kinds of conducting materials. On the currently used electrode materials for DE, an excellent review by Rosset and Shea[66] exists. Commonly used electrodes range from thin metal films (silver, gold),[67] carbon-based materials (carbon black, graphite, graphene)[41] or conductive nanowires such as CNTs[68] or silver nanowires (AgNWs).[69-71] Silver

---

[14] EPFL: Swiss Federal Institute of Technology in Lausanne.
[15] BRL: Bristol Robotics Laboratory.
[16] TUD: Technical University of Darmstadt.
[17] QMUL: Queen Mary University of London.

nanowires especially have attracted a great deal of interest in the last few years, due to their superior compliance, low thickness, high conductivity and the ability to enable the preparation of transparent electrodes. In the latter part of this chapter, the testing of three electrodes is described, which have been evaluated within the framework of this study: carbon black, silver ink and silver nanowires (Appendix A5).

2.1.2.4 Elastomers

As the most important components of a DE actuator, intrinsic properties of the dielectric elastomer, such as relative permittivity, breakdown strength and deformability, directly determine the performance of the system (Equation 2). During the 1990s and 2000s, a number of elastomers were tested and promising results were achieved from three materials, namely silicones, acrylics and polyurethanes.

Polyurethanes

Polyurethanes are basically suitable for use as DEs because of their high dielectric constant (> 5) and high electrical breakdown field (> 50 V/μm). However, due to their relatively high elastic modulus (> 1 MPa), polyurethane films are limited in their ability to generate large strains. Furthermore, the industrial production of some polyurethanes sorts requires strictly controlled safety conditions, due to the toxicity of isocyanates.[3, 72, 73] Furthermore, currently the relatively high glass transition temperature of Polyurethanes seems to be one of the main barriers of the industrialization.

Acrylics

Acrylic material has been a widely employed DE material. In the early stages of the DE research only acrylic adhesive tapes were available as off-the-shelf thin film elastomers. The publications of several research teams depicted the potentials of acrylic-based DE, e.g. commercially available VHB 4910 and VHB 4905, with respect to their strain performance (> 380%)[2, 74] and impressive energy density (3.4 MJ/m³).[40] They also possess comparatively high relative permittivity values ($\varepsilon_r \approx 5$).[2] However, the breakdown field of non-pre-stretched acrylic films is only about 18 V/μm;[75] moreover, mainly due to their pronounced viscoelastic behavior nowadays they are not considered as a technology of choice.[76]

Silicones

Silicones present a good combination of low dielectric loss and low elastic modulus. Also, the wide temperature range within which these materials can be used, the ease of preparation and the low price clearly outperform their counterparts. They are currently used in a diverse array of DE applications, though the low permittivity of commercially available silicones ($\varepsilon_r \approx 3$) is a considerable drawback. Several approaches exist to increase the relative permittivity of silicones. Some of them are described in the following section.

2.1.3 Silicone-based dielectric elastomers

A common method employed to improve the relative permittivity of silicones involves the addition of filler particles. One typical filler used in silicone elastomers is silica (SiO_2), which can enhance the deformability as well as the handling of the cured elastomers. However, by introducing interconnections between filler particles and polymer networks, the elastic modulus is often increased, which is a remarkable disadvantage for use as a DE, since the electromechanical deformation that can be generated is inversely proportional to the elastic modulus (Equation 2). Research has also focused on the addition of various conductive fillers such as aluminum oxide (Al_2O_3), titanium oxide (TiO_2) and barium titanium oxide ($BaTiO_3$) as well as organically modified montmorillonite (OMMT) with high relative permittivity values. Improvements of the overall performance appear rather limited, though, since the enhanced relative permittivity is often achieved at the cost of heightened stiffness, increased dielectric loss or a reduced breakdown field.[77]

To achieve a higher relative permittivity value, silicone/polymer blends have also been examined. In a work by Carpi et al.,[78] an approach preceded by blending the silicone elastomer with a highly polarizable conjugated poly(3-hexylthiophene) (PHT) was demonstrated, and encouraging results were reported that the blend yielded both significantly enhanced relative permittivity and elastic modulus, and therefore better actuation performance. However, as also reported in this work, these enhancements were also combined with an increase in dielectric loss. Further attempts to explore novel silicone-based DEs include incorporating a secondary network such as a CNT network into the silicone elastomer,[79-81] the grafting of dipole molecules onto the elastomer matrix[82] and building bimodal silicone interpenetrating networks,[83] to name just a few.

As mentioned above, the optimization of the properties of silicone networks still presents many challenges. The proper tuning of the mechanical and electrical properties requires a comprehensive understanding of the interplays between network structure and mechanical and electrical properties. For most material developments of silicone-based DEs, it is noteworthy that almost exclusively commercial materials are employed as the base material, such as Elastosil® P7670, Elastosil® RT625 from Wacker Chemie AG and Sylgard® 184 from Dow Corning. Only a few studies have directly

focused on tailor-making silicone elastomers for dielectric elastomers, which may be due to the complexity of formulating them in the first place, but it may also indicate that the required understanding about the structure-property relationship does not yet exist.

2.2 Chemistry of silicone-based dielectric elastomers

2.2.1 Cross-linking of silicone elastomers

Silicones, also known as polysiloxanes, are an important and interesting class in the family of elastomers. The name silicone was derived by Frederic Stanley Kipping in 1904,[84] to describe new compounds consisting of $-R_2SiO-$ as a repeat unit. In case of R = methyl, where the strong polar backbone of Si-O bonds is surrounded by organic methyl groups, it refers to a polydimethylsiloxane (PDMS) with the structure shown in Figure 7a. The repeat unit, $-(CH_3)_2SiO-$, is also often referred to as the D-unit, as the silicon atom is connected with two oxygen atoms (Figure 7b). Similarly, M-, T-, and Q-units are defined accordingly (Figure 7b).
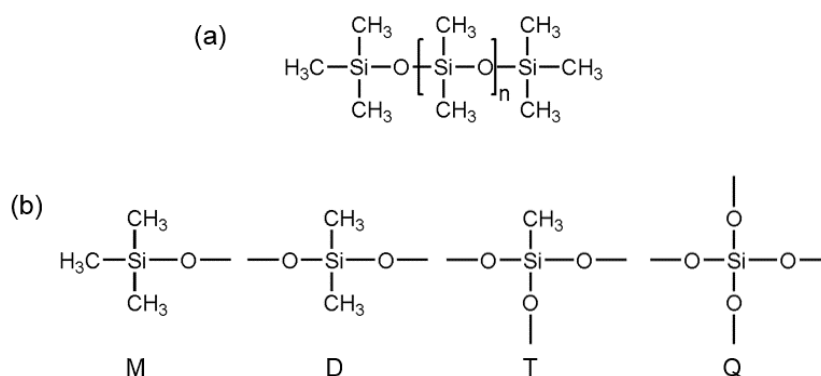
Figure 7. Chemical structure of (a) polydimethylsiloxane (PDMS) (b) M-, D-, T, Q-units.

The side group R can be also substituted by many other groups (i.e. vinyl, phenyl, hydride and alkyl groups). If the adjacent functional groups can react with each other and form new chemical bonds, e.g. via addition of vinyl group and hydrosilane group, a three dimensional network can be generated.

As can be seen from the chemical structure, silicones exhibit an unusual physicochemical combination of the inorganic backbone and organic side groups. For instance, the low electronegativity of Si (1.8) leads to a highly polarized Si-O bond, giving silicones good dielectric properties. These strongly polarized Si-O bonds could lead to strong intermolecular interactions without protection, but thanks to the methyl groups, a shielding effect helps to minimize chain-to-chain interactions. This low intermolecular interaction in silicones is also the reason for the high free

volume in silicones, which helps them achieve high permeability in the presence of oxygen, nitrogen and humidity. Furthermore, with the methyl groups pointing to the outside, silicones have hydrophobic surface characteristics, which make them particularly suitable as water repellents and in biocompatible applications. Also, such a -$(CH_3)_2$SiO- repeat unit has a relatively low rotational energy (3.3 kJ/mol), which explains the high flexibility of siloxane chains. This high flexibility is reflected by a low glass transition temperature ($T_g \approx$ -120°C), low melting temperature ($T_m \approx$ -40°C) and the low temperature of crystallization ($T_c \approx$ -75°C), enabling a broadly usable temperature range.

Silicones also have the advantage of excellent dielectric breakdown strength, good electric insulation and many more attributes, thus making them suitable for use in sealants, coatings, surfactants, adhesives, dielectric encapsulation, lubricants, etc.

Non-cross-linked silicones vs. cross-linked silicones

Silicones can be divided into non-cross-linked and cross-linked versions. Polydimethylsiloxane (PDMS), for example, is a common non-cross-linked silicone. It is fully methylated, linear or cyclic, and in this sense a non-functional polysiloxane. It is also fluid at low molecular weight and viscous at high molecular weight.

Cross-linked silicones, depending on their cross-linking density, are solids with variable levels of softness. Polysiloxanes contain functional groups such as vinyl or hydrosilane bonds. These functional groups can respond to each other via cross-linking reactions, by forming cross-linking joints between adjacent chains and thereby transforming loose polymer chains into a three-dimensional network. The cross-linking reaction can be performed in various ways such as by an addition reaction, a condensation reaction or with radical cations and so on. A schematic overview of a number of different silicone elastomer curing systems is illustrated in Figure 8.
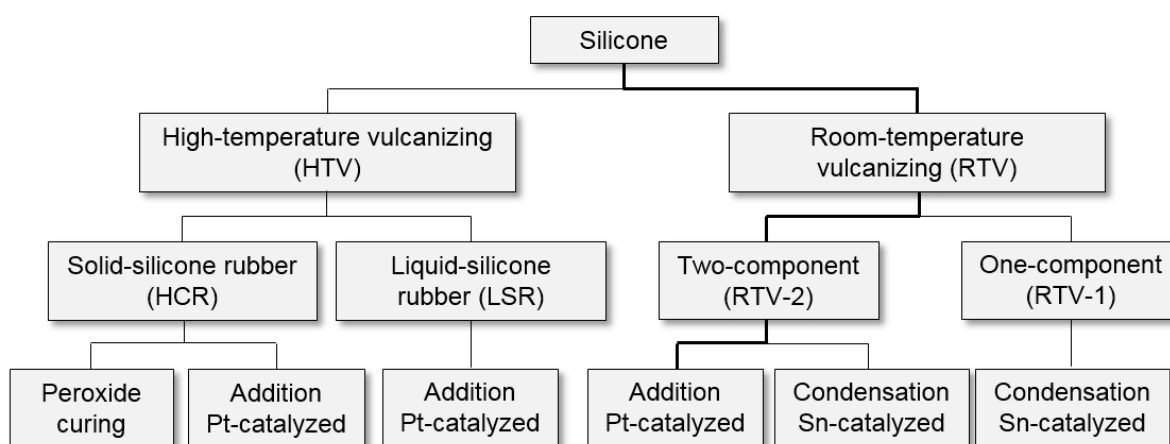

Figure 8. Schematic overview of the different cross-linking systems of silicone elastomers (according to references[85, 86]).

RTV vs. HTV

Generally speaking, based on cross-linking temperature, silicone elastomers can be classified as either high-temperature vulcanizing (HTV) silicones or room-temperature vulcanizing (RTV) silicones. As the name indicates, RTV cross-links at room temperature as soon as the parts are mixed, whereas the cross-linking of HTVs requires the application of presence of heat or irradiation to start. Traditionally, a RTV silicone can either be a condensation cross-linking silicone or an addition cross-linking silicone, the latter of which refers to a two-component system in which vinyl bonds react with hydrosilane bonds in the presence of a platinum catalyst. One-component RTVs are condensation cross-linking, while HTV silicones are generally addition cross-linking silicones. HTV silicones can be further divided into solid-silicone rubber (also high consistency rubber, HCR) and liquid-silicone rubber (LSR), based on the degree of cross-linking.

Two-component vs. one-component system

One-component RTV silicones use moisture in the air to form Si-O-Si bonds as cross-links, thus making this curing process strongly dependent on air humidity and the thickness of the mold. Two-component RTV silicones thus enjoy a major advantage over one-component RTVs, in that they do not require moisture; however, they do need skillful handling, as the two components have to be mixed together according to certain mixing ratios. Unlike a one- component system, two cross-linking mechanisms fall into this category, namely addition cross-linking and condensation cross-linking.

Addition vs. condensation cross-linking

Condensation cross-linking proceeds firstly through the hydrolysis of a cross-linker molecule with humidity in the air, to form a silanol group (Si-OH). These can further react via subsequent condensation reaction with other silanol groups to form Si-O-Si cross-links. This type of cross-linking is only applicable in applications that are not completely sealed, because during cross-linking a by-product (H_2O) is released. Thus, the major drawback is that the formed silicone usually contains voids. Hence, even though condensation cross-linking belongs to the RTV family, an elevated temperature is especially suggested, to allow volatiles to escape and prevent reversion.

The addition cross-linking system consists of a base part of vinyl-containing PDMS (known as pre-polymer) and a second part of curing agent (known as a cross-linker). Commercially available addition cross-linking systems are usually supplied in the form of two separate parts A and B. Typical addition cross-linking is achieved through a hydrosilylation reaction, whereby a vinyl-terminated PDMS chain binds to a hydrosilane unit of the cross-linker in the presence of a platinum catalyst (typically Karstedt's catalyst). A brief sketch of this hydrosilylation reaction is shown in Figure 9.

Compared to condensation cross-linking, one obvious advantage of addition cross-linking is that cross-linking can be accomplished under solvent-free conditions whereby no side-products are produced.
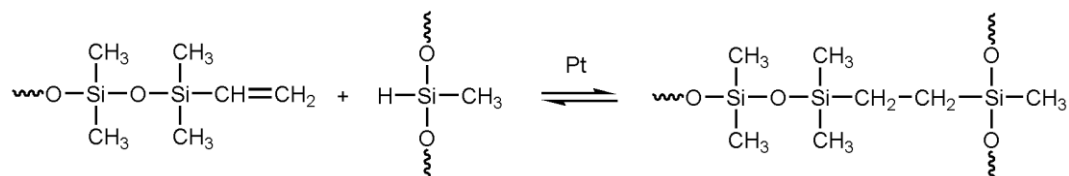
Figure 9. Brief sketch of a hydrosilylation reaction between vinyl and hydrosilane groups.

To build a three-dimensional network, a divinyl-terminated PDMS pre-polymer can be employed, while a cross-linker molecule has to contain more than two hydrosilane groups. The Karstedt's catalyst, the structure of which is illustrated in Figure 10a, has the following working principle (Figure 10b). Platinum binds initially with silane to form a ligand, and this Pt-ligand is then substituted and connected thereafter with the catalyst. Via reductive elimination the desired structure is generated and the Pt is released.
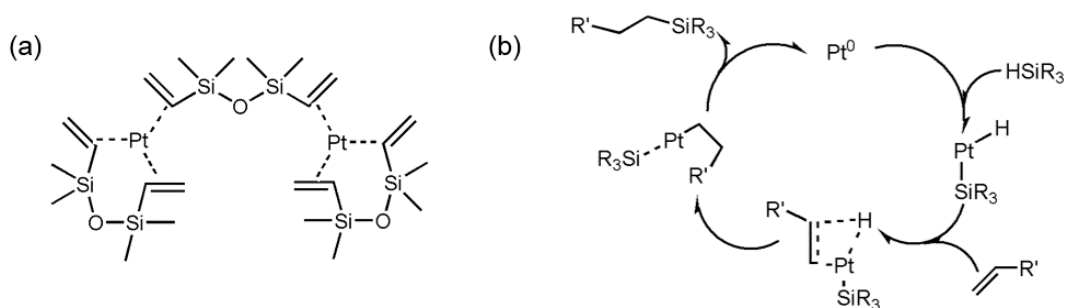
Figure 10. (a) Chemical structure and (b) catalytic cycle of Karstedt's catalyst (according to references[87, 88]).

The resulting three-dimensional structure is composed of long, easily reconfigured polymer chains interconnected with short chain cross-linkers (Figure 11). The cross-linking joints (Si-CH_2-CH_2-Si) act as supporting joints that ensure the network is capable of returning to its original configuration when the elastomer is subjected to cyclic mechanical deformation. In commercially available silicones, silica and silicone oil are commonly added as reinforcers and plasticizers, respectively.
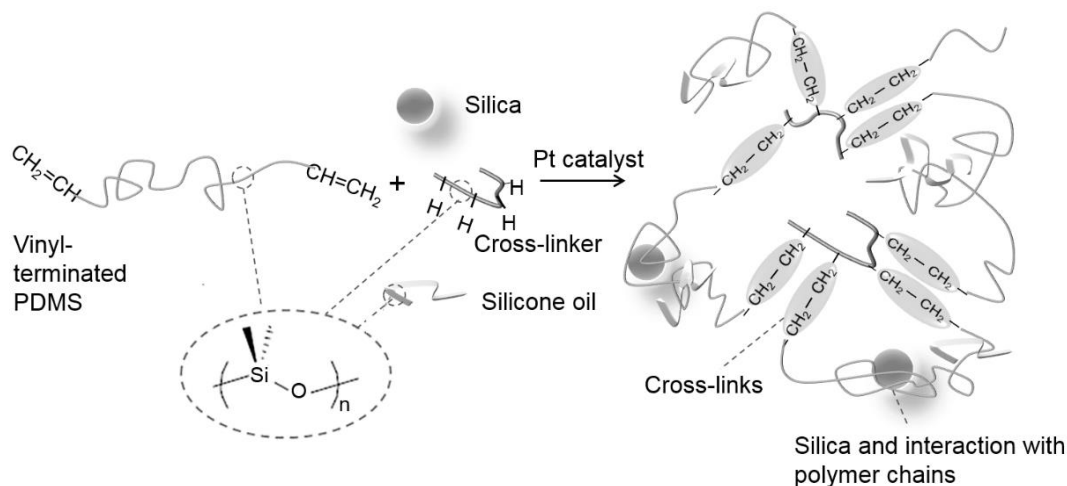
Figure 11. Schematic representation of the formation of a silicone network via a hydrosilylation reaction.

Several examples of commercially available addition cross-linking silicones used as DE materials are Elastosil® P7670, Elastosil® RT625 (both Wacker Chemie AG), Sylgard® 186 (Dow Corning) and NuSil® CF15-2186 (NuSil).

2.2.2 Factors influencing cross-linking

Researchers have never stopped seeking a deeper understanding of factors that may contribute to the cross-linking reaction, because this knowledge is especially vital for material design and optimization. This section provides a short overview of several most discussed factors in this regard, i.e. stoichiometric imbalance, molecular weight, functionality and filler additions.

Stoichiometric imbalance

Especially for two-part RTV silicones, a common approach to tune the elastomer's property is to change the mixing ratio of the two components during preparation. The stoichiometric imbalance of the system, r, is defined as the molar ratio of hydrosilane (Si-H) over vinyl (C=C) groups. As depicted in Figure 9, the hydrosilylation reaction is on a one-to-one basis with a theoretical stoichiometric balance of 1. In a real silicone network, especially at high molecular weight, dangling chains and steric hindrance play an essential role, so that a fully cross-linked network does not occur at theoretical stoichiometry but often at a substantially higher value.[89, 90]

An adequate amount of work has been devoted to the stoichiometric imbalance of silicone formulation as an important parameter. In a work by Chambon and Winter[91] the dependency of a cross-linked PDMS network's storage modulus on stoichiometry was investigated. It was established that the maximum storage modulus (G) was achieved with r close to 1.3 instead of the ideal value of 1. Larsen et al.[92] also reported the effect of stoichiometry on the elastic modulus (Y) and identified a saturation value of 1.2-1.5. According to Flory's theory of an ideal cross-linking process, for silicone networks prepared with different molecular weights or functionality, the PDMS system should reach a gel state for the stoichiometric ratio $r < 3$.[93]

A slightly higher amount of cross-linker is anticipated to compensate for steric hindrance and maximize the content of cross-linking.[94, 95] However, it is important to keep in mind that if the mixing ratio is moved far higher and away from the recommended ratio, a certain amount of cross-linker will be left in the network after the hydrosilylation reaction. For two-component RTV silicones, *thermal post-curing* is usually recommended by some silicone suppliers in order to consume excess hydrosilane groups. Nonetheless, the consistent mechanisms of thermal post-curing are still unclear. So far, though, it is acknowledged that by being subjected to heat, hydrosilane groups can possibly react with oxygen and humidity to form Si-O-Si bonds through a condensation reaction. In Figure 12 several possible reactions are illustrated, which may also occur in a combined form.
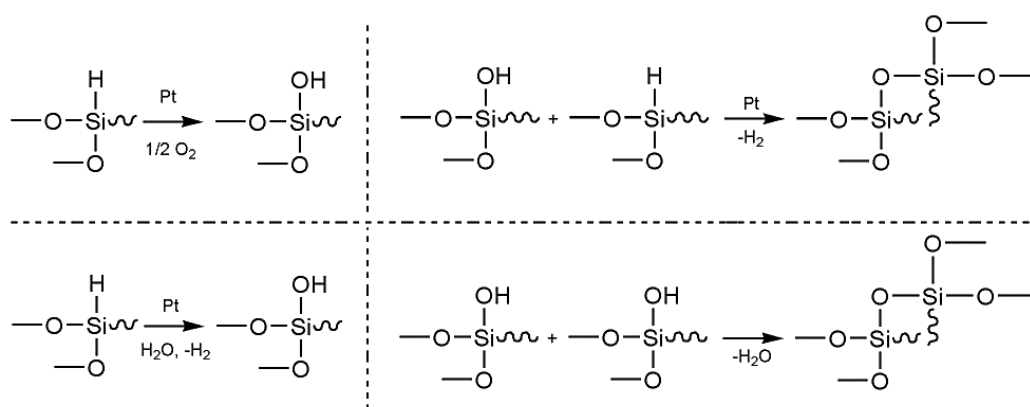
Figure 12. Possible side reactions of the Si-H group with H_2O or O_2 (modified from references[96]).

By lowering the amount of cross-linker, a reduction in the elastic modulus can indeed be obtained, albeit normally at the cost of a not fully completed cross-linking. The formed network thus displays a relatively sticky characteristic and a high amount of non-bonded PDMS chains. It has been observed, for instance, by Frankær et al.[97] that such a network is susceptible to high viscous loss and significant silicone migration during use. The optimum stoichiometric imbalances of a network that just meets the full conversion of cross-linking reactions need to be determined individually.

Molecular weight

A cross-linked elastomer network consists of polymer chains connected to each other via cross-linking joints. The average length of the polymer chains between cross-links is also an important factor influencing the cross-linking reaction. In case of vinyl-terminated PDMS, the average molecular weight of the formed network corresponds to the average molecular weight of the polymer. The chains need to be sufficiently long and reconfigurable in order to endure movement under mechanical stress, and to behave in soft and flexible ways at the bulk scale.

Functionality

To form a three-dimensional network, a vinyl-terminated PDMS chain requires a cross-linker with more than two functional groups per chain, as denoted by functionality (f). Previous investigations into the effect of functionality have shown contrasting results. Generally, it is acknowledged that higher functionality increases the rate of cross-linking, but steric hindrance might be an issue especially for polymers with high molecular weight and for cross-linkers with high functionality. For example, Braun and Mark[98] compared the use of cross-linkers with functionalities of 3, 4 and 40-50 in the preparation of PDMS networks and found that conversion decreased as functionality increased.

Fillers

Cross-linked elastomer properties can be tuned further by adding reinforcing fillers or plasticizers, dispersing agents, chain extenders, anti-oxidatives or other additives. The two most commonly used fillers are silica and silicone oil, which act as a reinforcer and a plasticizer, respectively. The compressive mechanism for the reinforcing effect of silica is still not fully clarified. So far, it is interpreted as an interaction force between polymer chains and filler particles. Silica is a synthetic form of silicon dioxide (SiO_2).[99] The common form is available as fumed silica, which is a pure, amorphous form of silicon dioxide produced via flame hydrolysis. Due to its hydrophilic property and high surface energy it tends to link together via hydrogen bonds. It is also capable of interacting with polymer chains via van der Waals forces.[100, 101] These physical constraints can also act as supporting joints, as the polymer is subjected to external stress and therefore strengthens the network. Hydrophobic and partially hydrophilic silica also exist, and these are prepared by chemically modifying hydrophilic silica with reactive silane. These modified silica (hydrophobic) shows less reinforcing capability compared to hydrophilic silica. Silica can be used in a wide range of commercially available silicones. Depending on the hydrophobic grades (fully/partially hydrophilic) and the concentrations of silica added (typically 10-60 wt.-%),[3] the mechanical properties of silicones can be very different.

The conventional choice of plasticizer for silicone elastomers is non-functional PDMS with low molecular weight. Its identical main chain structure ensures a good dispersion in the silicone matrix. Due to its low molecular weight, it shows a diluting effect that favors the distribution of silica particles and the processing of elastomers. However, the addition of these "free-moving", short PDMS chains may introduce problems with respect to long-term reliability.[3] Generally speaking, large amounts of mobile segments would also be expected to give rise to viscous losses in the material.

As the silica and silicone oil introduce competitive effects into a silicone network, the design of such silicone systems demands a thoughtful balance between reinforcement and dispersion. Also, it is necessary to keep possible effects of the added fillers in mind for long-term reliability issues.

2.2.3 Network structure

A cross-linked silicone, as mentioned above, has a three-dimensional network structure comprising of long, reconfigurable and flexible PDMS chains connected to multifunctional cross-linkers. To evaluate the network structure, several techniques can be exploited, such as FT-IR, MALDI-TOF, NMR, DSC or swelling measurements. FT-IR, MALDI-TOF and NMR are powerful tools employed to identify the chemical groups of the material. DSC can be used during cross-linking to track the cross-linking reaction, and after cross-linking to assess the crystallization/melting/glass transition behaviors of the material. Swelling measurement is a commonly used method to determine the cross-linking density of the material.

In this section, two essential intrinsic parameters evaluating the network structure, i.e. cross-linking density and degree of crystallization, are briefly introduced.

2.2.3.1 Cross-linking density

Cross-linking density (mol/mm³) describes the number of cross-linking joints (mol) per network volume (mm³). It can be measured using a swelling measurement, i.e. when solvent is added, the cross-linked network is capable of absorbing the solvent until an equilibrium is attained. The degree of swelling (%), as defined by the weight of adsorbed solvent in relation to the original weight of the elastomer, is strongly dependent on the density of effective cross-links in the skeletal structure, the interaction between the network and the solvent, the size of the solvent molecule and the temperature.

Based on the entropy change produced by swelling, the Flory-Rehner equation derives a relationship between the degree of swelling and cross-linking density.[102] The cross-linking density d of an elastomer is given by:

$$d = \frac{-(ln(1-\varphi_2) + \varphi_2 + \chi\varphi_2{}^2)}{V_1{}^m \varphi_2{}^{1/3}}$$

Equation 3

while for elastomers with sufficiently high swelling (sufficient low cross-linking density), this equation can be simplified to:

$$d = \frac{\varphi_2{}^{5/3}\left(\frac{1}{2}-\chi\right)}{V_1{}^m}$$

Equation 4

Where φ_2 is the volume fraction, χ is the Flory-Huggins interaction parameter (toluene/polysiloxane = 0.465)[233] and $V_1{}^m$ is the molar volume of the solvent.

The volume fraction φ_2 is defined as the ratio of solvent volume V_1 to the original volume V_0 of elastomer:

$$\varphi_2 = \frac{V_0}{V_0+V_1} = \frac{1}{1+\frac{V_1}{V_0}}$$

Equation 5

with

$$\frac{V_1}{V_0} = \frac{w_2-w_1}{w_1} \cdot \frac{\rho_1}{\rho_2}$$

Equation 6

where w_1 is the original weight of the elastomer, w_2 is the weight of the elastomer after swelling, ρ_1 is its density of the elastomer measured before swelling, and ρ_2 is the density of the solvent (toluene = 0.87 g/cm³ at 25°C).[103]

2.2.3.2 Degree of crystallization

A cross-linked elastomer is amorphous but can crystallize upon cooling. With the aid of DSC measurements, the crystallization peak can be detected at ca. -60°C. The formed crystallites give a melting peak at about -40°C in the subsequent heating run.[104] The degree of crystallization, calculated from the melting heat (ΔH_m) divided by the theoretical heat of fusion of a 100% crystalline PDMS (ΔH_{th} = 37.43 J/g),[105] expresses the amount of formed crystallites during cooling.

Crystallization kinetics are closely related to the presence of topological constraints in the cross-linked network, i.e. cross-linking density, chain length and un-bounded polymer chains. Classical crystallization theory, such as Hoffmann-Lauritzen's theory,[106-109] describes the crystallization process as a sequence of two steps: nucleation and crystal growth. Nucleation is a determining step whereby cross-linking joints, and solid micro-particles such as silica, act as nuclei to initiate the

further formation of a crystal. Subsequent crystal growth involves the incorporation of polymer chains on the crystal surface. The viscosity of the elastomer network and the flexibility of the polymer chain clearly affect this process.[108] Generally speaking, the more flexible the polymer chains, the better they can reorient and drive crystal growth. In this case, crystallization starts earlier and more "perfect" crystallites can be formed; moreover, the higher amount of crystallites leads to a higher melting heat so that the calculated degree of crystallization is higher. Therefore, there should exist a relationship between cross-linking density and the degree of crystallization.

2.3 Properties of silicone-based dielectric elastomer

2.3.1 Mechanical properties

As outlined above, a cross-linked elastomer is a three-dimensional network consisting of long polymer chains occasionally attached to one another via cross-links. For unfilled elastomers these cross-links are the primary valence bonds that are formed through cross-linking reactions between functional groups. For filled elastomers the interaction between the filler particles and the polymer chains can contribute as well. The excellent rotatability of Si-O-Si bonds, together with sufficient chain length, make it possible for polymer chains to undergo appreciable elongation.

While polymer chains are freely reconfigurable, each end of the chain is still bonded to cross-links. When elastomers are subjected to external deformation, polymer chains tend to align parallel to the direction of external deformation, whereas the positions of those cross-links are shifted along the direction of the external deformation. The deformed elastomer reaches a new state of equilibrium with lower entropy compared to that seen for a non-deformed elastomer.

When the external deformation is removed, polymer chains have the tendency to recover their initial configurations. In an ideal elastic state, polymer chains return to their initial locations completely, without loss of energy, just like a spring. However, an elastomer above its glass transition temperature additionally has a viscous nature that means it is able to "move" under stress, showing internal friction between the polymer chains. Respective internal friction during chain rearrangement leads to certain loss of energy through a loading cycle, as can be recognized by mechanical hysteresis, stress relaxation, creep and so on. The combination of these *elastic* and *viscous* natures is known as *viscoelasticity*. Silicone elastomers, for example, are a typical viscoelastic material, whereby elastic contribution normally dominates. Both elastic and viscous behaviors are essential for evaluating the mechanical performance of silicone elastomers. In this section, the fundamental aspects of the mechanical elasticity and viscoelasticity of silicones are introduced.

2.3.1.1 Elasticity

The rubber elasticity theory is a well-established theory thanks to extensive work by Guth and James,[110] Kuhn,[111] Flory and John-Rehner,[112] Gent[113] to name only a few. The elasticity of rubber is identified as the ability to undergo large deformation upon external stress and to recover its initial dimensions fully after the removal of external stress. Although it was firstly discovered on natural rubber,[114] the elasticity theory has become centrally important to polymer science. The rubber elasticity theory provides a first fundamental insight into the molecular origin of elasticity in rubber-like materials and the fundamental interconnections between network structure and mechanical elastic behaviors.

As depicted in Figure 13, the free energy needed to deform elastically a three-dimensional network along the uniaxial direction with a defined extension ratio λ is expressed as follows:

$$\Delta F_{el} = \frac{nRT}{2}(\lambda^2 + \frac{2}{\lambda} - 3)$$
<div align="right">Equation 7</div>

$$\lambda = \frac{L_i}{L_{i,0}} = \lambda_i^{macro} = \lambda_i^{micro} \quad \text{with} \quad i = x, y, z$$
<div align="right">Equation 8</div>

where R is the gas constant (8.314 J/(mol·K)), T is the absolute temperature and n is the number of cross-links per unit volume ($n = d \cdot V$).

L_x, L_y, L_z (or $L_{x,0}$, $L_{y,0}$ and $L_{z,0}$) are referred to the sample dimensions in the deformed (or non-deformed) state. The assumption for the relationship between macroscopic external deformation λ_i^{macro} and chain dimension λ_i^{micro} is based on the affine network, in which the displacement of the network points is similar to which of the deformed macroscopic elements (Figure 13).

And for an ideally incompressible material the relationship between deformations in each x-, y-, and z-directions can be formulated as:

$$\lambda_x \cdot \lambda_y \cdot \lambda_z = 1$$
<div align="right">Equation 9</div>

and

$$\lambda_x = \frac{<x^2>}{<x^2>_0} = \lambda, \; \lambda_y = \lambda_z = (1/\lambda)^{1/2}$$
<div align="right">Equation 10</div>

where $<x^2>_0$ and $<x^2>$ are the dimensions of non-deformed chain (with length x_0) and which of deformed chain (with length x) along the x-direction, respectively.
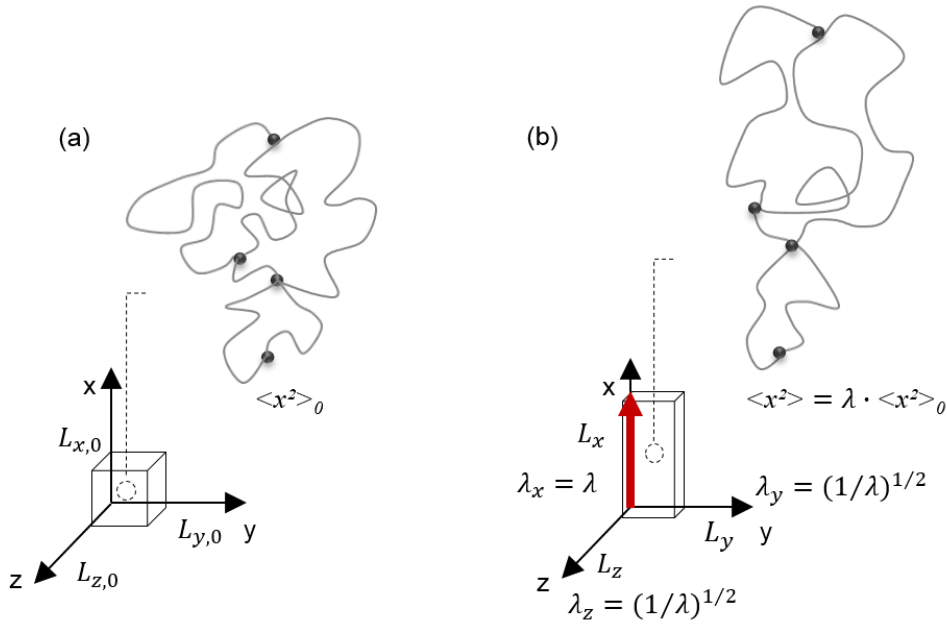
Figure 13. Deformation of an elastic network: (a) non-deformed elastomer, (b) the same elastomer under deformation (the lines represent polymer chains, the dots represent cross-links) (modified from references[112, 115]).

Based on Equation 7 and Equation 10, the stress σ can be presented as a function of $(\lambda - 1/\lambda^2)$:

$$\sigma = \frac{nRT}{V}\left(\lambda - \frac{1}{\lambda^2}\right)$$

Equation 11

It is thus evident that the stress (σ) of a network does not behave in a linear manner to extension (λ). As the strain S is defined as $\lambda - 1$, the slope of the σ - λ curve corresponds to the elastic modulus (Y):

$$Y = L_{i,0}\left(\frac{\partial\sigma}{\partial L_i}\right)_{T,V} = L_{i,0}\left(\frac{\partial\sigma}{\partial\lambda}\right)\left(\frac{\partial\lambda}{\sigma L_i}\right)$$

Equation 12

Introducing Equation 11 into Equation 12, and with $L_i/L_{i,0} = \lambda$, namely $\partial\lambda/\partial L_i = 1/L_{i,0}$, also $n/V = d$, Equation 12 is converted to:

$$Y = L_{i,0}\cdot dRT\cdot\left(1+\frac{2}{\lambda^3}\right)\cdot\frac{1}{L_{i,0}}$$

Equation 13

where it becomes clear that at small strain ($\lambda \rightarrow 1$, $S \rightarrow 0$) Equation 13 can be simplified to:

$$Y \approx 3dRT \qquad\qquad\qquad\qquad\qquad \text{Equation 14}$$

This means that in this small strain region the elastic modulus Y is proportional to the cross-linking density with a factor of 3. With increasing strain, the elastic modulus becomes lower. It is also evident that, based on the elastic modulus, the cross-linking density of the elastomer can also be derived.

Figure 14 shows the typical stress-strain curve of a silicone elastomer. The curve can be divided roughly into three regions. In the small strain region I (ca. 10%) the stress-strain curve is closely linear. This region is used to estimate the elastic modulus. In Region II the rise of stress in line with increasing strain slows down. According to Equation 11, in this region the stress-strain curve loses its linearity and the elastic modulus becomes lower as strain increases. From a macroscopic point of view, this can be explained by the rearrangement and "uncoiling" of the polymer chains. In Region III a steep rise in stress can be recognized, which is usually associated with the "stretching" of polymer chains. In other elastomers such as natural rubbers this region is also acknowledged as being related to strain-induced crystallization (SIC) in the material. However, for silicone elastomers, SIC has been observed rarely.[116-119]
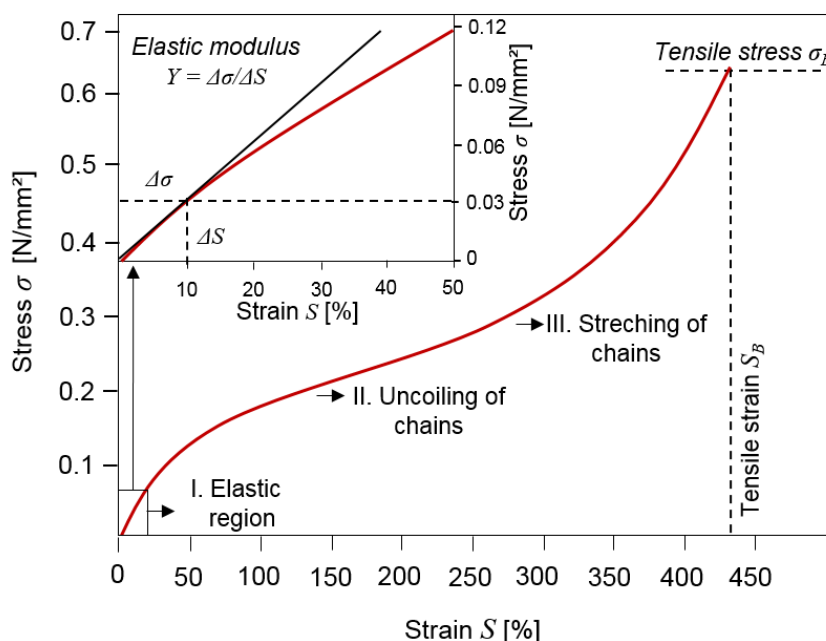

Figure 14. Typical stress-strain curve of an elastomer.

The above-mentioned derivation is based on the Neo-Hookean model,[120] which assumes that stress is proportional to strain for an elastic body. To attain a precise mathematical description of stress-strain behavior, diverse models can also be used, such as the Hooke model,[121] the Mooney-Rivlin

model[122, 123] and the Ogden model.[124] Many ongoing work is devoted to optimizing these models further.

2.3.1.2 Viscoelasticity

The central issue contributing to the mechanical behavior of elastomers is that there is a mixture of elastic and viscous behaviors, known as *viscoelasticity*. When an external force is applied to elastomer, part of the input energy is stored and used to reconfigure elastically the polymer chains. In the meantime, part of the energy is dissipated through molecular motions into heat as mechanical loss. Silicone elastomers have been regarded to have low viscous loss and a relatively dominant elastic contribution. However, it is worth keeping in mind that viscous behavior is associated with heat dissipation within the material, which may affect the properties of a material in relation to, for example, morphology, electrical properties and long-term reliability.

There are also various models describing viscoelastic behavior. A general expression, the so-called Kelvin-Voigt model, is given in Figure 15a. In this model the elastic fraction is symbolized by a spring element, while the viscous fraction is demonstrated by a dashpot element. The linear spring produces instantaneous deformation proportional to stress with a factor Y (elastic modulus), while the dashpot produces strain with a coefficient of viscosity η.
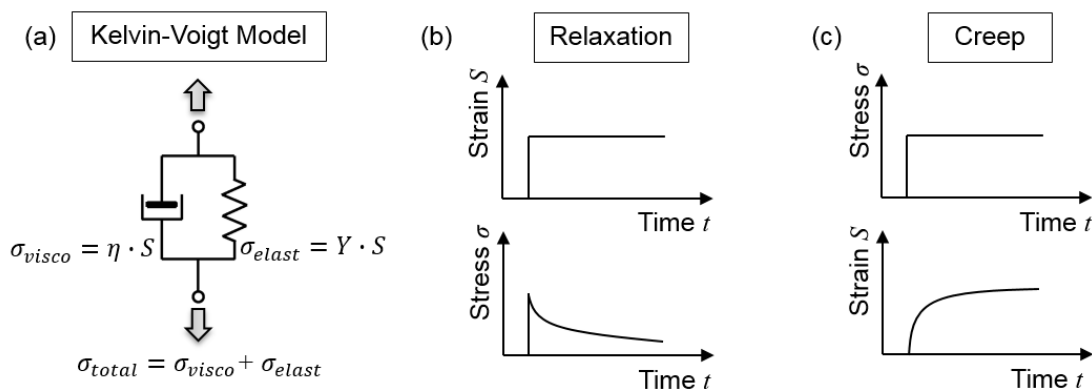

Figure 15. (a) Kelvin-Voigt model (b) stress relaxation (c) creep to demonstrate the viscoelastic behavior of a material (according to references[125, 126]).

The non-linear stress-strain behavior shown in Figure 14 is a direct result of viscoelasticity, and stress alternates non-linearly with strain and vice versa. Stress and strain also depend on the testing rate and duration time. The decrease in stress over time under constant strain is known as *stress relaxation* (Figure 15b). In a similar manner, at a constant level of stress the deformation of an

elastomer may show an increasing tendency, which in this case is acknowledged as *creep* (Figure 15c).

Upon cyclic loading, mechanical hysteresis is an important characteristic that evaluates the viscous behavior of the material (Figure 16a). In each hysteresis loop, the area under the stress-strain curve during loading corresponds to energy adsorbed by the material per unit volume. Respectively, the area under the unloading curve is the energy released by the material. The area between the uploading and unloading curves thus represents energy dissipated as mechanical loss.
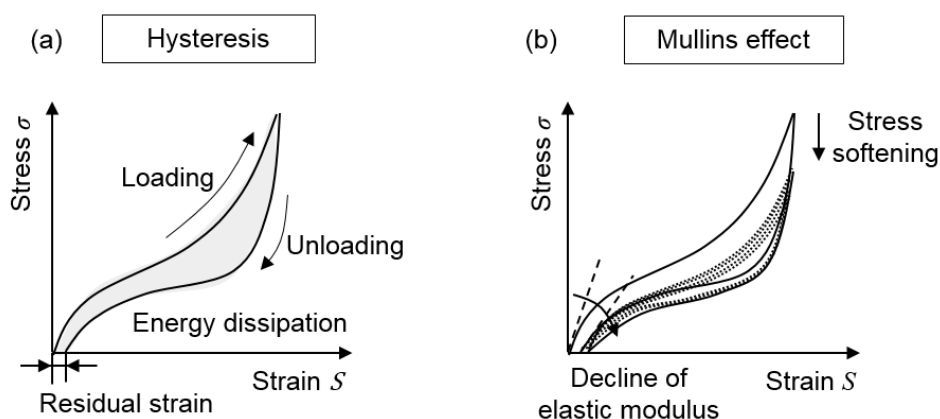

Figure 16. A typical (a) hysteresis curve of an elastomer during loading and unloading (b) the Mullins effect under constant strain (according to references[13, 125, 127]).

A further characteristic phenomenon upon cyclic loading is the so-called Mullins effect,[13, 15, 128] which describes the stress softening of elastomers (commonly filled elastomers) upon cyclic loading conditions (Figure 16b). At the molecular level it is currently described as the de-bonding of polymer chains from each other or from silica-particle surfaces.[129] This de-bonding leads to a steep decrease in stress at the same strain and thus to a decline in the elastic modulus of the material. It is also worth remarking that under a constant level of cyclic loading the Mullins effect is only significant within the first 10 load cycles, after which the polymer matrix reaches a state of equilibrium. Consequently, the Mullins effect needs to be considered as a transient physical effect. When a higher load level is applied to the same elastomer, the elastomer will show the Mullins effect once again.

As mentioned previously, the elastic modulus of elastomer is dependent on cross-linking density. A relationship between viscous properties and cross-linking density is expected as well. Generally speaking, higher cross-linking density leads to a higher elastic modulus and tensile strength. At this high cross-linking density, chain motions become more restricted, and the more restrained network is less capable of dissipating energy (namely also lower hysteresis). In polymer networks containing just a small number of cross-links, polymer chains between the cross-links can adopt more

conformations, and therefore more energy can be dissipated. This general relationship has been addressed by Mark et al.[130] (Figure 17).
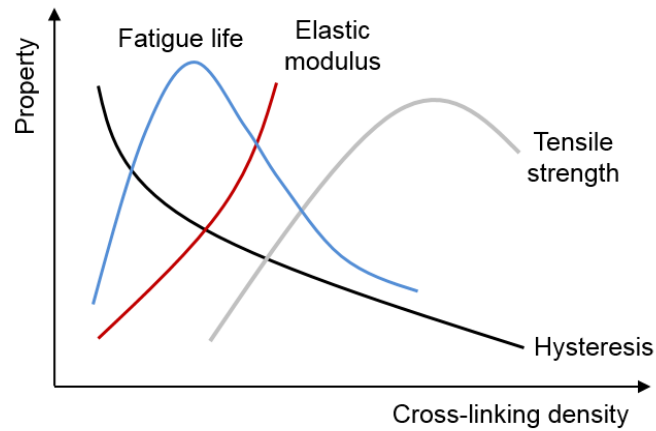

Figure 17. Mechanical properties as a function of the cross-linking density (according to reference[130]).

For silicone elastomers used as DE materials, low elastic moduli and low hysteresis are generally preferred, though the balance of which requires a thoughtful selection of cross-linking density. A further challenge is also understanding the combining effect of cross-linking density on the electrical properties and overall performance of a DE actuator. This will also be one mission of this present work.

In the following Section 2.3.2 some elementary aspects of electrical properties, i.e. relative permittivity and breakdown strength, are introduced.

2.3.2 Electrical properties

2.3.2.1 Relative permittivity

Relative permittivity

Permittivity is the most fundamental parameter of a dielectric material. Analogous to *resistance* for an insulating material, as well as *conductance* for a conductive material, *permittivity* quantifies the behavior of a dielectric material against an electrical field. However, different to resistance, which is a measure of the difficulty in passing an electric current through, and to conductance, which describes the ease with which an electric current passes, permittivity describes how easy it is to generate an electrical flux within the medium. Electric flux, also known as the flow of the electrical

field, is a result of polarization. A material with higher permittivity therefore possesses a higher tendency towards polarization, and therefore more electric flux can be generated.

At the macroscopic level, permittivity is related directly to the capacitance of the material. A dielectric material behaves like a parallel plate capacitor when an external electrical field is applied. Figure 18 exemplifies the situation when an external constant voltage (DC) is applied.
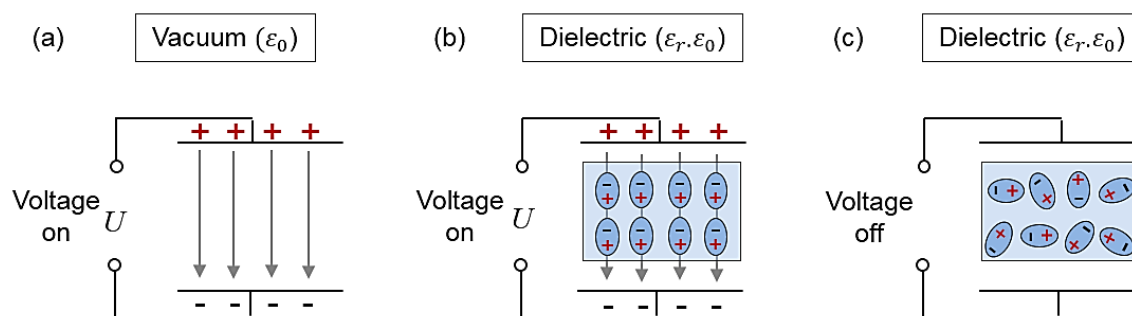

Figure 18. Brief sketch of the origin of permittivity of (a) vacuum (b) dielectric material consisting of dipoles subjected to an electrical field (c) dielectric material consisting of dipoles without an electrical field (according to reference[131]).

In case of a vacuum (Figure 18a), the relationship between the amount of free charge, Q, and the voltage drop, V, is $Q = C \cdot V$. The capacitance C of the capacitor follows the relationship:

$$C = \frac{\varepsilon_0 A}{d}$$
<div align="right">Equation 15</div>

where A is the active area, d is the distance of separation and ε_0 is the vacuum permittivity (8.85×10^{-12} F/m).

In this electrical field, an electrical displacement (also electric flux density) D originates from vacuum displacement and is given by:

$$D = \varepsilon_0 E_i$$
<div align="right">Equation 16</div>

where E_i are the components of the electrical field between the capacitor plates.

In the presence of a dielectric material, the charged particles (dipoles) involved in the material have the tendency to align themselves along the direction of the electric lines. The process, in which these

electrically loaded particles are displaced from their original states, in order to reach new equilibrium, is called *dielectric polarization*. As a result, electric displacement is increased to D_i:

$$D_i = \varepsilon E_i \qquad\qquad\qquad \text{Equation 17}$$

where ε is the permittivity of the system. Since part of the electric displacement is attributed to vacuum displacement, the dielectric polarization density P, contributing to electric density, is as follows:

$$P = D_i - \varepsilon_0 E_i = (\varepsilon - \varepsilon_0)E_i \qquad\qquad\qquad \text{Equation 18}$$

in which case relative permittivity ε_r is defined as:

$$\varepsilon_r = \frac{\varepsilon}{\varepsilon_0} \qquad\qquad\qquad \text{Equation 19}$$

and Equation 18 is converted to:

$$P_i = (\varepsilon_r - 1)\varepsilon_0 E_i \qquad\qquad\qquad \text{Equation 20}$$

The relative permittivity introduced above happens under constant voltage conditions. When the dielectric material is subjected to an alternating field, relative permittivity also displays frequency-dependent characteristics. This is due to the fact that at multiple frequency ranges various relaxation phenomena occur (will be introduced in the following paragraphs).

A definition of complex-valued relative permittivity is then employed, whereby the real and imaginary parts are separated:

$$\hat{\varepsilon}_r(\omega) = \varepsilon'_r(\omega) - i\varepsilon''_r(\omega) \qquad\qquad\qquad \text{Equation 21}$$

where $i = \sqrt{(-1)}$, $\omega = 2\pi f$

While ε'_r is the real part of relative permittivity denoting stored energy within the medium, ε''_r is the imaginary part of relative permittivity denoting the dissipation (or loss) of energy within the medium. The ratio of ε''_r over ε'_r is defined as loss factor $tan\delta$, which is a measure of the relative magnitude of energy loss.

$$tan\delta = \frac{\varepsilon''_r}{\varepsilon'_r} \qquad\qquad\qquad \text{Equation 22}$$

Generally speaking, when loss factor $tan\delta$ is infinitely small, the material can be considered as being perfectly dielectric without loss. In case of an infinitely large $tan\delta$, the material is fully conductive. Silicone materials are usually very good dielectric materials with relatively high ε'_r, low ε''_r and low $tan\delta$.

In this thesis, spectra of relative permittivity were measured using dielectric spectroscopy from 100 mHz to 300 kHz. The relative permittivity value at 10 Hz, at which the spectrum exhibited a plateau, was evaluated.

Dielectric polarization and relaxation

As mentioned above, the response of charged particles to an alternating field is frequency-dependent. The polarization of a material usually covers a wide range of relaxation phenomena, which are associated with characteristic frequency ranges.

Four types of polarization can be classified for dielectric materials:

- *Atomic (electronic) polarization* at 10^{14}-10^{15} Hz, due to the displacement of electron clouds within each atom upon exposure to an electrical field.
- *Ionic polarization* at 10^{10}-10^{12} Hz, due to displacement of oppositely charged neighboring ions in the presence of an electrical field.
- *Dipolar (orientation) polarization* at 10^4-10^6 Hz, due to the reorientation of dipole moments.
- *Interfacial polarization* in a low frequency range $< 10^3$ Hz, due to the space charge diffusion at electrode-specimen interfaces, or at the interface between two materials or between regions within a material.

Figure 19 presents an overview of these four polarization mechanisms. In general, a dielectric material exhibits more than one polarization mechanism, and therefore permittivity must be considered as a superimposed description. Nevertheless, the frequency dependency of these various polarization mechanisms suggests the corresponding polarization mechanism at a given frequency.
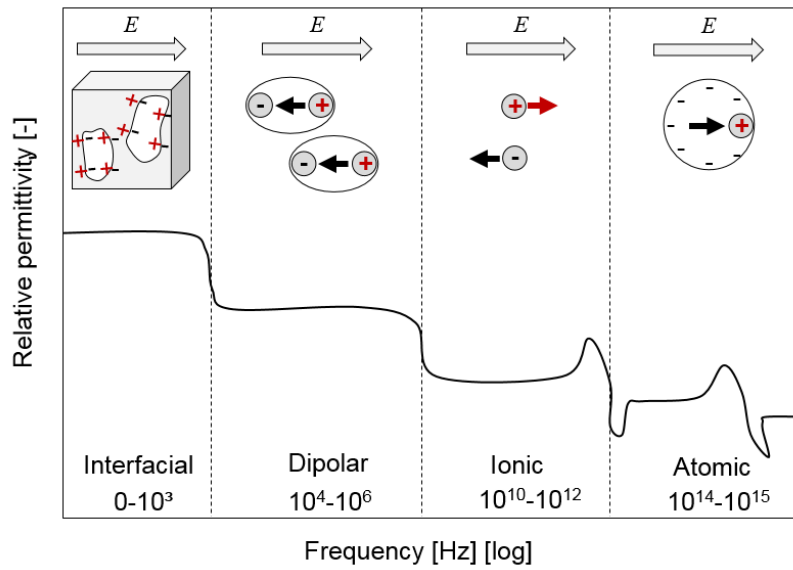
Figure 19. Overview of various polarization mechanisms and the characteristic frequency range (according to reference[132]).

For silicone elastomers, dipolar polarization is suggested as the predominant polarization process. This is due to the fact that the Si-O bonds of the main chain are highly polarizable and possess permanent dipole moments. Subjected to an electrical field, these dipole moments tend to reorient along the field. The net dipole moment per unit volume (dielectric polarization density) is therefore a summation of vectors over all molecular dipole types in the repeat unit, the polymer chain and every other chain in the system (Figure 20).

$$\vec{P} = \frac{1}{V} \sum_{\substack{all \\ chains}} \sum_{chain} \sum_{\substack{repeat \\ unit}} \vec{\mu_i}$$ Equation 23
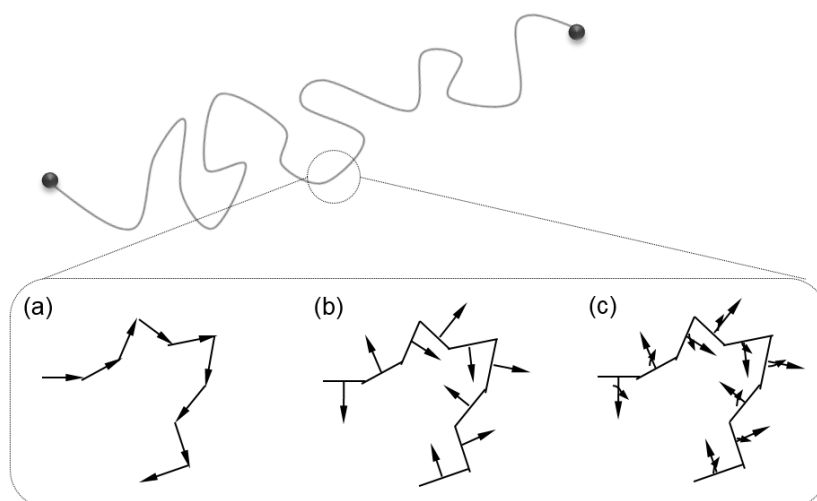
Figure 20. Different molecular motions contributing to dielectric polarization (according to reference[133]).

These molecular motions can be measured by different relaxation processes, for example α-relaxation, which describes the rotational movement of dipoles around the chain skeleton, and β-relaxation, which is related to the rotational fluctuations of diploe vectors of side groups, as well as normal-mode (α') relaxation, which indicates the fluctuation of the whole polymer chain.[133, 134]

These relaxation processes are also assigned to different frequency ranges and show also temperature-dependency. Theoretically, it is possible to distinguish between these relaxation processes by using proper temperatures and frequencies. For example, α-relaxation is also known as dynamic glass transition, because it is related to the glass transition of the material. This offers the chance to determine the dynamic glass transition temperature (T_g) as the temperature of maximum loss at the selected frequency. For elastomers with low T_g (ca. -120°C for silicone), a cooling process down to this temperature is therefore required.

Furthermore, the molecular structure, chain architecture and intermolecular interactions of a polymer also have an influence on relaxation and therefore on dielectric behavior. Though these relaxation processes are still not thoroughly understood, diverse mathematical models are intended on disclosing the microscopic description of the relaxation procedure. To name just a few, these models include the Debye model,[135] Volgel-Fulchel-Tammann-Hesse (VFTH), Williams-Landel-Ferry (WLF), the Harrilliak-Negami (HN) function[136, 137] and the Kohlrausch-Williams-Watts (KWW) function.[138] Experimentally it has been observed that the form of α-,β-relaxation peaks broadens with cross-linking in styrene-butyl acrylate copolymer.[134, 139, 140]

2.3.2.2 Breakdown strength

A dielectric material is evaluated by its ability to not only store energy within the medium, but also to resist the applied electrical field so that charges cannot pass through. At the moment that the medium is electrically passed through, an *electrical breakdown* (also *dielectric breakdown*) occurs. For solid insulating materials, this breakdown always ends up in permanent damage. Especially for DE materials, an electrical breakdown is of great importance for the application, since the operation of a DE device requires an electrical voltage preferably as high as possible. The voltage that the material suffers at breakdown is referred to as *breakdown voltage*, and this is the maximum voltage that a material can sustain. The corresponding electrical field is then defined as *breakdown strength*, which is deduced based on the thickness of the material.

Electrical breakdown covers extensive mechanisms, which can be categorized broadly into *intrinsic* and *extrinsic* breakdown.

An intrinsic breakdown occurs over a relatively short period of time (10^{-8} s)[141] and is related to damage at the molecular level within the material, i.e. chemical degradation, caused by the electrical field. With a sufficiently high electrical field, electrons may gain sufficient energy to form a conductive channel and lead to ionization. The Hippel low-energy theory,[142] for example, proposes that breakdown occurs when the applied electrical field is high enough to accelerate electrons to ionise further, thus building up an avalanche. The Fröhlich-based high-energy theory,[143, 144] in contrast, assumes that only electrons having sufficient ionization energy are accelerated by the applied field, which then leads to electrical breakdown.

Since the intrinsic breakdown is a measure of the inherent behavior of the medium, it needs to be measured in strictly controlled conditions and the specimen needs to be "perfectly" pure. In practice, the measured breakdown strength is commonly lower than the intrinsic breakdown strength of the medium, because there are certainly factors leading to extrinsic breakdown.

Prominent extrinsic breakdown mechanisms are as follows:[141, 145-148]

- *Thermal breakdown*: electric stress can be associated with significant heat build-up. If this generated heat cannot be dissipated sufficiently, the medium will suffer thermal stress. This may assist the chemical degradation/oxidation of the medium, leading to early breakdown compared to intrinsic breakdown.

- *Breakdown due to internal discharges*: when a dielectric medium contains cavities, inhomogeneities contaminations or voids, breakdown due to internal discharges may occur under an applied field. These voids or cavities are actually filled with air, and thus they have much lower breakdown strength ($E_{B, air} \approx 3$ V/μm) than the dielectric medium ($E_{B, silicone} \approx 30$ V/μm). These electrically loaded cavities will easily form a conductive channel within the material within a much lower electrical field than the intrinsic breakdown strength of the dielectric medium.

- *Electromechanical breakdown*: especially for dielectric elastomers an interplay between mechanical and electrical effects exists, and therefore a breakdown mechanism known as electromechanical breakdown is an important example. If electrical voltage applied on the electrodes, the electrostatic pressure that thins the elastomer layer is compensated by the internal elastic stress of the material. Once the electrical field further increases the electrostatic pressure cannot be balanced by the internal elastic stress, the so-called *electromechanical instability* (EMI) occurs and leads to the breakdown of the elastomer[149, 150] (Figure 21).
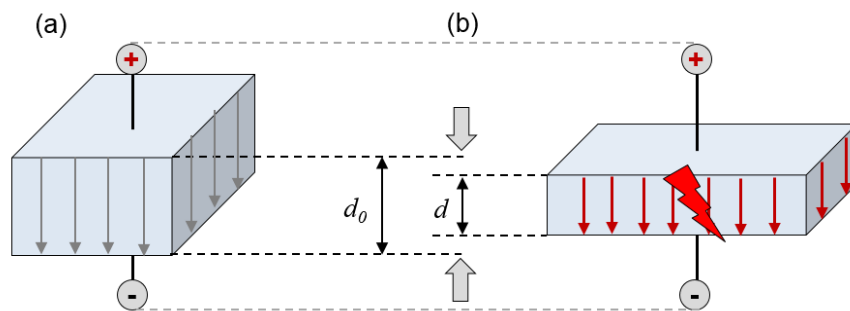
Figure 21. Brief sketch of electromechanical instability (EMI).

Breakdown limit based on EMI (E_{EMI}) can thus be calculated by equating these two effects:

$$\varepsilon_0 \varepsilon_r \frac{U^2}{2d^2} = Y \, ln\left(\frac{d_0}{d}\right)$$

Equation 24

where d_0 is the initial thickness of the dielectric elastomer film and d is the true thickness at the moment of breakdown.

By solving Equation 24, it becomes clear that when the thickness goes to zero, a critical voltage exists. This critical breakdown limit according to the EMI mechanism is thus given by:

$$E_{EMI} = \frac{U}{d_0} = 0.6 \left(\frac{Y}{\varepsilon_0 \varepsilon_r}\right)^{0.5}$$

Equation 25

This equation was first proposed by Stark-Garton[149] and has become one of the most well-accepted and well-established descriptions of EMI. However, it is worth noting that Equation 25 is actually a very unrealistic model, as it is based on infinitesimal thickness. Moreover, this model ignores factors such as inhomogeneity at the film's surface or within the medium, which may cause the inhomogeneous distribution of the electrical field within the dielectric medium and subsequent early breakdown.

Besides electromechanical instability (EMI), *electro-fracture breakdown*[151] and *filamentary electromechanical breakdown*[152] have also been proposed as possible reasons for electromechanical breakdown. In both cases the growth of a crack is considered to occur as a result of the coupled electromechanical stress. The filamentary electromechanical breakdown model suggests also that the strain energy additionally needed for crack propagation has to be counted when calculating the strain energy required for electromechanical breakdown. For dielectric elastomers, electromechanical instability (EMI) has been acknowledged as one of the most dominant breakdown mechanisms. Current research focuses mainly on the highly precise determination of electrical breakdown and on the modelling of electrical breakdown. In both areas a deeper understanding of electrical breakdown in DE materials is needed.

To investigate electrical breakdown in the present work, the major challenges are as follows:

- It has to be kept in mind that the measured breakdown strength is (E_B) referred to as *engineering* breakdown strength, which differs from *true* breakdown strength. The former is based on the initial thickness of the elastomer film, which is somehow lower than the *true* thickness of an elastomer film at the moment of EMI breakdown.

- The electrical breakdown due to EMI is thickness-dependent, as depicted in Equation 24. Furthermore, thickness may affect breakdown behavior, as the numbers of defects/voids in the medium scale with the volume and thickness of the specimen. These defects/voids may play a role in electrical breakdown.

- In practice, silicone films for DE applications are very thin (well below 200 µm). In the present work thin films with ca. 150 µm are investigated. For this low thickness, the measuring technique needs to be optimized in order to achieve statistically reliable results. For this purpose, an electrode facility is developed according to IEC 60243-1 with thin upper/lower electrodes. Further information about this test facility is introduced in the experimental part (Section 10.3.2).

- Although EMI has been considered as the main breakdown mechanism for dielectric elastomers, it is still unclear whether it is applicable to the mechanically/ electromechanically-aged specimens. As mentioned above, interplays between mechanical, electrical, thermal and chemical processes may take place when a specimen is subjected to an electrical voltage. From the viewpoint of polymer science, a further challenge is to offer interpretations at the molecular level about the interdependencies between breakdown strength and network structure, and then to use this understanding to address reliability-relevant concerns.

2.4 Reliability of dielectric elastomers

The reliability of silicone-based DEs is an essential issue that has been so far rarely investigated. Current research in the field of silicone-based DEs is mainly dedicated to three areas: material development, modelling and application. None of these topics can be separated from the reliability of the material: the developed material needs to show satisfying properties but also needs to sustain long-term loading; the modelling also requires an understanding of the possible time-variant changes of material parameters as well as their interdependencies; while a considerable amount of interesting applications have been introduced, the unknown long-term behavior strongly limits the industrialization of this material group.

There are indeed several problems impeding the investigation of the reliability of silicone-based DEs. First, the fundamental structure-property relationships of silicone-based DE materials are still unclear. Second, coupled electromechanical loads make the identification of underlying failure mechanisms even more difficult. Even in case of a sole mechanical and electric load, possible ageing mechanisms are often superimposed. Moreover, DE applications, particularly, must be capable of undergoing cyclic large deformation and cyclic high voltage, and for these severe load conditions there is still no clear statement on property changes or responsible ageing mechanisms.

In this section, a general introduction to reliability will be provided, including the common failure modes, general reliability theories and testing techniques. Emphasis will also be put on the Wöhler approach and Weibull analysis. Both of them will be employed in this thesis. Then, the current state of reliability investigations into DE actuators will be introduced. In the last subsection, a general overview of possible ageing mechanisms under mechanical, electrical and thermal loading found in the literature will be summarized, in order to give a glance into possible mechanisms on a molecular level.

2.4.1 General introduction to reliability

Reliability is a measure of the functionality of a system or a component under certain load conditions for a specified time period, in other words, when a system/component satisfies its expected performance. It is also important to note that reliability statements are only validated for defined load conditions and time ranges.

Load conditions and failure modes

Commonly applied load conditions can be mechanical, electrical, thermal stress or environmental influences such as exposure to pH, UV, etc. It is also common that several stresses are present in a combined form, such as mechanical-thermal stress, whereby thermal stress can arise from a thermal build-up during mechanical loading.

For most systems/components subjected to mechanical stress, mechanical fatigue is often the primary consideration. It is firstly established on metallic materials, and then also for polymeric materials. Underlying physical ageing has been well-studied, from the perspective of crack nucleation and propagation.

Techniques for reliability investigations

Depending on the load conditions and requirements, various techniques/methodologies can be employed. To address mechanical fatigue behavior, both an experimental approach and a statistic-assisted analysis are needed. Weibull analysis is a commonly used probabilistic fatigue analysis. The relationship between load conditions (stress or strain) and the cycle number that the system/components can sustain until failure (rupture or certain length of crack, etc.) is illustrated by the so-called Wöhler curve. Furthermore, computational modellings (e.g. finite element method) can be also very useful in generating models of mechanical fatigue in the early product development phase.

Accelerated testing can also be helpful in this regard. In the laboratory, failure upon a much harsher but nonetheless representative environment is generated by using much higher loads or much faster rates. In this case, different models, such as the Arrhenius model (for thermal stress), can be used to derive the relationship between the lifetime under laboratory conditions and the one under the actual load condition. For systems involving a number of subsystems or components, failure mode and effects analysis (FMEA), for instance, is also a commonly used method.

Wöhler tests

The Wöhler test is a classical and well-accepted approach to investigating the cyclic resistance of materials. It is named after August Wöhler, who established the method in 1850. Materials are subjected to cyclic sinusoidal loading until failure. The applied cyclic load can be applied as a *stress amplitude* σ_a or a *strain amplitude* S_a. For metallic materials, it is commonplace to use stress amplitudes, due to the small strain and high stress factors inherent in the material. The use of a strain-controlled approach is suggested for materials with large deformation and low strength, such as thin elastomer film, in which case an alternating strain can be controlled better than stress.[153-155] Moreover, the viscoelastic behavior of the elastomer makes stress-controlled Wöhler tests difficult,[155, 156] and so in the present work they are therefore performed by using a strain-controlled approach. The ratio of minimum strain (S_{min}) to maximum strain (S_{max}) is defined as the *R*-ratio, which is kept constant during Wöhler tests.

$$R = S_{min}/\, S_{max}$$
Equation 26

Strain amplitude S_a for cyclic sinusoidal loading (Figure 22a) is given as:

$$S_a = (S_{max} - S_{min})/2$$
Equation 27

By keeping the R-ratio constant, different strain amplitudes can be designed with different S_{min} and S_{max}. The R-ratio, strain amplitude S_a and the frequency of this cyclic loading influence the ultimate Wöhler curves and need to be defined prior to the experiments.

Specimens subjected to this cyclic loading will sustain a period of cycles but then eventually fail (rupture, certain length of crack, etc.). The number of cycles until the moment of failure is recorded as *cycle number to failure* N_f. Usually, more than one specimen needs to be tested under a given strain amplitude, because there exists a relatively large alternation of N_f. Also, in order to gain a relationship between S_a and N_f, several strain amplitudes are needed (Figure 22c).

By presenting the differently applied S_a on the y-axis and the N_f recorded on the x-axis on a double logarithmic scale, a linear relationship can be obtained in the range of 10^2-10^6 cycles. This period is called the *fatigue strength range*. The word *fatigue* refers to the *failure* of a material, caused by repeatedly applied loads in material science. This linear relationship between $Log(S_a)$ and $Log(N_f)$ is known as the *Wöhler curve*, and based on this relationship it is possible to predict the maximum cycle numbers that a specimen can sustain under arbitrary strain amplitude in this range.
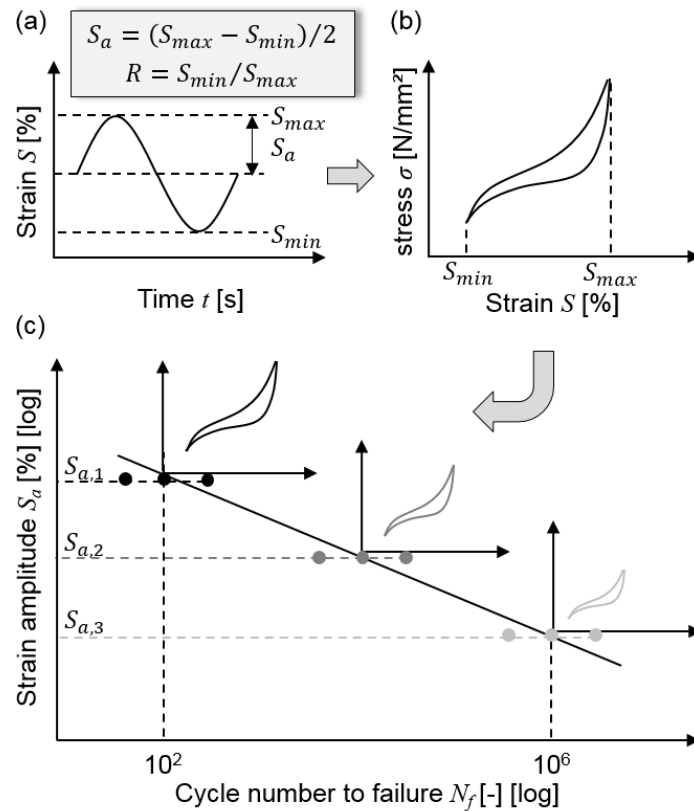
Figure 22. (a) Strain amplitude, maximum strain, minimum strain and R-ratio of a Wöhler test (b) corresponding stress-strain curve of a single loading cycle in a Wöhler test (b) the obtained Wöhler curve as the relationship between applied strain amplitudes and cycle numbers to failure.

Weibull analysis

While Wöhler tests provide an experimental approach to estimate/predict maximum cycle numbers of a material under cyclic load, Weibull analysis is a methodology for fatigue based on statistics. This distribution was first established by Waloddi Weibull in 1951.[157] Today, Weibull analysis has become a widely accepted analysis tool, not only in the field of reliability and material science, but also generally as a useful forecasting methodology. Especially for polymer science, the use of Weibull analysis has also been reported for polymers aged through electrical cycling.[12, 158, 159]

When a specimen is subjected to cyclic loads, the occurrence of failure (fatigue) has a time-dependent character. The distribution of the probability of failure is therefore cumulative and can be formulated by the following equation:[157, 160, 161]

$$F(x) = 1 - e^{-\left(\frac{t-t_0}{T-t_0}\right)^b}$$

Equation 28

where $F(x)$ is the cumulative failure probability or failure frequency (scaled to 100%), t is the operating time or cycle number, T is the scale parameter as characteristic lifetime during which a total of 63.2%[18] of the specimens have failed (also characteristic lifetime), b is the shape parameter as a slope of the fitting line in the probability plot and t_0 is time without failure (delay), which is usually the activation time of the acting failure mechanisms.

Assuming $t_0 \approx 0$, a simplified two-parameter equation (Equation 29) can be derived from Equation 28:

$$F(x) = 1 - e^{-\left(\frac{t}{T}\right)^b}$$

Equation 29

By applying this function to the probability plot, it is possible to determine how many specimens have failed or will fail up to a defined running time/cycle. The obtained parameters b and T are of great importance. The shape parameter b is the slope of the fitting line in the Weibull plot. $b < 1$ indicates "early" failure, $b = 1$ a "random" failure and $b > 1$ suggests a "wear-out" failure. T is known as the scale parameter and corresponds to the characteristic lifetime during which 63.2% failure probability is reached. In Figure 23 a typical Weibull plot is presented.

For tests with different sample sizes the probability of each specimen $F(x)$ can be estimated using mathematical approximations. For a sample size $N = 30$-60, the probability of each specimen can be assigned according to the following equation:[162]

$$F(x) = \frac{x - 0.3}{N + 0.4}$$

Equation 30

---

[18] 63.2% is defined under the assumption that $t = T$: in this case of $F(x) = 100\% \, (1 - 1/e) = 63.2\,\%$
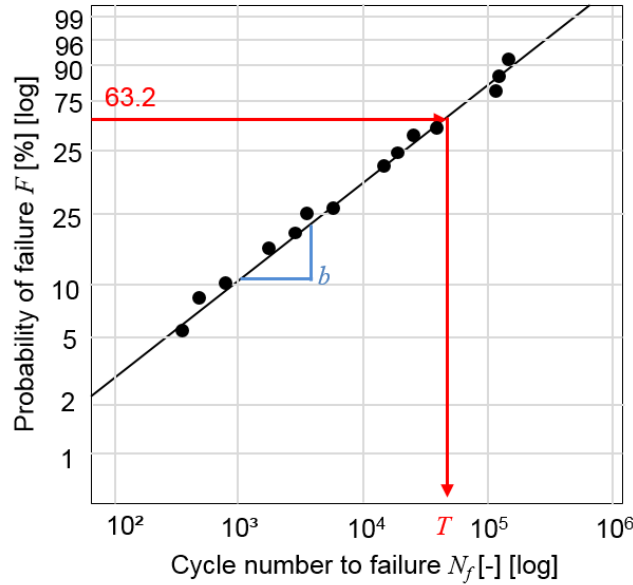
Figure 23. Example of a Weibull plot. T: characteristic lifetime at a 63.2% failure probability of failure.

2.4.2 Reliability investigations of dielectric elastomer actuators

So far, only very limited research has been published concerning the reliability and lifetime of DE actuators.[12, 159, 163] As mentioned above, this is mainly related to the unclarified structure-property relationships of the material, on the one hand; and the coupled loads of electrical high voltage and major mechanical deformation on the other hand.

Current studies therefore focus mainly on the system level of DE devices. Several failure modes for DEs can be suggested, such as mechanical rupture, electrical breakdown, pull-in instability, degradation of actuator performance, failure against aggressive media, etc. In the work of Matysek et al.[12] it was evident that electromechanical loading degraded the performance of a DE actuator over a long period of time. Accordingly, the lifetime of these DE actuators can be determined using Weibull analysis. However, the reasons for these deteriorations in performance remain still open.

There are several prevalent issues relating to the investigation into the reliability of silicone-based DE materials.

- First, load parameters for reliability testing must be thoughtfully and individually defined (coupled electrical/mechanical, torsion, tensile, compression, strain amplitude, voltage amplitude, voltage-driven or charge-driven, frequency, signal form, etc.).

- Second, test facilities need to be properly optimized or even custom made with respect to actuator configurations and load conditions (single-layer, multi-layer, stack actuator, roll actuator, resolution, measurement range, etc.). For specimens especially with low thickness and large

deformation, both accurately controlled testing and precise characterizations are essential. For planar actuators that require general pre-straining, the test setup needs to be designed to prevent early unintended effects (such as pre-damage to the specimen). In order to test multi-layer actuators, it is advisable to take the number of layers into consideration, because boundary conditions, adhesive properties between the layers and the inhomogeneity of the overall deformation may affect reliability results.[164] Although no universal definitions or setups can be registered, emphasis is currently also placed on specifying testing standards in the field of silicone-based DEs[164] in order to enable better comparisons between results attained by using different methods.

- Third, long-time and time-dependent testing are necessary, while accelerated testing may also be helpful. Ideally, the specimen should be tested under operating conditions as similar as possible to those of the intended application. However, it is also generally recommended that tests should be performed under worst-case stress scenarios, in order to characterize the critical influences on lifetime.[164] This certainly demands a comprehensive knowledge of the *critical load conditions* necessary for ageing the test specimen. For accelerated ageing tests, for example under elevated temperature conditions, great care has to be taken, because the underlying mechanisms can be complicated by associated thermal ageing.

- Also, in order to determine the lifetime of a DE device, a proper *end-of-life* criterion has to be defined and the lifetime determination needs to be performed according to statistical methods. The end-of-life criterion can be a mechanical rupture, an electrical breakdown or degradation in performance down to a certain level. Most important is that these criteria must be defined based on sufficient amounts of experimental data.

- Last but not least, as the goal of reliability investigation is not only about lifetime testing, but also about comprehending the underlying failure mechanisms, a deeper understanding of the fundamental relations or interactions between mechanical and electrical properties and the network structure is inevitable.

2.4.2 Possible ageing mechanisms

Depending on the load conditions, load duration, chemical formulations of the material as well as specimen configurations, different ageing mechanisms may take place, sometimes even in combined form. Besides physical mechanisms such as crack nucleation/propagation that take place under mechanical fatigue, it is also considered that the end-of-life of a material may possibly be associated with changes on the molecular level. Various ageing mechanisms have been reported in a diverse range of studies. In this section, the ageing mechanisms of polymeric materials under mechanical, electrical and thermal stresses, as found in the literature, are summarized, with the aim

of taking a quick glance at possible ageing mechanisms in general. In order to distinguish and identify ageing mechanisms at the material level, individual investigations are necessary.

Mechanical stress

The following mechanisms have been reported in the literature:

- Chain-scission, molecular fracture, fatigue of intermolecular bonds[18]
- Secondary cross-linking,[19] chemical degradation,[20, 21, 165, 166] oxidation[167]
- Mullins-type softening,[13, 14, 128, 129] disentanglement/chain slip,[23] damage of interactions between filler particles and polymers[13, 14, 128, 129]
- Formation of voids,[22, 23] formation of cavities/micro-cavities/internal defects,[168, 169] crack nucleation/propagation,[170-172] internal defects[173-177]
- Strain-induced crystallization (SIC) (rather typical in natural rubber and epoxy materials than in silicone materials)[116-119]
- Heat generation and associated thermal ageing[178-180]

Several of these mechanisms can be linked to each other, such as chain scission, degradation, oxidation and further cross-linking, and they are all related to chemical changes at the molecular level. External mechanical stress is suggested to change stress localization on polymer chains,[16, 17] leading to chain scission,[18] further cross-linking reactions[19] or chemical degradation.[20, 21, 165] During further cross-linking reaction, for addition RTV silicones in particular, there may exist a superimposed oxidation or hydrolysis reaction from Si-H to Si-OH. The formed Si-OH groups may condensate further with other Si-OH groups or react with Si-H groups from which additional Si-O-Si bonds form (Figure 12).[96]

Besides chemical changes, it has been acknowledged that mechanical stress may also physically alter the material. For mechanical fatigue, crack nucleation and propagation have been identified being possible when subjected to mechanical fatigue. For non-oriented polymer it was proposed by Kausch[22, 23] that chemical phenomena may not be the predominant causes of ageing, but that the structural weakening of a material during loading can also be related to physical phenomena like disentanglement, chain slip and void formation.

These ageing mechanisms certainly depend on the type of mechanical stress and the load duration. For example, the Mullins effect has been known to occur only in the first several load cycles (< 10 cycles), and also typically in instances of a sufficiently large amount of deformation. For non-cycled mechanical stress, it has been observed that compression/ tension stress may decrease the relative permittivity,[181] while sometimes it will increase the relative permittivity but decrease breakdown strength.[24] Furthermore, since stress distribution in case of compression and tension is very

different, even if deformation is equivalent the compressive load is well-acknowledged as being less destructive compared to tensile load.[113, 169, 172, 182, 183]

Electrical stress

Under electrical stress conditions, the major possible mechanisms are as follows:

- Chain-scission, molecular fracture, fatigue of intermolecular bonds[151, 184, 185]

- Secondary cross-linking[30-33], chemical degradation[28, 186], oxidation[27, 187, 188]

- Formation of cavities/micro-cavities/internal defects[185, 189, 190]

- Electrical breakdown and early breakdown[146]

- Hydrophobicity recovery, due to the diffusion of mobile low molecular weight polymer chains[34, 186, 191]

- Heat generation and associated thermal ageing[148, 187]

Also upon electrical stress, ageing mechanisms can take place in combined form. Several mechanisms are very similar to those seen for mechanical stress, for example the formation of cavities and micro-cavities. It has been reported by Parpal et al. [185] and Crine et al.[190] that micro-cavities may form as a result of electrical high voltage, and they also tend to coalesce to form cavities and thus lead to a final breakdown of the dielectric material. Chemical changes such as chain scission, degradation, oxidation and secondary cross-linking have also been evidenced in a good number of publications. It is also not surprising that a cross-linking reaction may be induced by electrical stress, as electron beam processing[192] and electron irradiation[193, 194] can be used to cross-link polymers. In addition, specimens stressed in electrical high voltage conditions are susceptible to heat generation.

Upon electrical stress, there are several individual ageing mechanisms that differ from mechanical stress. An increase in hydrophobicity, for example, has been often observed on electrically-aged specimens. It is understood as the diffusion of mobile low molecular weight chains, which can be associated with polymer degradation. Depending on the type of electrical stress, further individual ageing mechanisms have been proposed. These include:

- Partial electrical discharges: surface oxidation[195]

- Corona ageing: chemical reaction with water,[31] hydrophobic recovery[34]

- Electrical treeing: decrease in physical cross-linking joints, destruction of the connection between silica and PDMS[29]

- Dry-band arcing: scission and interchange, hydrolysis of siloxane bonds and hydrocarbon groups, oxidation of hydrocarbon groups[96]

- Electrical irradiation: decrease in molecular mobility, due to further cross-linking[196]

- DC exposure: chemical degradation[197]
- Gamma radiolysis: molecular weight changes, chain scission and cross-linking[198]

Thermal stress

Under thermal stress, the following ageing mechanisms have been reported:

- Cross-linking,[199, 200] oxidation[201]
- Chain scission,[202] degradation[203-205]
- Acceleration of chemical reactions[206, 207]
- Impact on mechanical, optical, electrical properties of the material[208]

Both mechanical and electrical stress may result in heat generation within the material. Upon thermal stress both oxidation[201] and degradation[203-205] have also been identified as possible ageing mechanisms. It is also known that when exposed to heat many chemical reactions may be accelerated. In the work by Hsu et al.[208] the effects of thermal ageing were also shown to have effects on the optical, mechanical and morphological properties of phenylmethylsiloxane-modified epoxy being used as an LED[19] encapsulate.

---

[19] LED: Light-Emitting Diode.

3 Preparation of Silicone Formulations

The first major challenge faced when investigating the reliability of silicone-based DE is that the chemical formulations of the used commercial silicone elastomer are undisclosed. Therefore, a benchmark formulation of silicone that was similar to the composition of the commercial material needed to be created. By varying the formulation parameters of this benchmark formulation an understanding of the material's structure-property relationships can be gained, and the ageing mechanisms can be further investigated. This chapter describes preparation of a benchmark material with properties similar to those of commercial silicone Elastosil® P7670 (Wacker Chemie AG).

To clarify the chemical structure of the commercial material, diverse techniques such as NMR, FT-IR, ICP-OES, MALDI-TOF and extraction measurement were employed. Based on the obtained information, several pre-polymers and cross-linkers were selected as possible candidates, allowing for the design of a basic formulation and for defining possible influencing formulation parameters (Section 3.1).

In Section 3.2, by discussing the influences of these formulation parameters' variations on cross-linking, a final formulation is specified as the *benchmark formulation*. Comparisons between the prepared benchmark material and the commercial material, in terms of their cross-linking density, mechanical tensile property, relative permittivity and breakdown strength, are also outlined.

Based on this benchmark material, the stoichiometric imbalance is then varied and a set of silicone materials is designed (Section 3.3). These silicone materials haven then been employed for subsequent investigations.

3.1 Characterization of commercial silicone material

3.1.1 Structural characterization

NMR

Elastosil® P7670 (abbreviated as Elastosil in this work) is an addition cross-linking, two-component silicone that vulcanizes at room temperature. As introduced in Section 2.2.1, a common reaction type for addition cross-linking is the hydrosilylation reaction between vinyl groups (C=C) and hydrosilane groups (Si-H) where platinum is present as a catalyst.

The two components of uncured Elastosil, referred herein to as part A and part B, were provided in form of highly viscous liquids. Curing reaction was performed by mixing A and B in the same weight proportions. In order to identify the chemical structures of the exact functional components in A and B, liquid-NMR (^{1}H, ^{13}C and ^{29}Si) measurements were firstly carried out.

Figure 24a and Figure 24b show the ^{1}H-NMR spectra of parts A and B. In both spectra, the signal groups between δ = 6.30 and 5.60 ppm are clearly ascribed to the chemical shifts of vinyl protons (-CH=CH$_2$). The three doublets "a", "b" and "c" can be assigned to the individual protons of the vinyl group, which is an indication that both A and B consist of terminated vinyl groups. The broad and strong signals around δ = 0 ppm belong to the methyl protons in the D-unit[20] (-OSi(CH$_3$)$_2$-), as marked by "d". Moreover, the peak "e" at δ = 0.16 ppm is shifted slightly downfield because of the adjacent vinyl group. Compared to Figure 24a, the spectrum of part B (Figure 24b) presents additionally a multiplet in the range of δ = 4.8 to 4.6 ppm, which corresponds to the Si-H group. Furthermore, the multiplets "g" and "f" can be assigned to the terminated Si-H groups and the Si-H groups on the PDMS backbone, respectively.

The ^{13}C-NMR spectra of parts A and B visualize consistent chemical structures. In both spectra of part A and part B shown in Figure 25a and Figure 25b, chemical shifts at δ = 131.8 and 139.6 ppm can be detected clearly; these are characteristic of the vinyl groups marked by "a" and "b". The significant resonance around δ = 0 ppm in both spectra is typical of the methyl group, while the small peak at δ = 1.03 ppm in Figure 25b is attributed to the silyl methyl group adjacent to the hydride groups, as labelled "e" and "f".

The ^{29}Si-NMR spectra of part A (Figure 26a) and part B (Figure 26b) suggest the same chemical structures proposed by ^{1}H-NMR and ^{13}C-NMR. In Figure 26a there are only two peaks visible at δ = -22.0 and 7.2 ppm, which indicate the D-unit (-OSi(CH$_3$)$_2$-) (labelled "b") and the M-unit[21] adjacent to the vinyl group (CH$_2$=CH-Si(CH$_3$)$_2$O-) (labelled "a"), respectively. In Figure 26b, the D-unit signal is clearly visible, while the M-unit signal is comparably weak. Signals in the range from -20 to 0 ppm can be ascribed to the Si-H groups, which exist in very small amounts.

---

[20] D-unit: one silicon atom is connected to two oxygen atoms ((CH$_3$)$_2$SiO$_2$).
[21] M-unit: one silicon atom is connected to one oxygen atom ((CH$_3$)$_3$SiO).
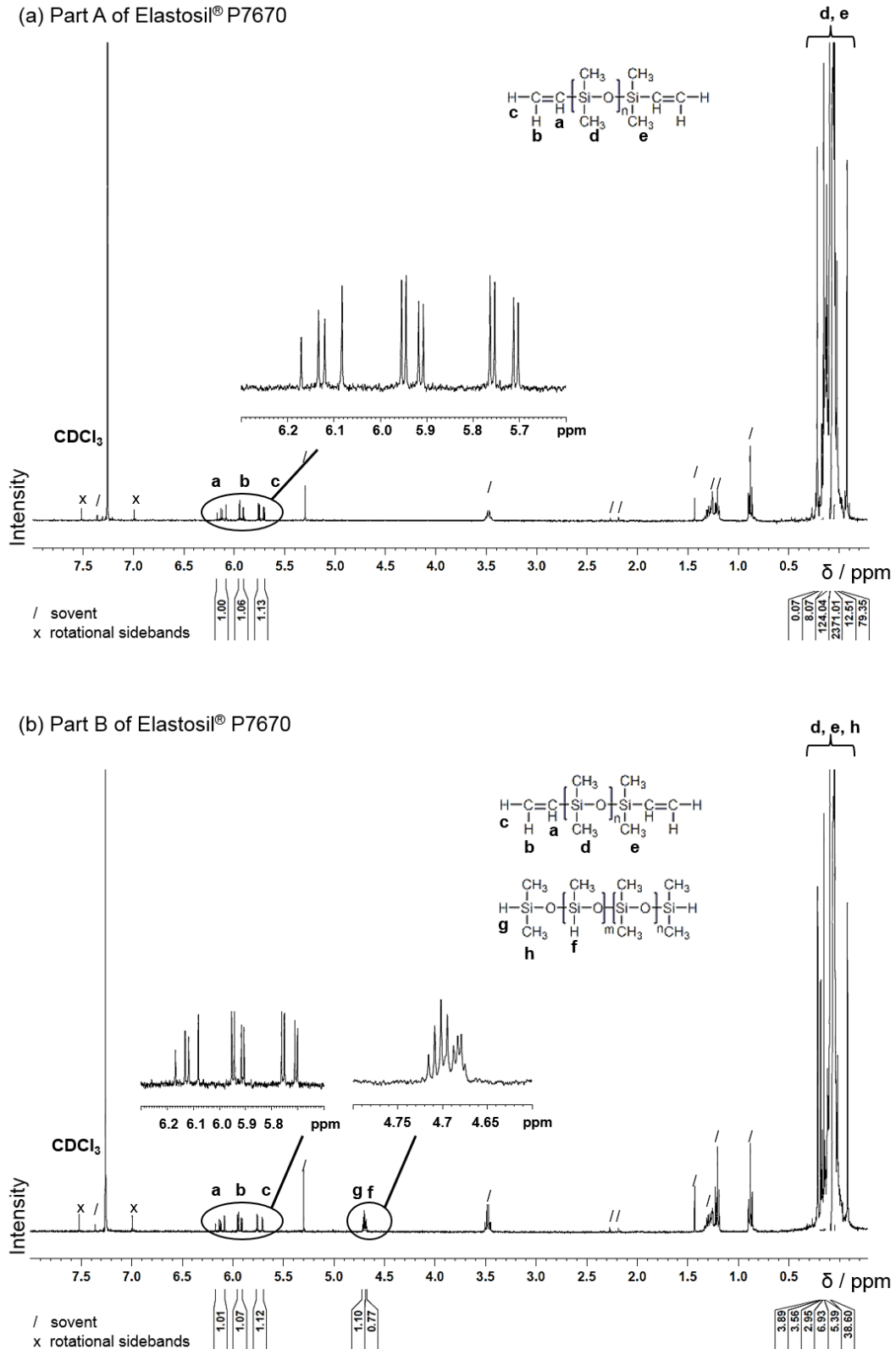
Figure 24. ^{1}H-NMR spectra of (a) part A and (b) part B of Elastosil® P7670. Chemical structures of the involved components can be deduced: both A and B involve vinyl groups. Part B contains also Si-H groups.
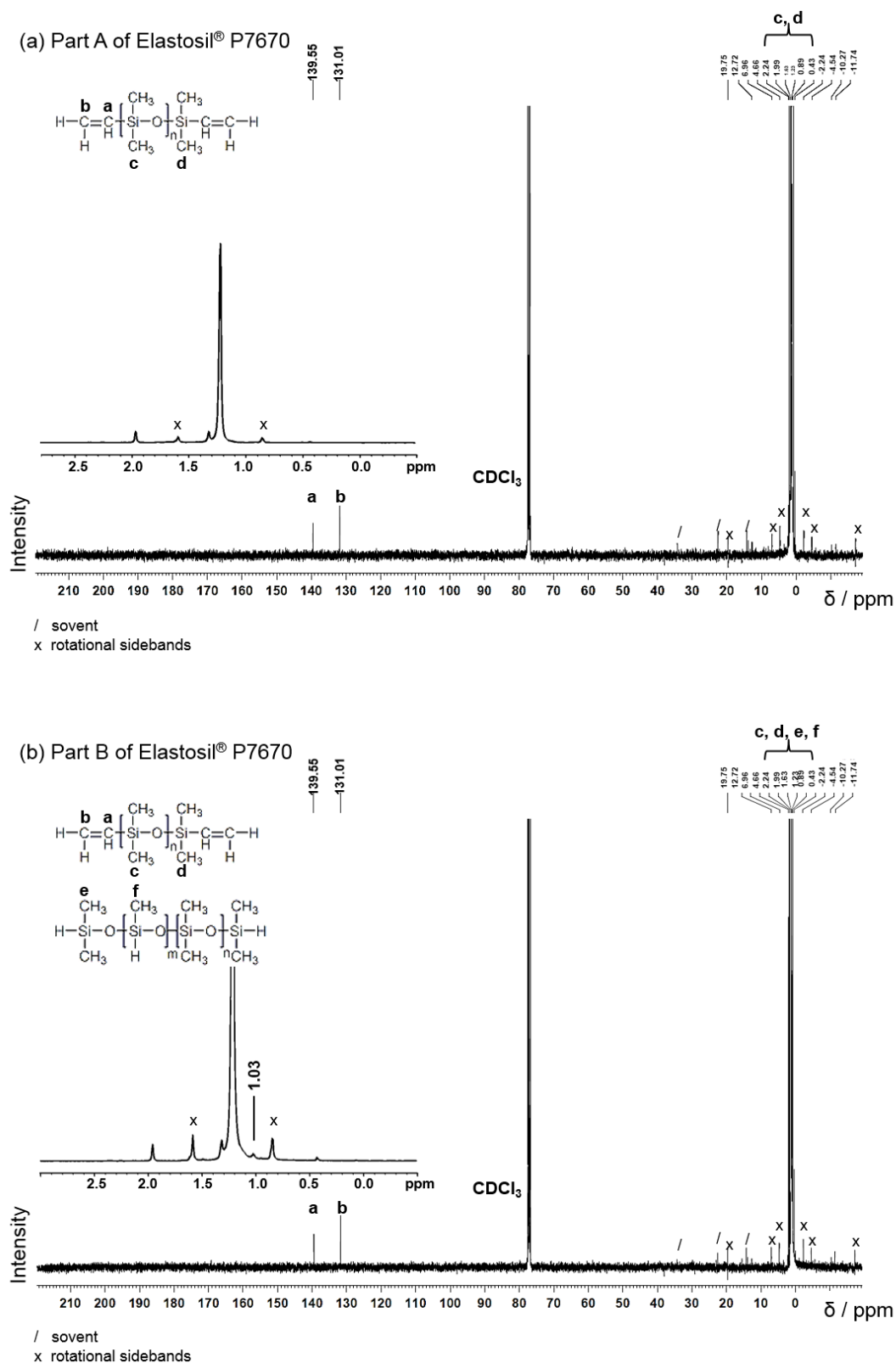
Figure 25. ^{13}C-NMR spectra of (a) part A and (b) part B of Elastosil® P7670. Chemical structures of the involved components can be confirmed: both A and B involve vinyl groups. Part B contains also Si-H groups.
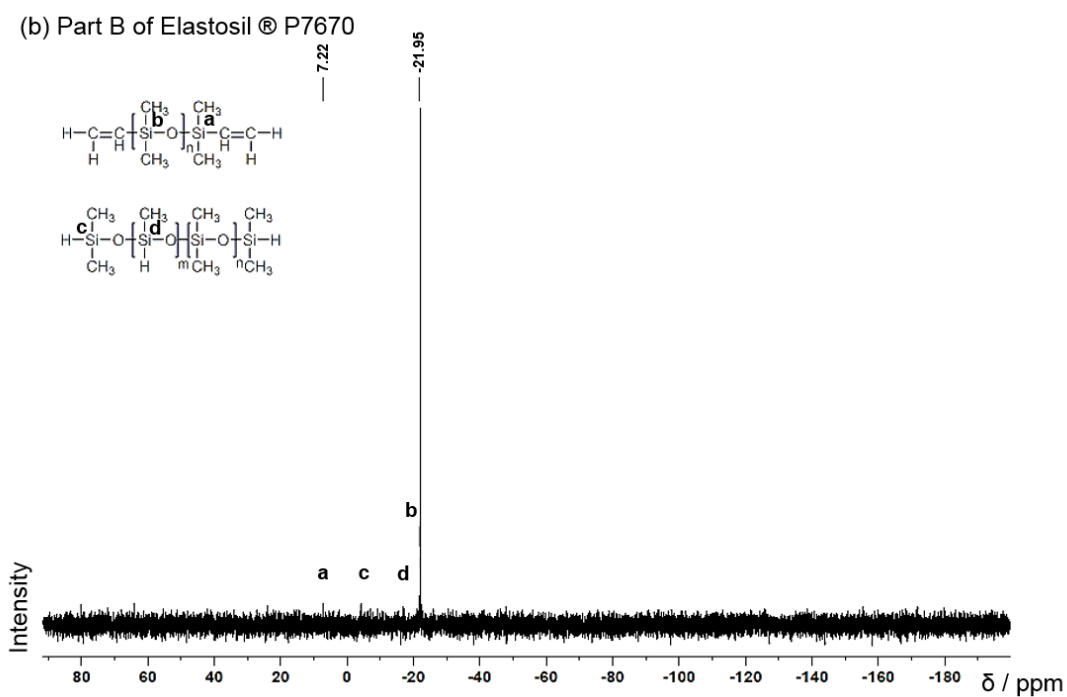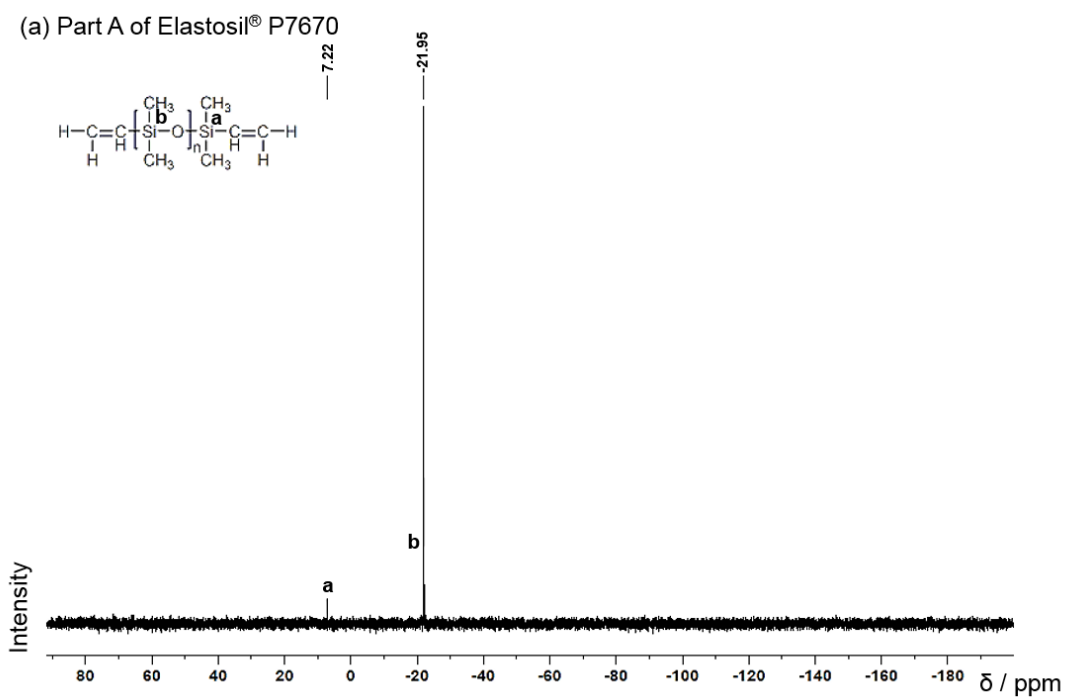
Figure 26. ^{29}Si-NMR spectra of (a) part A and (b) part B of Elastosil® P7670.

ATR-FT-IR

The chemical structures of parts A and B revealed by NMR measurements are supported by the FT-IR spectra shown in Figure 27. Typical chemical bonds of the involved components in A and B can be identified, for example C-H bonds in CH_3 groups at 2962 cm^{-1} (asymmetric stretching), Si-CH_3 bonds at 1260 cm^{-1}(symmetric stretching*)* and Si-O-Si bonds around 1014 cm^{-1} (asymmetric stretching). In both parts A and B, the stretching bands of the vinyl groups are only faintly evident due to the low relative content of the vinyl groups. In part B, the Si-H group at 2136 cm^{-1} (stretching) and 912 cm^{-1} (bending) are identifiable, as illustrated in Figure 28.
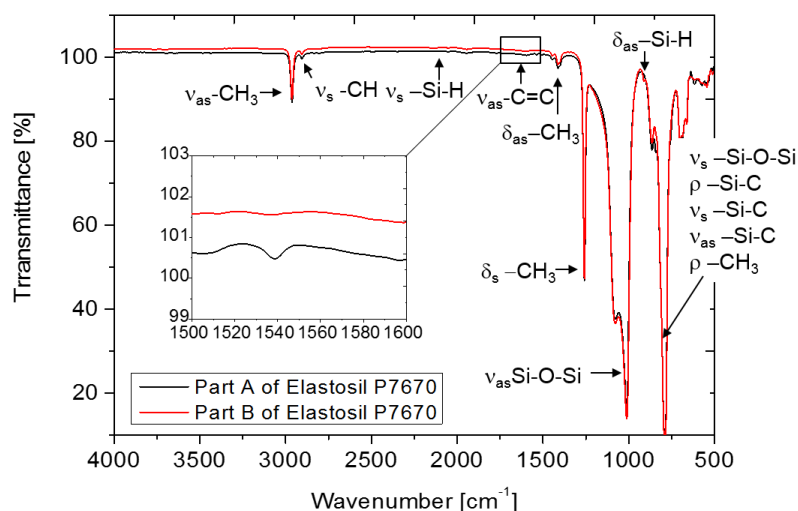
Figure 27. ATR-FTIR spectra of part A and B of Elastosil® P7670 ranging from 4000 to 500 cm^{-1}.
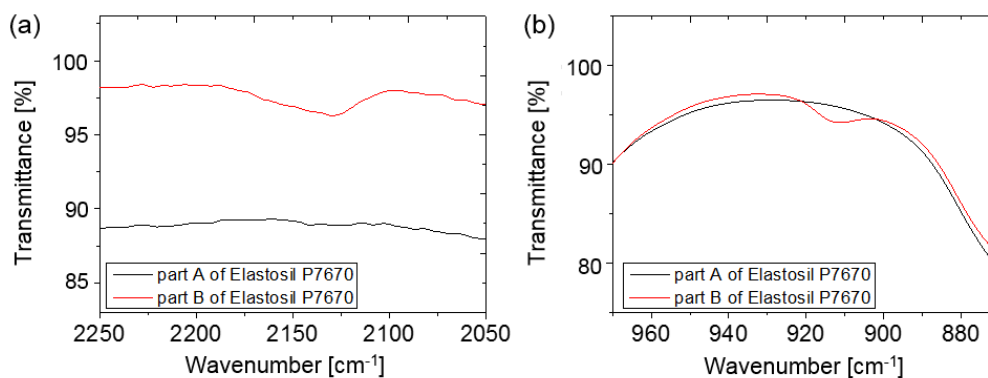
Figure 28. ATR-FTIR spectra of Si-H groups in part A and B of Elastosil® P7670 (a) stretching band of the Si-H group at 2136 cm^{-1} and (b) bending band for the Si-H group at 912 cm^{-1}. It confirms that part B contains Si-H groups.

ICP-OES

Based on the results from NMR and FT-IR, it is proposed that part A includes vinyl-terminated PDMS (abbreviated as vinyl-PDMS), while part B contains both vinyl-terminated PDMS and hydride-containing PDMS (abbreviated as SiH-PDMS). Hence, the assumption can be made that the platinum catalyst is only present in part A. To verify this hypothesis, ICP-OES measurements were performed to determine the content of platinum in A and B. Three independent measurements of each A and B were performed. No evidence of platinum in part B was detected, whereas in part A an average platinum concentration of ca. 9 ppm was acquired (Appendix 1). ICP-OES measurements cannot, however, provide information about the chemical structure of the platinum catalyst.

MALDI-TOF

To shed light on this issue, MALDI-TOF was employed. MALDI-TOF is a powerful tool for investigating the chemical structure of polymers.[209-211] This method functions by capturing polymer fragments ionized by proton or metal ion, it is based on the assumption that polymer fragments with different molecular weights can be equally ionized and detected. This in turn sometimes limits the interpretation of the mass spectrum, especially in quantitative analysis of polymer with high molecular weight and broad molecular weight distribution.[212, 213] This explains that the obtained mass spectra of parts A and B were not able to provide information regarding the exact molecular weights of the polymer. Although the exact molecular weights of components in parts A and B cannot be substantiated by using MALDI-TOF, the MALDI spectra presented in Figure 29 offer clear indications of the chemical structures and molecular weights of the repeat units in both A and B, as well as the chemical structure of the Pt catalyst in part A.

The spectrum of part A in Figure 29a allows for deducing the chemical structure of the platinum catalyst, which refers clearly to a classical Karstedt's catalyst, i.e. a Pt(0) complex, which contains both bridging and chelating divinyl ligands. This Karstedt's catalyst coupled with vinyl-PDMS has a complex structure, which is also illustrated in Figure 29a. Furthermore, it can be confirmed that the repeat unit of the PDMS pre-polymer in part A has an average molecular weight of 74.02 g/mol, which clearly refers to the D-unit ($-OSi(CH_3)_2-$). Detectable are the fractions with numbers of repeating units (n) from 6 to 36.

In a similar manner, based on the spectrum of part B (Figure 29b), the average molecular weight of the repeat unit of the PDMS pre-polymer in part B can be calculated, which also comes in at 74.02 g/mol. However, apart from this finding, no further information was gained.
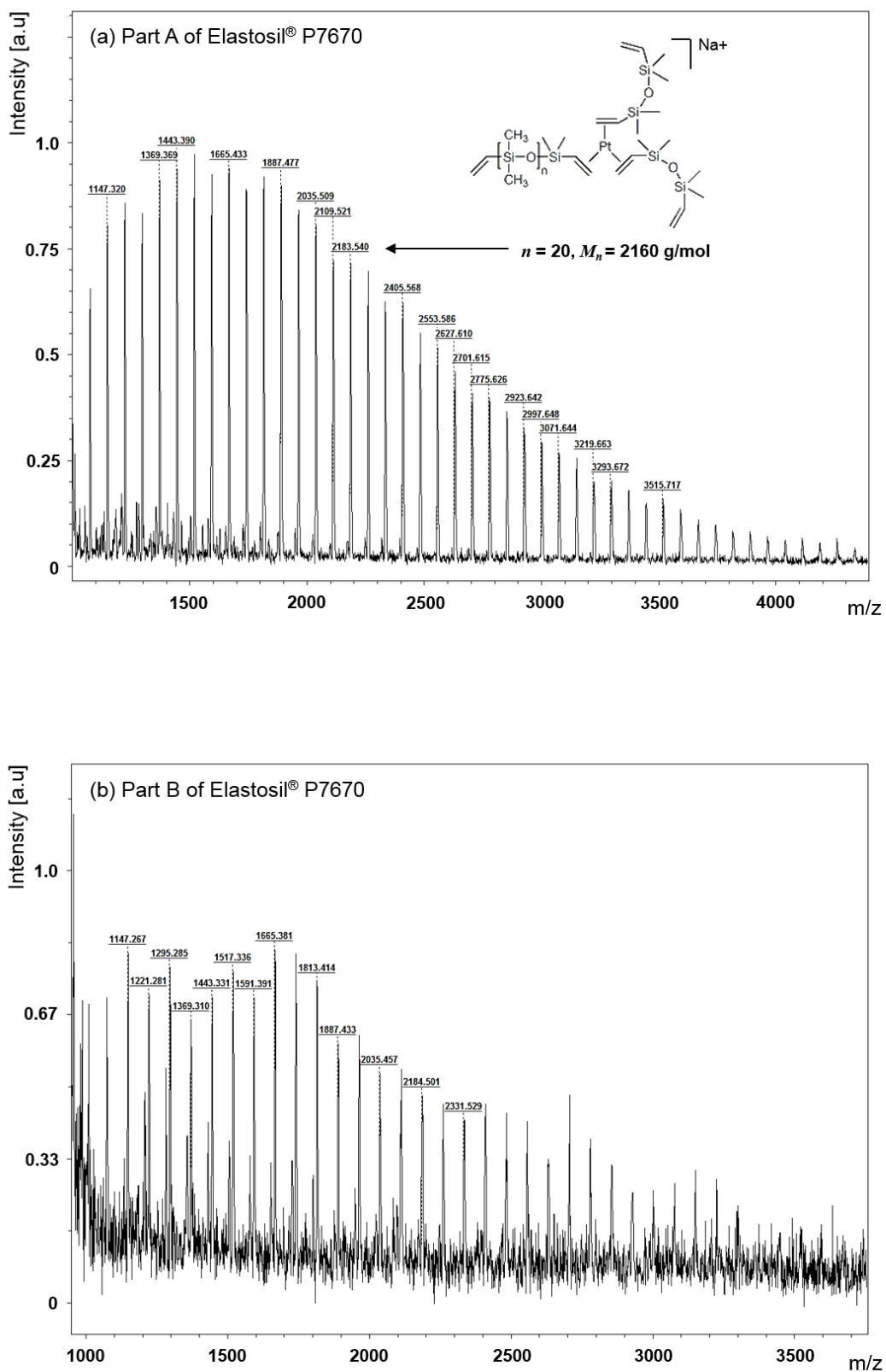
Figure 29. MALDI-TOF mass spectra of (a) part A and (b) part B of Elastosil® P7670. Repeat units of the components in A and B can be estimated. Part A contains Karstedt's catalyst.

Extraction measurement

It is common that commercially available silicone elastomers contain a substantial amount of fillers. The two most commonly employed fillers are silica and silicone oil. The former is used to reinforce the silicone elastomer, while the latter is especially of interest due to its lubricating property. Commonly used silicone oils are non-functionalized PDMSs (linear or cyclic), whose backbones consist of the same repeat unit (D-unit: $-OSi(CH_3)_2-$) as seen in the silicone matrix, thus ensuring a high compatibility with the silicone matrix, on the one hand; on the other hand, silicone oils with comparably low molecular weights compared to the siloxane matrix are usually preferred, making them disperse well in the siloxane matrix.[214]

To verify the content of silicone oil involved in Elastosil, cured Elastosil films were analyzed using extraction measurement. The extract was subsequently characterized by ^{1}H-NMR measurement to assess its chemical structure. Results showed that ca. 24 wt.-% of extract can be removed from Elastosil. This means that the actual content of silicone oil in Elastosil should be at least 24 wt.-% or even higher. Subsequent ^{1}H-NMR measurements (Figure 30) confirm that this extract refers to a linear, non-functionalized PDMS.
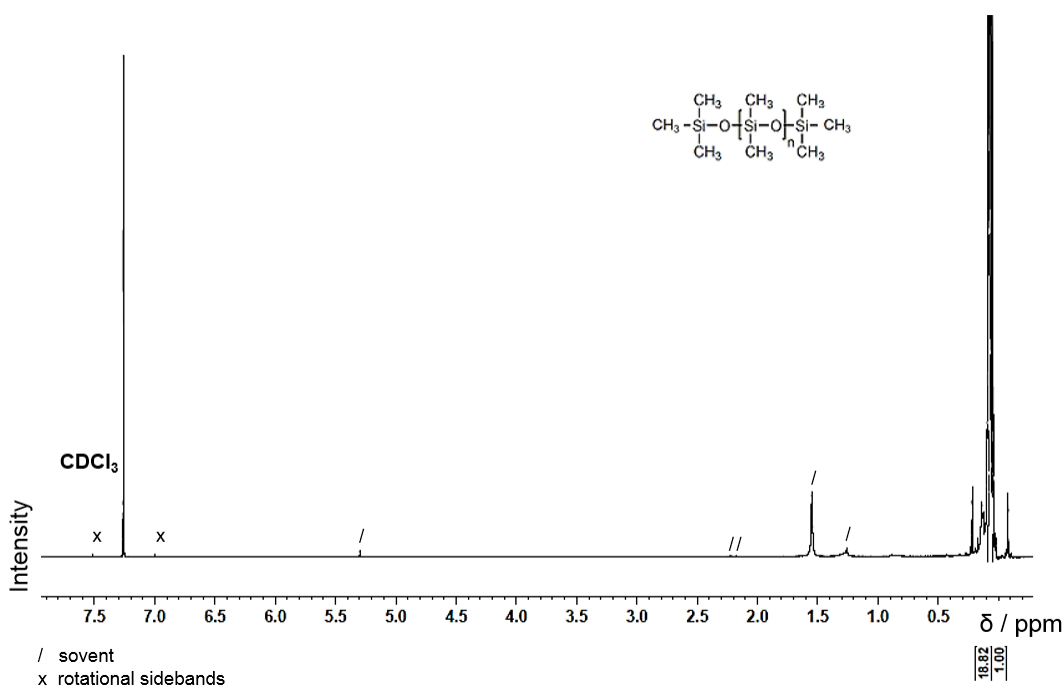
Figure 30. ^{1}H-NMR spectrum of the silicone oil extracted from Elastosil® P7670.

The relative integral of the D-unit's proton (δ = 0.08-0.06 ppm), calculated by using the proton of the terminated methyl group (δ = 0.046 ppm) as reference, was about 18.82. The number of D-units (n ≈ 9) and the molecular weight of the silicone oil (M_n ≈ 700 g/mol) could be therefore calculated. These

results were in close agreement with the molecular weight of a commercially available silicone oil AK35 from Wacker Chemie AG.

As mentioned above, silica is a further ingredient that finds use in commercial silicone elastomers. In contrast to silicone oil, silica is known for its ability to reinforce the siloxane matrix and to enhance the mechanical properties of a silicone elastomer.[99-101] Due to the opaque color of Elastosil, the general assumption can be made that silica is also involved therein. For preparation of the benchmark formulation, commercially available silica N20, which is a highly hydrophilic silica provided by Wacker Chemie AG, was used.

Based on the results so far, the chemical structures of the ingredients contained in Elastosil's parts A and B have been successfully identified: clear evidence was provided by NMR that part A contained vinyl-PDMS pre-polymer (functionality f = 2) while part B contained both vinyl-PDMS pre-polymer (f = 2) and SiH-PDMS cross-linker. Subsequent FT-IR measurements confirmed the existence of vinyl groups in part A, and the existence of vinyl and Si-H groups in part B. From ICP-OES, it was evident that the platinum catalyst was only present in part A. The concentration of the platinum catalyst was estimated. The chemical structure of the platinum catalyst was further identified as the Karstedt's catalyst by MALDI-TOF. Also MALDI-TOF confirmed the repeat unit of the PDMS involved in A and B. Furthermore, by using extraction measurements it was found that Elastosil involves silicone oil (> 24 wt.-%).

These information together established a good basis for the preparation of the benchmark material. However, the following questions remained still unclarified: what are the molecular weights of vinyl-PDMS in A and B respectively? What is the functionality (f) of the Si-H in cross-linker? To shed light on these issues, several investigations were performed and the respective results are outlined in the following Section 3.1.2.

3.1.2 Molecular weight calculations

Molecular weight of the pre-polymer

Several attempts were made to estimate the molecular weights of vinyl-PDMS in parts A and B. As a common method to determine molecular weights, GPC failed in this case to provide reliable information. This is related to the fact that the sensitivity of GPC measurements is strongly dependent on the chain structure,[215] molecular weight and viscosity of the polymer[216] and also on interactions between functional groups and polymer chains.[217]

MALDI-TOF can also, in principle, give information about the molecular weight of a polymer. However, as mentioned above, this method may be falsified easily, especially when quantifying large

polymer molecules that have high molecular weights and a broad range of molecular weight distributions.

A further possibility is the use of NMR spectra. ^{1}H-NMR is known as a good method for estimating the molecular weight of polymers. By determining the integrals, useful information can be acquired, including the number of repeat units.

Recalling Figure 24a and Figure 24b, the integrals of the D-unit can be calculated by using the integral of H_{vinyl} as reference. By multiplying this value by 2 (f = 2) and dividing it by 6 thereafter (one D-unit has six protons), the number of D-units ($n \approx$ 790) can be estimated. By substituting this value with the number of D-units in silicone oil ($n \approx$ 10, see Figure 30), the number of D-units in vinyl-PDMS can be estimated ($n \approx$ 780). The molecular weight of the vinyl-PDMS was deduced, which was ca. 60,000 g/mol. In Table 1 the values of the integrals of the D-unit and vinyl groups are summarized together with the chemical shifts derived from the ^{1}H-, ^{13}C- and ^{29}Si-NMR spectra. The approximate molecular weight of vinyl-PDMS, i.e. ca. 60,000 g/mol, corresponded roughly to that of commercially available vinyl-PDMS DMS-V41 ($M_n \approx$ 62,700 g/mol) from Gelest Inc.

Table 1. List of the chemical shifts of the ^{1}H-NMR spectra of part A of Elastosil® P7670, the corresponding assignments and the relative integral of the protons.

δ_H [ppm]	Relative integral in ^{1}H-NMR	Assignment
0.32 … -0.20	2371	–OSi(CH$_3$)$_2$-
6.3 … 5.6	3.2	Si-CH=CH$_2$

Molecular weight of the cross-linker

Similarly, it was possible to calculate the molecular weight of vinyl-PDMS in part B (Figure 24b), as about 50,000 g/mol. It is worth noting that in this case the D-unit of the SiH-PDMS cross-linker could not be distinguished from those of the vinyl-PDMS pre-polymer. Thus this molecular weight is only an approximate value. Nevertheless, this result allows for proposing DMS-V33 ($M_n \approx$ 43,000 g/mol) as a possible candidate for use in part B.

Table 2. List of the chemical shifts deduced from ^{1}H-NMR spectra of part B of Elastosil$^\circledR$ P7670, the corresponding assignments and the relative integral of the protons.

δ_H [ppm]	Relative integral in ^{1}H-NMR	Assignment
0.32 … -0.20	2037	-OSi(CH$_3$)$_2$-
6.3 … 5.6	3.0	Si-CH=CH$_2$
4.8 … 4.6	1.9	Si-H
4.72 … 4.69	1.1	SiH(CH$_3$)$_2$O-
4.69 … 4.67	0.8	-O-SiH(CH$_3$)-O-

Functionality of the cross-linker

In order to choose a proper candidate for the SiH-PDMS cross-linker in part B, the functionality of the Si-H group needed to be estimated. This was accomplished by comparing the integral areas of two different kinds of Si-H groups, i.e. terminated Si-H (SiH(CH$_3$)$_2$O-) and Si-H located on the siloxane backbone (-O-SiH(CH$_3$)-). As illustrated in Table 2, the latter has a proton fraction of 0.77, while the former has a fraction of 1 proton, and the total proton fraction for H$_{SiH}$ is 3.

HMS-151 produced from Gelest Inc. meets this condition. However, HMS-151 has only Si-H groups in the main chain. An alternative was C200 from Evonik AG. C200 has the same chemical structure as found in Elastosil, albeit much higher functionality (ca. 14-15).

3.1.3 Basic formulation

Structural characterization outlined in Section 3.1.1 allowed for finding the chemical structure of the compositions involved in parts A and B, and based on the molecular weight calculation in Section 3.1.2 possible candidates were proposed accordingly. These candidates were then employed to conceive a first formulation, referred to as the basic formulation. The chemical composition of this basic formulation is outlined in Table 3, in comparison to those of Elastosil. Similar to Elastosil, the basic formulation was also arranged into two separate parts, i.e. A and B. DMS-V41 or DMS-V33 (Gelest Inc.) were proposed as candidates for vinyl-PDMS, while the SiH-PDMS cross-linker may be replaced by HMS-151 (Gelest Inc.) or C200 (Evonik). SIP 6830.3 from Gelest Inc., which is a commercially available Karstedt's catalyst was selected as the catalyst. AK35 provided from Wacker Chemie AG was chosen as silicone oil. N20 also from Wacker Chemie AG was selected as silica.

This choice was based on its favorable hydrophilic property and thus stronger reinforcing effect compared to hydrophobic silica. Besides, based on the results so far, the concentration of platinum in the commercial material (part A) was quantified as ca. 9 ppm; the content of silicone oil was known to be > 24 wt.-%.

Table 3. Estimated chemical components of parts A and B of Elastosil® P7670, their chemical structures, molecular weights (M_n) and functionalities (f), and the corresponding candidate materials suggested for the preparation of a basic formulation.

#	Component	Chemical structure	M_n [g/mol]	f [a)][-]	Candidate [b)]
A	Vinyl-PDMS	$H_2C=C(H)-Si(CH_3)_2-[O-Si(CH_3)_2]_n-C(H)=CH_2$	ca. 60,000	2	V33 or V41
	Karstedt's catalyst		-	-	SIP 6830.3
	Silicone oil	$H_3C-Si(CH_3)_2-[O-Si(CH_3)_2]_n-O-Si(CH_3)_2-CH_3$	ca. 700	-	AK35
	Silica	SiO_2	-	-	N20
B	Vinyl-PDMS	$H_2C=C(H)-Si(CH_3)_2-[O-Si(CH_3)_2]_n-C(H)=CH_2$	ca. 50,000	2	V33, V41
	Cross-linker	$H-Si(CH_3)_2-[O-Si(CH_3)(H)]_m[O-Si(CH_3)_2]_n-Si(CH_3)_2-H$		ca. 3	HMS-151, C200
	Silicone oil	$H_3C-Si(CH_3)_2-[O-Si(CH_3)_2]_n-O-Si(CH_3)_2-CH_3$	ca. 700		AK35
	Silica	SiO_2	-	-	N20

a) Functionality of vinyl or Si-H groups of the chemical components in Elastosil® P7670.
b) Proposed candidates (commercially available products) for preparation of the basic formulation.

This basic formulation laid the foundation for the further development of the *benchmark formulation*. Clearly, in order to achieve the final benchmark formulation, several factors needed to be additionally studied, for instance, whether V33 or V41 should be used, or whether HMS-151 or C200 would be more appropriate. The suitable stoichiometric imbalance, as defined as the molar ratio of Si-H groups to vinyl groups, also needed to be discussed. Finally, the exact contents of silicone oil and silica, which would surely play an important role in the mechanical properties, also remained unclear. These four formulation parameters, namely stoichiometric imbalance, the molecular weight of vinyl-PDMS, the cross-linker and filler content were therefore defined as *influencing formulation parameters*. In the following Section 3.2, four series of formulations, i.e. I, II, III and IV, will be outlined. For these studies, varying ranges of the influencing factors needed to be defined previously.

In Table 4 a brief overview of these influencing formulation parameters is presented, together with the varying ranges that need to be discussed. For instance, stoichiometric imbalance (r) ranged from 1 to 3. The stoichiometric imbalance of addition-curing silicone, as introduced earlier (Section 2.2.2), needs to be generally higher than 1 and lower than 3.[91-93] The value $r = 3$ was chosen on purpose to make sure that excessive Si-H would remain in the network, so that possible phenomena as a result of these excessive Si-H groups could be further investigated.

Table 4. Defined influencing formulation parameters and varying ranges based on the basic formulation to further investigate possible influences of these formulation parameters and to prepare the benchmark formulation.

#	Influencing formulation parameter	Varying range
I	Stoichiometric imbalance (r)	1, 2 and 3
II	Molecular weight of vinyl-PDMS (M_n)	V33, V41
III	Cross-linker	HMS15, C200
IV	Filler content	AK35 (> 24wt.-%), N20

3.2   Preparation of benchmark formulation

In this section, it will be described how a benchmark formulation was finally developed. This required firstly a thorough investigation on the influences of different formulation parameters. The four influencing formulation parameters (Table 4), namely stoichiometric imbalance r, molecular weight

M_n, the cross-linker and filler content, are discussed individually in the following subsections. By varying only one parameter each time, while keeping other parameters constant, it is specified how these parameters contribute to cross-linking density and mechanical tensile properties. Finally, a formulation resulting in the most comparable properties to those of Elastosil has been derived.

3.2.1 Influences of formulation parameters

Based on the afore-outlined Table 3 and Table 4, the exact chemical formulations employed for the preparation of the four silicone formulations, i.e. I, II, III and IV, are listed in Table 5.

To evaluate the state of the cross-linked network, one of the most important intrinsic parameters is the cross-linking density. In case of a hydrosilylation reaction, the cross-links refer to ($-Si-CH_2-CH_2-Si-$) bonds formed between vinyl and Si-H groups. To determine cross-linking density, swelling measurements were employed. These were assisted by DSC measurements and ATR-FT-IR, in order to estimate the crystallization behavior of the cured network and to verify the chemical structure before and after cross-linking. Then, tensile tests were performed on all prepared networks to characterize their mechanical behaviors.

Table 5. Formulation parameters used for the preparation of silicone formulations with varied stoichiometric imbalance (r), molecular weight (M_n), cross-linker with functionality f and filler content.

#	Part A	Part B	r [-]	M_n [g/mol]	f [-]	Filler content [wt.-%]
I-1	DMS-V41, SIP6830.3	DMS-V33, HMS-151	1	51,000	4	-
I-2			2			
I-3			3			
II-1	DMS-V33, SIP6830.3	DMS-V33, HMS-151	2	43,000	4	-
II-2	DMS-V41, SIP6830.3	DMS-V33, HMS-151		51,000		
II-3	DMS-V41, SIP6830.3	DMS-V41, HMS-151		63,000		
III-1	DMS-V41, SIP6830.3	DMS-V41, HMS-151	1	63,000	4	-
III-2	DMS-V41, SIP6830.3	DMS-V41, C200			14-15	
IV-1	DMS-V33, SIP6830.3	DMS-V33, HMS-151	1.7	43,000	4	-
IV-2	DMS-V33, SIP6830.3, AK35	DMS-V33, HMS-151, AK35				24 wt.-% AK35
IV-3	DMS-V33, SIP6830.3, AK35, N20	DMS-V33, HMS-151, AK35, N20				24 wt.-% AK35, 4 wt.-% N20
IV-4	DMS-V33, SIP6830.3, AK35, N20	DMS-V33, HMS-151, AK35, N20				55 wt.-% AK35, 4.5 wt.-% N20

Influence of stoichiometric imbalance

Results from the swelling measurements shown in Figure 31 provide a clear indication that the cross-linking reaction is not completely accomplished at $r = 1$ (formulation I-1, Table 5). This is not surprising, since in a real network consisting of long polymer chains, the extent of a cross-linking reaction can be affected by chain mobility and by steric hindrance. In order to accomplish the cross-linking, a higher r value, such as $r = 2$ (formulation I-2), is needed. As depicted in Figure 31, an increase in the r value from 1 to 2 resulted in a significant increase in cross-linking density as well as in a significant decrease in swelling. It should be pointed out that the silicones studied herein were prepared in an inert atmosphere (N_2-filled glove box) and tested shortly after preparation. Since the hydrolysis reaction of the remaining Si-H groups in air and the following polycondensation reaction are much slower processes,[95, 218] the obtained results can be considered to reflect mainly the cross-linking accomplished by a hydrosilylation reaction.
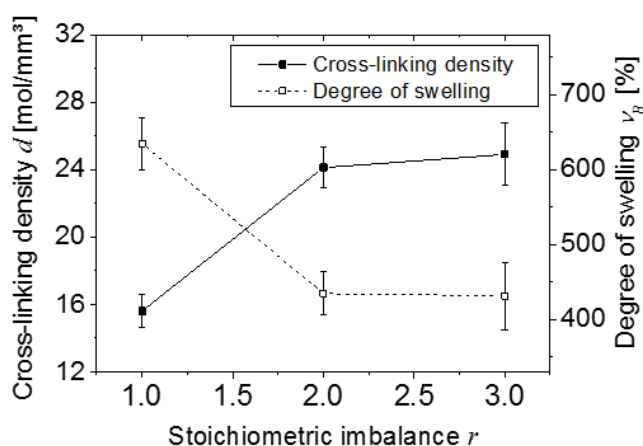
Figure 31. Dependence of cross-linking density d and degree of swelling v_B on stoichiometric imbalance r.

As can also be seen in Figure 31, a further increase in r up to 3 (formulation I-3) led only to a slight additional increase in cross-linking density. This was reached at the expense of a significant excess of hydrosilane groups, whereas at $r = 2$ a small amount of excessive hydrosilane groups can be seen, as revealed by the infrared spectra in Figure 32. Therefore, in order to ensure that samples were cross-linked to a maximum extent via hydrosilylation, and that their properties did not alter over time, all samples have to be prepared with $r = 2$ or even slightly lower under glove box conditions. For the preparation of series IV, a value of 1.7 was used.

The results presented herein on the effects of different r values are in good agreement with findings by other authors. Esteves et al.[95] have carried out an investigation on the effects of stoichiometric

imbalance using r = 1, 1.7 and 2.7. They found that by using r = 1 the formed network consisted of a large percentage of extractable material, while at r = 2.7 a significant excess of Si-H groups was determined. In the work by Larsen et al.[92] and Skov et al.[219], the equilibrium modulus of silicone networks was presented as a function of stoichiometric imbalance, and it was found that the maximum was reached by using an r value > 1.5.
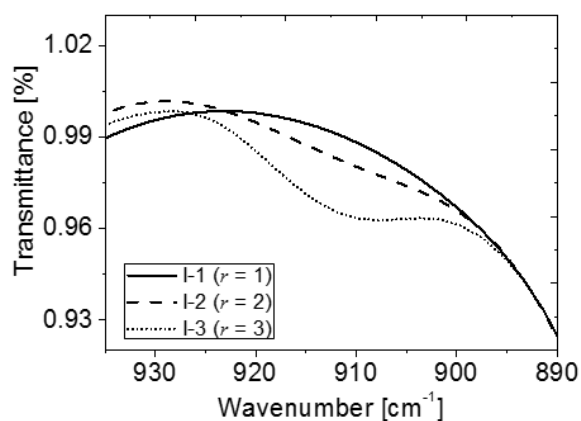
Figure 32. Bending band of hydrosilane group at 916 cm^{-1} in the ATR-FT-IR spectra of silicone formulations (series I) prepared with different stoichiometric imbalances r. For r = 2 and 3 an excess of Si-H groups after preparation was observed.

DSC measurements support the observation that a higher r value resulted in a more cross-linked network. By using DSC, the degree of crystallization (*cryst*) of the silicone networks were determined. These results are reported in Table 6, together with the estimated cross-linking densities and mechanical tensile properties of the investigated silicone formulations. It is seen that with a higher r value a more cross-linked network formed and the network showed a lower degree of crystallization.

Table 6. Estimated cross-linking density (d), degree of crystallization ($cryst$), tensile stress (σ_B), tensile strain (S_B), and elastic modulus (Y) of silicone networks prepared with different formulation parameters.

#	d [mol/mm³]	$cryst$ [%]	σ_B [MPa]	S_B [%]	Y [MPa]
I-1	15.6	69.3	0.15	201.3	0.16
I-2	24.1	64.9	0.25	86.5	0.61
I-3	24.9	62.6	0.22	61.5	0.83
II-1	27.6	63.7	0.29	67.2	0.67
II-2	24.1	64.9	0.25	86.5	0.61
II-3	19.2	65.7	0.23	105.7	0.47
III-1	15.2	70.1	0.18	126.4	0.25
III-2	14.8	73.8	0.12	123.3	0.14
IV-1	27.4	66.9	0.29	66.2	0.59
IV-2	26.9	75.5	0.23	124.6	0.18
IV-3	43.6	70.7	0.61	288.0	0.21
IV-4	52.9	80.5	0.66	344.4	0.13

Molecular weight influence

Effects of molecular weights of the different vinyl-PDMS pre-polymers were investigated on formulations II-1 (M_n = ca. 43,000 g/mol), II-2 (M_n = ca. 51,000 g/mol) and II-3 (M_n = ca. 63,000 g/mol). The results obtained from swelling measurements, DSC measurements and mechanical tensile testing are summarized in Table 6.

Evidently, the cross-linking density of the formed network strongly depended on the molecular weight of the vinyl-PDMS used. With increasing molecular weight, decreased cross-linking density was obtained, combined with a higher degree of crystallization and a lower elastic modulus. This is because by using a pre-polymer with higher molecular weight, long molecule segments are introduced between the individual cross-links, whereby resulting in a looser network.

Influence of the cross-linker

As also summarized in Table 6, based on the investigations on formulations III-1 and III-2, it was found that the use of a cross-linker with higher functionality formed a network with lower cross-linking density, a higher degree of crystallization and a lower elastic modulus. While this is in contrast to the general observation that higher f values of a cross-linker increase the netpoint density,[220] the results herein are consistent with a study by Braun and Mark,[98] who also reported that in the formation of PDMS-gels by using cross-linkers with increased functionality (f = 3, 4, 40-50) the total conversion decreased, because the degree of entanglements increases as functionality increases.

The finding of insufficient cross-linking by using a cross-linker with higher functionality was confirmed by DSC measurements of the curing behavior (Figure 33). The formulation III-2 obviously cured slower than the III-1 system, and its cross-linking temperature was shifted to higher temperature. This decelerated cross-linking observed with high functionality cross-linkers provided support for steric hindrance and accounted for the resultant insufficient cross-linking and poor mechanical stiffness. Also, the presence of excessive functional groups may increase the risk of further secondary reactions, as mentioned previously. In order to avoid these effects, the HMS-151 cross-linker is used in the benchmark formulation.
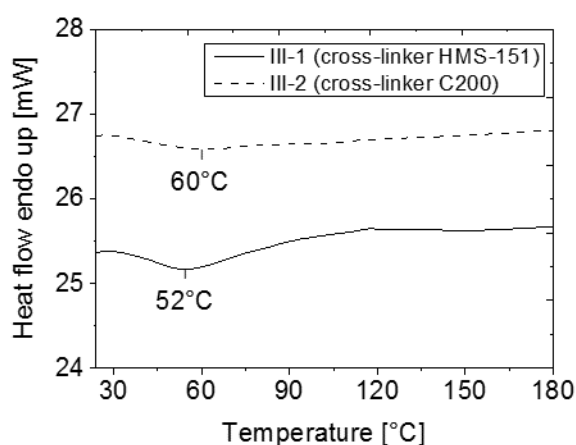
Figure 33. DSC thermograms recorded during cross-linking reaction of silicone formulations (series III) prepared with different cross-linkers. The III-2 prepared with C200 cured slower than III-1.

Influence of the filler

In formulations IV-1 to IV-4, an r value of 1.7 instead of 2 was employed. As outlined previously, this r value was chosen in order to accomplish cross-linking to a maximum extent while avoiding excess Si-H groups. DMS-V33 was used as a pre-polymer because of its relatively low viscosity, which

favored mixing with silica. HMS-151 was used as cross-linker, since a cross-linker with higher functionality impedes cross-linking reaction as shown previously. Formulation IV-1 was prepared without fillers and used as a reference.

As can be seen from the stress-strain curves (Figure 34), silicone oil and silica generated dramatic effects on the mechanical behavior. The addition of 24 wt.-% of silicone oil into unfilled silicone (from IV-1 to IV-2) significantly lowered the elastic modulus but enhanced tensile strain. This occurred in line with a reduced cross-linking density and an increased degree of crystallization (Table 6). Further addition of 4 wt.-% of silica (from IV-2 to IV-3) fed competing effect into the network, leading to a significant enhancement in both tensile strain and tensile strength. The elastic modulus increased, indicating an increased network density caused by silica-polymer interactions. Associated with this increased cross-linking density, the mobility of the polymer chain was negatively affected, thereby leading to a decrease in the degree of crystallization in IV-3 compared to IV-2 (Table 6).
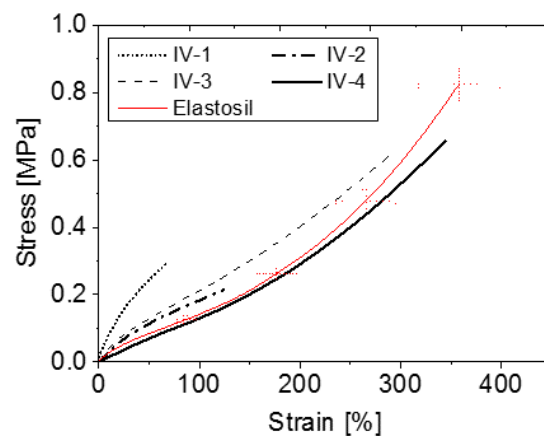
Figure 34. Stress-strain curves of silicone formulations (series IV) prepared with different contents of silicone oil and silica. It is shown that silica and silicone oil resulted in competing effects on the stress-strain behavior. The formulation IV-4 showed a stress-strain behavior comparable to the one of commercial Elastosil.

Accordingly, by varying the amounts of silicone oil and silica, it was possible to tune the mechanical properties quite precisely. With respect to the application of silicone as a dielectric elastomer, large deformability and low elastic modulus are usually the two primary requirements. In order to further improve deformability, an additional increase in the silica content was needed. Concomitantly, to adjust the viscosity to the processing conditions, more silicone oil had to be added as well. In this context, the results of formulations IV-2 and IV-3 are reported only to show the effects of silicone oil and silica. In fact, many more formulations were prepared and characterized. The final formulation IV-4 presented in Table 6 and Figure 34 showed satisfactory mechanical properties in terms of

tensile strain (344%), tensile stress (0.66 MPa) and elastic modulus (0.13 MPa). These values were very comparable to those of Elastosil® P7670, as illustrated in Figure 34.

3.2.2 Benchmark formulation

Chemical composition of benchmark formulation

In view of the above-outlined results, formulation IV-4 was defined as the benchmark formulation. It is renamed here as E2. Table 7 documents the formulation parameters used (can be compared with Table 5). As discussed in the previous section, the choice of V33 as the vinyl-PDMS was based on its molecular weight and viscosity, which favored the subsequent mixing of silica. HMS151 was chosen as the cross-linker because of its Si-H functionality, which was similar to the one in the Elastosil's cross-linker, despite the fact that its chemical structure was slightly different. The stoichiometric imbalance was set to 1.7, at which the cross-linking conversion might reach a relatively high content, while the amount of excessive Si-H groups should not be significant. Next, 55 wt.-% of AK35 and 4.5 wt.-% N20 were added to ensure mechanical tensile properties similar to those of Elastosil.

It is important, however, to point out that this formulation was not the only possibility that had characteristics similar to those of commercial Elastosil. In fact, as demonstrated in the previous section, cross-linking density and mechanical properties can be tuned by varying the different formulation parameters. The systematic investigations of these formulation parameters, as outlined so far, help to establish a deeper understanding of the influences.

Table 7. Formulation parameters used for preparation of benchmark material E2.

Parameter	Value
r [a]	1.7
$[DMS]_A : [DMS]_B : [HMS]_B$ [b]	1 : 0.92 : 1.63
Content of silica (N20)	55 wt.-%
Content of silicone oil (AK35)	4.5 wt.-%
Concentration of platinum	9 ppm

[a] Molar ratio of Si-H groups to vinyl groups.
[b] Molar ratios of DMS-V33 and HMS-151 in part A and B. DMS is shortened from DMS-V33, while HMS is shortened from HMS-151.

Properties of benchmark material

As introduced in Chapter 2, there are three most important parameters that directly determine the performance of an actuator made of dielectric elastomer. These are the elastic modulus Y, relative permittivity ε_r, and breakdown strength E_B. A comparison of these properties, between the developed benchmark material E2 and Elastosil® P7670, was also carried out. Results are summarized in Table 8, together with their cross-linking densities and degrees of crystallization.

Table 8. Cross-linking density (d), degree of crystallization ($cryst$), elastic modulus (Y), relative permittivity (ε_r) and breakdown strength (E_B) of prepared benchmark material E2 in comparison with Elastosil® P7670.

#	d [mol/mm³]	$cryst$ [%]	Y [MPa]	ε_r [a] [-]	E_B [b] [V/µm]
Benchmark material E2	52.91 ± 2.89	80.53 ± 3.77	0.13 ± 0.02	2.94 ± 0.09	34.78 ± 3.89
Elastosil® P7670	58.66 ± 4.47	74.33 ± 2.82	0.15 ± 0.01	2.86 ± 0.02	40.71 ± 3.65

[a] Relative permittivity values derived from frequency spectra at 10 Hz.
[b] Breakdown tests performed on thin films with ca. 150 µm thickness.

Differences in these properties between the benchmark materials and commercial Elastosil were only minor. It is evident that the benchmark material exhibited only a slightly lower cross-linking density, compared to Elastosil, whilst the degree of crystallization was a little higher. The benchmark material showed a lower elastic modulus, as can also be seen in the stress-strain curves (Figure 34). The relative permittivity of the benchmark material was a little higher, while its breakdown strength was slightly lower.

3.3   Materials for further investigations

For subsequent investigations, a series of materials was designed based on the benchmark material E2. The stoichiometric imbalance r was varied: while E2 was prepared by using $r = 1.7$, formulations E1 and E3 were prepared by using $r = 1.3$ and 3 respectively. The exact ratios yielding these r values are given in Table 9.

Table 9. Molar ratios of DMS-V33 and HMS-151 in part A and B used for the preparation of E1, E2 and E3 with different stoichiometric imbalances r.

#	r	$[DMS]_A : [DMS]_B : [HMS]_B$
E1	1.3	1 : 0.94 : 1.26
E2	1.7	1 : 0.92 : 1.63 [a]
E3	3	1 : 0.87 : 2.80

[a]   See also Table 7.

The main reason, why the stoichiometric imbalance r was chosen as the varying parameter, was based on the hypothesis that some possible property changes induced by mechanical and electromechanical ageing may be related to the chemical identity of the material. According to the literature survey introduced in Chapter 2, the content of excessive Si-H groups and their further reactions may play a role in long-term behaviors upon mechanical and electromechanical ageing.

To study the possible influences of the excessive Si-H groups, three different r values were used. In addition to the r value of 1.7, which has been suggested so far as a possible stoichiometric imbalance of a virtually completed conversion, r values of 1.3 and 3 were additionally proposed for further investigation. The latter one ($r = 3$) was seen to produce a significant amount of excessive Si-H after hydrosilylation reaction (Section 3.2.1). By using $r = 1.3$ it was intended to gain a not fully cross-

linked network. The previously discussed r value of 1 was abandoned because the network after curing was almost still in a liquid form, which made further characterizations very difficult. The influences of those three r values on the properties of the formed network structures as well as on their mechanical and electromechanical ageing behavior will be presented in Chapter 4, 5 and 6, respectively.

3.4   Summary

In summary, the aim of developing the benchmark material was successfully fulfilled. A systematic approach is described. Impressions of correlations between the formulation parameters, the formed network structure and the mechanical tensile properties of the silicone elastomers were achieved.

The developed benchmark material E2 laid the foundation for further studies. Two materials, E1 and E3, were additionally designed. The three silicone formulations, i.e. E1, E2 and E3, differed from each other in terms of various levels of stoichiometric imbalance r used (r = 1.3, 1.7 and 3, respectively). They were employed for subsequent investigations, to compare their long-term behavior and to illustrate possible relations between property changes and network structures.

4 Structure-Property Relationships

The aim of this chapter is to establish a fundamental understanding about interdependencies between a silicone's network structure and its mechanical and electrical properties. Silicone materials (E1, E2 and E3), prepared by using varied stoichiometric imbalances (r = 1.3, 1.7 and 3, Table 9) were employed. They were processed into thin films and thoroughly characterized in terms of their network structures (cross-linking density, degree of crystallization), mechanical properties (elastic modulus, hysteresis) and electrical properties (relative permittivity, breakdown strength). The obtained results, reported in Section 4.1 to 4.4, helped to derive the fundamental relationships between the network structures, mechanical and electrical properties of DE materials.

4.1 Influence of stoichiometric imbalance on network structure

As visualized in Figure 35, the increase in the r value from 1.3 to 1.7 caused a significant increase in cross-linking density, as also indicated by a decrease in the swelling of the formed network. These results confirmed that the cross-linking reaction was incomplete at r = 1.3, however, went however to completion starting at r = 1.7. These results aligned well with the results shown previously in Section 3.2.1, in that from r = 1 to r = 2 a significant increase in cross-linking took place.
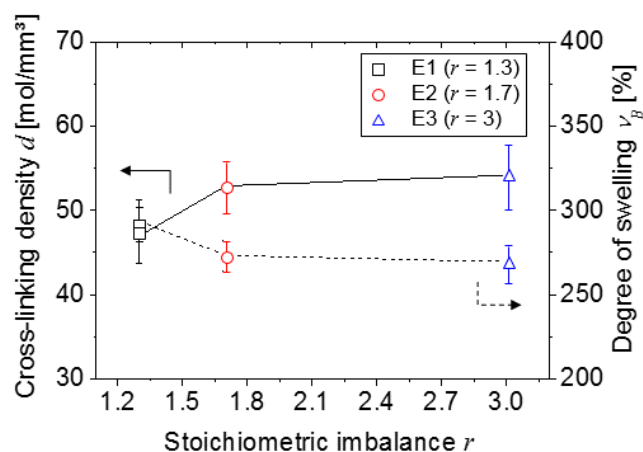
Figure 35. Dependence of cross-linking density d and degree of swelling v_B on the stoichiometric imbalance r of silicone networks E1, E2 and E3 prepared using different stoichiometric imbalances.

The influence of r on the network structure of cross-linked elastomers was further verified by their crystallization behavior observed in DSC measurements (Figure 36). In all spectra (Figure 36a), the crystallization peak T_c was easily detected during the cooling scan around -66°C. The position of the crystallization peak moved to a lower temperature in line with an increasing r value. The melting temperature T_m of all networks was also clearly detected upon reheating around -40°C, and its position also moved slightly to a lower temperature following an increase in r (Figure 36b). This effect was also quantified by the calculated degree of crystallization ($cryst$, Table 10), which shows that higher r values resulted in lower degrees of crystallization. As discussed previously in Section 3.2.1, crystallization and melting behavior have been acknowledged as influenceable by varying the network structure. A more densely cross-linked network reduces chain mobility, hinders the crystal growth process and thereby lowers the tendency towards crystallization. Consequently, crystallization starts later and fewer crystallites are formed. The smaller crystallites, together with the smaller content of crystallites, lower both the melting point and the melting heat.
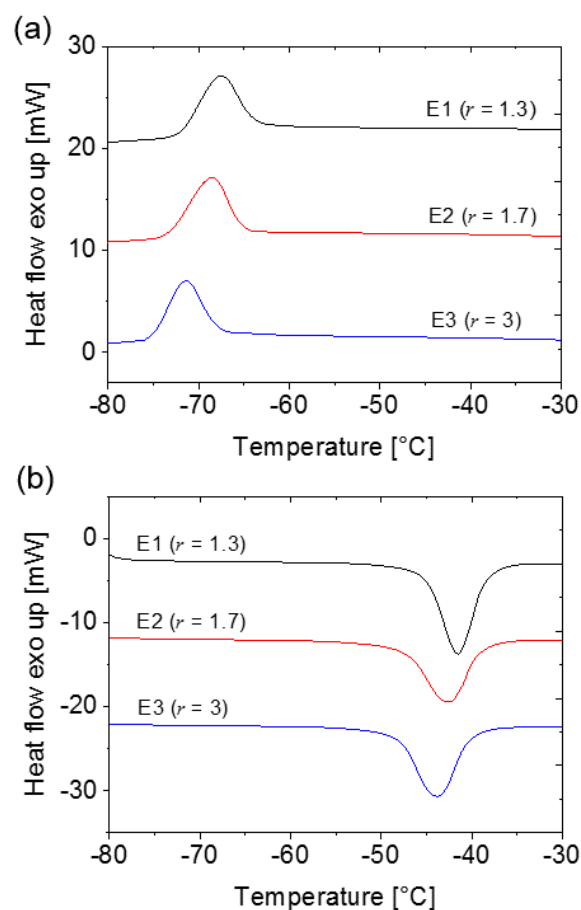
Figure 36. DSC (a) cooling and the subsequent (b) heating curves of silicone networks E1, E2, and E3 prepared using different stoichiometric imbalances. The curves are offset for clarity.

Table 10. Cross-linking density (d), degree of crystallization ($cryst$), elastic modulus (Y), relative permittivity (ε_r) and breakdown strength (E_B) of E1, E2 and E3 in relation to the stoichiometric imbalance.

#	r	d [mol/mm³]	$cryst$ [%]	Y [MPa]	ε_r [-]	E_B [V/µm]
E1	1.3	46.99 ± 3.29	87.06 ± 2.50	0.10 ± 0.01	3.19 ± 0.08	30.10 ± 2.00
E2	1.7	52.91 ± 2.89	80.53 ± 3.77	0.13 ± 0.02	2.94 ± 0.09	34.78 ± 3.89
E3	3	56.88 ± 3.18	80.91 ± 3.42	0.15 ± 0.01	2.89 ± 0.11	35.37 ± 3.41

4.2   Influence of stoichiometric imbalance on elastic modulus

When the stoichiometric imbalance increased from 1.3 to 3, the elastic modulus was enhanced by nearly 50% (Figure 37, Table 10). These results are consistent with the previous results discussed in Section 3.2.1 and in Table 6 (from I-1 to I-3).
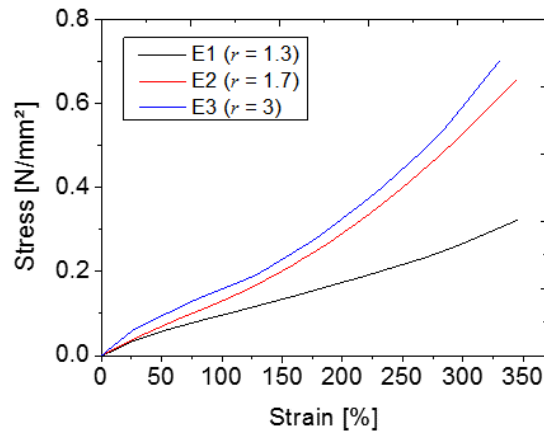
Figure 37. Stress-strain curves of silicone networks E1, E2 and E3 prepared using different stoichiometric imbalances.

Considering the diagram of stoichiometric imbalance vs. elastic modulus (Figure 38), the gain in the elastic modulus was much more pronounced in the initial part (increasing r from 1.3 to 1.7) than in the subsequent part of the diagram (increasing r from 1.7 to 3). It is also interesting to note here that the change in elastic modulus showed the same trend as the change in cross-linking density with regard to stoichiometric imbalance.

The observed correlation between cross-linking density d and elastic modulus Y (Figure 38) can be explained according to the rubber elasticity theory,[112] where a polymer chain in a cross-linked network is considered as an elastic spring. As the strain increases, these cross-linking netpoints, as well as the connected polymer chains, deform in the straining direction. Elasticity is derived from the ability of long polymer chains to reconfigure themselves, while the cross-linking netpoints ensure that the elastomer will return to its configuration once the stress has been removed. An increase in the density of cross-linking netpoints has the effect of adding more elastic springs into the network, thus resulting in a larger external force needed to deform the structure.

Another important aspect of mechanical properties describing the viscous characteristics of an elastomer is the mechanical hysteresis behavior. The respective results of E1, E2 and E3 are presented in Appendix 3.
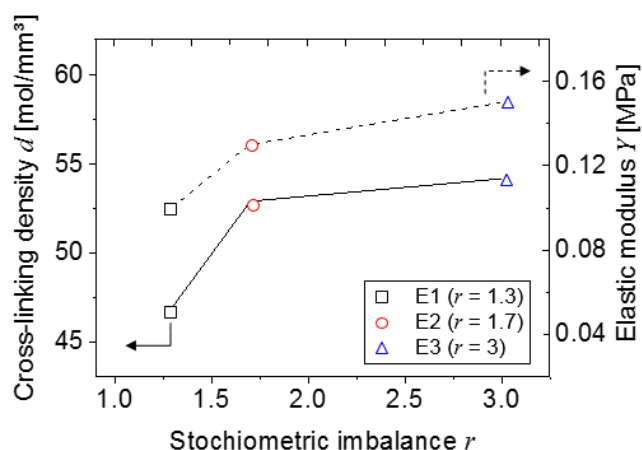
Figure 38. Dependency of cross-linking density d and elastic modulus Y on the stoichiometric imbalance r of silicone networks E1, E2 and E3.

4.3   Influence of stoichiometric imbalance on relative permittivity

Figure 39 shows the plot of relative permittivity vs. frequency for E1, E2 and E3. The plateau level of the relative permittivity curve shows the relative permittivity of the material, while the slight increase at low frequencies is presumable a result of the low frequency dispersion at the material-electrode interface.[221]

A comparison between the three materials showed that the network formed with the lowest stoichiometric imbalance had the highest relative permittivity. An increase in the r values from 1.3 to 3 led to about a 9% decline in relative permittivity (from 3.2 to 2.9). The majority of this drop occurred in the range from 1.3 to 1.7. Although differences in the relative permittivity of the samples were rather low, these deviations were probably due to alterations in the mobility of the dipoles.[133, 222] As discussed previously, high stoichiometric imbalance was correlated with higher cross-linking density and therefore a more restrained molecular structure, as reflected by the lower degree of crystallization (Table 10). This therefore impeded the reorientation of the dipoles and resulted in lower permittivity. For a better illustration, this inverse relationship between cross-linking density and relative permittivity is demonstrated in Figure 40.
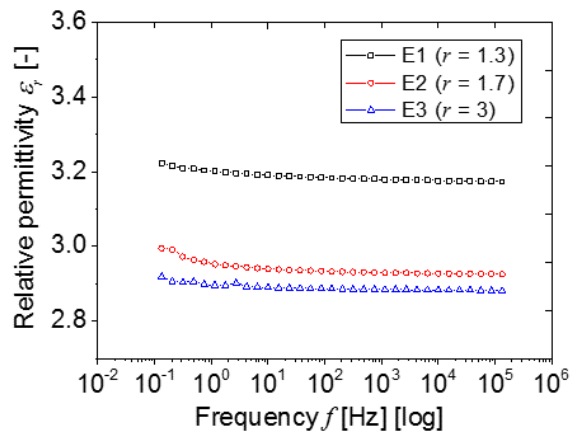
Figure 39. Dependency of relative permittivity on the frequency of silicone networks E1, E2 and E3 prepared using different stoichiometric imbalances.
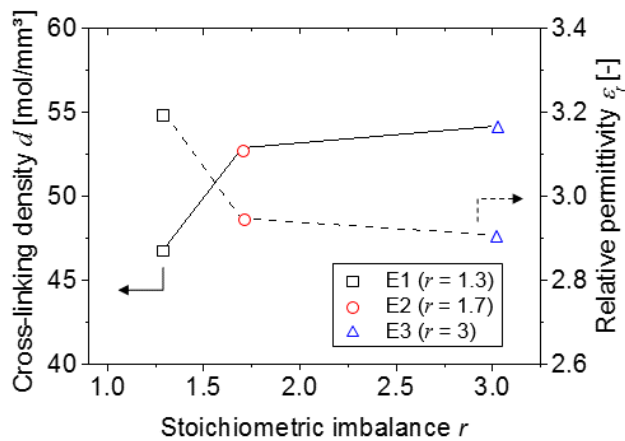
Figure 40. Dependency of cross-linking density d and relative permittivity ε_r on the stoichiometric imbalance r of silicone networks E1, E2 and E3.

It is also important to note that the permittivity value presented in Figure 39 and Figure 40 refers to the relative permittivity ε_r, which is a complex value consisting both a real part ε'_r and an imaginary part ε''_r (Section 2.3.2.1). The real part is related to stored energy within the medium, whereas the imaginary part corresponds to the dissipation (or loss) of energy within the medium. The ratio of ε''_r over ε'_r, defined as the loss factor $tan\delta$, is a further essential parameter evaluating the dielectric property of the medium.

As shown above, a silicone network prepared with higher stoichiometric imbalance exhibited lower relative permittivity. In line with this finding, it is worth noting that the imaginary part ε''_r and the loss factor $tan\delta$ of the material E3 were also the lowest among the three materials (Figure 41b and Figure

41c). It is also evident that the spectra of the imaginary part ε''_r and $tan\delta$ displayed a strong frequency dependency. The shape of the frequency spectra of ε''_r and $tan\delta$ may be influenced by cross-linking. Generally, with increased cross-linking, the spectrum shifted towards the lower frequency range, as a result of more restricted segmental motion and longer corresponding relaxation times. Furthermore, by comparing Figure 41a with Figure 39, it can also be seen that the real part determined predominately the relative permittivity of the material, whilst the imaginary part was relatively low. The loss factor $tan\delta$ is far below 1, indicating that the prepared silicone networks can be considered as low-loss dielectric (nearly, though not exactly, lossless).
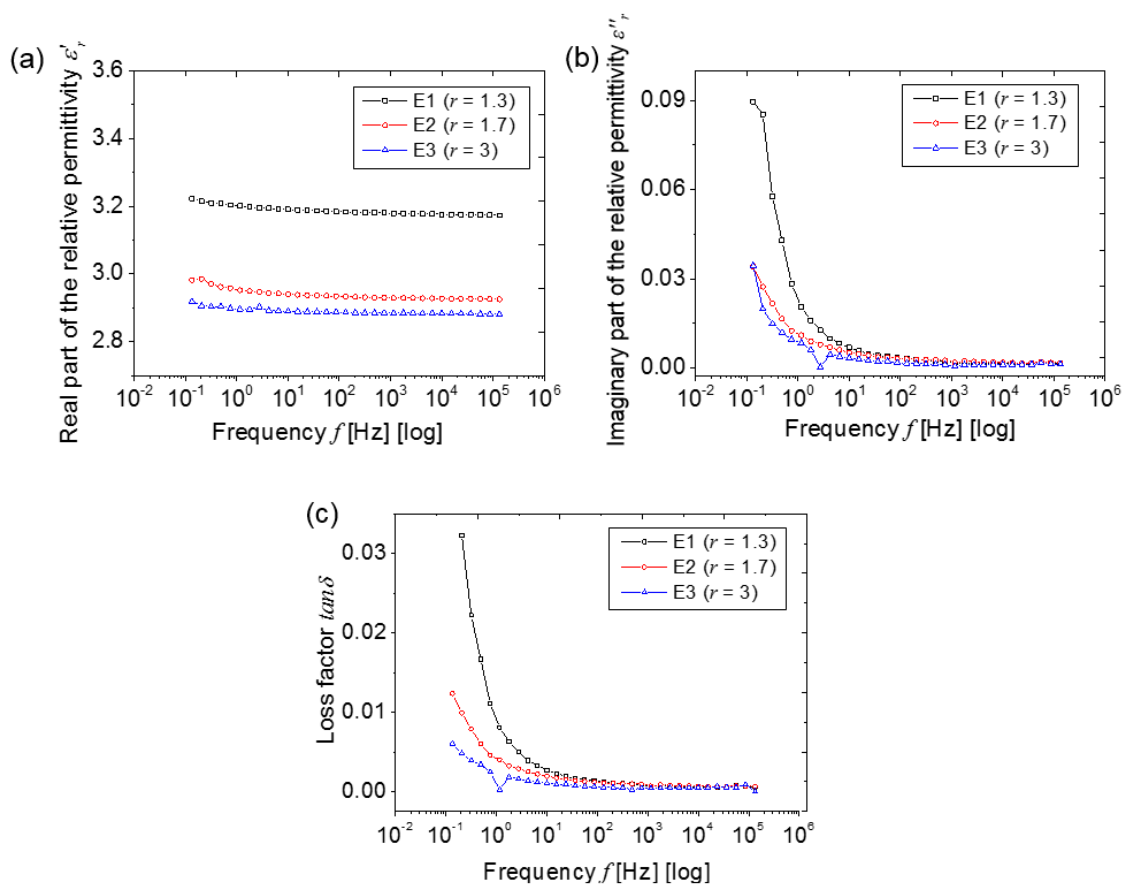
Figure 41. Frequency spectra of (a) the real part of the relative permittivity ε'_r (b) the imaginary part of the relative permittivity ε''_r and (c) loss factor $tan\delta$ of silicone networks E1, E2 and E3 prepared using different stoichiometric imbalances.

4.4 Influence of stoichiometric imbalance on breakdown strength

As introduced in Section 2.2.3.2, the Stark-Garton model (Equation 24) is a well-accepted model to mathematically describe the extrinsic breakdown that is a result of the electromechanical instability (EMI). A correlation between the measured breakdown strength (E_B) and breakdown strength

calculated through the Stark-Garton model (E_{EMI}) can help to identify whether the breakdown is caused primarily through EMI. However, it must be kept in mind that the measured breakdown strength refers to the so-called *engineering* breakdown strength, which is approximated through the measured voltage and the initial thickness of the sample. As a matter of fact, the measured breakdown strength is usually lower than the calculated value, since the *true* thickness of the elastomer film at the moment of breakdown is somehow lower than the initial thickness (Section 10.3.1).

Based on the previous measurements of elastic modulus and relative permittivity, the values of E_{EMI} can be calculated for E1, E2 and E3. Figure 42 compares variations in the calculated E_{EMI} values and the measured breakdown strengths in relation to the *r* value. The calculated E_{EMI} values displayed nearly the same trend as the measured breakdown ones, which indicated that the electromechanical instability (EMI) mechanism was well applicable for the prepared silicone films. The observed increase in breakdown strength, in line with increasing stoichiometric imbalance, also agreed well with the experimental results reported by Kollosche and Kofod.[223]
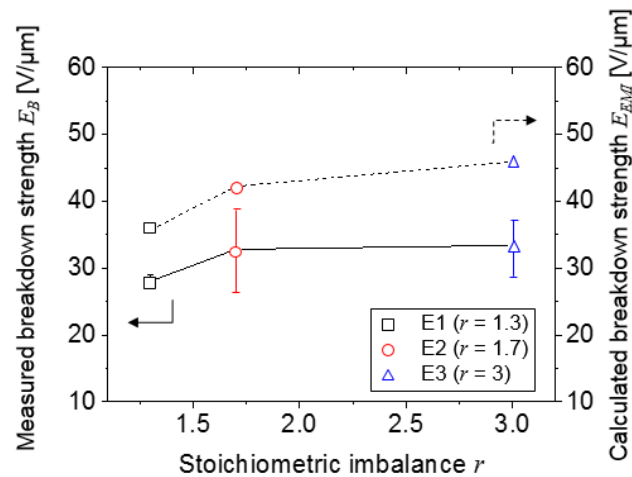
Figure 42. Comparison between calculated breakdown strength E_{EMI} and measured breakdown strength E_B of silicone networks E1, E2 and E3 in relation to the stoichiometric imbalances.

4.5 Summary

Fundamental relationships between network structure and mechanical and electrical properties of silicone DE were successfully established. Figure 43 illustrates a brief overview of the proposed relationships: higher stoichiometric imbalance formed network with higher cross-linking density and lower chain mobility. The increased cross-linking density resulted in an increased elastic modulus. Meanwhile, the decreased chain mobility was responsible for a more restricted dipole-motion under

electric field, thereby explaining the lowered elastomer relative permittivity. The increased elastic modulus and the decreased relative permittivity together led to a heightened breakdown strength under electromechanical instability (EMI).
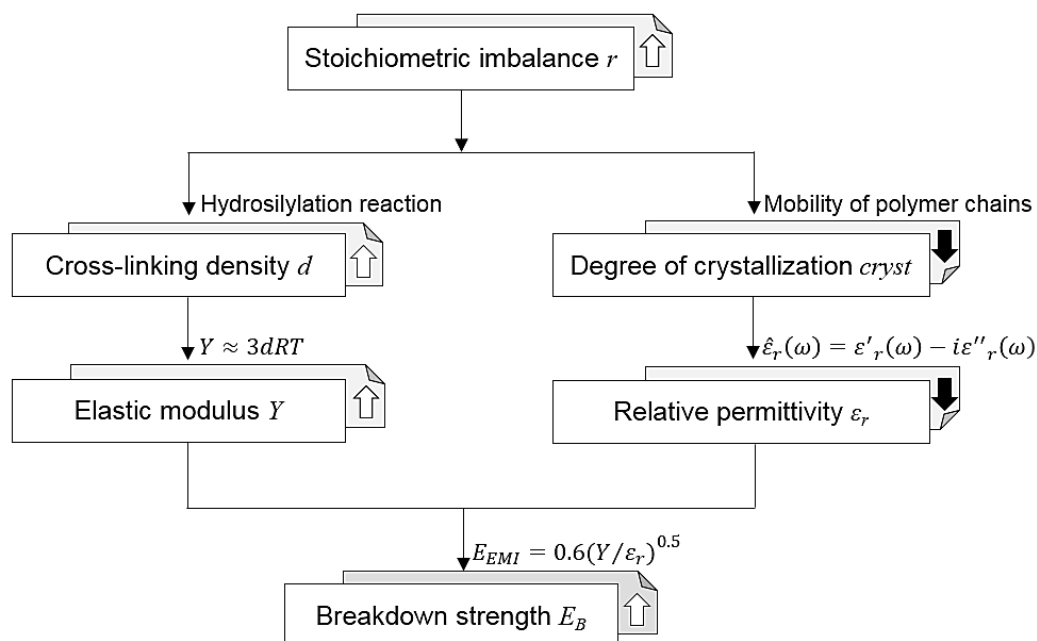
Figure 43. Proposed structure-property relationships between network structure, mechanical and electrical properties of silicone materials prepared with varied stoichiometric imbalance.

Furthermore, by comparing the mechanical and electrical properties of E1, E2 and E3, it became also evident that variations in the stoichiometric imbalance had a greater influence on mechanical properties than on electrical properties. By increasing the r value from 1.3 to 3, a rise in the elastic modulus by 50% (from 1.0 to 1.5 MPa) was observed, whereas the relative permittivity only slightly decreased by 9% (from 3.2 to 2.9); the breakdown strength was enhanced by 17% (from 30.1 to 35.4 V/µm). This information is important for tuning the properties of materials according to their applications. For DE actuators, it has been generally acknowledged so far that materials with lower cross-linking density are preferred, since higher relative permittivity and a lower elastic modulus will generate larger actuator deformation under the same electrical voltage. However, this lower cross-linking density also leads to a decreased breakdown strength as well as to a higher dielectric loss, as presented in this chapter.

The correlations obtained here are of fundamental importance for all further investigations on the ageing mechanism of thin silicone films under mechanical and electromechanical ageing conditions.

5   Mechanical Ageing

DE materials in dielectric devices usually undergo cyclic deformations in service. Thus, a sufficient sustainability of the materials is one of the major concerns for the reliability of the device, which has a twofold meaning. Firstly, the materials should not mechanically fail within a prescribed lifetime. Secondly, the properties of the materials should be, ideally, less affected by mechanical loading.

The possible ageing effects due to mechanical loading has its origin in the alterations of chemical structure. Thus, this chapter describes the investigations on the long-term behavior of dielectric elastomers under mechanical cyclic loading, and provides first insights into the correlations between the property changes and structural changes of the material.

Thin silicone films of E1, E2 and E3 were prepared and mechanically cycled until rupture (referred to as *fatigued* specimens) using a displacement-controlled Wöhler approach. Characteristic lifetimes of E1, E2 and E3 were estimated based on a Weibull analysis (Section 5.1). The fatigued specimens were then characterized in order to illustrate the possible effects of mechanical fatigue. Network structure, elastic modulus, relative permittivity and breakdown strength were measured. Results are presented in Section 5.1 to 5.5. Based on these results, correlations between the property changes and structure changes are derived. Possible influences of mechanical fatigue on the performance of an actuator are discussed in Section 5.6. Finally, mechanical ageing of the commercial material Elastosil® P7670 was also investigated. Section 5.7 reveals the comparison of the results between Elastosil and the benchmark material E2.

5.1   Mechanical fatigue behavior

If materials are cyclically loaded far below their mechanical strength for sufficiently long time, they will still rupture in the end. This is also known as fatigue phenomenon (see Section 2.4.1). Fatigue behaviors of E1, E2 and E3 are presented in Figure 44a in form of Wöhler curves, which present linear relationships between the applied strain amplitudes (S_a) and the corresponding cycle numbers to failure (N_f) under a double logarithm. To quantify the lifetime of the material, the characteristic lifetime T was assessed by using Weibull analysis (Figure 44b), where T is defined as the cycle number at a 63.2% failure probability[157, 162] (Section 2.4.1). The obtained lifetime values of E1, E2

and E3 are listed in Table 11, together with the stoichiometric imbalances, cross-linking densities and elastic moduli.
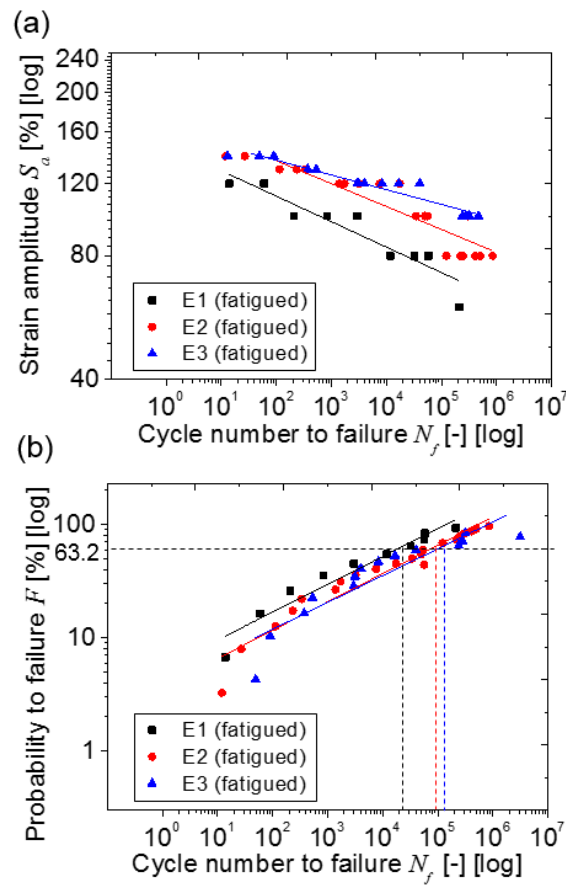
Figure 44. (a) Wöhler curves of thin silicone films E1, E2 and E3. R = 0.2, f = 0.5 Hz (b) Weibull plots to estimate the characteristic lifetime.

It can be seen that with increasing stoichiometric imbalance (from E1 to E3) the Wöhler curve of the material moved to a higher cycle number to failure. Correspondingly, the material showed an improved lifetime, along with an increased cross-linking density and an enhanced elastic modulus. This observed correlation between cross-linking density, elastic modulus and characteristic lifetime supports the inherent strengthening mechanisms.[112, 224, 225] According to rubber elasticity theory,[112] a higher density of cross-linking netpoints generates more support for the rearrangement of molecular chains, in which case the inherent resistance of the material becomes more pronounced.

Table 11. Characteristic lifetimes (T) of thin silicone films E1, E2 and E3 with respect to the stoichiometric imbalance (r), cross-linking density (d) and elastic modulus (Y).

#	r	d [mol/mm³]	Y [MPa]	T [cycle]
E1	1.3	47.0	0.10	15290
E2	1.7	52.9	0.13	81680
E3	3	55.9	0.15	102826

5.2   Effects of mechanical fatigue on network structure

The fatigued specimens were then characterized in terms of cross-linking density (d), variations of which are plotted against the corresponding cycle number to failure (N_f) (Figure 45). Intact specimens without mechanical loading are also shown in Figure 45 as references with a cycle number of 1. Cross-linking density (d) of the intact specimen increased with increasing r value from E1 to E3 (recall Chapter 4, Table 10). It is worth noting that the data presented in Figure 45 are average values from at least four measurements.

The fatigued specimens showed different cross-linking densities at different r values, and also as a function of the strain amplitude S_a. Among fatigued E1 no significant variations of d became visible. This is different with E2: as encircled in Figure 45 by the red ellipse, there the cross-linking density exhibited a maximum in the fatigued samples ruptured at a strain amplitude of 120% (corresponding to $N_f = 10^3$-10^4). With E3 (blue ellipse in Figure 45), a similar maximum was observed at a strain amplitude of 140% (corresponding to $N_f = 10$-100). These significant changes in cross-linking density d appeared to be related to S_a and N_f. Therefore, the position (S_a, N_f) of the maximum in d is defined in this work as the so-called *critical load condition*, where N_f is the maximum cycle number that a specimen can sustain under a given S_a, as retrieved from the Wöhler curve (Figure 44a).
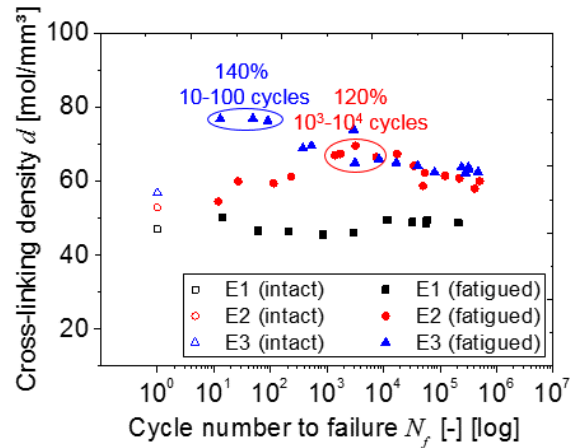
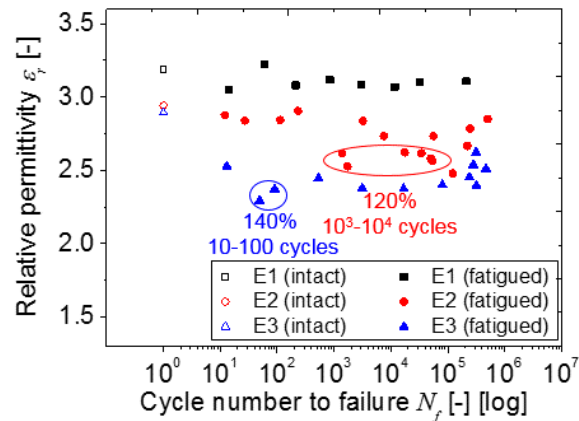**Figure 45.** Cross-linking density of intact and mechanically fatigued thin silicone films E1, E2 and E3. The fatigued specimens were cycled until rupture. The d values shown were average values. Maximums of the d values were observed on specimens fatigued at *critical load conditions* (marked by ellipses).

Considering the differences of the cross-linking density d between intact and fatigued samples, it seems interesting to determine how $d(S_a, N)$ was increasing as a function of the number of load cycles $N < N_f$. Those specimens, which have been mechanically cycled but not ruptured are denoted as *cycled*. They differ from the *intact* specimens, which were not cycled at all, and the *fatigued* specimens, which were cycled until rupture. In Figure 46 the dashed curves show $d(S_a, N)$ for E3 on a logarithmic N-scale. Filled symbols and a solid line display the ultimate cross-linking densities $d(S_a, N_f)$. It is seen that for a given strain amplitude the cross-linking density increased monotonously with increasing load cycles. Moreover, this increase was only significant when the specimens were loaded under a relatively large strain amplitude (e.g. 140%). In case of a moderate strain amplitude (e.g. 100%), no significant changes in cross-linking density occurred during the entire service life.
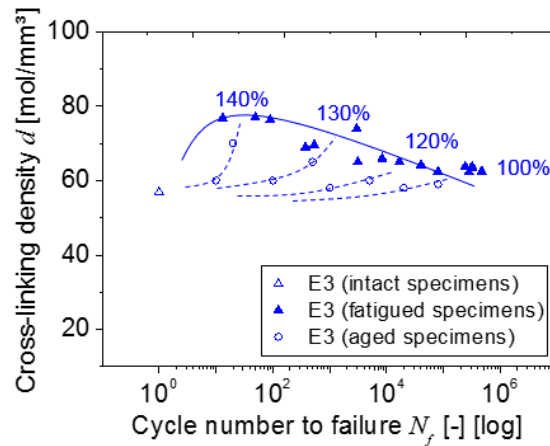
Figure 46. Cross-linking density of intact, cycled and fatigued thin films E3. For a given strain amplitude the cross-linking density increased monotonously with increasing load cycles.

The difference in the *critical load conditions* between the different materials E1, E2 and E3 is clearly related to their different contents of Si-H groups (recall Figure 45).[226] Those unreacted Si-H groups may lead to a mechanically-induced, secondary cross-linking under cyclic loading, thus increasing the cross-linking density. E1 had the smallest excess in hydrosilane and thus showed no significant changes in cross-linking density after mechanical fatigue. E2 and E3 had a moderate, respectively large amounts of excess of hydrosilanes. As a result, a minor, a respectively significant increase in cross-linking density were observed in fatigued E2 and E3 specimens. At the same S_a and N_f (e.g. 140%/10-100 cycles), the higher values of final cross-linking densities in fatigued E3 specimens indicated a faster increase in cross-linking density.

A mechanically-induced secondary cross-linking process is therefore suggested as the underlying mechanism within the silicone material under mechanical stress, which may occur in two different ways. First, upon external strain, unreacted functional groups may come into contact, which leads to further cross-linking reactions thereby forming additional CH_2-CH_2 bonds. Second, along with a decrease in the thickness of the specimen and the extension of the specimens' surface under severe deformation, oxygen and humidity can be transmitted/permeated into the silicone material with more ease. Particularly the presence of humidity may induce polycondensation reactions between hydrosilane groups, thereby forming additional Si-O-Si cross-links.

To illustrate changes in the chemical structure after mechanical fatigue, FT-IR spectrum of a fatigued E3 specimen (S_a = 140%, N_f = 90) is compared with an intact E3 specimen. As illustrated in Figure 47, no new peak appeared, and all peak positions for the fatigued specimen were not shifted compared to the intact example. Nevertheless, the Si-O-Si stretching peak in the range of 1000-

1100 cm^{-1} showed a slightly increased relative intensity in the fatigued specimen, confirming the formation of additional Si-O-Si bonds after mechanical fatigue. These Si-O-Si bonds indicated polycondensation reactions between hydrosilane groups. However, evidence of H_2O, which may also be produced during such polycondensation reactions, was not found.
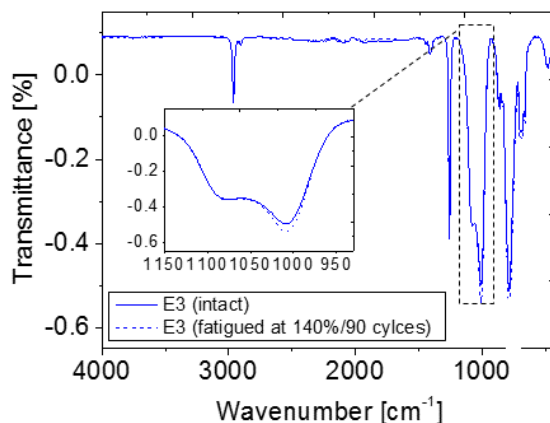
Figure 47. ATR-FT-IR spectra of an intact and a fatigued E3 specimen (140%/90 cycles). In the fatigued E3 specimen an increase of Si-O-Si intensity was observed.

Also the decreased chain mobility attained from DSC measurements verifies the increased cross-linking density in the fatigued specimen. The positions of both crystallization peak (ca. -66°C) and melting peak (ca. -40°C) are moved to lower temperatures in the fatigued E3 specimen (Figure 48). Furthermore, in the fatigued specimen the degree of crystallization $cryst$ was also observed to be lower (Figure 49).

As can also be seen in Figure 49, the minimum in the $cryst$ value was present under the aforementioned *critical load conditions* of "120%/10^3-10^4 cycles" for E2, and "140%/10-100 cycles" for E3, respectively. For E1 no significant changes in cross-linking density and no associated changes in the degree of crystallization were detected.
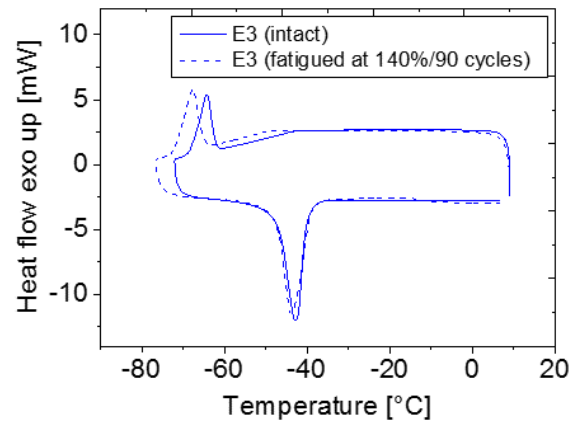
Figure 48. DSC thermographs of an intact and a fatigued E3 specimen (140%/90 cycles). This fatigued E3 specimen exhibited lowered crystallization temperature (ca. -66 °C) and melting temperature (ca. -40 °C).
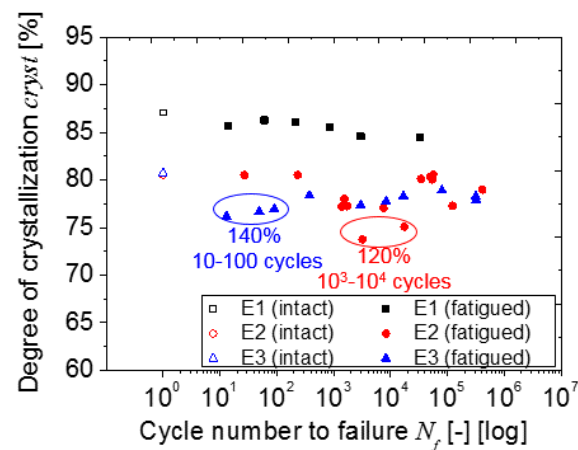
Figure 49. Determined degree of crystallization of fatigued specimens and intact specimens of thin silicone films E1, E2 and E3. The fatigued specimens were cycled until rupture. The *cryst* values shown were average values. Minima of the *cryst* values were observed on specimens fatigued at *critical load conditions* (marked by ellipses).

5.3   Effects of mechanical fatigue on elastic modulus

During fatigue tests, stress-strain curves of each specimen were recorded periodically. The stress-strain curve of the last load cycle before rupture was used to determine the elastic modulus of the fatigued specimen. Figure 50 shows the elastic modulus of each fatigued specimen against the corresponding cycle number to failure. As references, the elastic moduli of the intact specimens are

also presented in Figure 50. E1, E2 and E3 prepared with different stoichiometric imbalances displayed different elastic moduli in their intact states.
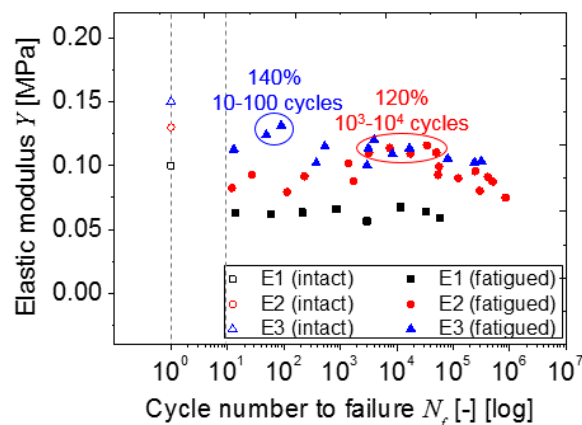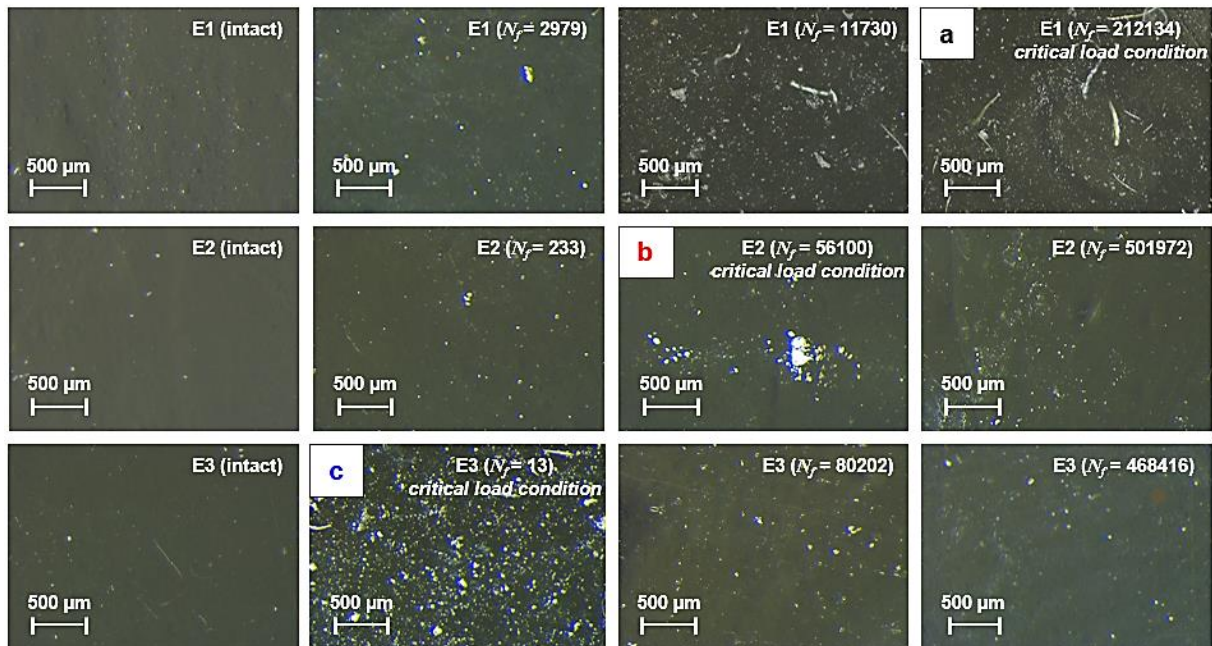

Figure 50. Elastic modulus of intact and mechanically fatigued thin silicone films E1, E2 and E3. The fatigued specimens were cycled until rupture. The Y values shown were average values. In the first 10 load cycles significant drops of Y became evident. Among fatigued specimens the maxima of the Y values were observed on specimens fatigued at *critical load conditions* (marked by ellipses).

Among fatigued specimens, variation of the elastic modulus with the cycle number to failure also differed in E1, E2 and E3. It can be generally divided into two stages: the first stage referred to specimens fatigued at the highest strain amplitude by the smallest cycle numbers (around 10 cycles), where significant declines in elastic moduli were observed in all three materials compared to the intact specimens. In specimens fatigued under lower strain amplitudes by higher cycle numbers, variation in their elastic moduli with the corresponding cycle number to failure showed same trend as seen for the cross-linking density (Section 5.2, Figure 45). In other words, the Y of all fatigued E1 showed virtually no difference, whereas in E2 and E3 the maxima of Y were found in specimens that were fatigued at their *critical load conditions*, namely "120%/10^3-10^4 cycles" and "140%/10-100 cycles", respectively.

The good agreement between changes in the elastic modulus after 10 cycles and changes in cross-linking density is attributed to the rubber elasticity theory.[112, 227]

The pronounced drop in the elastic modulus in specimens fatigued by 10 cycles originates from the so-called Mullins effect (Section 2.3.1.2), which is currently understood as the physical debonding of polymer chains from each other or from silica particle surfaces, which are initially connected via van der Waals forces.[129] Such debonding leads to a steep decrease in stress for the same strain and

thus to a decline in elastic modulus of the material (Figure 51). It is also worth noting that under cyclic loading the Mullins effect only occurs within the first 10 load cycles, after which the polymer matrix reaches a state of equilibrium. Thus, the Mullins effect must be considered as a transient physical effect, whereas further changes in the elastic modulus across a longer time range may indicate changes in the network structure, which in turn confirms the observations outlined in Section 5.2.
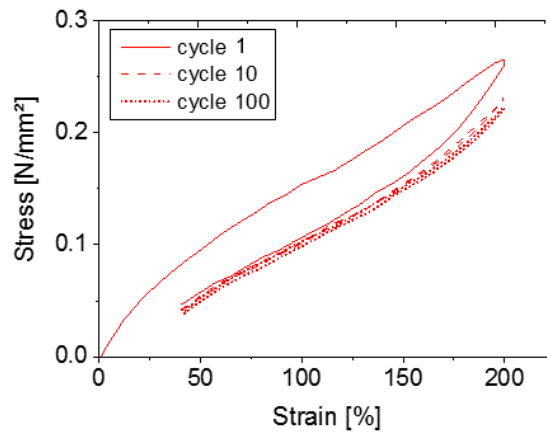
Figure 51. Stress-strain curves of cycle 1, cycle 10 and cycle 100 during mechanical testing to demonstrate the Mullins effect. Data recorded were from an E2 specimen loaded at S_a = 80% and R = 0.2.

5.4   Effects of mechanical fatigue on relative permittivity

Measured values of relative permittivity of intact and fatigued specimens of E1, E2 and E3 are plotted against the corresponding cycle number to failure in Figure 52. The intact specimens showed different relative permittivity values due to the different r values used for preparation.

For fatigued E1, there was no significant difference in relative permittivity, whereas for fatigued E2 and E3 variations in relative permittivity displayed opposite trends with respect to the variation in cross-linking density (recall Figure 45). Also, the relative permittivity of E2 reached a minimum in specimens fatigued at 120% amplitude by 10^3-10^4 cycles, where the *critical load condition* was identified for E2. In E3, such a minimum of relative permittivity also correlated well with the *critical load condition* of E3, i.e. "140%/10-100 cycle".

Figure 52. Relative permittivity of intact and mechanically fatigued thin silicone films E1, E2 and E3. The fatigued specimens were cycled until rupture. The ε_r values shown are average values. Maxima of the ε_r values were observed on specimens fatigued at *critical load conditions* (marked by ellipses).

The correlation between relative permittivity and cross-linking density has been discussed previously in Section 4.3. The underlying mechanism is understood in terms of the motion of permanent molecule dipoles in an electric field. In silicone elastomers, relative permittivity is proportional to the freedom of the molecular dipoles of the polymer chains in reorienting themselves under an applied electrical field. Increased cross-linking density in the fatigued E2 and E3 specimens led to a more restrained network structure, which impeded the reorientation of the molecule dipoles and therefore led to lowered relative permittivity.

In line with the decrease in relative permittivity, the loss factor $tan\delta$ decreased as well. This is reflected by a shift of the $tan\delta$ vs. f spectra to lower frequency range (Figure 53), wherein the frequency spectra of $tan\delta$ for E1, E2 and E3 are compared between intact specimens and those fatigued at *critical load conditions*. Changes in the real part of relative permittivity (ε'_r) and the imaginary part of relative permittivity (ε''_r) in fatigued specimens as a function of frequency are given in Appendix 4.1.
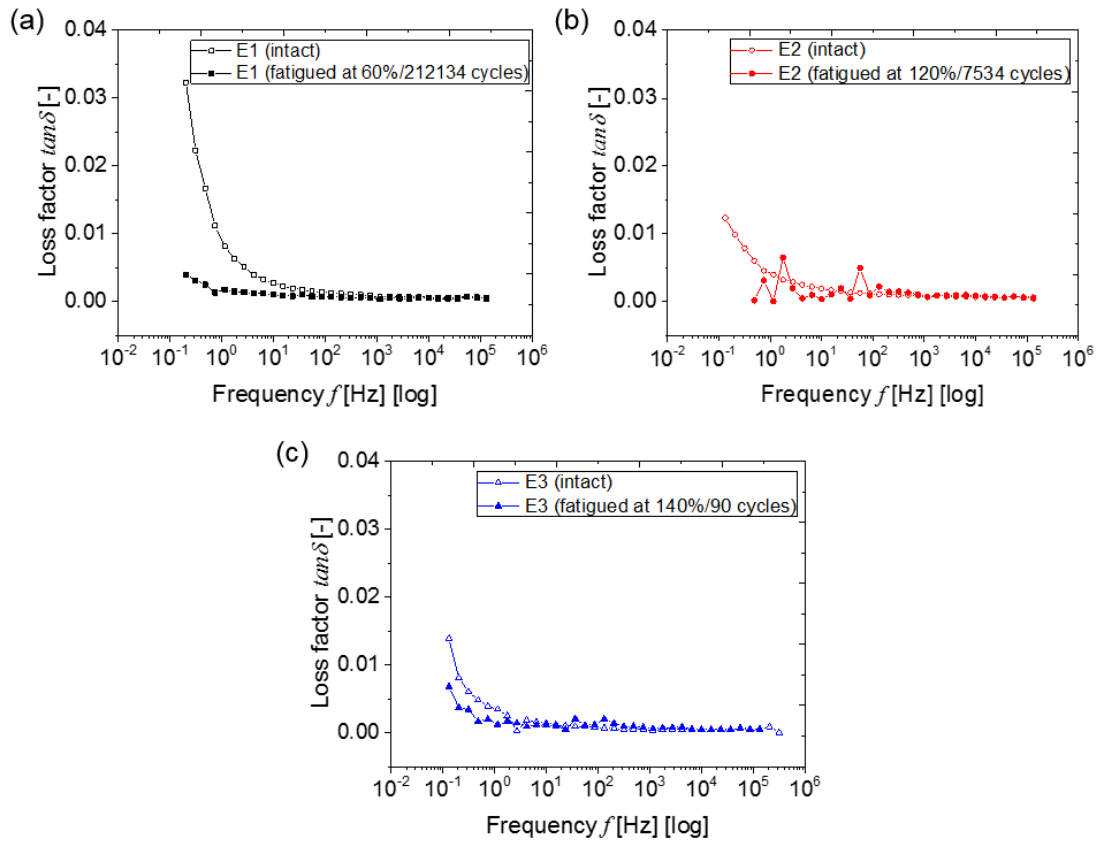
Figure 53. Spectra of loss factor as a function of frequency for (a) intact E1 and fatigued E1 (60%/212134 cycles), (b) intact E2 and fatigued E2 (120%/7534 cycles) and (c) intact E3 and fatigued E3 (140%/90 cycles). Fatigued specimens showed decreased $tan\delta$ values.

5.5   Effects of mechanical fatigue on breakdown strength

Based on the elastic modulus and the relative permittivity previously measured, the theoretical EMI breakdown strength of the fatigued specimens was estimated using the Stark-Garton model (Equation 31, Section 2.3.2.2).[149, 228, 229] In Figure 54, both the theoretical and measured breakdown strengths of the fatigued specimens of E1, E2 and E3 are plotted against their corresponding cycle numbers to failure.

Specimens of E1, E2 and E3, fatigued by 10 cycles, exhibited drops in breakdown strength (both calculated and measured values). This is related to the fact that these specimens had significantly lowered elastic moduli due to the Mullins effect. Among the fatigued specimens, particularly for E1, it is seen that the calculated breakdown strengths aligned well with the measured ones. For E2 the calculated values were also in good accordance with the measured values, except for the specimens fatigued at "120%/10^3-10^4 cycles", as marked by the red ellipse (also by "b"). In E3 a relatively large

discrepancy between the calculated and the measured values became evident. This was especially noticeable in specimens fatigued at "140%/10-100 cycles", as marked by the blue ellipse and by "c".
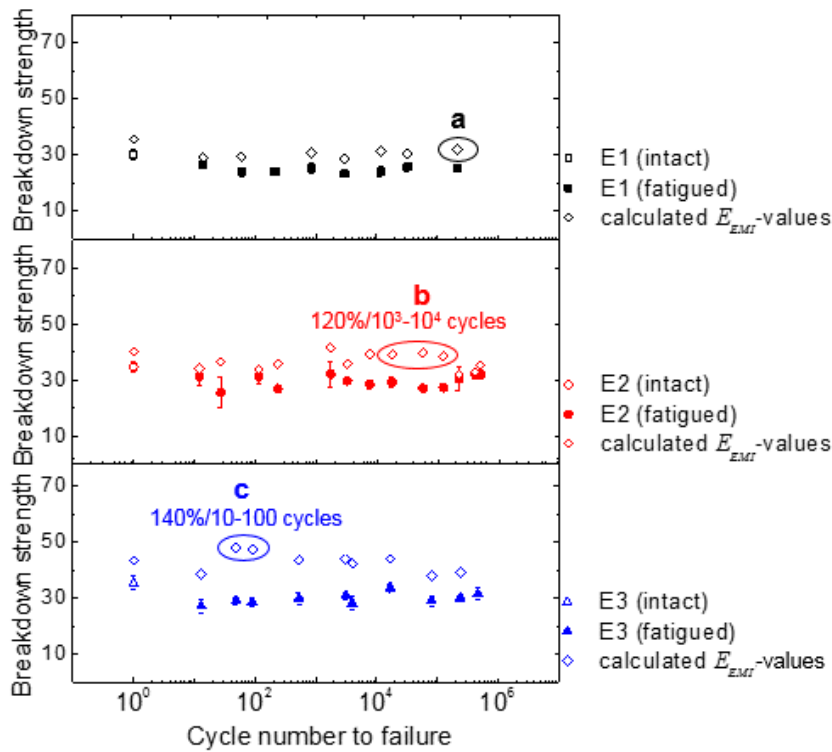
Figure 54. Comparison between the calculated breakdown strength (E_{EMI}) and the measured breakdown strength (E_B) of intact and mechanically fatigued thin silicone films E1, E2 and E3. The fatigued specimens were cycled until rupture. At specimens fatigued at *critical load conditions* (marked by "b" and "c") the differences between calculated and measured breakdown values were more significant.

Such a discrepancy is probably related to the fact that the basic assumption of the EMI model has been violated due to the mechanical fatigue effects. The EMI model considers elastomers as homogeneous continual, without microscopic defects, which can lead to inhomogeneities in the electrical field. However, as shown in the microscopic graphs of the specimens' surfaces (Figure 55), from E1 to E3 there was an increasing trend for inhomogeneities in the ruptured specimens, due to mechanical stress. The E2 and E3 specimens fatigued at their *critical load conditions*, as marked by "b" and "c" respectively, suffered from the formation of inhomogeneities on the surface. In the fatigued E1 specimen, which was fatigued over 212134 cycles (marked by "a"), the formation of inhomogeneities was rather insignificant. These surface inhomogeneities are locally weakened points, where early electromechanical instability (EMI) may occur, thereby leading to a lower

measured breakdown value than expected. In essence, the higher the inhomogeneities content, the larger the discrepancy between theoretical and experimental values.

Figure 55. Optical micrographs of intact and mechanically fatigued thin silicone films E1, E2 and E3. The fatigued specimens were cycled until rupture. With specimens fatigued at *critical load conditions* (marked by "b" and "c") formation of inhomogeneities at the surface was observed. From "b" to "c" the number of surface inhomogeneities increased.

Furthermore, the amount of inhomogeneities in a fatigued specimen appears proportional to the damage accumulation in the material prior to failure occurring. E3 had a much higher cross-linking density compared to E1. Thus, its network was denser, and could withstand more damage, either in terms of a higher strain amplitude or in terms of a larger number of cycles to failure, as shown in the Wöhler curves in Figure 44a. The same is true for specimens fatigued under *critical load conditions*, where significant secondary cross-linking occurred (represented by "b" and "c"). More inhomogeneities were found in these specimens, due to a higher degree of damage, which led to the pronounced discrepancy shown in Figure 54.

Based on these results, it is concluded that the main cause of the decrease in the measured breakdown strength is the Mullins effect in the first several load cycles. In the long-term range, due to the formation of surface inhomogeneities the breakdown strengths of all ruptured specimens did not differ much from each other. This means that no variation in the breakdown electrical field E_{EMI}

is to be expected for a DE device. However, specimens fatigued at *critical load conditions* may suffer early breakdowns due to the inhomogeneities at the surfaces.

5.6   Effects of mechanical fatigue on actuator performance

As outlined in Sections 5.2 and 5.3, specimen fatigued under the *critical load condition* showed a higher cross-linking density, which was responsible for an increase in elastic modulus and simultaneously for the decrease in relative permittivity. Both of these changes will reduce the potential to generate large deformation (Equation 2, Section 2.1.2.1). In other words, even a sole mechanical ageing episode will produce detrimental effects on actuator performance. However, these detrimental effects are only expected at the *critical load condition* of the material. Note that the possible effects of electrical high voltage are here initially neglected (which will be discussed in the next chapter). In this case, as shown in Figure 56, the final actuation deformations for the E2 and E3 specimens fatigued under their *critical load conditions* (marked by ellipses) are expected to be much lower compared to specimens fatigued under non-critical load conditions.
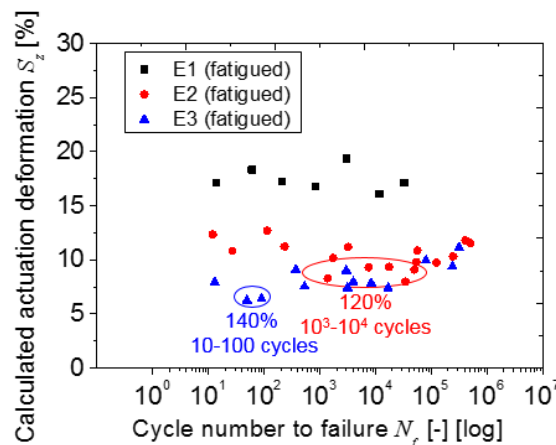
Figure 56. Calculated actuation deformation that generated by fatigued E1, E2 and E3 specimens. Calculation was based on an electrical field of 20 V/µm (defined arbitrary). Specimens fatigued at *critical load conditions* (marked by ellipses) will produce lower actuator deformations.

5.7   Comparison with commercial material

Since E2 was prepared as the benchmark material for the commercial Elastosil® P7670, it was necessary to compare their mechanical ageing behaviors. The obtained Wöhler curve and corresponding Weibull plot of Elastosil are presented in Figure 57a and Figure 57b.

Commercial Elastosil showed similar mechanical fatigue behaviors. The estimated characteristic lifetime of Elastosil (T = 109038 cycles) was only slightly higher than the one of E2 (T = 81680 cycles). This difference is probably due to the preparation technique of the commercial material and the better quality of the formed thin films.
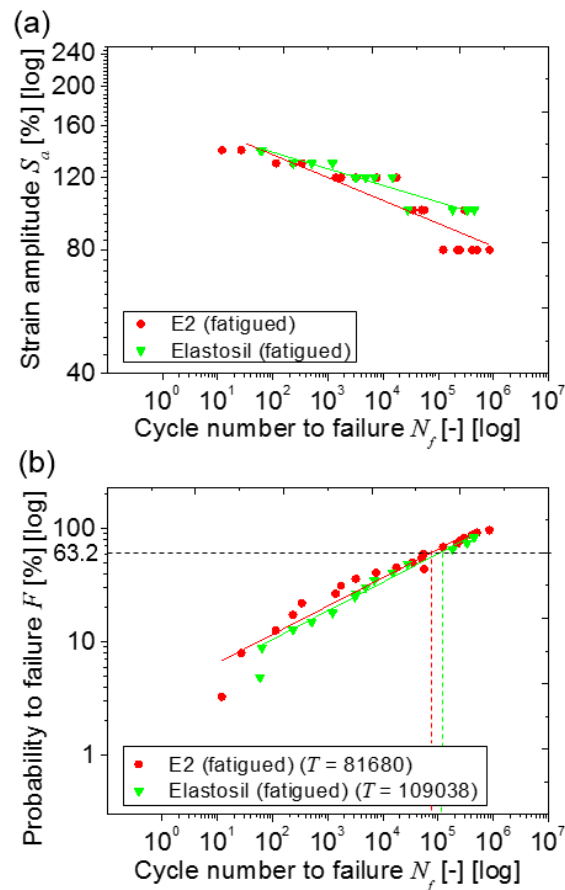
Figure 57. (a) Wöhler curves and (b) Weibull plots of Elastosil® P7670 were comparable with those of the benchmark material E2.

After being mechanically fatigued, comparable property changes and structural changes occurred in Elastosil. Figure 58 provides an overview of the estimated changes in cross-linking density, degree of crystallization, elastic modulus, relative permittivity, breakdown strength and actuator deformation that can be generated by these fatigued specimens.
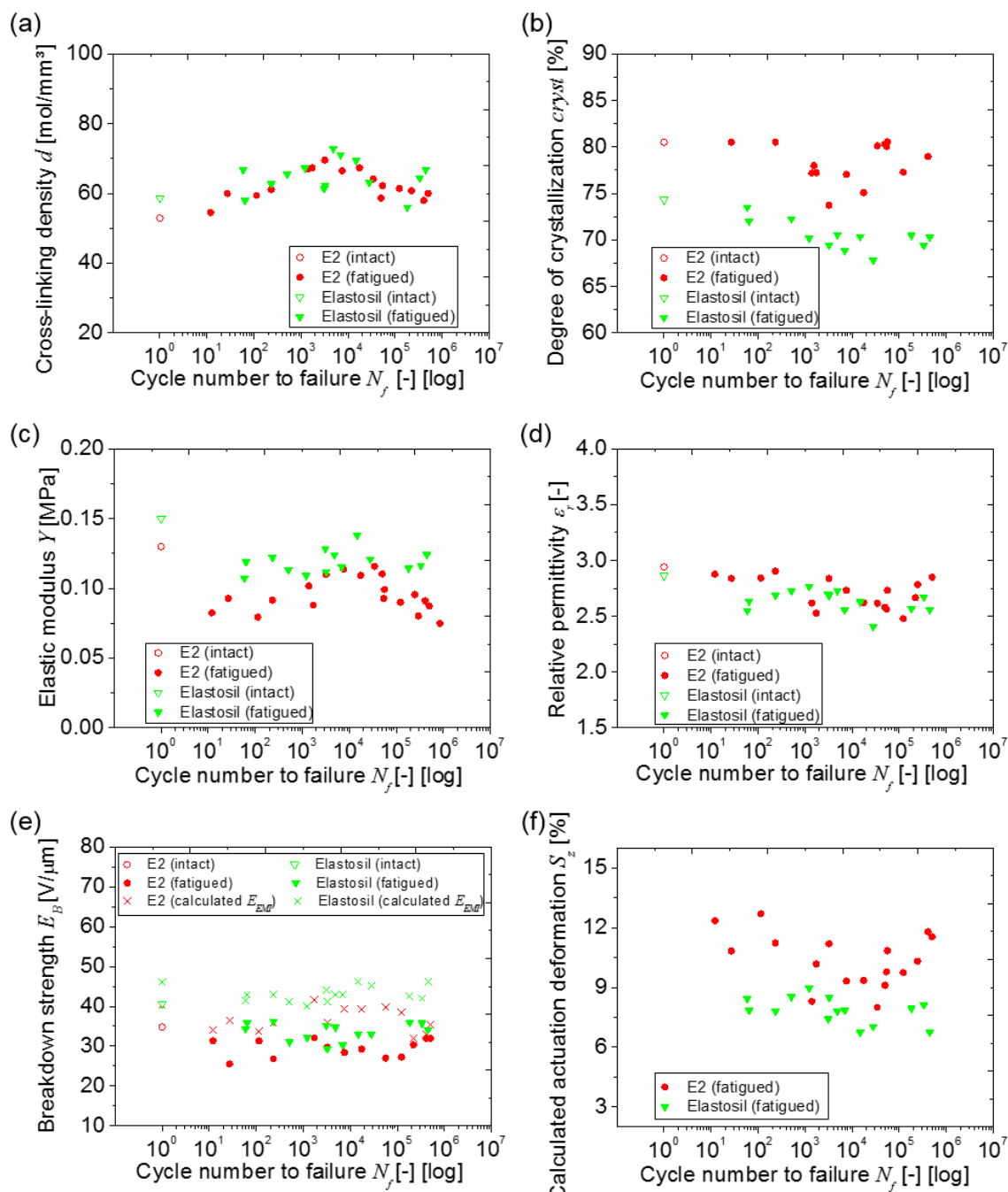
Figure 58. Changes in (a) cross-linking density, (b) degree of crystallization, (c) elastic modulus, (d) relative permittivity, (e) breakdown strength and (f) calculated strain deformation of intact and fatigued thin films Elastosil® P7670. Results were comparable with those of benchmark material E2.

In general, Elastosil behaved very similarly to the benchmark material E2. Changes in cross-linking density in Elastosil and E2, in particular, were very consistent among each other. The maximum d values were achieved on specimens fatigued at "120%/ca. 10^4 cycles" - a *critical load condition* that was also observed with E2.

Variations in elastic modulus also showed two stages. A significant drop in the elastic modulus occurred in the first 10 load cycles arising from the Mullins effect as outlined above. In specimens fatigued at higher cycle numbers, the secondary cross-linking fed an additional increase in stiffness into the material. Specimens fatigued at the above-mentioned *critical load condition* (120%/ca. 10^4 cycles) presented the highest values among the specimens fatigued in a long time range.

Relative permittivity is inversely proportional to cross-linking density. This is attributed to the chain mobility of the silicone network, as discussed previously. With Elastosil (Figure 58d vs. Figure 58a), this relationship was also be confirmed: associated with the increase in cross-linking density in Figure 58a, relative permittivity decreased, and the minimum value was reached at a *critical load condition* (120%/ca. 10^4 cycles).

Breakdown strength was influenced both by the elastic modulus and relative permittivity. Since these were both directly related to the cross-linking density of the material, breakdown strength can be interpreted as being dependent on cross-linking density as well. As shown in Figure 58e, the short-term fatigued specimens mainly undergo the Mullins effect and therefore present a significant decline in E_B. Specimens fatigued by higher cycle numbers also experienced intrinsic structural changes of secondary cross-linking. Consequently, the elastic modulus increased while relative permittivity decreased. Under the *critical load condition* a maximum breakdown field E_{EMI} was therefore expected. Furthermore, the measured values were especially lower than the calculated values in this region. The reason for this is proposed in Section 5.5 as the occurrence of surface inhomogeneities. With Elastosil, this assumption was also supported by comparing the surface characteristics of specimens that fatigued under different conditions (Figure 59). The large amount of surface inhomogeneities, as observed on the specimen fatigued under the *critical load condition* (120%/ca. 10^4 cycles), can cooperate with electromechanical instability (EMI) and lead to lower breakdown values than expected.
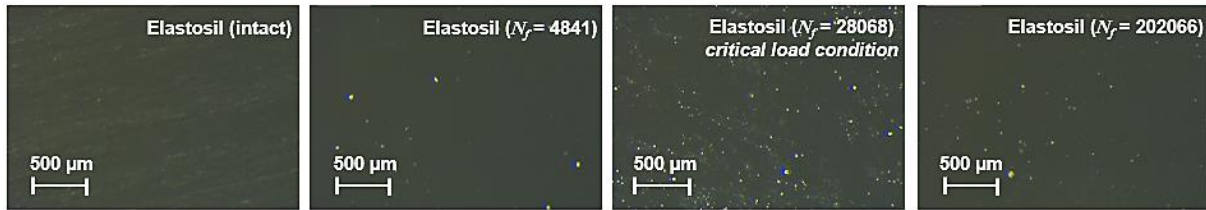
Figure 59. Optical micrographs of intact and mechanically fatigued thin films Elastosil® P7670. For specimens fatigued at *critical load conditions* inhomogeneities were found at the surface.

In Figure 58b and Figure 58f, effects of mechanical fatigue on the degree of crystallization, and on the calculated actuator deformation, became also evident. In fatigued specimens, the $cryst$ value declined as a direct consequence of mechanically-induced secondary cross-linking. The lowest values were given by specimens fatigued under the *critical load condition* (120%/ca. 10^4 cycles). The results of the calculated actuator deformation (Figure 58f) show that specimens fatiguing under *critical load conditions* exhibited reduced performance.

The good accordance of the results between the commercial Elastosil and the benchmark material E2 supports the conclusions made so far. At the end of the mechanical lifetime, DE silicones suffer structural changes and property changes, though to different extents. The significance of these effects of mechanical fatigue is strongly dependent on both the strain amplitude applied and the content of excessive hydrosilanes in the material. For different applications of the material in DE devices, the *critical load conditions* of DE materials needs to be especially considered.

5.8   Summary

The mechanical ageing behavior under mechanical cyclic ageing condition (mechanical fatigue), and effects of mechanical fatigue on silicone-based DE materials has been investigated. The key points of this chapter can be summarized as follows.

➢   Effects of mechanical cyclic loading have been demonstrated.
Mechanical fatigue can produce detrimental effects on the elastic modulus, relative permittivity and breakdown strength of the material. All of the changes in mechanical and electrical properties were found to correlate with changes in network structure, i.e. in cross-linking density and in degree of crystallization. Changes in mechanical and electrical properties will collectively degrade the potential of a DE actuator to generate sufficient actuation deformation.

> ➢ *Critical load conditions* have been defined.

All of the structure changes and property alternations were found to be most significant for specimens fatigued under certain load conditions, defined as *critical load conditions*. For the tested materials prepared with different stoichiometric imbalances, *critical load conditions* strongly depended on the contents of excessive hydrosilane groups. For E3 the *critical load condition* was found to be "140%/10^3-10^4 cycles", while for E2 it is "120%/10-100 cycles". E1 sustained no significant structural alterations, and thus no *critical load condition* was defined. Knowledge about these *critical load conditions* and resultant changes in network structure and material properties are essential for the design and application of DE actuators according to their service loads.

> ➢ The underlying mechanisms of silicone elastomers upon mechanical ageing have been proposed.

These are briefly illustrated in Figure 60. In the first 10 load cycles, the Mullins effect was responsible for the significant drop in elastic modulus, while cross-linking density and relative permittivity remained unaffected. This decline in the elastic modulus led to a decline in breakdown strength based on electromechanical instability (EMI).
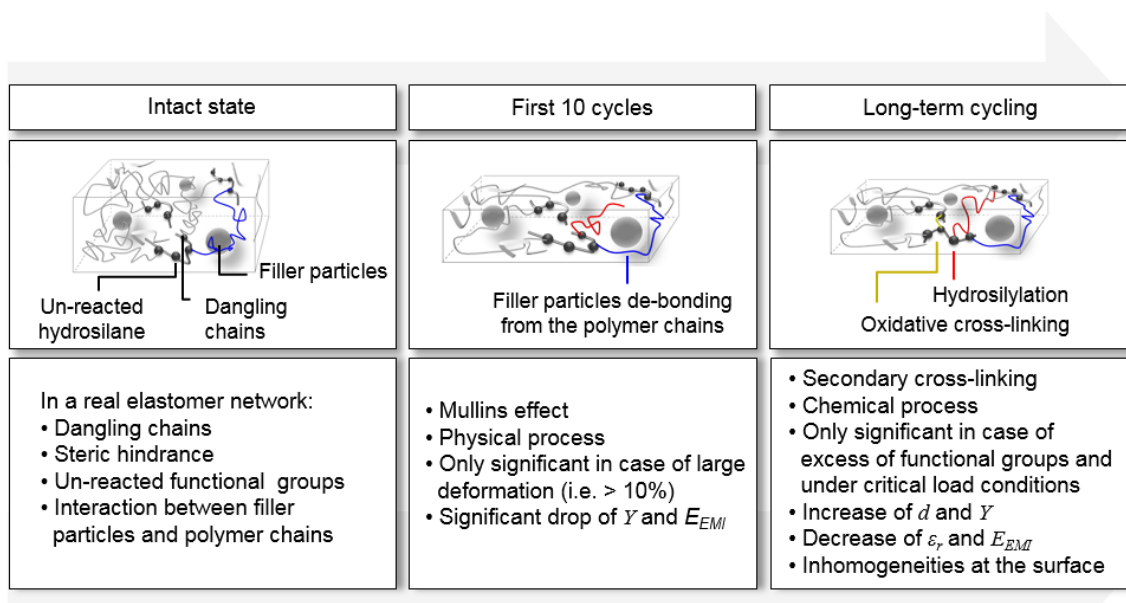
Figure 60. Proposed ageing mechanisms of a silicone elastomer upon mechanical ageing.

A more predominate mechanism in the longer term was the mechanically-induced secondary cross-linking by excess hydrosilanes. Such a change in network structure was also found to be associated with a pronounced increase in elastic modulus and a decline in relative permittivity in those specimens. Depending on the content of excessive hydrosilane groups in the network structure,

there were different *critical load conditions* for different elastomers, under which maximum changes in material properties were observed after fatigue. Under *critical load conditions*, a substantial amount of inhomogeneities formation was also observed at the surface of the thin silicone films after fatigue. This can cooperate with electromechanical instability (EMI) and resulted in even lower breakdown strength compared to expected E_{EMI} values.

The results achieved in this chapter provide valuable insights into the long-term behavior of silicone-based DE materials under mechanical cyclic loading. It is especially worth noting that the deteriorating effects caused by sole mechanical loading are only significant in case of *critical load conditions*. At moderate deformations such as < 100% (recall Section 5.2, Figure 46), no significant property changes should be expected. In practice, the deformation that a real DE actuator undergoes can be far below 100%, and the coupled *electromechanical* loading may introduce additional damages/changes into the material. Therefore, it is necessary to discuss the long-term behavior and the underlying mechanisms of the material under such load conditions. This will be discussed in the following Chapter 6.

6 Electromechanical Ageing

The aforementioned results confirmed that a sole mechanical cyclic loading can induce the secondary cross-linking of and cause various property changes in silicone-based DE materials under certain *critical load conditions*. Chapter 6 will consider electromechanical loading, a more realistic load condition, where the mechanical deformation is produced by electrical actuation.

For this purpose, thin silicone films prepared with varied stoichiometric imbalances were coated with compliant silver nanowire electrodes and then electromechanically cycled under alternating high voltage (V_{PP} = 2 kV, V_{DC} = 1 kV, f = 0.5 Hz) up to around 10^5 cycles. Note that the electromechanical ageing tests were not based on the Wöhler approach, instead, they were carried out under a constant electrical load for various timespans. This was due to the fact that, as mentioned in Section 10.5.3, during testing no linear relationship between electrical voltage amplitude and cycle number up to electrical failure (under double-logarithm) was observed. The self-prepared silver nanowire electrodes exhibited high compliance, low thickness and excellent conductivity (Appendix 5). After ageing tests, the electrodes were removed and the bare thin silicone films were examined. Changes in network structure, elastic modulus, relative permittivity, breakdown strength and actuator performance are illustrated in Section 6.1 to 6.5. Results gained from the benchmark material E2 are also compared with that of the commercial silicone material Elastosil® P7670 in Section 6.6. In Section 6.7, emphasis is placed on comparing mechanical ageing and electromechanical ageing.

6.1 Effects of electromechanical ageing on network structure

In Figure 61, cross-linking density of the intact and electromechanically aged thin silicone films are plotted with respect to the load cycles. The cross-linking densities of E1, E2 and E3 differed from each other due to the different r values used.

Among the electromechanically aged specimens, variations in cross-linking density in E1, E2 and E3 were clearly dependent on the cycle numbers. In all three materials, cross-linking density increased monotonously in line with increasing load cycles. During the early stage of the tests (< 10^3 cycles), cross-linking densities in all E1, E2 and E3 remained nearly constant. With a subsequent increase in load cycles (> 10^3 cycles), increasing cross-linking density trends were observed with all three silicone materials.

Also, the stoichiometric imbalance (r) had an impact on this long-term variation in cross-linking density after 10^3 cycles. As the stoichiometric imbalance increased, the onset of the increase in cross-linking density started at lower cycle numbers, while the total rise in cross-linking density was higher.
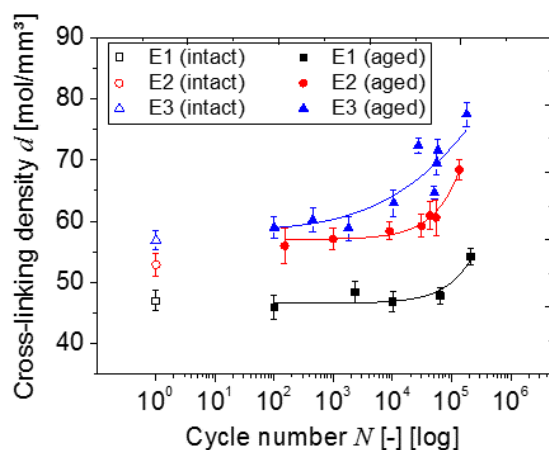
Figure 61. Cross-linking density of intact and electromechanically aged thin silicone films E1, E2 and E3. The d values increased with increasing load cycles. From E1 to E3 the overall increase became more significant.

These results indicate that excessive hydrosilanes involved in the specimens play an important role in the long-term behavior under electromechanical ageing. The observed increase in cross-linking density suggests a secondary cross-linking of the excess hydrosilanes. Theoretically, the secondary cross-linking reaction of hydrosilane groups can be initiated either mechanically[17, 19] or electrically.[27-29, 35] As mentioned in Chapter 5, the most significant increases in cross-linking density corresponded to the *critical load conditions*. It was proposed that excess Si-H bonds can form Si-CH_2-CH_2-Si joints via hydrosilylation reactions, or Si-O-Si bonds via oxidative reactions.

To verify changes in the chemical structure after electromechanical ageing, infrared spectra were recorded on intact and electromechanically aged specimens. In Figure 62 a comparison between an intact and an aged E3 specimen is presented. In the aged specimen, the broad stretching band in 3000-3500 cm^{-1}, which is typical of H_2O, is clearly detected. This suggests that H_2O is involved within the material after electromechanical ageing. Also, the Si-O-Si stretching peak in 1000-1100 cm^{-1} shows a slight increase in its relative intensity after ageing. Meanwhile, the Si-H bending peak at 916 cm^{-1} show slightly decreased intensity. It is also worth noting that these structural changes were more significant on specimens aged over a longer period. All of these observations confirmed the presence of the oxidative cross-linking reaction of hydrosilane groups.
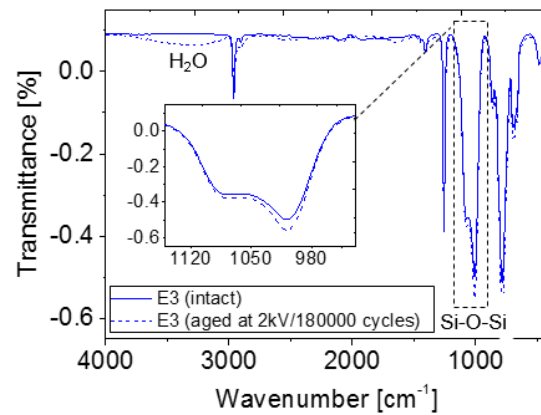
Figure 62. ATR-FT-IR spectra of an intact E3 specimen and an electromechanically aged E3 specimen (2 kV/180000 cycles).

Additionally, the increased cross-linking density in the aged specimen is verified by the decreased chain mobility, as observed by DSC measurements. In an aged specimen with increased cross-linking density, both crystallization and melting peak were shifted to lower temperatures (Figure 63). The resulting *cryst* value also decreased correspondingly (Figure 64). From E1 to E3 this trend became more significant. The decline of *cryst* values scaled also inversely with the increase of cross-linking density presented in Figure 61.
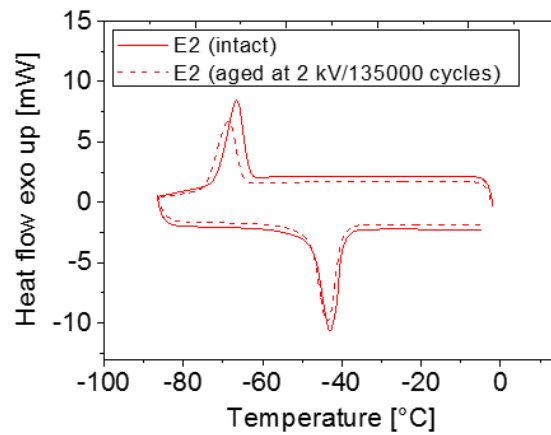
Figure 63. DSC thermographs of an intact E2 specimen and an electromechanically aged E2 specimen (2 kV/135000 cycles).
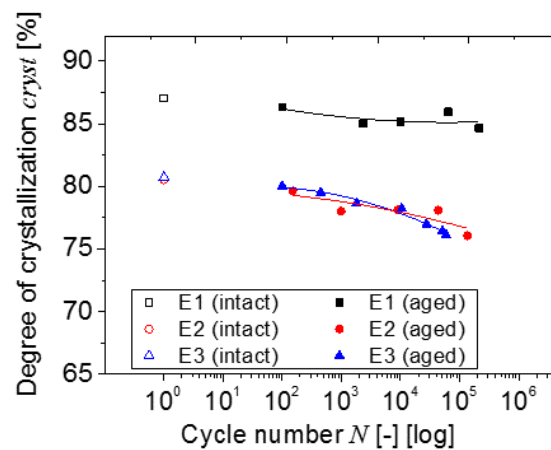
Figure 64. Degree of crystallization of intact and electromechanically aged thin silicone films E1, E2 and E3. The $cryst$ values decreased with increasing load cycles. From E1 to E3 the total decrease became more significant.

6.2   Effects of electromechanical ageing on the elastic modulus

Tensile tests were performed on the electromechanically aged thin silicone films. In Figure 65 the measured elastic moduli of aged specimens are plotted against their corresponding cycle numbers. As references the elastic moduli of intact specimens are also shown. The three materials E1, E2 and E3 showed different elastic moduli in the intact states due to different r values used for preparation.

As the load cycle increased, all three materials showed rising trends in the elastic modulus. E1 only presented a relatively slight increase after 10^5 cycles, whereas in E2 and E3 increases in the elastic moduli were already pronounced after 10^4 and 10^3 cycles respectively. After 10^5 cycles, the

increases compared to the intact state become 30, 54 and 87% for E1, E2 and E3, respectively. These changes generally scaled with the corresponding changes in cross-linking density revealed by Figure 61 (15, 29 and 36%). Such a proportional correlation between elastic modulus with cross-linking density is supported by rubber elasticity theory.[112]
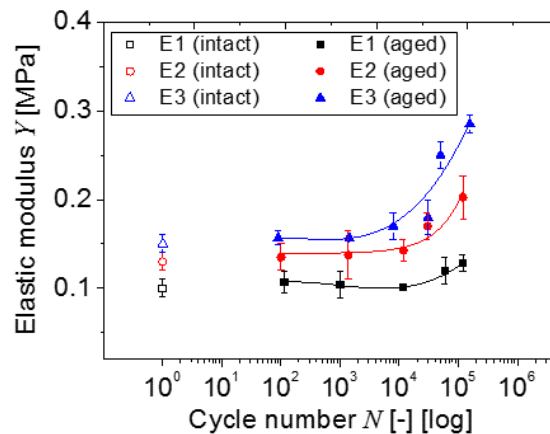
Figure 65. Elastic modulus of intact and electromechanically aged thin silicone films E1, E2 and E3. The Y values increased with increasing load cycles. From E1 to E3 the total increase became more significant.

6.3   Effects of electromechanical ageing on relative permittivity

Dielectric spectroscopy provided further important information about the ageing mechanisms of the silicone network. The dependence of relative permittivity on cross-linking density has been outlined in Section 4.3. In the treated frequency range the dielectric characteristic of silicone is governed mainly by dielectric relaxation phenomena. Figure 66 plots the relative permittivity of the electromechanically aged thin silicone films of E1, E2 and E3 against the corresponding cycle number.
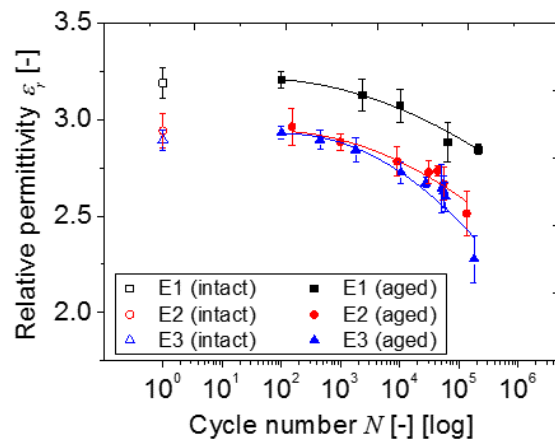
Figure 66. Relative permittivity of intact and electromechanically aged thin silicone films E1, E2 and E3. The ε_r values decreased with increasing load cycles. From E1 to E3 the total decrease became more significant.

For E1 in its intact state, cross-linking density did not reach the maxima due to the incomplete cross-linking reaction (recalling Section 4.1, Figure 35). Free-moving molecular side chains resulted in high relative permittivity for E1 (Figure 41), but because of the viscous nature of their movements the resulting $tan\delta$ was high as well (Figure 67). Although some rise in cross-linking density occurred during electromechanical ageing, the cross-linking density of E1 remained below the one of E2 and E3 (Figure 61). Consequently, the relative permittivity of aged E1 was higher than the relative permittivity of E2 and E3.

The concomitant decrease in $tan\delta$ (Figure 67) with growing number of cycles confirms that the viscous movement of the side chains was reduced through the increasing number of cross-links.

The frequency plots of the real part of relative permittivity (ε'_r) and the imaginary part of the relative permittivity (ε''_r) of E1, E2 and E3, before and after electromechanically ageing, are demonstrated in Appendix 6.
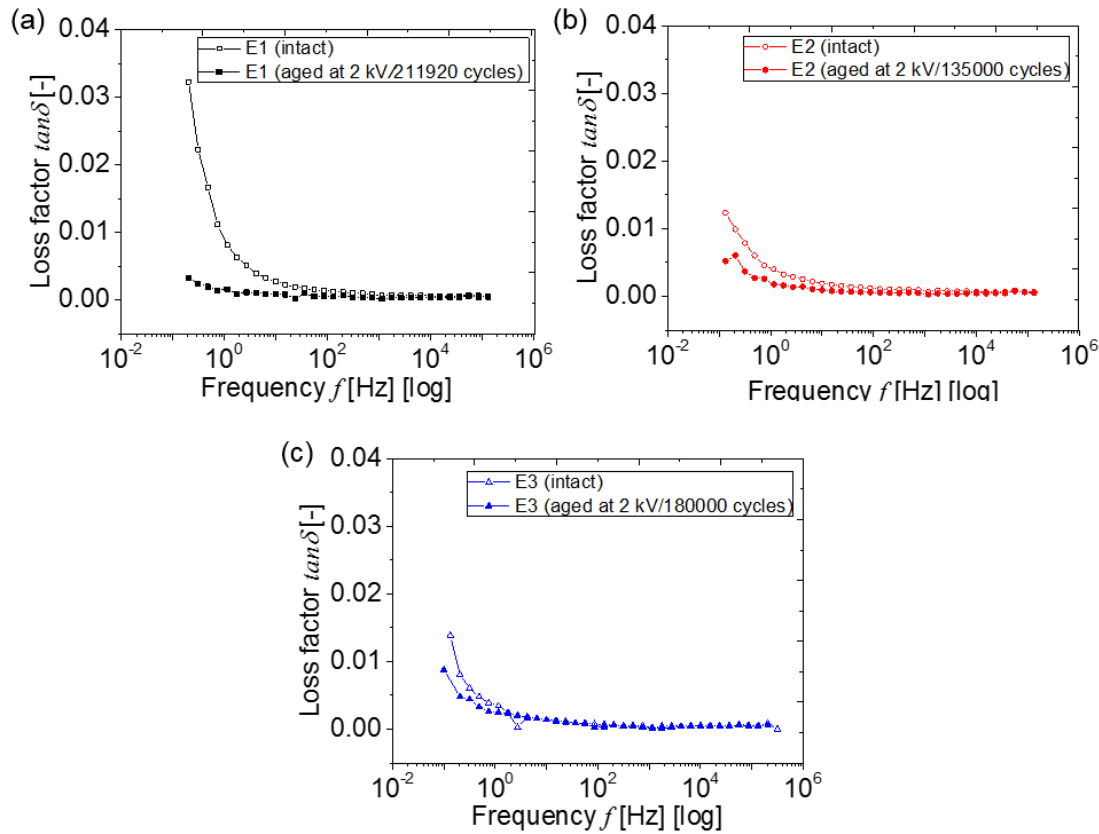
Figure 67. Spectra of loss factor $tan\delta$ as a function of frequency for (a) intact E1 and aged E1 (2 kV/211920 cycles), (b) intact E2 and aged E2 (2 kV/136000 cycles) and (c) intact E3 and aged E3 (2 kV/180000 cycles). Fatigued specimens showed decreased $tan\delta$ values.

6.4   Effects of electromechanical ageing on breakdown strength

Due to the increase in elastic modulus and the decrease in relative permittivity, as presented in Sections 5.2 and 5.3, breakdown strength is expected to increase with increasing load cycles. In Figure 68, the calculated E_{EMI} values are compared with the measured breakdown strength E_B for E1, E2 and E3.

It is evident that the measured breakdown strength increased in line with increasing load cycles. Furthermore, with the increasing r value from E1 to E3, the increase in breakdown strength became more significant. After 10^5 cycles the breakdown strength of E1, E2 and E3 was enhanced by 30, 44 and 78%, respectively.
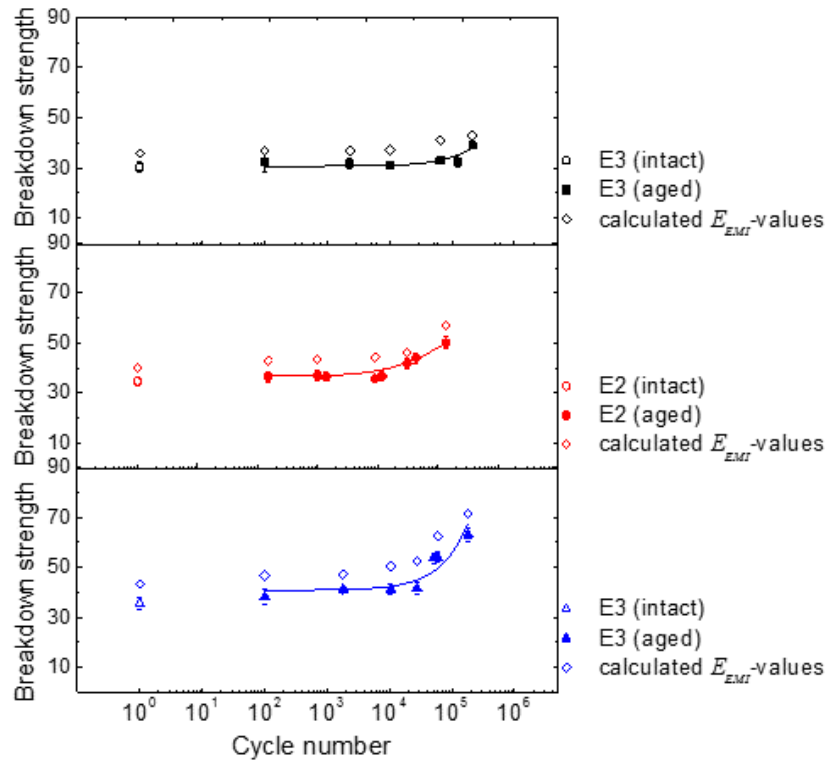
Figure 68. Comparison between the calculated breakdown strength (E_{EMI}) and the measured breakdown strength (E_B) of intact and electromechanically aged thin silicone films E1, E2 and E3. Both calculated and measured values showed increase with increasing load cycles. From E1 to E3 the total increase became more significant. The calculated and measured values were in good agreement.

It can also been seen that the calculated and measured values are in good agreement. The calculated E_{EMI} values in all E1, E2 and E3 sample were only slightly lower than the measured E_B values. This is, as discussed previously, related to the fact that the measured values are referred to the so-called *engineering* breakdown strength. The accordance between calculated and measured breakdown strength confirms that the change in breakdown strength in aged specimens is attributed to changes in the elastic modulus and relative permittivity caused by electromechanical ageing.

To verify whether additional ageing effects such as changes to surface characteristics also took place, all aged specimens were examined using optical microscopy. Figure 69 compares the surface characteristics of intact specimens with several aged (with moderate and large cycle numbers) E1, E2 and E3 specimens. Some alternations were visible at the surface of the aged specimens, but the size and depth of the surface inhomogeneities were considered to be rather insignificant.
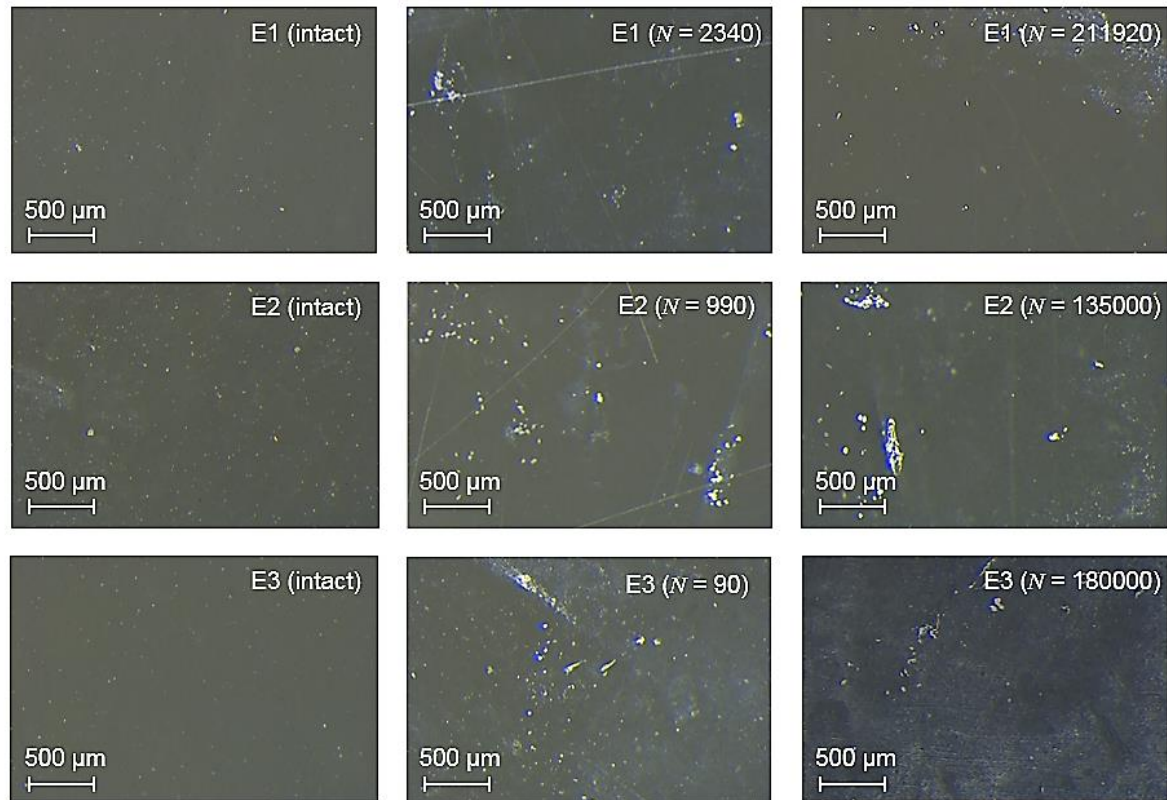
Figure 69. Optical micrographs of intact and electromechanically aged thin silicone films E1, E2 and E3. Formation of surface inhomogeneities was insignificant.

6.5   Effects of electromechanical ageing on actuator performance

On the one hand, the decrease in relative permittivity and the increase in stiffness of the material keep the operation away from the electromechanical instability (EMI) limit. This explains why, during the whole testing of up to 10^5 cycles, no breakdown occurred. On the other hand, decreasing electrostatic force and deformation reduce the performance of the actuator made of these silicone films, which confirms the lowered virtual actuator deformation during testing.

Actuation deformation in thickness S_z of each aged E1, E2 and E3 specimens was calculated. Declines of about 69, 55 and 41%, respectively, of their initial values are revealed in Figure 70. These results agree well with the experimental observations reported by Matysek et al.,[12] that after 1.44×10^6 cycles actuation deformation dropped off to about 60% of the initial state. Based on the aforementioned results in present work, plausible explanations about the degrading of actuation performance are provided.
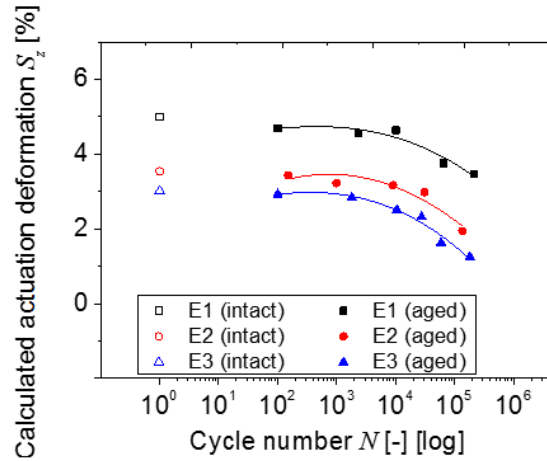
Figure 70. Calculated actuation deformation during electromechanical ageing of E1, E2 and E3 specimens. Calculation was based on the applied electrical voltage (2 kV) and the thickness of ca. 150 µm. The S_z values decreased with increasing load cycles. From E1 to E3 the total decrease became more significant.

6.6   Comparison with commercial material

The procedure developed so far to investigate the effects of electromechanical ageing was also applied to commercial Elastosil® P7670. In Figure 71, the estimated changes in cross-linking density, degree of crystallization, elastic modulus, relative permittivity, breakdown strength and actuator deformation are illustrated against the cycle numbers that the specimens underwent, and in comparison with the benchmark material E2. It is evident that Elastosil behaved very similarly to E2 under electromechanical loading.

The increase in cross-linking density (Figure 71a) in line with an increasing cycle number probably arose from electrically-induced cross-linking, as discussed in Section 6.2. This was directly responsible for the monotonic increase in elastic modulus (Figure 71c), the decrease in degree of crystallization (Figure 71b), and the respective decrease in relative permittivity (Figure 71d). According to electromechanical instability (EMI), the E_{EMI} values were expected to increase, and these were well verified by measured E_B values in Figure 71e. No obvious sign of surface inhomogeneities at the Elastosils' surface was observed (Figure 72). The increase in elastic modulus shown in Figure 71c, together with the decrease in relative permittivity shown in Figure 71d, led not only to the enhancement of breakdown strength (Figure 71e), but also the degradation of actuator deformation (Figure 71f).
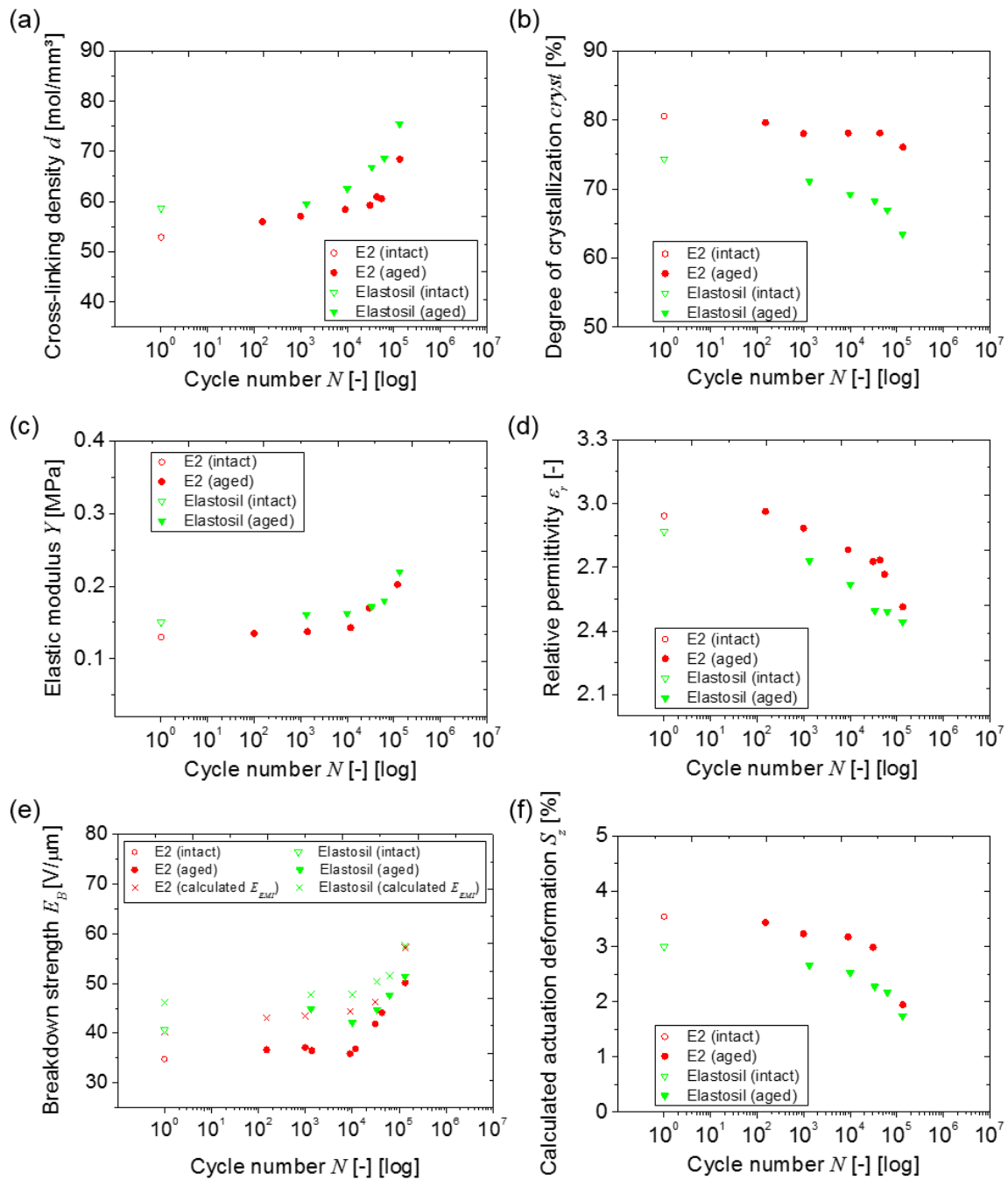
Figure 71. Changes in (a) cross-linking density, (b) degree of crystallization, (c) elastic modulus, (d) relative permittivity, (e) breakdown strength and (f) calculated strain deformation of intact and electromechanically aged thin films Elastosil® P7670. Results were comparable with those of benchmark material E2.
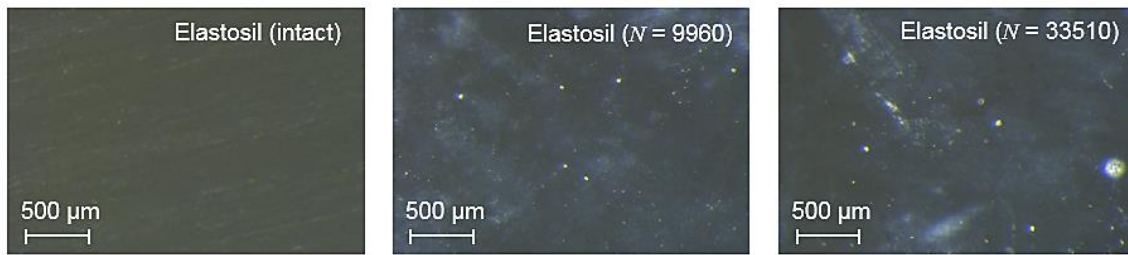
Figure 72. Optical micrographs of intact and electromechanically aged thin films Elastosil® P7670. Formation of surface inhomogeneities was insignificant.

In conclusion, the effects of long-term electromechanical cycling observed in the benchmark material are validated by the commercial material. Furthermore, the underlying interdependencies between property changes and structural changes in the material are well confirmed.

6.7   Comparison with mechanical ageing

Comparing the aforementioned results of electromechanical ageing with the results of mechanical ageing presented in Chapter 5, some interesting features can be found:

➢   Upon electromechanical ageing, the mechanically-induced cross-linking effects can be neglected due to the small degree of actuator deformation. The increase in cross-linking density observed upon electromechanical ageing is suggested to be attributed to electrical effects:

In order to clarify whether the electrical field or mechanical deformation is responsible for the observed rise in cross-linking density upon electromechanical ageing, some specimens were exposed solely to mechanical cycling. The idea was to put the specimens under the same mechanical stress as the electrostatic contraction caused by electromechanical loading. Since the applied test bench can only stretch the specimens in lengthways, a strain amplitude causing a stress state equivalent to the stress state caused by the electrostatic contraction was calculated. The calculation was based on the *principle strain theory* (Appendix 7) of incompressible materials.[230-232] The calculated uniaxial equivalent strain was about 5%.

Specimens mechanically aged upon 5% deformation over 10^5 cycles were characterized. As shown in Figure 73, such a purely mechanical cycling did not cause any rise in cross-linking density and no associate changes in elastic modulus, relative permittivity or breakdown strength. It can be therefore proposed that the observed increase in cross-linking density upon electromechanical loading is mainly attributed to the alternating electric high voltage.
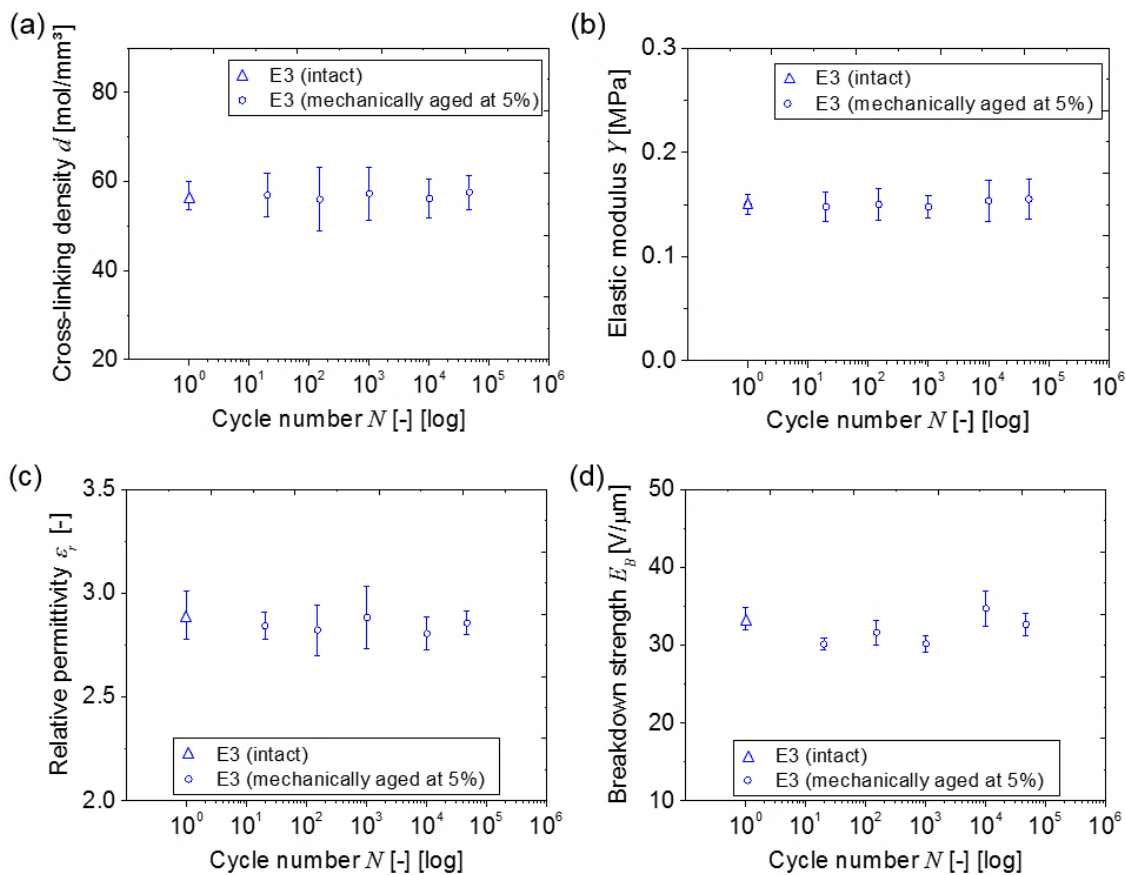
Figure 73. (a) Cross-linking density, (b) elastic modulus, (c) relative permittivity and (d) breakdown strength of material E3 mechanically cycled at a strain amplitude of 5%. Changes of these properties were insignificant.

➢ The secondary cross-linking induced by high electric voltage is more significant than that induced by mechanical loading:

Upon mechanical ageing, the increase in cross-linking density of a silicone material was only pronounced in specimens fatigued under *critical load conditions* and in materials containing excessive hydrosilane groups. Even though both of these criteria were fulfilled, if one compares the infrared spectra of the electromechanically aged specimen and that of a mechanically fatigued specimen (Figure 62 vs. Figure 47), no clear evidence of H_2O was visible in mechanically fatigued specimen.

Upon electromechanical ageing, even though the mechanical actuation deformation was far below the required *critical load condition* of the silicone material, the observed magnitude of the increase in cross-linking density was significant (Figure 61). And even in E1, which underwent no property changes upon mechanical ageing at all, an increase in cross-linking density upon electromechanical

ageing became evident. Moreover, the infrared spectra of the electromechanically aged specimen clearly confirmed the formation of H_2O.

In other words, the increase in cross-linking of the silicone-based DE is more prone to electromechanical ageing than to mechanical ageing. Note that if the actuator deformation of a DE material can be large enough to cause associated mechanical ageing, both mechanical effects and electrical effects will together contribute to the increase in cross-linking density and property changes in the material.

It becomes clear that mechanical and electromechanical ageing share some common characteristics, and also display differences in several aspects:

The following common characteristics can be concluded:

- *Cross-linking density*: in both cases there is a risk of the secondary cross-linking of excessive hydrosilane groups, which leads to increased cross-linking density.
- *Degree of crystallization*: in line with the increased cross-linking density, the chain mobility of the network becomes more restricted. The degree of crystallization therefore decreases.
- *Relative permittivity*: both mechanical ageing and electromechanical ageing can lead to the deterioration of relative permittivity, due to the increase in cross-linking density and a decrease in the chain mobility of the material.
- *Breakdown strength*: for both mechanically or electromechanically aged specimens, the main breakdown mechanism is verified as the electromechanical instability (EMI). Measured breakdown values (E_B) are consistent with breakdown values (E_{EMI}) calculated using Stark-Garton model.

Differences can be summarized as follows:

- *Significance of secondary cross-linking*: the increase in cross-linking density is more prone to electromechanical ageing, as mentioned above.
- *Elastic modulus*: upon mechanical ageing and significant deformation, the elastic modulus is reduced by the so-called Mullins effect which dominates in the first 10 load cycles. Thereafter, the change in the elastic modulus follows the proportional dependence on the change in cross-linking density according to rubber elasticity. Upon electromechanical ageing at a high voltage but minimal deformation, no Mullins effect is present, and the elastic modulus increases in line with the increase in cross-linking density.
- *Breakdown strength*: unlike via mechanical ageing, the detrimental effect of surface inhomogeneities formation does not occur in case of electromechanical ageing. Thus, the calculated E_B values show better agreement with the E_{EMI} values for electromechanically aged specimens.

6.8   Summary

The following key points can be summarized based on the results outlined in the current chapter:

➢   Effects of electromechanical ageing have been identified.

Electromechanical cycling can promote increase in cross-linking density, increase in elastic modulus, decrease in relative permittivity and an increase in breakdown strength according to electromechanical instability (EMI). These phenomena were detected in all three silicone materials. Silicone containing a higher amount of excessive hydrosilanes showed a stronger increasing tendency.

➢   Mechanisms of electromechanical ageing have been proposed.

The electrically-induced secondary cross-linking process was suggested as the underlying mechanism. An overview of this proposed mechanism is sketched briefly in Figure 74. Besides the increased cross-linking density estimated using swelling measurements, further direct evidences for this were produced by infrared spectra, in which the formation of H_2O and additional Si-O-Si bonds have been observed. Also, associated with increased cross-linking density, the mobility of the polymer chains declined, as reflected by the lowered degree of crystallization measured by DSC.

The secondary cross-linking is suggested as the predominant ageing mechanism upon electromechanical ageing. Unlike mechanical ageing (Figure 60), the Mullins effect upon electromechanical ageing can be neglected due to the small actuator deformation.

Intact state	Long-term loading
Filler particles Un-reacted hydrosilanes Dangling chains	Hydrosilylation Oxidative cross-linking
In a real elastomer network: • Dangling chains • Steric hindrance • Un-reacted functional groups • Interaction between filler particle and polymer chains	• Secondary cross-linking • Chemical process • More significant than mechanical ageing • Also dependent on the content of excessive Si-H • Increase of d, Y and E_{EM} • Decrease of ε_r • No visible surface inhomogeneities

Figure 74. Proposed ageing mechanisms of a silicone elastomer upon electromechanical ageing.

➢ A comparison between electromechanical and mechanical ageing has been performed.

By comparing electromechanical ageing with sole mechanical ageing at an equivalent degree of deformation, it was proposed that at the small electromechanical deformation (about 5%) the observed increase in cross-linking density was mainly attributed to the electrically-induced secondary cross-linking process. Furthermore, the oxidative cross-linking of hydrosilane groups became more significant under electromechanical ageing.

Knowledge gained in this chapter produces the first consistent picture of the long-term reliability of silicone-based DE materials under electromechanical ageing during service. Also the comparison between mechanical and electromechanical ageing behaviors helps to understand different mechanisms of mechanically-induced and electromechanically-induced effects.

7 First Comparisons with Post-Cured Material

The aforementioned results concerning mechanical and electromechanical ageing effects suggested that the main reason for possible property changes and performance degradation is the secondary cross-linking by excessive hydrosilane groups. Therefore, it is legitimate to ask if long-term stability might be improved if the excessive hydrosilane groups are subjected to a *post-curing*, after preparation but before use.

Post-curing via thermal treatment is usually recommended by silicone suppliers. To do this, silicone, after cross-linking reaction, is thermally treated in an oven over a substantial period of time. Although this process is widely recommended and well accepted, the consistent mechanisms of this post-curing process still remain unclear. In contrast, as introduced in Section 2.2.1, the term *thermal post-curing* may refer to a complex mechanism that involves further hydrosilylation or oxidative cross-linking with oxygen and humidity. How these reactions take place and how they participate with each other are, nevertheless, not only questions about chemistry, but also about statistics. The formed network structure of such a *post-cured* material should therefore be regarded as a mixture of diverse kinds of cross-linking joints, which in turn may hinder the interpretation of underlying ageing mechanisms. Therefore, the present thesis was so far focused on silicone formulations without thermal post-curing.

To give a first comparison of long-term ageing behaviors between a thermally post-cured material and a non-treated material, the following investigations are carried out. Self-prepared silicone E3 was selected to perform this comparison, because E3 contained a significant amount of excessive hydrosilanes. After a cross-linking reaction at room temperature, some E3 films were thermally treated at 120°C overnight. Properties of those post-cured E3 samples are presented in Section 7.1. Mechanical ageing tests were then performed on thin films of these post-cured E3. The fatigued specimens were analyzed in terms of structural changes and property changes. These results are outlined in Section 7.2 in comparison with E3 specimens without post-curing. Similarly, electromechanical ageing tests were also carried out on post-cured E3 specimens. The effects of electromechanical ageing are evaluated and compared to those on E3 without post-curing in Section 7.3.

Nevertheless, it is important to keep in mind that the results presented in this chapter are only the preliminary outcomes, since the exact reactions of a thermal post-curing are still unclear. In order to

achieve consistent statements on the ageing mechanisms of post-cured material, it is necessary to perform further, more detailed work in this area.

7.1   Properties of post-cured material

After thermal post-curing, cross-linking density, elastic modulus, relative permittivity and breakdown strength of the thermally post-cured E3 were compared with E3 without post-curing. Results are summarized in Table 12.

Table 12. Cross-linking density (d), elastic modulus (Y), relative permittivity (ε_r) and breakdown strength (E_B) of post-cured E3 were comparable with those of E3 without post-curing.

#	d [mol/mm³]	Y [MPa]	ε_r [-]	E_B [V/µm]
E3	56.88 ± 3.18	0.15 ± 0.01	2.89 ± 0.11	35.37 ± 3.41
E3 post-cured	63.86 ± 0.07	0.20 ± 0.05	2.89 ± 0.03	35.75 ± 0.50

It is notable that post-curing led to a minor increase in cross-linking density, together with a slight increase in elastic modulus. Differences in terms of relative permittivity and breakdown strength, however, were insignificant. These properties were also observed to be constant during storage over 3 weeks at room temperature (Appendix 8).

7.2   Mechanical ageing

Thin post-cured E3 films were mechanically fatigued using the Wöhler approach. As shown in Figure 75a, the Wöhler curves of E3 and post-cured E3 were closely superimposed on each other. The determined characteristic lifetime of the post-cured E3 (T = 117236 cycles) was only slightly higher than that of E3 (T = 102826 cycles), as illustrated in Figure 75b.
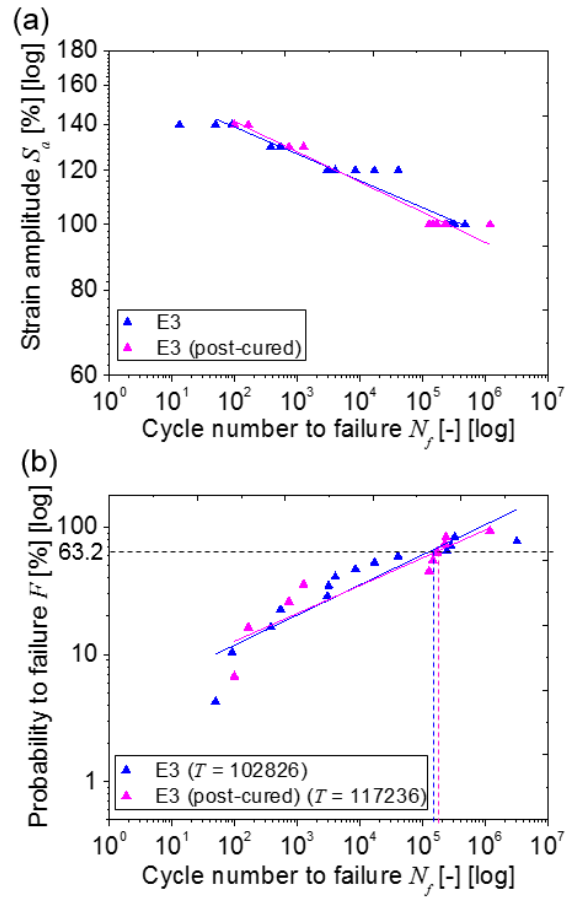
Figure 75. (a) Wöhler curves (b) Weibull plots of post-cured E3 were comparable with those of E3 without post-curing.

The fatigued specimens were characterized in terms of their changes in network structure, as well as in mechanical and electrical properties. The results of changes in cross-linking density, degree of crystallization, elastic modulus, relative permittivity and breakdown strength, and respective changes in actuator deformation are demonstrated in Figure 76.
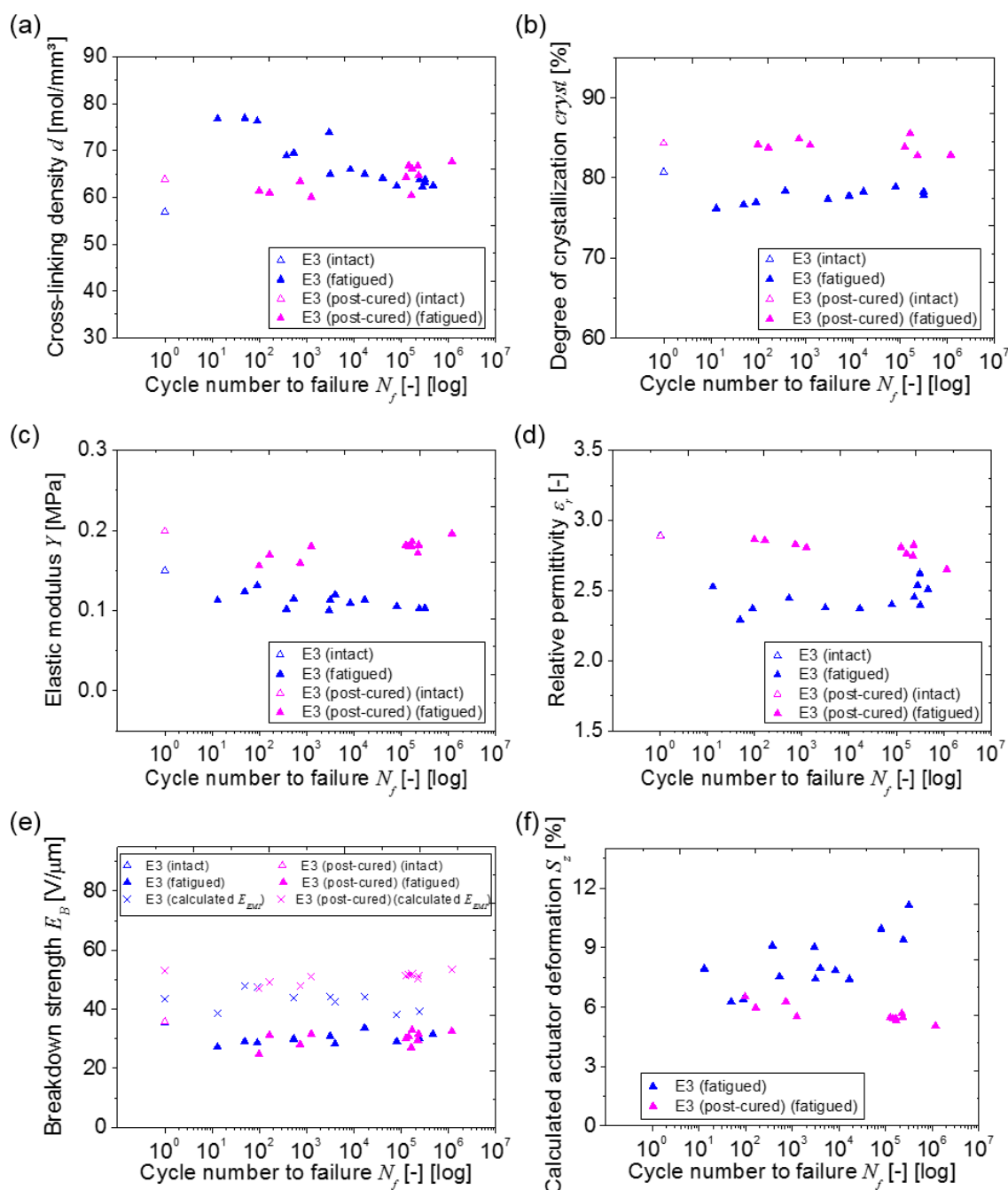
Figure 76. Changes in (a) cross-linking density, (b) degree of crystallization, (c) elastic modulus, (d) relative permittivity, (e) breakdown strength and (f) calculated strain deformation of intact and mechanically fatigued post-cured E3. The results were comparable with those of E3 without post-curing.

In general, the fatigued post-cured E3 showed less property changes compared to E3. Unlike E3, in which a *critical load condition* at "140%/10-100 cycles" was clearly observed, the post-cured E3 did not present significant property changes under these load conditions. Noticeable, however, was the presence of the Mullins effect in the first several load cycles on the post-cured E3 (Figure 76c). This effect was responsible for the significant decline in elastic modulus of specimens fatigued under this load condition. The general correlations between cross-linking density, degree of crystallization, elastic modulus and relative permittivity, as outlined in Chapter 2, can also be well recognized on the post-cured E3.

The breakdown strengths of all fatigued specimens also decreased (Figure 76e), mainly due to the involvement of the Mullins effect during loading. It is also interesting to note that for post-cured E3, discrepancies between the calculated E_{EMI} values and measured E_B values were higher than for E3. Nevertheless, no significant surface inhomogeneity was detected on the surface of fatigued post-cured E3 (Figure 77). This may indicate that the Start-Garton model probably needs additional modifications to be applied on post-cured silicone materials.

The calculated actuator deformation that can be produced at 20 V/µm of post-cured E3 showed a declining tendency. Specimen fatigued at 100%/ca. 10^5 cycles showed an obviously reduced ability to generate actuation, presumably due to its relatively high elastic modulus and low relative permittivity.
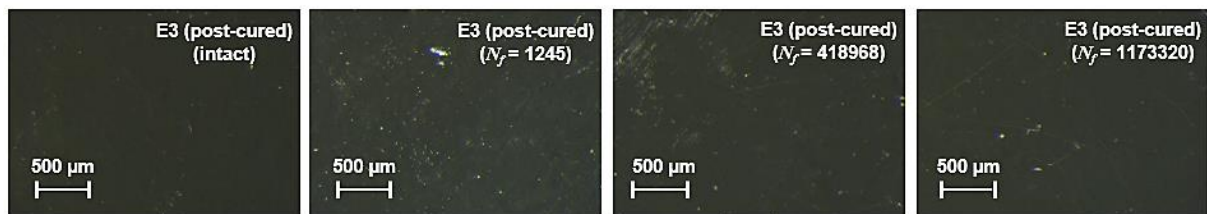
Figure 77. Optical micrographs of intact and mechanically fatigued post-cured E3. No surface inhomogeneities at the surface were visible.

7.3   Electromechanical ageing

Effects of electromechanical ageing on post-cured E3 were also examined. The results are presented in Figure 78, in comparison with E3. The post-cured E3 also showed more stable properties under electromechanical ageing, compared to the E3 without post-curing. Nevertheless, the increasing tendency of cross-linking density (Figure 78a) and elastic modulus (Figure 78c), as well as the decreasing degree of crystallization (Figure 78b) and relative permittivity (Figure 78d), can be observed after cycling over 10^5 cycles.
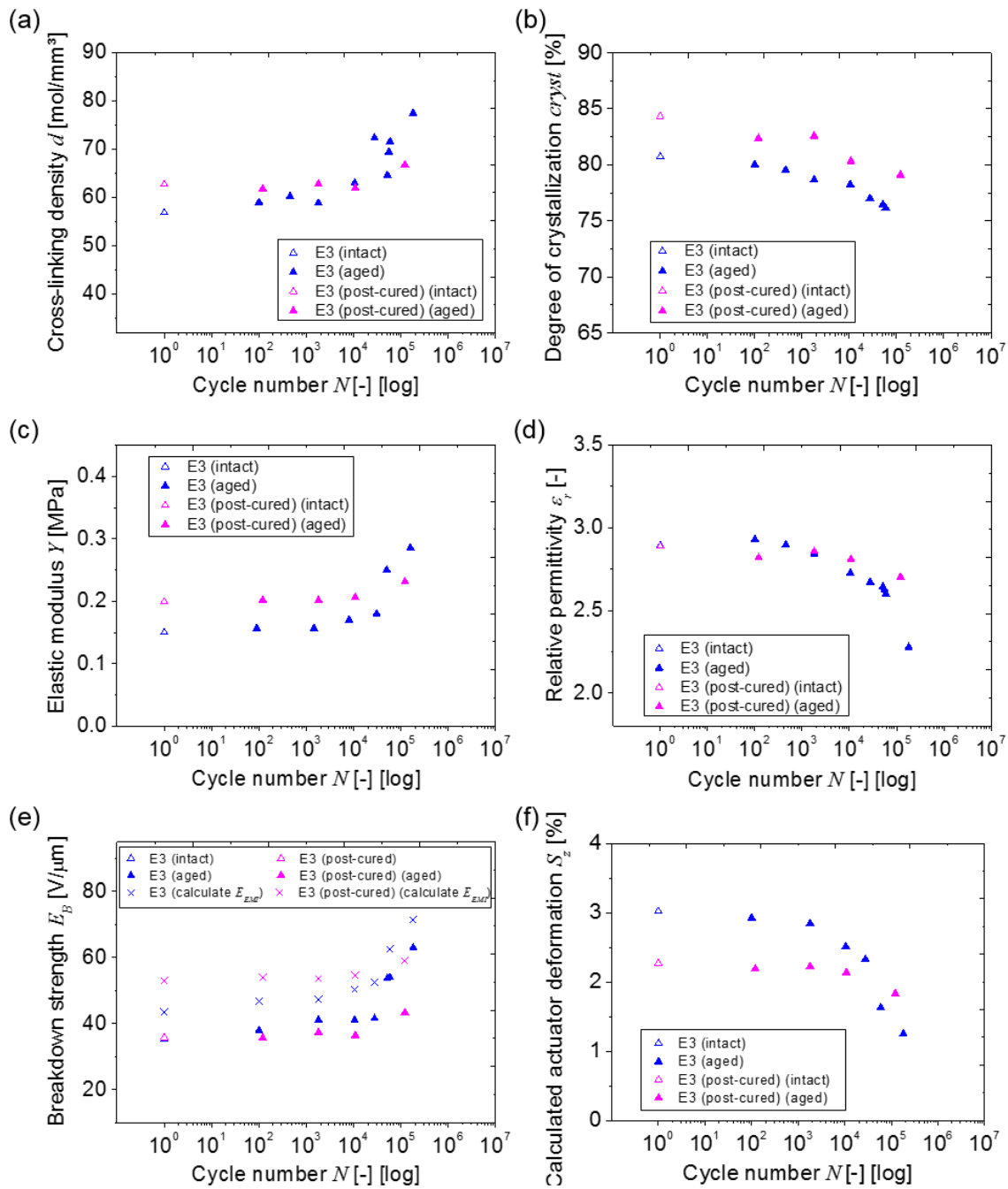
Figure 78. Changes in (a) cross-linking density, (b) degree of crystallization, (c) elastic modulus, (d) relative permittivity, (e) breakdown strength and (f) calculated strain deformation of intact and electromechanically aged post-cured E3. The results were comparable with those of E3 without post-curing.

Breakdown strength displayed an increasing tendency as well (Figure 78e). This can be explained by the increasing elastic modulus (Figure 78c) and decreasing relative permittivity (Figure 78d). It is also evident (Figure 78e), that with the electromechanically aged post-cured E3 specimens the discrepancy between calculated E_{EMI} values and measured E_B values was generally higher than for E3. From the surface images (Figure 79) no visible surface inhomogeneity was detected.

The actuator deformation that can be generated under the test condition (2 kV) decreased slightly after 10^5 cycles (Figure 78f). This was a result of the increased elastic modulus and decreased relative permittivity of these specimens.
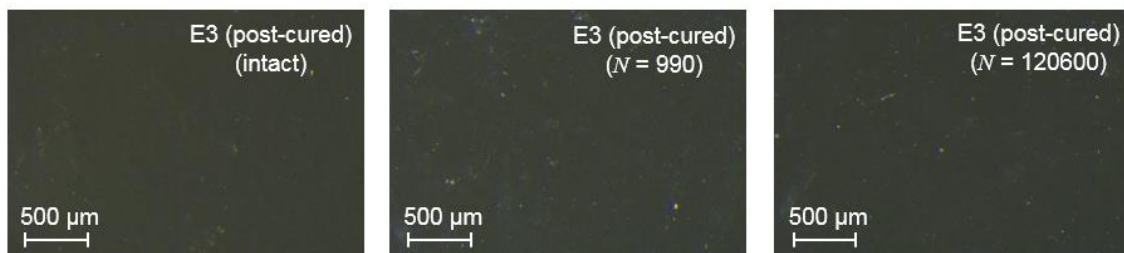
Figure 79. Optical micrographs of intact and electromechanically aged post-cured E3. No surface inhomogeneities at the surface were visible.

7.4   Summary

Based on the results outlined in Section 7.2 and Section 7.3, thermal post-curing is observed to favor long-term stability under mechanical and electromechanical ageing conditions. This therefore also confirms the findings in Chapters 4 and 5, that excessive hydrosilane groups in non-treated silicone materials are indeed playing a critical role in the long-term reliability.

Although the method thermal post-curing appears to be promising, it has to be kept in mind that thermal post-curing was also evidenced to somewhat stiffen the material, which may deteriorate actuator performance compared to non-treated material, as documented in Section 7.1. Also, as mentioned at the beginning of this chapter, this study was not able to disclose the underlying mechanisms behind the favorable effects observed experimentally. In order to gain a consistent picture of thermal post-curing and the effects of mechanical and electromechanical ageing on these post-cured materials, further research is still necessary.

8   Conclusion

Silicone-based dielectric elastomer is a promising novel actuator technology with a wide range of potential applications. Despite many advantageous properties of these materials, a lack of information concerning their reliability restricted the commercialization of the technology until now. In this thesis, the influences of both mechanical and electromechanical ageing on the long-term behaviors of silicone-based DE materials were analyzed, and the underlying mechanisms were clarified.

As a first step, a benchmark material with chemical structures and properties similar to those of the commercial silicone Elastosil® P7670 was successfully developed. Then, by varying the stoichiometric imbalance in its formulation, the structure-property relationships of the prepared silicone materials were investigated systematically. It was found that the silicone network synthesized with a higher stoichiometric imbalance showed a higher cross-linking density and a lower chain mobility. This increased cross-linking density resulted in an increased elastic modulus as well as in a decreased relative permittivity, which was due to the more restricted dipole motion upon electric field. The increased elastic modulus and decreased relative permittivity together led to a higher electromechanical instability (EMI) limit.

These investigations were then followed by mechanical fatigue tests performed on the prepared thin silicone films. It was found that the mechanical fatigue increased the cross-linking density, as a result of mechanically-induced secondary cross-linking of the excessive hydrosilane groups. This change of network structure in turn increased the elastic modulus and decreased the relative permittivity of the material, both of which can lead to a decreased deformation of the structure and thus to a deterioration in the performance of the actuator. These structural changes were found most significant in specimens fatigued under the so-called *critical load conditions*. For materials prepared with different stoichiometric imbalances, the load conditions considered as critical were strongly dependent on the contents of excessive hydrosilane groups. This information is essential for selecting the most suitable silicone materials for DE actuators.

In the last part, the prepared elastomer films were coated with compliant silver nanowire electrodes on both sides and then subjected to cyclic electromechanical loads via the applied alternating high voltage. As in mechanical ageing, with increasing load cycles an increase in the cross-linking density together with an increase in the elastic modulus and a decrease in relative permittivity were observed, which led to the significant deterioration of actuation deformation. By comparing with the results of

mechanically aged specimens under an equivalent strain, the underlying mechanism of electromechanical ageing was identified as the electrically-induced cross-linking of hydrosilane groups.

Results in this work show that for silicone-based DE materials, the structural characteristics, mechanical and electrical properties and their reliability behaviors during long-term loading are closely interconnected. In addition, they also give the positive message that reliability of actuators made of dielectric elastomers can be tailored by using proper chemical formulations of the material.

For material development, it is, however, worth noting that there may exist no optimal chemical formulation that generally fits all applications: a loosely cross-linked elastomer exhibits low stiffness, high relative permittivity, and its structural changes are less significant during long-term loading; however, it may suffer from low breakdown strength, high dielectric loss, and a short mechanical lifetime. In practice, tradeoffs will need to be made based on the actual load conditions and reliability requirements. Therefore, it is worthwhile performing further detailed studies on the necessary tradeoffs between performance-related properties and reliability-related properties of silicone-based DE materials.

The methodologies developed in the present work can also be used in future work to perform more detailed investigations on thermally post-cured materials, which were only preliminarily investigated in this work. Moreover, they can be applied to the testing of dielectric materials with more complex network structures, such as dielectric elastomer composite with conductive fillers, elastomer blends and interpenetrating polymer networks.

Furthermore, the illustrated interactions between the mechanical and electrical properties during long-term loading can also contribute to future studies in the areas of numerical modeling and lifetime prediction of silicone-based dielectric elastomers.

9 Zusammenfassung

Silikonbasierte dielektrische Elastomere (DE) haben ein großes Interesse geweckt für den Einsatz als flexiblen Aktoren. Trotz zahlreicher attraktiver Eigenschaften herrscht dennoch eine gewisse Unsicherheit im Hinblick auf eine wirtschaftliche Vermarktung dieser Technologie. Vor diesem Hintergrund bestand die Zielsetzung der vorliegenden Arbeit darin, einerseits das Langzeitverhalten von silikonbasierten dielektrischen Elastomeren zu untersuchen und andererseits die zugrundeliegenden Schadensmechanismen aufzuklären.

Um eine Basis für die vorliegende Arbeit zu schaffen, wurde zunächst eine Formulierungsbasis für ein Materialsystem entwickelt, das ähnliche Zusammensetzungen und Eigenschaften wie das eingesetzte kommerzielle Elastosil® P7670 besaß (Kapitel 3). Durch Variation des stöchiometrischen Verhältnisses zwischen Hydrosilanen und Vinyl-Gruppen wurde anschließend eine Reihe von Silikonmaterialien hergestellt. An diesen Materialien wurde systematisch untersucht, wie sowohl die Netzwerkstruktur als auch die mechanischen und elektrischen Eigenschaften mitandern korrelieren (Kapitel 4).

Mithilfe der hergeleiteten Struktur-Eigenschafts-Beziehung wurde als nächstes das Langzeitverhalten der Materialien unter mechanischer Ermüdung untersucht. Es wurde festgestellt, dass die mechanisch ermüdeten Silikonmaterialien auch Veränderungen bezüglich Netzpunktdichte, Elastizitätsmodul, Permittivität und Durchschlagfestigkeit erlitten. Die mechanisch-induzierte Nachvernetzung von nicht abreagierten überschüssigen Si-H Gruppen erwies sich als ein dominierender Mechanismus, der für die Eigenschaftsänderungen hauptsächlich verantwortlich war. Außerdem konnte festgestellt werden, dass diese chemischen Nachvernetzungsreaktionen und die resultierenden Eigenschaftsänderungen nur ab einer bestimmten *kritischen Last* stattfanden, die wiederum von der Menge der restlichen Si-H Gruppen im Material abhing.

Aufbauend auf den gewonnenen Erkenntnissen wurde in Kapitel 6 die elektromechanische Ermüdung untersucht. Durch Beschichtung mit elastischen Silber-Nanodraht Elektroden, konnte die Silikonfolie beim Anlegen einer elektrischen Spannung (V_{pp} = 2 kV, V_{DC} = 1 kV) eine mechanische Verformung von ca. 5% erzeugen. Mit zunehmender Belastungszyklenzahl wurde eine signifikante Zunahme des Elastizitätsmoduls, eine Abnahme der Permittivität, eine Abnahme der Durchschlagsfestigkeit und Verschlechterung der Verformung beobachtet. Als zugrundeliegenden

Mechanismus wurde im Material auch eine Nachvernetzung festgestellt, die aufgrund der geringfügigen Verformung auf eine elektrisch-induzierte Nachvernetzung hindeutete.

Die aus dieser Arbeit gewonnenen Erkenntnisse sind die ersten im Hinblick auf die Etablierung eines grundlegenden Verständnisses auf dem Gebiet der Zuverlässigkeit von dielektrischen Elastomeren.

Für die anwendungsorientierte Materialentwicklung ist es von großer Bedeutung, dass die Eigenschaften und das Langzeitverhalten des DE-Materials durch Variation seiner Netzwerkstruktur maßgeschneidert werden können. Allerdings ist es auch bemerkenswert, dass es für unterschiedliche Lastbedingungen kein universal einsetzbares Material gibt. Vielmehr muss für den individuellen Einsatzfall jeweils ein maßgeschneiderter Kompromiss gefunden werden. Weiterführende Arbeiten werden sich voraussichtlich verstärkt mit dieser individuellen Anpassung beschäftigen.

Außerdem bieten die bislang erarbeiteten Ansätze Möglichkeiten für zahlreiche weitere Untersuchungen an. So können weitere Silikonelastomere wie z.B. thermisch-nachvernetzte Silikonmaterialien, und neuartige Silikonmaterialien mit komplexeren Netzwerkstrukturen wie z.B. mit alternativen funktionellen Gruppen nachfolgend modifizierte Silikonmaterialien, erprobt werden.

Darüber hinaus können die im Rahmen dieser Arbeit erhaltenen Struktur-Eigenschafts-Beziehungen und ihren Wechselwirkungen unter Langzeitbedingungen dazu beitragen zukünftig die Zuverlässigkeitsstudien simulationsgestützt zu vertiefen.

10 Experimental

10.1 Characterization of the commercial silicone material

10.1.1 Materials

Elastosil® P7670 (Wacker Chemie AG, Germany, abbreviated as Elastosil) was investigated as a commercial silicone material. It is a two-component, addition cross-linking silicone elastomer, provided in both uncured and cured states. Uncured Elastosil was supplied in two separate components, i.e. parts A and B, both of which were highly viscous liquids with a viscosity of ca. 1800 mPa·s. The densities (at 23°C) of A and B were 1.01 g/cm³ and 1.05 g/cm³, respectively, while the mixing ratio for cross-linking between A and B was 1:1. Curing time was about 20 min (at 23°C). The cured Elastosil® P7670 came in the form of thin translucent films with a thickness of ca. 150 µm. Tensile strength was ca. 1.8 N/mm², tensile strain was ca. 600%, and the elastic modulus was ca. 1.5 MPa.

10.1.2 Characterization

To determine the chemical structure of Elastosil and the corresponding molecular weight, diverse techniques were employed. Both the uncured parts A and B in uncured form, and the cured thin Elastosil films, were characterized. An overview of the analytical methods employed is given in Figure 80.
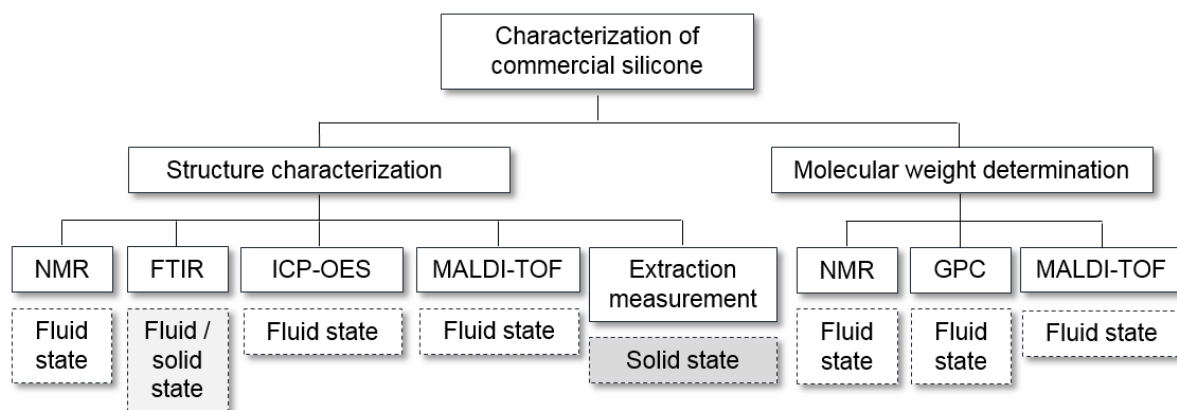
Figure 80. Employed analytical methods for characterizing commercial silicone material.

Nuclear magnetic resonance spectroscopy (NMR)

^{1}H-NMR: Approx. 80 mg of the uncured liquid part was dissolved in 1 mL deuterated chloroform (CDCl$_3$) in a sealed vial and analyzed using one-dimensional ^{1}H-NMR spectroscopy. The spectrometer was a Bruker Avance 400 (400 MHz) instrument (Bruker Optik GmbH, Ettlingen, Germany). Tetramethylsilane (TMS) was used as the internal standard, and measurements were performed by the author at the University of Stuttgart.

^{13}C-NMR: Measurements were carried out on a Bruker Avance 400 (400 MHz) instrument by using TMS as internal standard. The solvent was deuterated CDCl$_3$ at a concentration of ca. 200 mg/mL. Measurements were performed by the author at the University of Stuttgart.

^{29}Si-NMR: ^{29}Si-NMR spectra were recorded on a Bruker Avance 250 (79.5 MHz) using deuterated CDCl$_3$ as a solvent and TMS as the internal standard. The concentration of the test sample was ca. 200 mg/mL. Measurements were performed by the author and Dr. Dongren Wang at the University of Stuttgart.

Fourier transform infrared spectroscopy (FT-IR)

ATR-FT-IR data were acquired ranging from 4000 to 300 cm^{-1} using a Bruker IFS 66v/s equipped with a ZnSe crystal ($n_{ZnSe} \approx 2.4$, $\theta = 60°$) and an MCT detector. The nominal resolution was 4 cm^{-1}, and the number of scans was 500. Test samples were placed directly onto the sample holder for measurement, which was performed by the author at the University of Stuttgart.

Inductively coupled plasma atomic emission spectroscopy (ICP-OES)

To determine the content of platinum (Pt) in the parts A and B, ICP-OES measurements were performed on an ICP spectrometer (Spectro Analytical Instruments GmbH, Kleve, Germany). Three independent measurements were performed. Sample solutions for ICP-OES measurements were prepared using the ashing procedure, whereby approximately 0.2 g of the sample was placed in a crucible made of polytetrafluoroethylene (PTFE), and 5 mL nitric acid (HNO$_3$, 65%), 0.5 mL hydrofluoric Acid (HF, 38%), 1 mL hydrogen peroxide (H$_2$O$_2$, 30%), and 1 mL hydrochloric acid (HCl, 37%) were added. The crucible was then closed in a muffle furnace (MLS-ETHOS, MLS GmbH, Leutkirch, Germany) and heated gradually up to 200°C according to the temperature program shown in Table 13. After cooling down to 30°C the sample/acid mixture was filtered through filter paper, and then dissolved into 50 mL solution with distilled water for ICP-OES measurements. Measurements were performed by the author and Mr. Mike Wendel at the University of Stuttgart.

Table 13. Temperature program for sample preparation for ICP-OES measurements.

Step	Duration [min]	Power [W]	End temperature [°C]
1	20	700	150
2	20	800	200
3	60	800	200
4	60	0	30

Matrix-assisted laser desorption/ionization (MALDI-TOF)

MALDI-TOF spectra were acquired on a Brucker Autoflex III instrument equipped with an integrated nitrogen laser (337 nm, 5 ns). Time-of-flight (ToF) mass analysis was performed in reflector mode. Dichloromethane (DCM) was used as a solvent (10 mg/mL) and 2,4-dihydroxybenzoic acid (DHBA) as a matrix (10 mg/mL). Sodium iodide (NaI) was used to generate positive ions. The probe tip was made of stainless steel. Measurements were performed by Dr. Dongren Wang at the Institut für Textilchemie und Chemiefasern in Denkendorf (ITCF, Germany).

Extraction measurement

A total of 10.1060 g of Elastosil in its cured form was put into a 250 mL round-bottom flask, and 150 mL n-heptane was added. The mixture was heated in an oil bath at 50°C for 72 h. The extract was weighed (2.4467 g) and filtrated using a PTFE filter (40 μm). In all, 2 mL of the filtrate were analyzed using ^{1}H-NMR. Measurements were performed by the author at the University of Stuttgart.

Gel permeation chromatography (GPC)

GPC measurements for the uncured parts A and B were carried out at PSS Polymer Standards Service GmbH (Mainz, Germany). PDMS standards were used for calibration. Based on the calibration curve, average molecular weight values were calculated using PSS-WinGPC UniChrom software. Test samples for GPC measurements were prepared by using a 15 mg polymer sample dissolved in 3 mL of toluene (5.0 mg/mL). This sample solution was then filtered through filter paper (1.0 μm). For measurements 50 μL of the filtrate were injected into a GPC instrument using an auto-sampler (PSS SECurity 1260). The elution rate was 1.0 mL/min. The eluate was firstly passed through a pre-column (5 μm, 100 Å, 8.0 mm x 50 mm) and then through three consecutive columns

(all 5 µm, 8.0 mm x 50 mm) having different pore sizes, i.e. 100 Å, 1000 Å and 10^5 Å, respectively. Detection was carried out by employing a refractive index detector; all measurements were conducted at room temperature.

10.2 Preparation of silicone formulations

10.2.1 Materials

Two vinyl-terminated polydimethylsiloxanes (PDMS), i.e. DMS-V33 (M_n = 43,000 g/mol, f = 2, abbreviated as V33) and DMS-V41 (M_n = 62,700 g/mol, f = 2, abbreviated as V41), were purchased from Gelest Inc. (Morrisville, USA) and used as pre-polymers. Two types of cross-linkers were employed, i.e. HMS-151 (f = 4, M_n = 1,900-2,000 g/mol, Gelest Inc.) and C200 (f = 14-15, M_n = 4,500 g/mol, Evonik Hanse GmbH, Geesthacht, Germany). The hydrosilane (Si-H) groups of HMS-151 were located within the main chain, whereas C200 additionally allowed for terminal Si-H groups. A Karstedt's platinum catalyst (SIP6830.3), which is platinum-divinyltetramethyldisiloxane complex with 3-3.5 wt.-% of platinum already dissolved in vinyl-terminated polydimethylsiloxane, was purchased from Gelest Inc. For the cross-linking reaction, it was dissolved in the aforementioned PDMS pre-polymer, giving a platinum concentration of ca. 0.1 wt.-%. Fumed silica HDK N20 (abbreviated as N20) and silicone oil AK35 (both Wacker Chemie AG, Burghausen, Germany) were used as fillers. Highly hydrophilic-fumed silica N20 has a specific surface area of ca. 170-230 m^2/g, while AK35 silicone oil is a linear, non-functionalized PDMS with an average molecular weight of around 700 g/mol.

10.2.2 Preparation of the silicone networks

The preparation of the benchmark silicone material was also performed by mixing two separate parts, A and B, in the same weight ratio, similarly to Elastosil. Part A contained a pre-polymer and a catalyst, while part B contained a pre-polymer and the cross-linker. Four formulation parameters were systematically varied: The stoichiometric imbalance (r), the molecular weight of the pre-polymer, the cross-linker, and the filler content. Four series of silicone networks, i.e. I, II, III, and IV (Table 5), were prepared accordingly.

Stoichiometric imbalance (r) was defined as the molar ratio of hydrosilane groups over vinyl groups (Equation 31).[68, 97]

$$r = \frac{[SiH]}{[vinyl]} = \frac{[cross-linker] \cdot f}{[pre-polymer] \cdot 2} \qquad\qquad \text{Equation 31}$$

Generally, in order to reach a fully cured state, it is necessary to have a certain excess of hydrosilane beyond the theoretical balance (r = 1) but lower than 3. The stoichiometric imbalance value for attaining a virtually complete reaction needs to be investigated individually. The value r = 3 was chosen on purpose, in order to ensure a significant amount of excessive Si-H would remain in the network after hydrosilylation cross-linking, so that possible phenomena as a result of excessive Si-H groups can be illustrated further. To attain Series I (I-1, I-2, and I-3) with different stoichiometric imbalances (1, 2, and 3, respectively), the molar ratios for the pre-polymer and cross-linker in parts A and B were varied. For Series II, the molecular weight of the pre-polymer was varied by using V33 (II-1), V41 (II-2) and a one-to-one mixture of V33 and V41 (II-3) for the preparation. The same cross-linker (HMS-151) was used, and no filler was added. The corresponding molecular weights were therefore ca. 43,000, 51,000, and 63,000 g/mol, respectively. For Series III, V41 was used as a pre-polymer. By using different cross-linkers, i.e. HMS-151 and C200, silicone formulations III-1 and III-2 were prepared accordingly. For the preparation of Series IV, different amounts of silica and silicone oil were used. They were mechanically stirred (at least 30 min) into both A and B. V33 was used as a pre-polymer and HMS-151 as a cross-linker. The r value was 1.7.

Mixing of A and B was conducted with the aid of a two-component static mixer (10 mL/1:1) purchased from Adchem GmbH (Wendelstein, Germany). Identical weights of parts A and B were emptied into the two separated tubes of the static mixer and degassed in a vacuum oven overnight. To prepare a silicone film, the two components were pushed through the mixer and the mixture was then deposited onto a carrier foil made of polyethylene terephthalate (PET) (Figure 81a). The surfaces of the PET carrier foil were pre-treated inside O_2-plasma (200 W, 1 min). This mixture was then degassed in a vacuum oven for ca. 1 min (Figure 81b). A second PET foil was then placed on top of the mixture and a mechanical doctor blade was drawn along the top foil to obtain a film with a defined thickness (Figure 81c). Within a few minutes, a significant increase in viscosity was observed, and within ca. 30 min the mixture turned into a film. The formed silicone films (Figure 81d) were then stored overnight at room temperature. All procedures were carried out at room temperature inside an N_2-filled glove box.
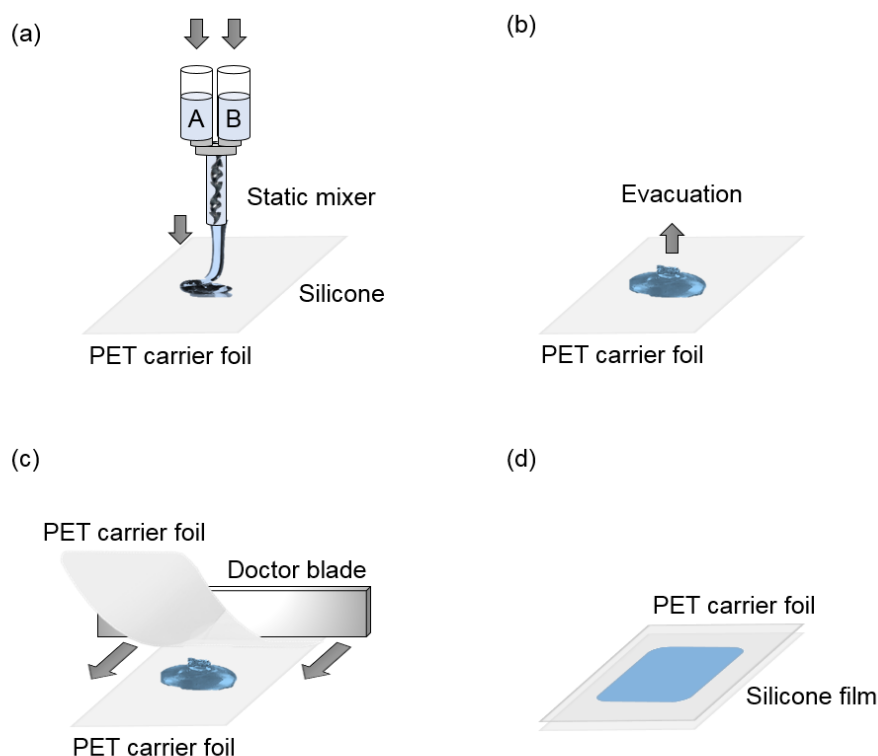
Figure 81. Preparation process for silicone film.

The homogeneity of the formed films was verified by optical microscopy. For further characterizations the formed silicone films were removed from the PET foils and cut into proper geometries.

10.2.3 Characterization

To determine the cross-linking density of the formed silicone material, swelling measurements were carried out. By using DSC, the crystallization behavior was studied in detail, and it was also possible to follow the curing reaction. In order to detect residual hydrosilane groups inside the formed networks, ATR-FT-IR was used. All prepared networks were also subjected to mechanical tensile tests.

Swelling measurements

Swelling measurements were performed at room temperature using toluene. A strip of cured silicone was weighed, put in a 50 mL flask, and 30 mL toluene were added. After 24 hours, the sample was quickly and carefully dried with paper tissue. The sample was again weighed, using a weighing pan with a lid, in order to prevent solvent evaporation. The degree of swelling (v_B) and cross-linking density (d) were calculated according to the Flory-Rehner equation (Equation 4), whereby the Flory-

Huggins interaction parameter for polysiloxane/toluene was 0.465.[233] The density of the cured elastomer was determined prior to swelling with the aid of a pycnometer. Densities of toluene (0.865 g/cm^3 at 25°C) and water (0.997 g/cm^3 at 25°C), and their dependence on temperature, were taken from the literature.[234] For each sample at least four measurements were carried out. Measurements were performed by the author at the University of Stuttgart.

Differential scanning calorimetry (DSC)

To determine the crystallization behavior of cured silicones, DSC measurements were performed on a DSC Q2000 apparatus (TA Instruments, New Castle, USA). Strips of cured silicone, weighing ca. 8-12 mg, were enclosed in standard Al-pans (50 µL). The overall scan speed was 10 °C/min. Samples were held at 30°C for 1 min, cooled from 30 to -90°C, and then reheated to 0°C. The second cooling/heating cycle was used for interpretation. Degrees of crystallization *cryst* in % were calculated from the melting enthalpies $\mathit{\Delta H_m}$ using the literature value of $\mathit{\Delta H_{th}}$ *of* 37.43 J/g as the perfect fusion heat.[104] Measurements were performed by the author and Ms. Erna Muks at the Institut für Textilchemie und Chemiefasern in Denkendorf (ITCF).

To follow the curing reaction, DSC measurements were carried out on a PerkinElmer DSC 400 instrument. Nitrogen was used as purge gas with a flow rate of 20 mL/min. Standard Al-pans (30 µL) were filled with ca. 10 mg of sample mixture and sealed inside a glove box. Two consecutive runs, between 20 and 220°C, using a heating rate of 10 °C/min were conducted. The first heating run was used for interpretation, and three measurements were performed for each sample. Measurements were carried out by the author at the University of Stuttgart.

ATR-FT-IR spectroscopy

To detect any remaining hydrosilane groups in the cross-linked networks, measurements were carried out shortly after the networks had been cross-linked. A sample slice was placed onto the sample holder. Spectra were then recorded on an Alpha FT-IR spectrometer (Bruker Optik GmbH, Ettlingen, Germany) in the region of 4000 to 400 cm^{-1}. Signals at $\bar{v}$ = 916 cm^{-1} assigned to the bending vibration of the hydrosilane (Si-H) groups were used for this purpose. Notably, the stretching band of the silane groups near 2136 cm^{-1} could not be distinguished particularly well, because it overlapped with a second band which probably originated from the background (noise) of the MCT detector.[95] Measurements were performed by the author at the University of Stuttgart.

Mechanical tensile tests

Dumbbell-shaped samples were cut from each film sheet. The thickness of the specimens for the tensile tests was 2 mm. Tests were performed on a Zwick Z020 (Zwick, Ulm, Germany) at room temperature with a test speed of 200 mm/min. Stress-strain curves were recorded along with tensile strength and tensile strain. Based on the stress-strain curve, an elastic modulus Y was calculated. The results reported herein are the average values of at least five specimens. Measurements were performed by the author at the Robert Bosch GmbH.

Optical microscopy

The surface characteristics of the prepared elastomer films were studied using a Leica M60 microscope coupled to a Leica MC120HD camera (Leica Mikrosysteme Vertrieb GmbH, Wetzlar, Germany). Measurements were performed by the author at the Robert Bosch GmbH.

White light interferometry

White light interferometry (CyberSCAN CT100, cyberTECHNOLOGIES GmbH, Eching-Dietersheim, Germany) was carried out using a high-resolution, non-contact profilometer to determine the thickness (2D mode) and the surface characteristics (3D mode) of the prepared silicone films. The test setup consisted of a white light sensor and an additional x-, y-motion system on a granite platform. Sensors were available at a z-resolution down to 3 nm and a measurement range up to 25 mm. For each specimen at least five independent measurements were carried out. Measurements were performed by the author at the Robert Bosch GmbH.

10.3 Structure-property relationships

10.3.1 Materials

Based on the developed benchmark material (E2) (also IV-4), the stoichiometric imbalance r was varied to prepare silicone materials E1 ($r = 1.3$) and E3 ($r = 3$). All other formulation parameters remained the same: DMS-V33 was used as pre-polymer, while HMS-151 was used as cross-linker. Karstedt's catalyst SIP6830.3 was employed as a catalyst. All three silicone networks contained silica N20 (4.5 wt.-%) and silicone oil AK35 (55 wt.-%).

The mixing process for parts A and B, and the preparation of silicone films, was performed according to the procedure illustrated in the previous section (Section 10.2.2, Figure 81). For investigations, thin silicone films were processed with a thickness of ca. 150 μm. This thickness provided results with satisfying statistics and also ensured good handling. All prepared thin films showed

homogenous surface characteristics and no obvious agglomerates of the silica particles, as shown in Figure 82.
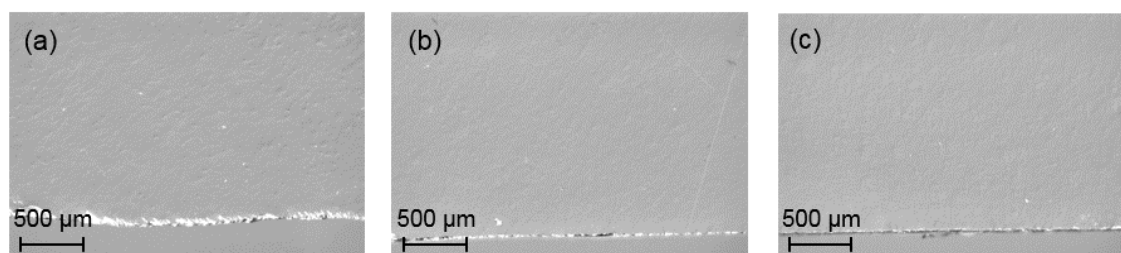
Figure 82. Optical micrographs of the surface characteristics of prepared thin silicone films (a) E1, (b) E2, and (c) E3.

10.3.2 Characterization

In addition to the characterizations of cross-linking density, degree of crystallization, infrared spectroscopy and elastic modulus introduced in Section 10.2.3, the prepared thin silicone films of E1, E2, and E3 were also characterized in terms of mechanical hysteresis behavior, relative permittivity and dielectric breakdown strength.

Mechanical hysteresis tests

Mechanical hysteresis behavior was recorded using the aforementioned tensile test facility (Zwick Z020) at a testing rate of 200 mm/min. The test specimen was a rectangular strip of thin silicone film (50 mm free length, 25 mm width, ca. 150 µm thickness, according to ISO 527-3). Measurements were performed by the author at the Robert Bosch GmbH.

Dielectric spectroscopy

The relative permittivity of the prepared silicone films was determined by a broadband dielectric analyzer (Novocontrol, Montabaur, Germany). Permittivity spectra were recorded from 100 mHz up to 300 kHz. Relative permittivity values were derived from permittivity spectra at 10 Hz; all measurements were carried out at room temperature using a sample cell (BDS 1200, Novocontrol) with two gold-sputtered electrodes (10 mm in diameter, BDS 1301, Novocontrol). For each specimen at least five independent measurements were carried out. Measurements were performed by the author at the Robert Bosch GmbH.

Dielectric breakdown test

The test setup for the dielectric breakdown tests involved a HS 0111 instrument from Thalheimer Transformatorenwerke GmbH. An electrode setup was designed and fabricated by the author according to IEC 60243-1 standard, especially suitable for the characterization of soft elastomer thin films (Figure 83). It consisted of two electrodes (diameter 6 mm, tip radius 1 mm) made of a copper-zinc alloy, which were placed vertically in an isolated holder. The upper electrode was allowed to slide freely into the guide of the holder and touch the specimen's surface.
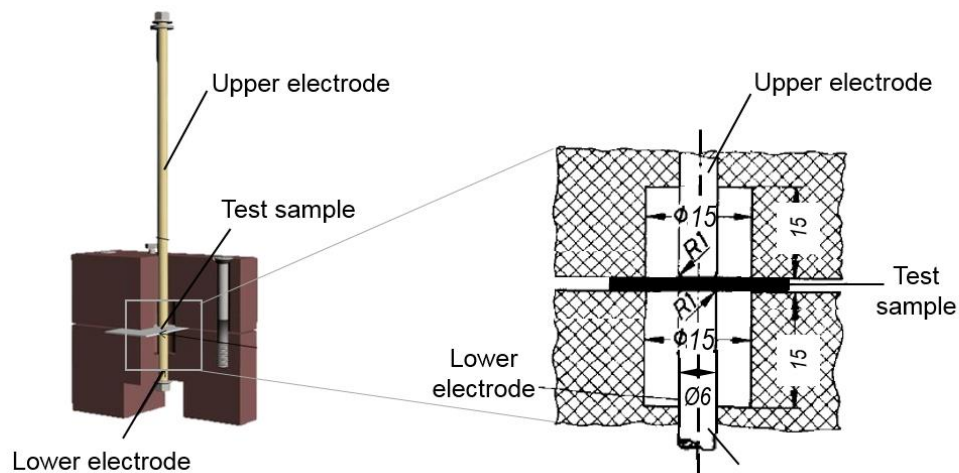
Figure 83. Self-developed electrode setup for dielectric breakdown tests of thin silicone films.

During testing, an AC (50 Hz) voltage was applied and increased at a rate of ca. 500 V/s until breakdown occurred. All tests were performed at room temperature. The critical field strength was calculated with respect to the initial thickness of the material, referred to as *engineering* breakdown strength. The initial thickness of the elastomer film was determined using a white light interferometer. Since the initial thickness of the sample was somehow higher than the real thickness under electrostatic pressure and under the weight of the upper electrodes, the estimated engineering breakdown strength was somehow lower than the *true* breakdown strength. At least five independent measurements were carried out; these were performed by the author at the Robert Bosch GmbH.

10.3.3 Storage tests on E3

Since E3 contained a high amount of hydrosilane groups after hydrosilylation, it was necessary to verify whether its properties had remained constant during storage over the time range equivalent to the ageing tests. The prepared E3 films were stored at room temperature over 23 days (almost the

maximum time duration investigated under mechanical ageing and electromechanical ageing). E3 films stored up to 48 h (2 day), 120 h (5 days), 168 h (7 days), and 552 h (23 days) were characterized in terms of cross-linking density, elastic modulus, relative permittivity, and breakdown strength.

10.4 Mechanical ageing

10.4.1 Materials

Self-prepared thin silicone films E1, E2, and E3, and the commercial material Elastosil, were mechanically fatigued (cycled until rupture). The film thickness was ca. 150 µm. The preparation process for E1, E2, and E3 is described in Section 10.2.2. The properties of the three thin films before mechanical cycling (referred to as *intact* specimen) are summarized in Table 10 (Section 4.1).

10.4.2 Mechanical fatigue tests

The mechanical testing facility for the thin silicone films (Figure 84) was developed by the author together with Mr. Jonas Fischer (Technical University of Darmstadt). It contained three independent loading units, each of which enabled a maximum displacement of 600 mm in the axial direction. Test specimens were rectangular strips 50 mm in free length and 25 mm in width (according to ISO 527-3). Specimens were mounted by clamps with rounded edges. Crack propagation from the edges was not observed. The lower jaw was driven by a linear motor, and in the upper jaw a load cell was mounted (maximum force 50 N, resolution 10 mN).

Figure 84. Self-developed testing facility for mechanical fatigue testing of thin silicone films.

Due to the non-linear behavior of the elastomer, mechanical fatigue tests were performed based on the Wöhler approach under strain-controlled conditions. Displacement was described as a sinusoidal

pulse at a frequency of 0.5 Hz. Six different strain amplitudes (S_a) were used (140, 130, 120, 100, 80 and 60% of initial length). The R-ratio, defined as the load minimum divided by the load maximum, was held at 0.2. For example, for S_a = 80%, specimens were cycled from 40 up to 200%.

Each specimen was cyclically loaded until rupture, which was defined as the *failure* of the specimen. The final cycle number that a specimen sustained until failure was recorded as N_f. For each material experiments were repeated 2-7 times[22], because in Wöhler tests N_f values are known to vary considerably. These ruptured specimens are denoted here as *fatigued* specimens, in contrast to *intact* specimens without any mechanical loading. The relationship between applied strain amplitude (S_a) and cycle number to failure (N_f) was characterized by the Wöhler curve, which is a linear fitting of the data points in the double logarithmic diagram. Based on the obtained Wöhler curve the characteristic lifetime (T) was estimated by using Weibull analysis as the cycle number at a 63.2% failure probability.

A further definition of *cycled* specimens is also mentioned in this thesis. These specimens were only mechanically cycled up to a given cycle number, which was lower than the N_f value. These *cycled* specimens were therefore not ruptured. Cycling tests were performed for E3 to verify the changes in cross-linking density during the load duration before rupture. Strain amplitudes employed were 140, 130, 120 and 100%.

During testing, stress-strain curves were recorded periodically to estimate the elastic modulus. The *fatigued* specimens were characterized with respect to their network structure as well as mechanical and electrical properties. The *cycled* specimens were then characterized with respect to changes in cross-linking density. All measurements were performed by the author at the Robert Bosch GmbH.

10.4.3 Characterization

Details on swelling measurements, ATR-FT-IR spectroscopy, DSC measurements, mechanical tensile testing, dielectric spectroscopy, breakdown tests and optical microscopy are outlined in Section 10.2.3 and Section 10.3.2.

10.5   Electromechanical ageing

10.5.1 Materials

Thin silicone films of E1, E2, E3, and Elastosil® P7670 were investigated. The film thickness was ca. 150 µm. The preparation process for E1, E2, and E3 is described in Section 10.2.2. For electromechanical ageing tests, silicone films were coated with compliant electrodes on both sides.

---

[22] The exact numbers of experiments refer to the corresponding Figures (Figure 44, 57, 75).

Three different types of electrodes were evaluated, i.e. carbon black, silver ink, and silver nanowire. The properties of these three electrode materials are outlined in Appendix 5. The silver nanowire exhibited low thickness, high compliance, and good conductivity, it was therefore chosen for preparing the specimens for electromechanical tests.

10.5.2 Preparation of silver nanowire electrodes

A solution of silver nanowire AgNW (SLV-NW-35, 10 mg/mL in 2-propanol) was purchased from BlueNano Inc. (Charlotte, USA). For preparation, 250 µL of the purchased AgNW solution was diluted in 50 mL of 2-propanol and then filtrated using a vacuum. A hydrophilic PTFE membrane filter (JVWP09025, pore size 0.1 µm), purchased from Merckmilipore (Darmstadt, Germany), was used for filtration. Thereafter, AgNWs were left on the PTFE filter while 2-propanol was fully removed. The PTFE filter was then cut into rectangles to a size of 25 mm × 35 mm. AgNWs were then transferred from this PTFE filter onto the surface of a thin silicone film. A schematic representation of this preparation process is shown in Figure 85. The preparation was performed by the author at the University of Stuttgart.
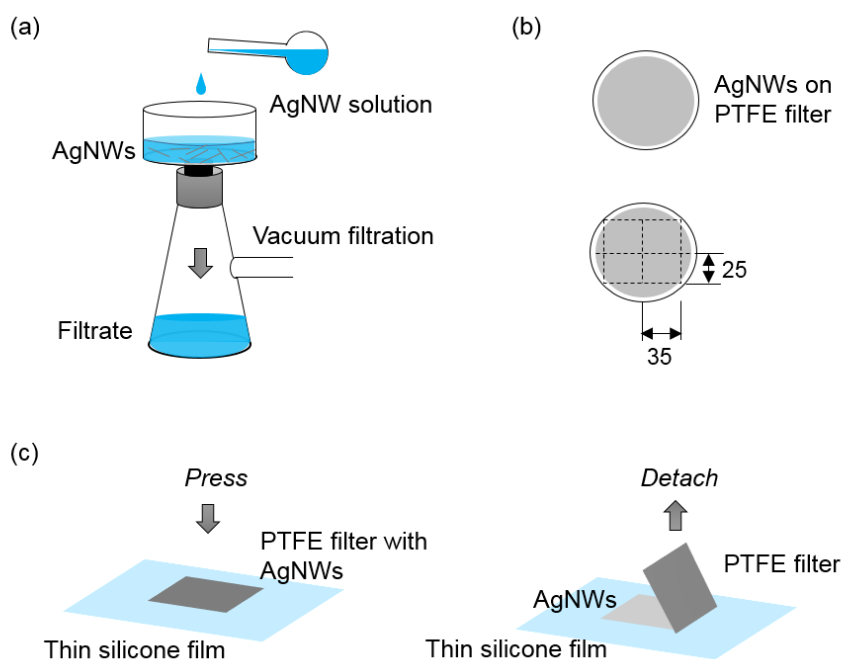
Figure 85. Preparation process for the silver nanowire (AgNW) electrode, (a) vacuum filtration (b) cut electrode with proper geometry, (c) transfer of silver nanowire (AgNW) onto the surface of a thin silicone film.

The prepared AgNW electrode showed an average thickness of ca. 3.1 µm, measured by white light interferometry. The electrode had low sheet resistance, both in the non-stretched (ca. 2.4 Ω/sq) and in the 10%-stretched state (ca. 86.0 Ω/sq). These resistance measurements were performed according to the so-called *four-points method*,[235, 236] using a test facility developed by Fraunhofer IST (Braunschweig, Germany) (Appendix 5). The surface of the prepared electrode was homogenous, as examined by optical microscopy (Figure 86a) and white light interferometry (Figure 86b).
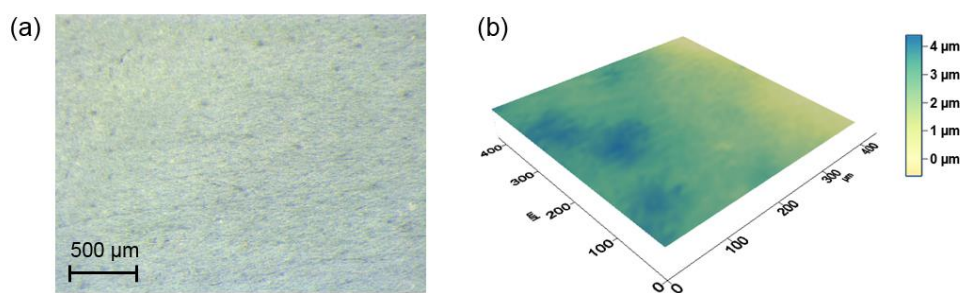
Figure 86. Surface characteristics of prepared silver nanowire electrode (a) optical surface image (b) 3D scan image measured by white light interferometer.

10.5.3 Electromechanical ageing tests

The test specimen used for electromechanical ageing tests comprised of one thin silicone film (ca. 150 mm x 150 mm) coated with AgNW electrodes (25 mm x 35 mm) on both sides. This gave an active area of ca. 25 mm x 25 mm (Figure 87a, b). Two copper wires with a diameter of 0.2 mm were connected to both electrodes using a silicone-based conductive paste (XCS 80255-1, Henkel, Germany). The coated silicone film was then placed onto a PTFE frame (2 mm in thickness) for testing (Figure 87c, d).
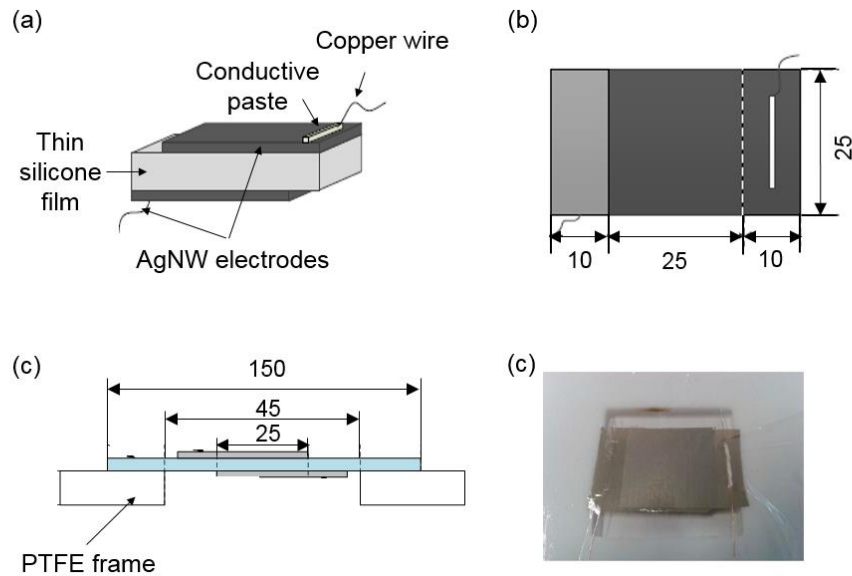
Figure 87. Geometry of the test specimen for electromechanical ageing tests.

The test setup is presented in Figure 88. An input signal was generated by a voltage generator (Agilent 33250A) and then multiplied by a high-voltage amplifier (TRek, Model 5/80) at a magnification of 2000. The test specimen was then connected to a real-time monitor, which measured the output signals of voltage $V(t)$ and the actuator's current $I(t)$. A web camera (Logitech C310) was placed about 40 cm above the test specimen to record actuator deformation (Figure 88a). All electromechanical ageing tests were carried out by applying a sinusoidal voltage of 2 kV (V_{pp} = 2 kV, V_{DC} = 1 kV) (Figure 88b) at 0.5 Hz up to several certain cycle numbers (ca. 10, 100, 10^3, 10^4 and 10^5 cycles). The applied voltage of 2 kV was chosen to avoid short-term breakdown and to generate an observable surface deformation of about 5% (approximate value due to the inhomogeneity of local deformations, see Figure 88c). Note that the electromechanical ageing tests were not based on the Wöhler approach but under a constant electrical load over given timespans. This was due to the fact that during testing no linear relationship between electrical voltage amplitude and cycle number up to electrical failure (double logarithmic) was observed.
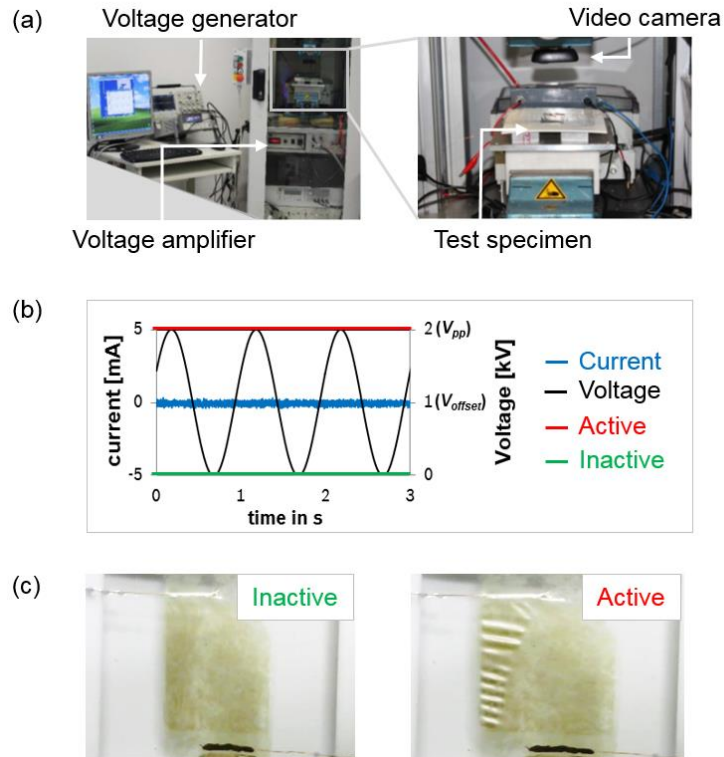
Figure 88. (a) High-voltage test setup for electromechanical ageing tests (b) sketch of the applied voltage and measured current (c) recorded images of inactive and active states of a test specimen during testing.

After ageing, the AgNW electrodes were removed using an adhesive foil and the bare silicone films were cut into proper size for subsequent characterization. In the present work, these thin silicone films after electromechanical ageing tests are referred to as electromechanically *aged* or *cycled* specimens. Sample preparation and measurements were performed by the author at the Robert Bosch GmbH.

10.5.4 Characterization

Details on swelling measurements, ATR-FT-IR spectroscopy, DSC measurements, mechanical tensile testing, dielectric spectroscopy, electrical breakdown testing, and optical microscopy are described in Section 10.2.3 and Section 10.3.2.

10.5.5 Comparison between electromechanical and mechanical ageing

The sole mechanical cycling tests at an equivalent deformation (ca. 5%) were performed on the mechanical fatigue test facility introduced in Section 10.4.2. Since the applied test facility can only

stretch specimens in the longitudinal direction, a strain amplitude causing stress equivalent to the one caused by electrostatic contraction was calculated. The calculation was based on the *principle strain theory*[230, 232, 237] of incompressible materials, which is briefly addressed in Appendix 7.

10.6 First comparisons with the post-cured material

Self-prepared silicone material, E3, was selected to investigate the long-term behavior of post-cured material, because E3 contained a significant excess of hydrosilanes. The post-curing process was conducted by heating the prepared E3 films overnight at 120°C. Storage tests were performed on post-cured E3 specimens, i.e. up to 48 h (2 day), 120 h (5 days), 168 h (7 days), and 552 h (23 days). These specimens were characterized in terms of cross-linking density, relative permittivity and breakdown strength. The post-cured E3 films were also subjected to mechanical fatigue tests and electromechanical ageing tests. Changes in network structure as well as mechanical and electrical properties were analyzed afterwards.

List of Abbreviations

DE	Dielectric Elastomer
EAP	Electroactive Polymer
EMI	Electromechanical Instability
PDMS	Polydimethylsiloxane
DSC	Differential Scanning Calorimetry
NMR	Nuclear Magnetic Resonance Spectroscopy
FT-IR	Fourier-Transform Infrared Spectroscopy
ATR	Attenuated Total Reflection
GPC	Gel Permeation Chromatography
ICP-OES	Inductively-Coupled Plasma Optical Emission Spectrometry
MALDI-TOF	Matrix-Assisted Laser Desorption/Ionization with Time-of-flight (ToF) Mass Analysis
IPG	Ionic Polymer Gel
IPMC	Ionic Polymer-Metal Composite
CP	Conductive Polymer
CNT	Carbon Nanotube
LCE	Liquid-Crystalline Elastomer
JPL	Jet Propulsion Laboratory of NASA (National Aeronautics and Space Administration)
CTS	Compliant Transducer Systems
FAPS	Institute for Factory Automation and Production Systems
ESNAM	European Scientific Network for Artificial Muscles
EMPA	Swiss Federal Laboratories for Materials Science and Technology
BRL	Bristol Robotics Laboratory
EPFL	Swiss Federal Institute of Technology in Lausanne
BMBF	German Ministry of Research
TUD	Technical University of Darmstadt
QMUL	Queen Mary University of London
OMMT	Organically Modified Montmorillonite
PHT	Poly(3-hexylthiophene)
M-Unit	$(CH_3)_3SiO$
D-Unit	$(CH_3)_2SiO_2$
T-Unit	$(CH_3)SiO_3$
Q-Unit	SiO_4
RTV	Room-Temperature Vulcanizing
HTV	High-Temperature Vulcanizing

HCR	High Consistency Rubber (Also Solid-Silicone Rubber)
LSR	Liquid-Silicone Rubber
DC	Direct Current (DC Voltage = Constant Voltage)
AC	Alternating Current (AC Voltage = Alternating Voltage)
pH	Numeric Scale of Acidity/Basicity
UV	Ultraviolet
FMEA	Failure Mode and Effects Analysis
LED	Light-Emitting Diode
Elastosil	Elastosil® P7670 (commercial silicone material, Wacker Chemie A)
AK35	WACKER® AK 35 (commercial silicone oil, Wacker Chemie AG)
N20	WACKER® HDK N20 (commercial silica,Wacker Chemie AG)
DMS	Commercial Vinyl-Terminated Polydimethylsiloxane, Gelest Inc.
HMS	Commercial Methylhydrosiloxane-Dimethylsiloxane Copolymer, Gelest Inc.
C200	Commercial Hydrosilane-Terminated Methylhydrosiloxane-Dimethyl-siloxane Copolymer, Evonik Hanse GmbH
SIP6830.3	Commercial Karstedt's Platinum Catalyst, Gelest Inc.
$CDCl_3$	Deuterated Chloroform
TMS	Tetramethylsilane
PTFE	Polytetrafluoroethylene
DCM	Dichloromethane
DHBA	2,4-Dihydroxybenzoic Acid
PET	Polyethylene Terephthalate
IEC	International Electrotechnical Commission
ISO	International Organization for Standardization
AgNW	Silver Nanowire

List of Tables

List of Figures

References

[1]   W. Noll, Properties of Technical Products, in *Chemistry and Technology of Silicones*, Academic Press, London, **1968**, p. 437.

[2]   J. D. W. Madden, N. A. Vandesteeg, P. A. Anquetil, P. G. A. Madden, A. Takshi, R. Z. Pytel, S. R. Lafontaine, P. A. Wieringa, I. W. Hunter, *IEEE-JOE* **2004**, *29*, 706.

[3]   F. B. Madsen, A. E. Daugaard, S. Hvilsted, A. L. Skov, *Macromol. Rapid Commun.* **2016**, *37*, 378.

[4]   A. O'Halloran, F. O'Malley, P. McHugh, *J. Appl. Phys.* **2008**, *104*, 071101.

[5]   R. F. Shepherd, F. Ilievski, W. Choi, S. A. Morin, A. A. Stokes, A. D. Mazzeo, X. Chen, M. Wang, G. M. Whitesides, *Proc. Natl. Acad. Sci.* **2011**, *108,* 20400.

[6]   S. Shian, R. M. Diebold, D. R. Clarke, *Opt. Express* **2013**, *21*, 8669.

[7]   M. Matysek, P. Lotz, T. Winterstein, H. F. Schlaak, Dielectric elastomer actuators for tactile displays, in *Third Joint Eurohaptics Conference and Symposium on Haptic Interfaces for Virtual Environment and Teleoperator Systems*, Salt Lake City, **2009,** p. 290.

[8]   Y. Fouillet, O. Fuchs, S. Maubert, M. Cochet, F. Baleras, C. Chabrol, N. David, R. Campagnolo, *Procedia Eng.* **2012**, *47*, 314.

[9]   M. Giousouf, G. Kovacs, *Smart Mater. Struct.* **2013**, *22*, 104010.

[10]   R. Pelrine, R. Kornbluh, Q. Pei, J. Joseph, *Science* **2000**, *287*, 836.

[11]   H. B. Callen, *Phys. Rev.* **1949**, *76*, 1394.

[12]   M. Matysek, P. Lotz, H. F. Schlaak, *IEEE Trans. Dielectr. Electr. Insul.* **2011**, *18*, 89.

[13]   L. Mullins, *Rubber Chem. Technol.* **1969**, *42*, 339.

[14]   F. Bueche, *J. Appl. Polym. Sci.* **1960**, *4*, 107.

[15]   S. Cantournet, R. Desmorat, J. Besson, *Int. J. Solids Struct.* **2009**, *46*, 2255.

[16]   C. Svaneborg, R. Everaers, G. S. Grest, J. G. Curro, *Macromolecules* **2008**, *41*, 4920.

[17]   M. M. Caruso, D. A. Davis, Q. Shen, S. A. Odom, N. R. Sottos, S. R. White, J. S. Moore, *Chem. Rev.* **2009**, *109*, 5755.

[18]   R. S. Porter, A. Casale, *Polym. Eng. Sci.* **1985**, *25*, 129.

[19]   B. Terselius, U. W. Gedde, J. F. Jansson, Mechano-chemical phenomena in polymers, in *Failure of Plastics*, Carl Hanser Verlag, München, **1986**, p. 273.

[20]   H. Staudinger, H. F. Bondy, *Ber. Dtsch. Chem. Ges.* **1930**, *63*, 734.

[21]   W. Kauzmann, H. Eyring, *J. Amer. Chem. Soc.* **1940**, *62*, 3113.

[22]   H. H. Kausch, *Polymer Fracture: Polymers/Properties and Applications*, Springer, New York, **1978**, p. 251.

[23]   H. H. Kausch, C. J. G. Plummer, *Polymer* **1994**, *35*, 3848.

[24]   S. Zakaria, L. Yu, G. Kofod, A. L. Skov, *Mater. Today Commun.* **2015**, *4*, 204.

[25]   F. B. Madsen, S. Zakaria, L. Yu, A. L. Skov, *Adv. Eng. Mater.* **2016**, *18,* 1154.

[26]   Z. Suo, *Acta Mech. Solida Sin.* **2010**, *23*, 549.

[27]   C. W. Reed, S. W. Cichanowski, *IEEE Trans. Dielectr. Electr. Insul.* **1994**, *1*, 904.

[28]   J. L. Goudie, M. J. Owen, T. Orbeck, A review of possible degradation mechanisms of silicone elastomers in high voltage insulation applications, in *Conference on Electrical Insulation and Dielectric Phenomena (CEIDP)*, Proc. IEEE, Atlanta, **1998**, p. 120.

[29]   Y. X. Zhou, Q. Nie, Z. Z. Chen, R. Liu, *J. Phy. Conf. Ser.* **2009**, *183*, 012013.

[30]   I. Prasertsung, S. Damrongsakkul, N. Saito, *Plasma Process Polym.* **2013**, *10*, 792.

[31]   F. Galantini, G. Gallone, F. Carpi, *IEEE Trans. Dielec. Electr. Insul.* **2012**, *19*, 1203.

[32]   V. V. Kochervinskii, M. A. Shcherbina, N. P. Bessonova, V. I. Gerasimov, S. N. Udra, D. V. Petkieva, A. S. Pavlov, N. A. Shmakova, N. V. Kozlova, *Polym. Sci. Ser. A* **2013**, *55*, 540.

[33]   F. Virlogeux, D. Bianchini, F. Delor-Jestin, M. Baba, J. Lacoste, *Polym. Int.* **2004**, *53*, 163.

[34]   H. Hillborg, U. W. Gedde, Hydrophobicity recovery of polydimethylsiloxane after repeated exposure to corona discharges. Influence of crosslink density, in *1999 Annual Report Conference on Electrical Insulation and Dielectric Phenomena (CEIDP)*, Proc. IEEE, Austin, **1999**, p. 751.

[35]   D. Andjelkovic, N. Rajakovic, *Electr. Eng.* **2001**, *83*, 83.

[36]   W. C. Roentgen, *Ann. Phys. Chem.* **1880**, *11*, 771.

[37]   M. P. Sacerdote, *J. Phys.* **1899**, *31*, 282.

[38]   M. Eguchi, *Phil. Mag.* **1925**, *49*, 178.

[39]   V. L. Finkenstadt, *Appl. Microbiol. Biotechnol.* **2005**, *67*, 735.

[40]   R. E. Pelrine, R. Kornbluh, *Dielectric Elastomers as Electromechanical Transducers: Fundamentals, Materials, Devices, Models and Applications of an Emerging Electroactive Polymer Technology*, Elsevier Science, Amsterdam, **2008**, p. 14.

[41]   R. Pelrine, R. Kornbluh, G. Kofod, *Adv. Mater.* **2000**, *12*, 1223.

[42]   S. Mohsen, J. K. Kwang, *Smart Mater. Struct.* **2001**, *10*, 819.

[43]   T. Ikeda, *Fundamentals of Piezoelectricity*, Oxford University Press, Oxford, **1996**, p. 196.

[44]   R. Kornbluh, J. Eckerle, G. Andeen, Artificial muscle: The next generation of robotic actuators, in *4th World Conference of Robotics Research*, SME Paper, Pittsburg, **1991**, p. 91.

[45]   R. Kornbluh, R. Pelrine, J. Eckerle, J. Joseph, Electrostrictive polymer artificial muscle actuators, in *IEEE International Conference on Robotics and Automation (ICRA)*, Proc. IEEE, **1998**, p. 2147.

[46]   R. Kornbluh, A. Wong-Foy, R. Pelrine, H. Prahlad, B. McCoy, *Mater. Res. Soc. Symp. Proc.* **2010**, *1271*, 1271.

[47]   R. J. Eckerle, S. Chiba, Review of artificial muscle approaches, in *3rd International Symposium on Micro Machine and Human Science (MHS)*, Nagoya, **1992**, p. 1.

[48]   R. A. Anderson, *Phys. Rev. B* **1986**, *33*, 1302.

[49]   R. Pelrine, R. D. Kornbluh, J. Eckerle, P. Jeuck, S. Oh, Q. Pei, S. Stanford, Dielectric elastomers: generator mode fundamentals and applications, in *Smart Structures and Materials 2001: Electroactive Polymer Actuators and Devices (EAPAD)*, Proc. SPIE, Newport Beach, **2001**, p. 148.

[50]   Á. Pintér, I. Dénes, *IET Sci. Meas. Technol.* **2015**, *9*, 570.

[51]   S. C. B. Mannsfeld, B. C. K. Tee, R. M. Stoltenberg, C. V. H. H. Chen, S. Barman, B. V. O. Muir, A. N. Sokolov, C. Reese, Z. Bao, *Nat. Mater.* **2010**, *9*, 859.

[52]   K. Guggi, *J. Phys. D Appl. Phys.* **2008**, *41*, 215405.

[53] H. R. Choi, K. Jung, N. H. Chuc, M. Jung, I. Koo, J. Koo, J. Lee, J. Lee, J. Nam, M. Cho, Y. Lee, Effects of prestrain on behavior of dielectric elastomer actuator, in *Smart Structures and Materials 2005: Electroactive Polymer Actuators and Devices (EAPAD)*, Proc. SPIE, San Diego, **2005**, p. 283.

[54] R. D. Kornbluh, R. Pelrine, J. Joseph, R. Heydt, Q. Pei, S. Chiba, High-field electrostriction of elastomeric polymer dielectrics for actuation, in *Symposium on Smart Structures and Materials*, Proc. SPIE, Newport Beach, **1999**, p. 149.

[55] R. Pelrine, R. Kornbluh, J. Joseph, S. Chiba, Electrostriction of polymer films for microactuators, in *10th Annual International Workshop on Micro Electro Mechanical Systems (MEMS)*, Proc. IEEE, Nagoya, **1997,** p. 238.

[56] K. Jung, J. Nam, Y. Lee, H. Choi, Micro inchworm robot actuated by artificial muscle actuator based on nonprestrained dielectric elastomer, in *Smart Structures and Materials 2004: Electroactive Polymer Actuators and Devices (EAPAD)*, Proc. SPIE, San Diego, **2004**, p. 357.

[57] R. D. Kornbluh, R. Pelrine, Q. Pei, R. Heydt, S. Stanford, S. Oh, J. Eckerle, Electroelastomers: applications of dielectric elastomer transducers for actuation, generation, and smart structures, in *Smart Structures and Materials 2002: Industrial and Commercial Applications of Smart Structures Technologies*, Proc. SPIE, San Diego, **2002**, p. 254.

[58] N. Hosoya, S. Baba, S. Maeda, *J. Acoust. Soc. Am.* **2015**, *138*, 424.

[59] O. A. Araromi, I. Gavrilovich, J. Shintake, S. Rosset, M. Richard, V. Gass, H. R. Shea, *IEEE/ASME Trans. Mechatronics* **2015**, *20*, 438.

[60] E. Biddiss, T. Chau, *Med. Eng. Phys.* **2008**, *30*, 403.

[61] S. Kim, C. Laschi, B. Trimmer, *Trends Biotechnol.* **2013**, *31*, 287.

[62] F. Carpi, G. Frediani, S. Turco, D. De Rossi, *Adv. Funct. Mater.* **2011**, *21*, 4002.

[63] C. Jordi, S. Michel, E. Fink, *Bioinspir. Biomim.* **2010**, *5*, 026007.

[64] R. Jonathan, Y. Bryan, C. Andrew, *Bioinspir. Biomim.* **2012**, *7*, 036009.

[65] M. Matysek, P. Lotz, K. Flittner, H. F. Schlaak, *Polymer* **2010**, *7642*, 76420D.

[66] S. Rosset, H. R. Shea, *Appl. Phys. A* **2012**, *110*, 281.

[67] I. M. Graz, D. P. J. Cotton, S. P. Lacour, *Appl. Phys. Lett.* **2009**, *94*, 071902.

[68] W. Yuan, P. Brochu, H. Zhang, A. Jan, Q. Pei, Long lifetime dielectric elastomer actuators under continuous high strain actuation, in *Electroactive Polymer Actuators and Devices (EAPAD)*, Proc. SPIE, San Diego, **2009**, p. 7287.

[69] J.-H. Choi, J. Ahn, J.-B. Kim, Y.-C. Kim, J.-Y. Lee, I.-K. Oh, *Small* **2016**, *12*, 1840.

[70] S. Yun, X. Niu, Z. Yu, W. Hu, P. Brochu, Q. Pei, *Adv. Mater.* **2012**, *24*, 1321.

[71] P. Lee, J. Lee, H. Lee, J. Yeo, S. Hong, K. H. Nam, D. Lee, S. S. Lee, S. H. Ko, *Adv. Mater.* **2012**, *24*, 3326.

[72] K. Wongtimnoi, B. Guiffard, A. Bogner-Van de Moortèle, L. Seveyrat, J. Y. Cavaillé, *Compos. Sci. Technol.* **2013**, *85*, 23.

[73] T. Chen, J. Qiu, K. Zhu, J. Li, *Mater. Des.* **2016**, *90*, 1069.

[74] Y. Bar-Cohen, Electroactive polymers: current capabilities and challenges, in *Smart Structures and Materials 2002: Electroactive Polymer Actuators and Devices (EAPAD)*, Proc. SPIE, San Diego, **2002**, p. 02.

[75] G. Kofod, P. Sommer-Larsen, R. Kornbluh, R. Pelrine, *J. Intell. Mater. Syst. Struct.* **2003**, *14*, 787.

[76] S. Michel, X. Q. Zhang, M. Wissler, C. Löwe, G. Kovacs, *Polym. Int.* **2010**, *59*, 391.

[77]   M. Molberg, D. Crespy, P. Rupper, F. Nüesch, J.-A. E. Månson, C. Löwe, D. M. Opris, *Adv. Funct. Mater.* **2010**, *20*, 3280.

[78]   F. Carpi, G. Gallone, F. Galantini, D. De Rossi, *Adv. Funct. Mater.* **2008**, *18*, 235.

[79]   H. Li, H. Liu, J. Li, D. Wei, Y. Wang, B. Song, *Sci. Eng. Compos. Mater.* **2015**, *22*, 215.

[80]   L. Liu, Z. Zhang, J. Li, T. Li, Y. Liu, J. Leng, *Compos. B. Eng.* **2015**, *78*, 35.

[81]   G. Fabia, B. Sabrina, C. Valter, G. Giuseppe, *Smart Mater. Struct.* **2013**, *22*, 055025.

[82]   B. Kussmaul, S. Risse, G. Kofod, R. Waché, M. Wegener, D. N. McCarthy, H. Krüger, R. Gerhard, *Adv. Funct. Mater.* **2011**, *21*, 4589.

[83]   C. Tugui, G. Stiubianu, M. Iacob, C. Ursu, A. Bele, S. Vlad, M. Cazacu, *J. Mater. Chem. C.* **2015**, *3*, 8963.

[84]   N. R. Thomas, *Silicon* **2010**, *2*, 187.

[85]   H. Dodiuk, S. H. Goodman, *Handbook of Thermoset Plastics*, William Andrew Inc., New York, **2013**, p. 555.

[86]   P. Jerschow, *Silicone Elastomers*, Smithers Rapra Publishing, London, **2002**, p. 137.

[87]   B. D. Karstedt, US Patent 3, **1973**, *775*, 452,

[88]   B. Marciniec, H. Maciejewski, C. Pietraszuk, P. Pawluc, J. Gulinski, *Hydrosilylation: A Comprehensive Review on Recent Advances*, Springer Science+Business Media B.V., Berlin **2009**, p. 176.

[89]   C. W. Macosko, G. S. Benjamin, *Pure Appl. Chem.* **1981**, *53*, 1505.

[90]   C. W. Macosko, J. C. Saam, *Polym. Bull.* **1987**, *18*, 463.

[91]   F. Chambon, H. H. Winter, *J. Rheol.* **1987**, *31*, 683.

[92]   A. L. Larsen, K. Hansen, P. Sommer-Larsen, O. Hassager, A. Bach, S. Ndoni, M. Jørgensen, *Macromolecules* **2003**, *36*, 10063.

[93]   P. J. Flory, *J. Am. Chem. Soc.* **1941**, *63*, 3083.

[94]   A. L. Larsen, P. Sommer-Larsen, O. Hassager, e-*Polymers* **2004**, *050*, 1.

[95]   A. C. C. Esteves, J. Brokken-Zijp, J. Laven, H. P. Huinink, N. J. W. Reuvers, M. P. Van, G. de With, *Polymer* **2009**, *50*, 3955.

[96]   K. Seog-Hyeon, E. A. Cherney, R. Hackam, K. G. Rutherford, *IEEE Trans. Dieletric. Electr. Insul.* **1994**, *1*, 106.

[97]   S. Frankær, M. Jensen, A. Bejenariu, A. Skov, *Rheol. Acta* **2012**, *51*, 559.

[98]   J. L. Braun, J. E. Mark, B. E. Eichinger, *Macromolecules* **2002**, *35*, 5273.

[99]   E. M. Dannenberg, *Rubber Chem. Technol.* **1975**, *48*, 410.

[100]   E. M. Dannenberg, *Trans. Inst. Rubber Ind.* **1966**, *42*, 26.

[101]   I. Drogin, T. H. Messenger, *Proc. 3rd Rubber Techn. Conf.*, Cambridge W. Heffer & Sons Ltd., Cambridge, **1954**, p. 585.

[102]   P. J. Flory, J. Rehner, *J. Chem. Phys.* **1943**, *11*, 521.

[103]   L. H. Sperling, Crosslinked Polymers and Rubber Elasticity, in *Introduction to Physical Polymer Science*, John Wiley & Sons Inc., Hoboken, **2005**, p. 427.

[104]   M. I. Aranguren, *Polymer* **1998**, *39*, 4897.

[105]   J. Jancar, Structure-Property Relationships in Thermoplastic Matricles, in *Advances in Polymer Science*, Springer, Berlin, **1999**, p. 1.

[106] J. D. Hoffman, G. T. Davis, J. I. Lauritzen Jr., The Rate of Crystallization of Linear Polymers with Chain Folding, in *Treatise on Solid State Chemistry*, Plenum Press, New York, **1976**, p. 497.

[107] L. Mandelkern, *Polym. J.* **1985**, *17*, 337.

[108] L. Mandelkern, *Crystallization Of Polymers,* McGraw Hill, New York, **1964**, p. 191.

[109] B. Wunderlich, *Macromolecular Physics. Volume 2: Crystal Nucleation, Growth, Annealing*, Academic Press, New York, **1976**, p. 1.

[110] H. M. James, *J. Chem. Phys.* **1947**, *15*, 651.

[111] W. Kuhn, *J. Polym. Sci.* **1946**, *1*, 380.

[112] P. J. Flory, J. Rehner, *J. Chem. Phys.* **1943**, *11*, 512.

[113] A. N. Gent, W. V. Mars, Strength of Elastomers, in *The Science and Technology of Rubber,* Academic Press, Boston, **2013**, p. 473.

[114] J. Gough, *Philos. Mag.* **1806**, *24*, 103.

[115] P. J. Flory, *Principles of Polymer Chemistry*, Cornell University Press, New York, **1953**, p. 464.

[116] I. J. Rao, K. R. Rajagopal, *Int. J. Solids Struct.* **2001**, *38*, 1149.

[117] S. Toki, T. Fujimaki, M. Okuyama, *Polymer* **2000**, *41*, 5423.

[118] J.-M. Chenal, C. Gauthier, L. Chazeau, L. Guy, Y. Bomal, *Polymer* **2007**, *48*, 6893.

[119] P.-H. Sung, S.-Y. Wu, *Polymer* **1998**, *39*, 7033.

[120] C. W. Macosko, *Rheology: Principles, Measurements, and Applications*, Wiley-VCH Verlag, New York, **1994**, p. 37.

[121] A. C. Ugural, S. K. Fenster, *Advanced Strength and Applied Elasticity*, Prentice Hall College Div, New Jersey, **1981**, p. 88.

[122] M. Mooney, *J. Appl. Phys.* **1940**, *11*, 582.

[123] R. Rivlin, *Phil. Trans. R. Soc. A* **1948**, *241*, 379.

[124] R. W. Ogden, *Proc. R. Soc. A* **1972**, *326*, 565.

[125] M. A. Meyers, K. K. Chawla, *Mechanical Behavior of Materials*, Cambridge University Press, Cambridge, **2009**, p. 688.

[126] N. G. McCrum, C. Buckley, C. B. Bucknall, *Principles of Polymer Engineering*, Oxford University Press, New York, **1997**, p. 118.

[127] A. E. H. Love, *A Treatise on the Mathematical Theory of Elasticity*, Cambridge University Press, London, **2013**, p. 120.

[128] A. Dorfmann, R. W. Ogden, *Int. J. Solids Struct.* **2004**, *41*, 1855.

[129] D. E. Hanson, M. Hawley, R. Houlton, K. Chitanvis, P. Rae, E. B. Orler, D. A. Wrobleski, *Polymer* **2005**, *46*, 10989.

[130] A. Y. Coran, Vulcanization, in *The Science and Technology Of Rubber*, Academic Press, San Diego, **1994**, p. 326.

[131] G. Kofod, *Dielectric Elastomer Actuators*, *Ph.D. Dissertation*, The Technical University of Denmark, **2001**.

[132] B. Kussmaul, *Modifizierung von Silikonelastomeren mit organischen Dipolen für Dielektrische Elastomer Aktuatoren*, *Ph.D. Dissertation*, University of Potsdam, **2013**.

[133] A. Schönhals, Dielctric properties of amorphous polymers, in *Dielectric Spectroscopy of Polymeric Materials: Fundamentals and Applications*, ACS Publisher, Washington, **1997**, p. 81.

[134] A. Schönhals, E. Schlosser, *Colloid Polym. Sci.* **1989**, *267*, 125.

[135] P. Debye, *Polar molecules,* The Chemical Catalog Company Inc., New York, **1929**, p. 172.

[136] S. Havriliak, S. Negami, *J. Polym. Sci.* **1966**, *14*, 99.

[137] S. Havriliak, S. Negami, *Polymer* **1967**, *8*, 161.

[138] G. Williams, D. C. Watts, *Trans. Faraday. Soc.* **1970**, *66*, 80.

[139] J. K. W. Glatz-Reichenbach, L. Sorriero, J. J. Fitzgerald, *Macromolecules* **1994**, *27*, 1338.

[140] E. Schlosser, A. Schönhals, *Colloid Polym. Sci.* **1989**, *267*, 133.

[141] R. J. Seeger, E. Teller, *Phy. Rev.* **1939**, *56*, 352.

[142] A. V. Hippel, R. S. Alger, *Phys. Rev.* **1949**, *76*, 127.

[143] H. Fröhlich, *Phys. Rev.* **1939**, *56*, 349.

[144] R. Cooper, *Br. J. Appl. Phys.* **1966**, *17*, 149.

[145] J. Blok, D. G. LeGrand, *J. Appl. Phys.* **1969**, *40*, 288.

[146] L. A. Dissado, J. C. Fothergill, *Electrical Degradation and Breakdown in Polymers*, IET, London, **1992**, p. 271.

[147] V. Rajini, K. Udayakumar, *IEEE Trans. Dielectr. Electr. Insul.* **2009**, *16*, 834.

[148] N. Yoshimura, S. Kumagai, *IEEE Trans. Dielectr. Electr. Insul.* **1999**, *6*, 632.

[149] K. H. Stark, C. G. Garton, *Nature* **1955**, *176*, 1225.

[150] H. Wang, Z. Zeng, Electric Breakdown Model for Super-Thin Polyester Foil, in *Polyester*, InTech, Rijeka, **2012**, p. 359.

[151] H. R. Zeller, W. R. Schneider, *J. Appl. Phys.* **1984**, *56*, 455.

[152] J. C. Fothergill, Filamentary electromechanical breakdown in polymers, in *4th International Conference on Conduction and Breakdown in Solid Dielectrics (ICSD)*, Proc. IEEE, Sestri Levante, **1992,** p. 323.

[153] F. Abraham, T. Alshuth, S. Jerrams, *Mater. Des.* **2005**, *26*, 239.

[154] T. Alshuth, F. Abraham, S. Jerrams, *Rubber Chem. Technol.* **2002**, *75*, 635.

[155] D. Radaj, M. Vormwald, *Ermüdungsfestigkeit: Grundlagen für Ingenieure*, Springer, Berlin-Heidelberg, **2007**, p. 15.

[156] D. Radaj, M. Vormwald, *Advanced Methods of Fatigue Assessment*, Springer, Berlin-Heidelberg, **2013**, p. 227.

[157] W. Weibull, *J. Appl. Mech.* **1951**, *18*, 293.

[158] Q. Zhuang, P. H. F. Morshuis, X. Chen, S. Meijer, J. J. Smit, Z. Xu, Life prediction for epoxy resin insulated transformer windings through accelerated aging tests, in *10th International Conference on Solid Dielectrics (ICSD)*, Proc. IEEE, Postdam, **2010,** p. 1.

[159] P. Lotz, M. Matysek, H. F. Schlaak, Lifetime of dielectric elastomer stack actuators, in *Electroactive Polymer Actuators and Devices (EAPAD)*, Proc. SPIE 7976, San Diego, **2011**, p. 7976.

[160] E. S. Lindquist, *Probabilist. Eng. Mech.* **1994**, *9*, 191.

[161] W. Weibull, *A Statistical Theory of the Strength of Materials*, Generalstabens Litografiska Anstalts Forlag, Stockholm, **1939**, p. 12.

[162] J. W. McPherson, *Reliability Physics and Engineering: Time-To-Failure Modeling*, Springer, New York, **2010**.

[163] P. Lotz, M. Matysek, H. F. Schlaak, Climatic influences on the lifetime of dielectric elastomer stack actuators, presented at *International conference on Electromechanically Active Polymer (EAP) transducers & artificial muscles (EuroEAP)*, Pisa, **2011**.

[164] C. Federico, A. Iain, B. Siegfried, F. Gabriele, G. Giuseppe, G. Massimiliano, G. Christian, J.-M. Claire, K. William, K. Guggi, K. Matthias, K. Roy, L. Benny, M. Marc, M. Silvain, N. Stephan, O. B. Benjamin, P. Qibing, P. Ron, R. Björn, R. Samuel, S. Herbert, *Smart. Mater. Struct.* **2015**, *24*, 105025.

[165] H. Staudinger, *Die Hochmolekularen Organischen Verbindungen - Kautschuk und Cellulose,* Springer, Berlin, **1932**.

[166] M. A. Natov, S. V. Vasil'eva, V. S. Kabaivanov, *Polym. Sci. USSR* **1969**, *11*, 1467.

[167] K. Jacobson, B. Stenberg, B. Terselius, T. Reitberger, Oxidation of stressed polymers as studied by chemiluminescence, in *Ageing Studies and Lifetime Extension of Materials*, Kluwer Academic/Plenum Publisher, New York, **2001**, p. 253.

[168] A. N. Gent, C. Wang, *J. Mater. Sci.* **1991**, *26*, 3392.

[169] A. N. Gent, *Rubber Chem. Technol.* **1990**, *63*, 49.

[170] W. Schütz, *Eng. Fract. Mech.* **1996**, *54*, 263.

[171] W. V. Mars, A. Fatemi, *Int. J. Fatigue* **2002**, *24*, 949.

[172] A. N. Gent, P. B. Lindley, *P Roy. Soc. A-Math. Phy.* **1959**, *249*, 195.

[173] S. N. Zhurkov, V. A. Zakrevskyi, V. E. Korsukov, V. S. Kuksenko, *J. Polym. Sci., Part B: Polym. Phys.* **1972**, *10*, 1509.

[174] S. N. Zhurkov, V. S. Kuksenko, A. I. Slutsker, *Strength Mater.* **1971**, *3*, 162.

[175] S. N. Zhurkov, V. E. Korsukov, *J. Polym. Sci. Phys. Ed.* **1974**, *12*, 385.

[176] A. A. Griffith, *Phil. Trans. R. Soc. A* **1921**, *221*, 163.

[177] E. David, J. L. Parpal, J. P. Crine, *IEEE Trans. Dielectr. Electr. Insul.* **1996**, *3*, 248.

[178] N. Ranc, D. Wagner, P. C. Paris, *Acta Mater.* **2008**, *56*, 4012.

[179] D. Zhu, R. A. Miller, *Mater. Sci. Eng. A* **1998**, *245*, 212.

[180] I. Constable, J. G. Williams, D. J. Burns, *J. Mech. Eng. Sci.* **1970**, *12*, 20.

[181] D. Nguyen Dang, B. Peraudeau, S. Cohendoz, S. Mallarino, X. Feaugas, S. Touzain, *Electrochim. Acta* **2014**, *124*, 80.

[182] A. N. Gent, E. A. Meinecke, *Polym. Eng. Sci.* **1970**, *10*, 48.

[183] D. Zenkert, M. Burman, *Compos. Sci. Technol.* **2009**, *69*, 785.

[184] D. Chinh, J. L. Parpal, J. P. Crine, *IEEE Trans. Dielectr. Electr. Insul.* **1996**, *3*, 237.

[185] J. L. Parpal, J. P. Crine, D. Chinh, *IEEE Trans. Dielectr. Electr. Insul.* **1997**, *4*, 197.

[186] R. S. Gorur, G. G. Karady, A. Jagota, M. Shah, A. M. Yates, *IEEE Trans. Power Del.* **1992**, *7*, 525.

[187] J. P. Reynders, I. R. Jandrell, *IEEE Trans. Dielectr. Electr. Insul.* **1999**, *6*, 620.

[188] V. Ollier-Durbault, B. Gosse, *IEEE Trans. Dielectr. Electr. Insul.* **1998**, *5*, 935.

[189] T. Ebke, A. Khaddour, D. Peier, Degradation of silicone gel by partial discharges due to different defects, in *8th International Conference on Dielectric Materials, Measurements and Applications (DMMA)*, Proc. IEEE, Edinburgh, **2000**, p. 202.

[190] J. P. Crine, J. L. Parpal, C. Dang, *IEEE Trans. Dielectr. Electr. Insul.* **1997**, *143*, 395.

[191] J. Kim, M. K. Chaudhury, M. J. Owen, T. Orbeck, *J. Colloid Interface Sci.* **2001**, *244*, 200.

[192] M. A. Imam, J. Shaik, K. R. Vijaya, *Int. J. Nanosci.* **2016**, *15*, 1650004.

[193] A. J. Berejka, D. Montoney, M. R. Cleland, L. Loiseau, *Nukleonika* **2010**, *55*, 97.

[194] R. S. Maxwell, S. C. Chinn, D. Solyom, R. Cohenour, *Macromolecules* **2005**, *38*, 7026.

[195] B. Ma, S. M. Gubanski, H. Hillborg, *IEEE Trans. Dielectr. Electr. Insul.* **2011**, *18*, 1984.

[196] I. Stevenson, L. David, C. Gauthier, L. Arambourg, J. Davenas, G. Vigier, *Polymer* **2001**, *42*, 9287.

[197] R. Polansky, P. Prosr, V. Mentlik, M. Pinkerova, *Prz. Elektrotechniczny* **2012**, *88*, 249.

[198] D. J. T. Hill, C. M. L. Preston, D. J. Salisbury, A. K. Whittaker, *Radiat. Phys. Chem.* **2001**, *62*, 11.

[199] J. M. Spruell, M. Wolffs, F. A. Leibfarth, B. C. Stahl, J. Heo, L. A. Connal, J. Hu, C. J. Hawker, *J. Am. Chem. Soc.* **2011**, *133*, 16698.

[200] L. Ślusarski, *J. Therm. Anal. Calorim.* **1984**, *29*, 905.

[201] K. Xiang, G. Huang, J. Zheng, X. Wang, G. Li, J. Huang, *J. Polym. Res.* **2012**, *19*, 1.

[202] P. M. Visakh, A. Yoshihiko, *Thermal Degradation of Polymer Blends, Composites and Nanocomposites*, Springer, Switzerland, **2015**, p. 157.

[203] G. Camino, S. Lomakin, M. Lazzari, *Polymer* **2001**, *42*, 2395.

[204] G. Camino, S. Lomakin, M. Lageard, *Polymer* **2002**, *43*, 2011.

[205] F.-S. Chuang, H.-Y. Tsi, J.-D. Chow, W.-C. Tsen, Y.-C. Shu, S.-C. Jang, *Polym. Degrad. Stabil.* **2008**, *93*, 1753.

[206] M. Celina, K. T. Gillen, R. Assink, *Polym. Degrad. Stabil.* **2005**, *90*, 395.

[207] S. Ciutacu, P. Budrugeac, I. Niculae, *Polym. Degrad. Stabil.* **1991**, *31*, 365.

[208] C.-W. Hsu, C.-C. M. Ma, C.-S. Tan, H.-T. Li, S.-C. Huang, T.-M. Lee, H. Tai, *Mater. Chem. Phys.* **2012**, *134*, 789.

[209] M. S. Montaudo, C. Puglisi, F. Samperi, G. Montaudo, *Rapid Commun. Mass Spectrom.* **1998**, *12*, 519.

[210] C. Schneider, M. Sablier, B. Desmazières, *Rapid Commun. Mass Spectrom.* **2008**, *22*, 3353.

[211] S. M. Hunt, G. A. George, *Polym. Int.* **2000**, *49*, 633.

[212] C. A. Jackson, W. J. Simonsick Jr, *Curr. Opin. Solid State Mater. Sci.* **1997**, *2*, 661.

[213] G. Montaudo, M. S. Montaudo, C. Puglisi, F. Samperi, *Rapid Commun. Mass Spectrom.* **1995**, *9*, 1158.

[214] C. Zhang, L. Liu, Z. Zhang, K. Pal, J.-K. Kim, *J. Macromol. Sci., Phys.* **2011**, *50*, 1144.

[215] G. Shah, *Express Polym. Lett.* **2008**, *2*, 829.

[216] K. Mojsiewicz-Pieńkowska, *J. Chromatogr. B* **2008**, *865*, 1.

[217] I. V. Blagodatskikh, M. V. Sutkevich, N. L. Sitnikova, N. A. Churochkina, T. A. Pryakhina, O. E. Philippova, A. R. Khokhlov, *J. Chrom. A* **2002**, *976*, 155.

[218] S. K. Patel, S. Malone, C. Cohen, J. R. Gillmor, R. H. Colby, *Macromolecules* **1992**, *25*, 5241.

[219] A. L. Skov, P. Sommer-Larsen, Physical and chemical properties of dielectric elastomers, in *Dielectric Elastomers as Electromechanical Transducers: Fundamentals, Materials, Devices,*

Models and Applications of an Emerging Electroactive Polymer Technology, Elsevier Science, Amsterdam, **2008**, p. 25.

[220] Y. Song, L. Wang, R. Gyanda, R. Sakhuja, M. Cavallaro, D. C. Jackson, N. K. Meher, D. A. Ciaramitaro, C. D. Bedford, A. R. Katritzky, R. S. Duran, *J. Appl. Polym. Sci.* **2010**, *117*, 473.

[221] A. K. Jonscher, *J. Phys. D: Appl. Phys.* **1999**, *32*, R57.

[222] J. Qiang, H. Chen, B. Li, *Smart Mater. Struct.* **2012**, *21*, 025006.

[223] M. Kollosche, G. Kofod, *Appl. Phys. Lett.* **2010**, *96*, 071904.

[224] G. R. Hamed, *Rubber Chem. Technol.* **1994**, *67*, 529.

[225] K. Cho, W. J. Jang, D. Lee, H. Chun, Y.-W. Chang, *Polymer* **2000**, *41*, 179.

[226] M. Zhang, I. Denes, M. R. Buchmeiser, *Macromol. Mater. Eng.* **2016**, *301*, 337.

[227] M. Zhang, I. Denes, M. R. Buchmeiser, *Macromol. Chem. Phys.* **2016**, *217*, 1558.

[228] H. Kim, F. Shi, *IEEE Trans. Dieletric. Electr. Insul.* **2001**, *8*, 248.

[229] J. R. Laghari, W. J. Sarjeant, *IEEE Trans. Power Electron.* **1992**, *7*, 251.

[230] E. M. Arruda, M. C. Boyce, *J. Mech. Phy. Solids* **1993**, *41*, 389.

[231] M. Gordon, *Br. Polymer J.* **1976**, *8*, 39.

[232] A. Dorfmann, K.N.G. Fuller, R.W. Ogden, Shear, *Int. J. Solids Struct.* **2002**, 37, 1845.

[233] L. R. G. Treloar, *The Physics of Rubber Elasticity*, Oxford University Press, New York, **1975**, p. 141.

[234] W. M. Haynes, *CRC Handbook of Chemistry and Physics*, CRC Press, Boca Raton, **2013**, p. 6-7/15-25.

[235] M. Zhang, I. Denes, Y. Xue, M. R. Buchmeiser, *Macromol. Chem. Phys.* **2016**, *217*, 1729.

[236] L. J. Van der Pauw, *Philips Res. Rep.* **1958**, *13*, 1.

[237] M. Gordon, *Br. Polym. J.* **1976**, *8*, 39.

[238] W. V. Mars, A. Fatemi, *Rubber Chem. Technol.* **2004**, *77*, 391.

[239] V. Giurgiutiu, S. E. Lyshevski, Electroactive and Magnetoactive Materials, in *Micromechatronics: Modeling, analysis, and design with MATLAB,* CRC Press, Boca Raton, **2016**, p. 537.

State of Originality

I hereby certify that the dissertation entitled

Reliability of Dielectric Elastomers

is entirely my own work except where otherwise indicated. Passages and ideas from other sources have been clearly indicated.

Name: _____

Signature: _____

Date: _____

Appendix

A1   ICP-OES measurements

ICP-OES measurements were performed to determine the content of platinum in parts A and B. Results recorded no evidence of platinum in part B. In part A an average platinum concentration of ca. 9 ppm was measured. Data are summarized in Table A1.

Table A1. Results of ICP-OES measurements to determine the concentration of platinum in part A of Elastosil® P7670.[a]

#	Pt concentration [mg/L]	Sample weight [g]
Reference	< -0.0015	0
#1	0.0434	0.215
#2	0.0604	0.195
#3	0.0184	0.266
Mean value	0.0407	0.225

a) The concentration of platinum in part A is given by:
$[Pt] = 0.0407$ mg/L x 50 mL /0.225g = 9.04 mg/kg ≈ 9 ppm

A2   Properties of E3 during storage at room temperature

Since the self-prepared silicone material E3 contained a significant excess of hydrosilane groups after hydrosilylation, it was necessary to verify whether the properties of E3 remained stable during storage over the time range required for ageing tests, which was about 23 days. After storage for 48 h (2 day), 120 h (5 days), 168 h (7 days) and 552 h (23 days), the E3 films were characterized in terms of changes in cross-linking density, elastic modulus, relative permittivity and breakdown strength. Results shown in Figure A1 confirm that these properties remained constant within experimental error.
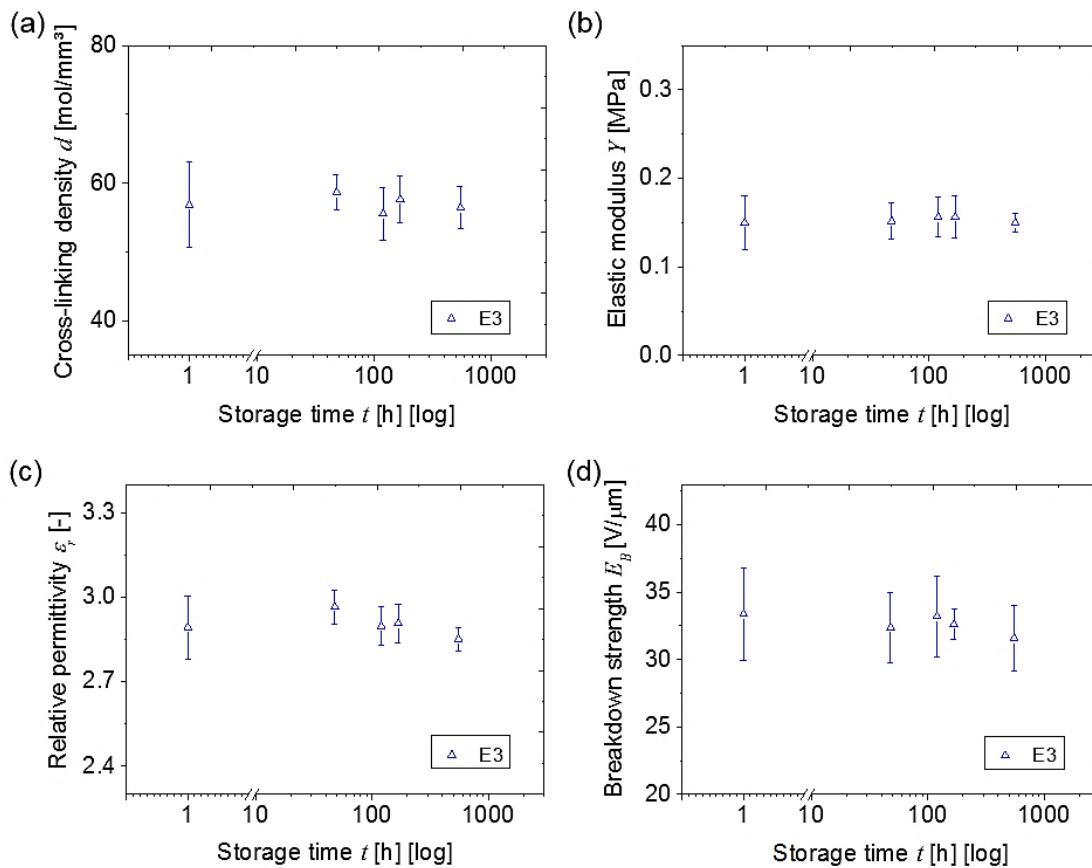
Figure A1. (a) Cross-linking density (b) elastic modulus (c) relative permittivity and (d) breakdown strength of E3 thin films stored at room temperature up to a maximum 23 days (552 h). Variations in these properties were insignificant.

A3   Hysteresis behavior of E1, E2 and E3

Figure A2 presents the hysteresis loops of the three silicone networks in the first loading cycles with maximum strains of 300%. In each hysteresis loop, the area under the stress-strain curve during uploading is the energy per unit volume adsorbed by the material. Accordingly, the area under the unloading curve is the energy released by the material, while the area between the uploading and unloading curves represents the energy dissipated as mechanical loss. In this study, the $W_d\%$ ratio between this dissipated energy and the total energy absorbed during uploading was used to compare the magnitude of hysteresis in different materials (Table A2).

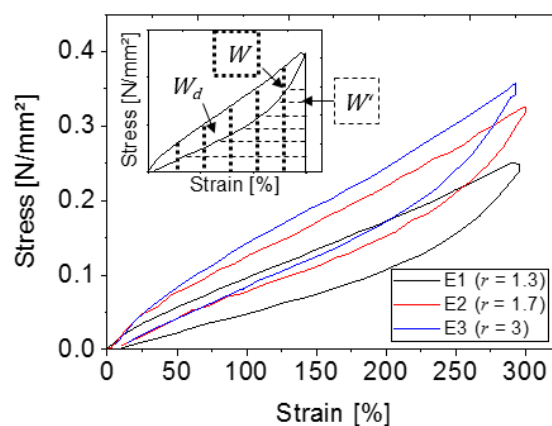**Figure A2.** Hysteresis loops of the silicone networks E1, E2, and E3. Curves were recorded during the first load cycles. The maximum strain was 300%.

Table A2. Integrated values of total adsorbed energy W, total released energy W', total dissipated energy W_d, and percentage of dissipated energy $W_d\%$ for the thin silicone films with different stoichiometric imbalances.

#	r	W [J/mm³]	W' [J/mm³]	W_d [J/mm³]	$W_d\%$ [%]
E1	1.3	0.39	0.25	0.13	35
E2	1.7	0.51	0.38	0.14	27
E3	3	0.55	0.39	0.16	29

It is evident that the material E1, prepared with the lowest stoichiometric imbalance, showed the largest hysteresis $W_d\%$. With E2 and E3 the difference in the $W_d\%$ was insignificant. Together with the increased elastic modulus from E1 to E2 and E3, which was a result of increased cross-linking density, the observed lowered hysteresis was consistent with observations reported by Mars et al.[238]

In subsequent load cycles the hysteresis $W_d\%$ decreased significantly due to the so-called Mullins effect.[15] As shown in Figure A3, after two to five cycles the material reached a stable state during chain rearrangement. Hysteresis was stabilized at a much smaller value and the viscous character declines significantly. The material E1, which had the highest hysteresis $W_d\%$ in the first load cycle, also showed the highest stabilized value at around 0.6%. The lowest hysteresis value of only 0.09% in a steady state was observed with E2.
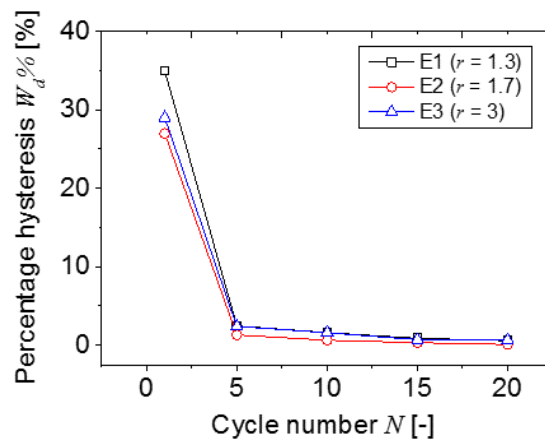
Figure A3. Changes in the percentage hysteresis $W_d\%$ in the first 20 load cycles for the E1, E2, and E3 silicone films.

Low hysteresis is important, since the energy conversion ratio[23] of the actuation components should be as high as possible.[239] Besides, thermal impact caused by hysteresis loss should be minimized. However, due to the low frequency used in the cycling tests (0.5 Hz), and because of the volume:surface ratio of the sample (low thickness and large surface), no considerable temperature rise was observed.

A4 Effect of mechanical fatigue on relative permittivity

A4.1 Self-prepared silicone materials

As shown in Section 5.4, mechanical ageing led to a decrease in both relative permittivity ε_r and the loss factor $tan\delta$. In Figure A4 the frequency spectra of the real part of permittivity (ε'_r) and the imaginary part of permittivity (ε''_r) for E1, E2, and E3, both in intact states and in fatigued states under the corresponding *critical load conditions*, are demonstrated. Declines in the ε'_r corresponded well with declines in the relative permittivity (Figure 52), while declines in the ε''_r corresponded well with those in $tan\delta$ (Figure 53). From E1 to E3, the decreasing trend became more significant. Note that the ε'_r and ε''_r curves were average value curves from at least three measurements. The ε''_r curves were additionally smoothed, due to their strong frequency dependency.

---

23 Energy conversion ratio is defined as the output mechanical energy divided by the input electrical energy. Mechanical hysteresis behavior contributes also to the electromechanical energy loss.

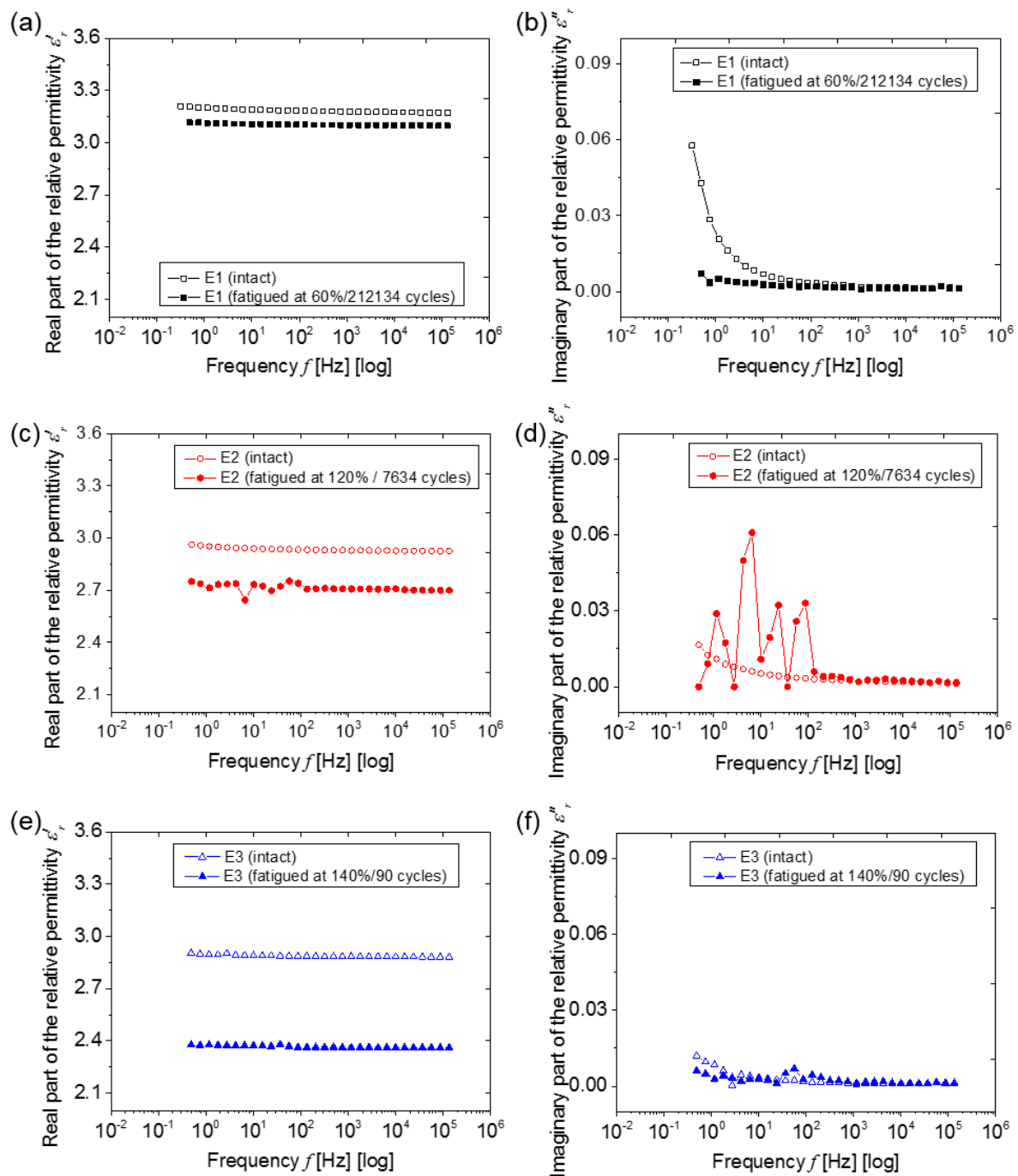**Figure A4.** Frequency spectra of the real part of the relative permittivity (ε'_r) and the imaginary part of the relative permittivity (ε''_r) of intact and fatigued (at *critical load conditions*) E1, E2, and E3 specimens.

A4.2 Commercial material

The decline in relative permittivity ε_r in fatigued Elastosil specimens with respect to the cycle number to failure was presented previously in Figure 58. It was also evident that alternations in ε_r in Elastosil aligned well with those in the benchmark material E2. The *critical load condition* of Elastosil was also "120%/ca. 10^4 cycles".

Figure A5 shows the frequency spectra of the intact Elastosil specimen in comparison with the Elastosil specimen fatigued under "120%/3105 cycles". It is evident that the real part of permittivity declined in line with the declined relative permittivity, which was shown in Figure 58d. By comparing Figure A5a with the previous Figure A4c, the accordance between Elastosil and E2 can also be confirmed. The change in the imaginary part of mechanically fatigued Elastosil was insignificant (Figure A5b).
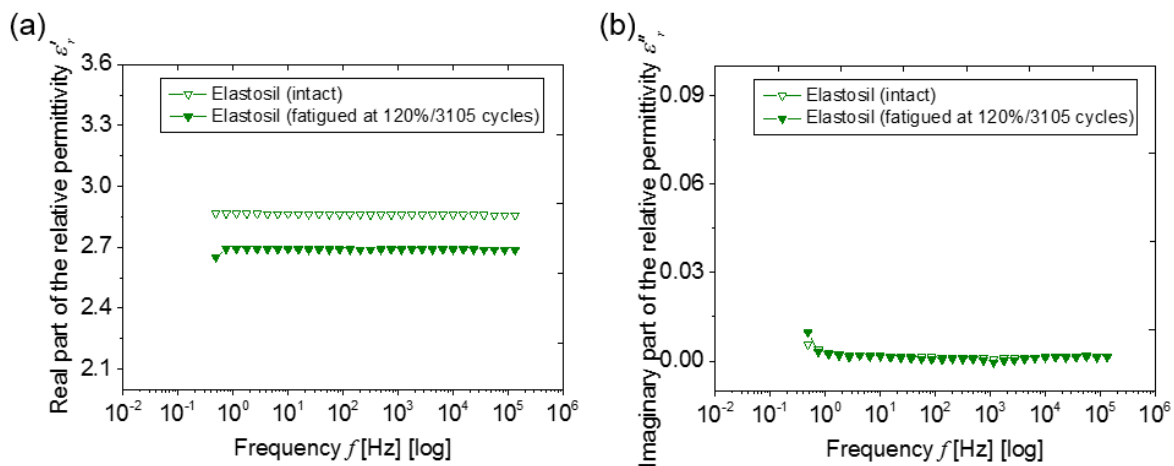

Figure A5. Frequency spectra of the real part of the relative permittivity (ε'_r) and the imaginary part of the relative permittivity (ε''_r) of intact and fatigued (at *critical load conditions*) Elastosil® P7670 specimens.

A4.3 Post-cured material

Comparisons of property changes induced by mechanical ageing between E3 and post-cured E3 have been illustrated in Figure 76. Unlike E3, which had *critical load condition* at ca. "140%/10-100 cycles", the post-cured E3 displayed a more significant property change in specimens fatigued under higher cycle numbers. In Figure A6, ε'_r and ε''_r spectra in relation to the frequency of the fatigued post-cured E3 specimen under 80% and after 1173320 cycles are illustrated, in comparison with the intact post-cured E3 specimens. In Figure A6a the imaginary part of permittivity decreased in the fatigued specimens, in line with the decreased complex permittivity shown in Figure 76. The total

decrease (Figure A6a) was lower than for the non-treated E3 (Figure A4e). The alternation of the imaginary part in mechanically fatigued post-cured E3 was insignificant (Figure A6b).
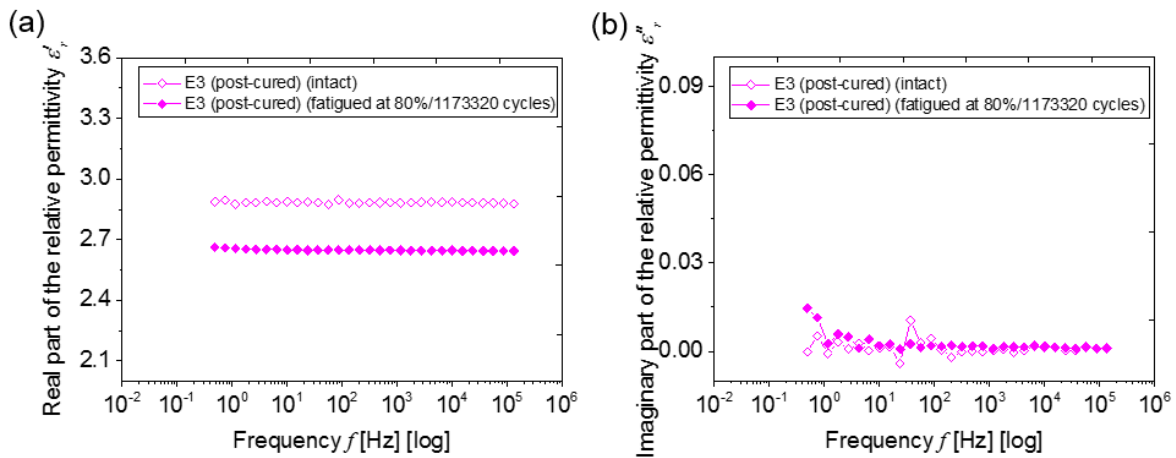

Figure A6. Frequency spectra of the real part of the relative permittivity (ε'_r) and the imaginary part of the relative permittivity (ε''_r) of intact and fatigued (at *critical load conditions*) post-cured E3 specimens.

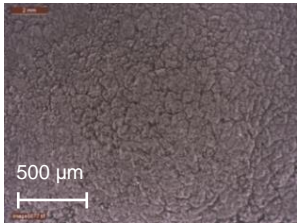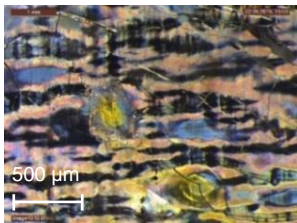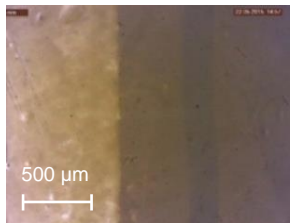## A5   Evaluation of different electrode materials

Chapter 6 aimed at investigating the electromechanical ageing behavior of dielectric elastomers. As introduced in Section 2.1.2.1, the deformation equation (Equation 2) did not take the influence of electrodes into account by assuming them as infinitely thin and compliant. In order to minimize the influence of electrodes on the performance of the test specimen, three different types of electrodes were firstly evaluated, i.e. carbon black, silver ink, and silver nanowire.

- Carbon black electrodes were coated onto the silicone's surface via a spray process. The carbon black (Graphit 33, carbon black in liquid propane and butane) was purchased from CRC Industries Deutschland GmbH (Iffezheim, Germany). Preparation was performed by the author at the Robert Bosch GmbH.

- Silver ink (NPS-JL) was purchased from Harima Chemicals Group (Japan). Coating was performed by using an inkjet printer (Dimatix DMP 2831) at Hahn-Schickard Gesellschaft (Stuttgart). In order to achieve good adhesion between the silicone substrate and the silver ink, the silicone substrate was pre-treated in an O_2-plasma (1-10 s, 20-60 W) at the Hahn-Schickard Gesellschaft.

- Silver nanowire electrodes were prepared by vacuum filtration of the AgNW solution, which was purchased from BlueNano Inc. (Charlotte, NC, USA). After filtration, the AgNW was transferred

from the Teflon filter onto the silicone's surface. No pre-treatment was needed for the silicone substrate.

All three electrode materials were investigated in terms of their surface characteristics (optical microscopy, white light interferometry), thickness (white light interferometry), sheet resistances in both the non-stretched and stretched states (four-points method[235, 236]), and breakdown behavior (electromechanical ageing test facility). Results are summarized in Table A3.

Table A3. Estimated surface characteristics, thickness, sheet resistivity, and breakdown voltage of the carbon black, silver ink, and silver nanowire electrode materials.

	Carbon black	**Silver ink**	**Silver nanowire**
Optical surface image			
Thickness [μm]	9.6	5.9	3.1
Sheet resistance (non-stretched) [Ω/sq]	566	0.2	2.4
Sheet resistance (stretched) [Ω/sq]	6.8×10^4	1.9×10^4	86.0
Breakdown Voltage [kV]	3.8	1	2.4

Surface characteristics

Cracks and clusters were found on the surface of the prepared carbon black electrodes. The cracks were generated during preparation, which were clear indications of the insufficient compliance of the

electrode. If the surface of the elastomers was not very homogenous or the drying rate too slow, clusters could also form on the elastomers during the spray process. On the surface of the silver ink electrode, cracks and flaws were also clearly observed. These were probably the result of the inkjet printing process and the pre-treatment of the silicone film, which was necessary to enhance adhesion between the silver ink and silicone. The silver nanowire electrode showed no obvious cracks and a more homogenous surface.

Thickness

The silver nanowire electrode showed favorable thickness in the nanometer range.

Sheet resistance

The sheet resistance of the electrode was measured using the so-called *four-point method*.[235, 236] The test instrument, developed by Fraunhofer IST (Germany), is shown in Figure A7. A sphere was located in the middle of the instrument, while the elastomer film was mounted onto the test frame, above the sphere. By moving the sphere in a perpendicular direction, the elastomer film can be stretched to a certain degree. Tests were carried out under two different states: a non-stretched state for 10 s and a stretched state for 10 s. In the stretched state, the film expanded by about 10%. Sheet resistances of the elastomer films in both non-stretched and stretched states were recorded. Data reported in Table A3 were average values obtained over 100 cycles. As shown in Table A3, upon 10% strain the sheet resistance of the silver ink electrode increased from about 0.2 Ω/sq to 1.9×10^4 Ω/sq, which became about 10^5 times greater. This ratio was also large for carbon black electrodes (about 119-times), while for silver nanowire electrodes it was about 36.6 times greater.
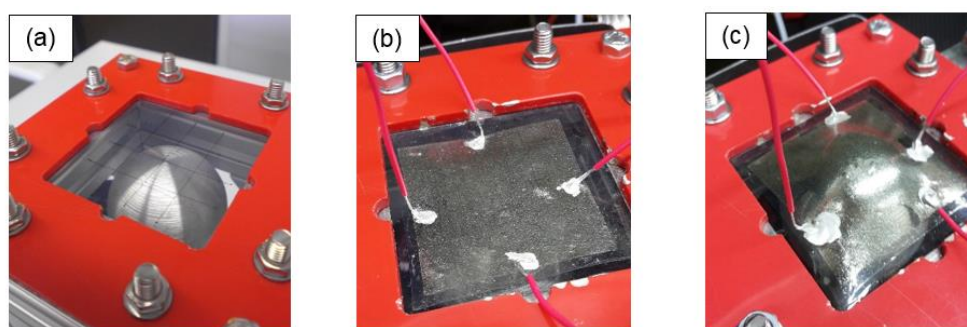

Figure A7. Test instrument for sheet resistivity measurements (a) top view (b) a silver ink electrode implemented into the test frame (non-stretched state) (c) the same electrode stretched to 10%.

Breakdown voltage

Elastosil films with a thickness of ca. 80 µm were coated with the three electrode materials and tested for electrical breakdown. The voltage, at which a breakdown was observed, was recorded. Since the Elastosil film has a breakdown strength of ca. 30 V/µm, the theoretical breakdown voltage was expected to be at least 2.4 kV.

As shown in Table A3, test specimens coated with carbon black electrode showed the highest breakdown voltage (ca. 3.8 kV). One possible reason was the high sheet resistance of carbon black electrodes. Samples coated with silver ink showed flash points at a voltage of 1 kV, which was far lower than the expected breakdown voltage (ca. 2.4 kV). This might indicate that the elastomer substrate was partially damaged by the plasma treatment before coating. Specimens with a silver nanowire electrode showed a reasonable breakdown voltage of ca. 2.4 kV. At the moment of breakdown, on the surface of the silver nanowire electrode, a small brown dot appeared, albeit the specimen remained functional.

A6   Effect of electromechanical ageing on relative permittivity

A6.1   Self-prepared silicone materials

The detrimental effects of electromechanical ageing on relative permittivity ε_r have been shown in Figure 66. From E1 to E3 the decreasing trend of ε_r became more significant due to the more significant secondary cross-linking at higher Si-H group excess. The respective decrease in $tan\delta$ with the increasing number of cycles (Figure 67) also confirmed that the viscous movement of the side chains was reduced through an increasing number of cross-links.

The frequency plots of the real part of permittivity (ε'_r) and the imaginary part of the permittivity (ε''_r) of E1, E2, and E3, before and after electromechanically ageing, are shown in Figure A8. All aged specimens were electromechanically cycled under 2 kV for up to 10^5 cycles.

Figure A8. Frequency spectra of the real part of the relative permittivity (ε'_r) and the imaginary part of the relative permittivity (ε''_r) of intact and electromechanically aged E1, E2, and E3 specimens.

It is evident that the aged specimens showed declines in both the real parts and the imaginary parts. From E1 to E3 the decrease of ε'_r became more pronounced, which corresponded well with the

decrease in relative permittivity ε_r shown in Figure 66. In Figures A8b, A8d, and A8f, the peaks of the imaginary part shifted to lower frequency in the electromechanically aged specimens.

A6.2   Commercial material

A comparison of electromechanical ageing behavior of Elastosil and the benchmark material E2 was shown in Figure 71. Figure A9 shows the frequency spectra of ε'_r and the ε''_r of intact and electromechanically aged Elastosil. It is evident that the decline in the real part ε'_r in Elastosil was comparable to that in E2 (Figure A8c). The change in the imaginary part after electromechanical ageing was insignificant (Figure A9b).
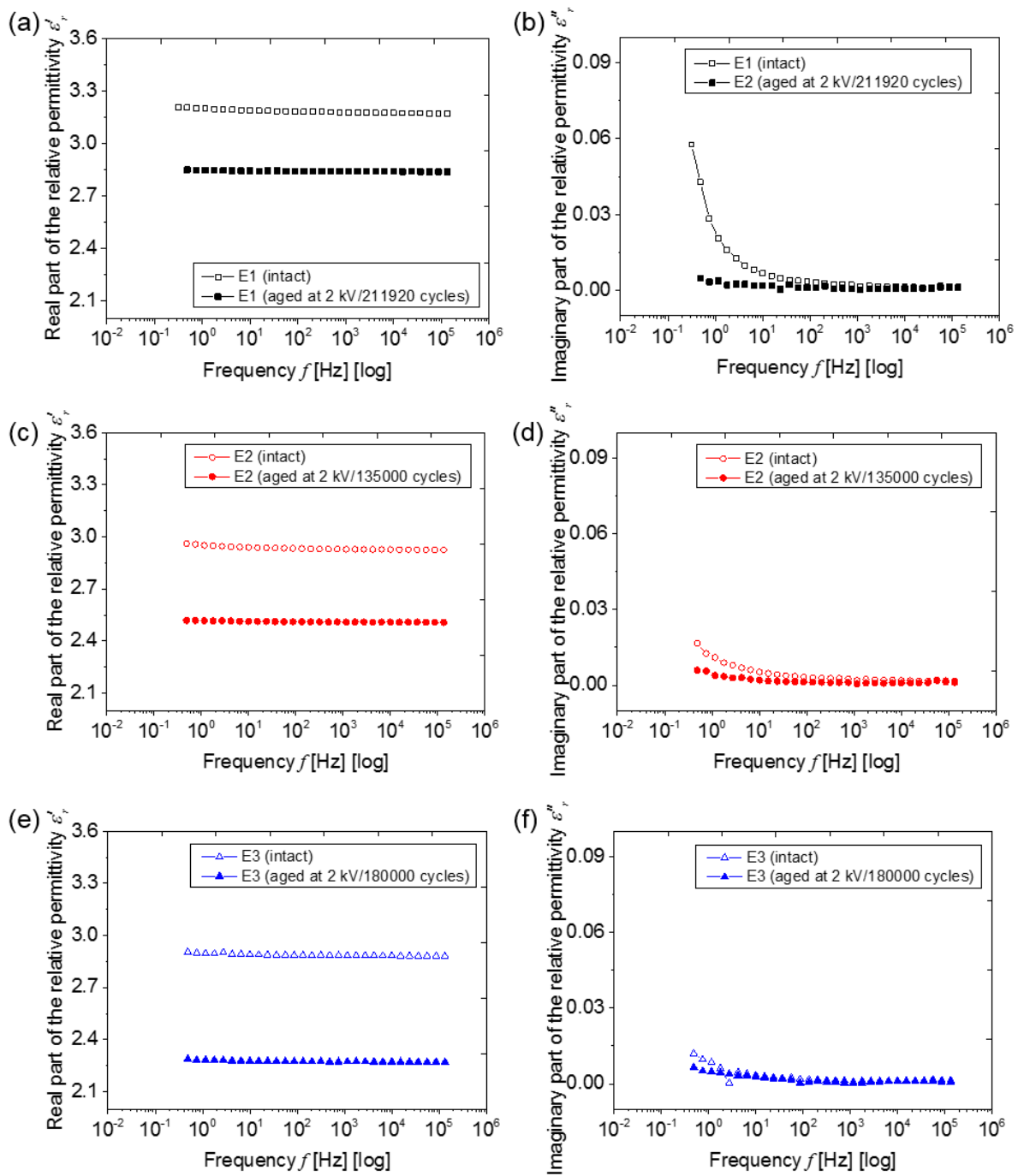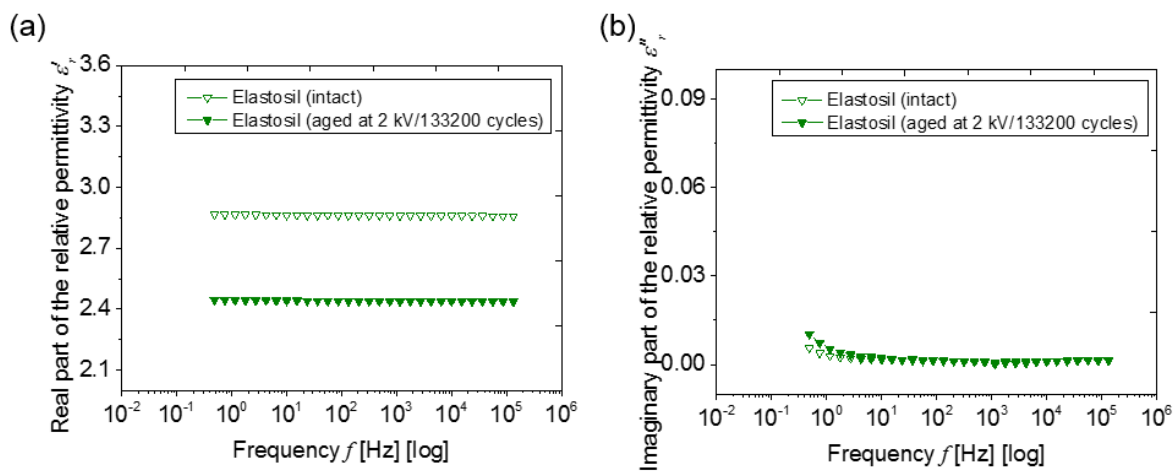

Figure A9. Frequency spectra of the real part of the relative permittivity (ε'_r) and the imaginary part of the relative permittivity (ε''_r) of the intact and electromechanically aged Elastosil® P7670 specimen.

A6.3   Post-cured material

Comparisons of electromechanical ageing behavior between E3 and post-cured E3 have been presented in Figure 78. The frequency spectra of ε'_r and ε''_r of post-cured E3 are shown here Figure A10. A decrease in ε'_r in the aged post-cured E3 is evident. By comparing Figure A10a with Figure A8e, it is also evident that ε'_r changes in the aged post-cured E3 were less significant than in E3. This verifies the enhanced stability via post-curing. The change in the imaginary part in the aged post-cured E3 was insignificant (Figure A10b).
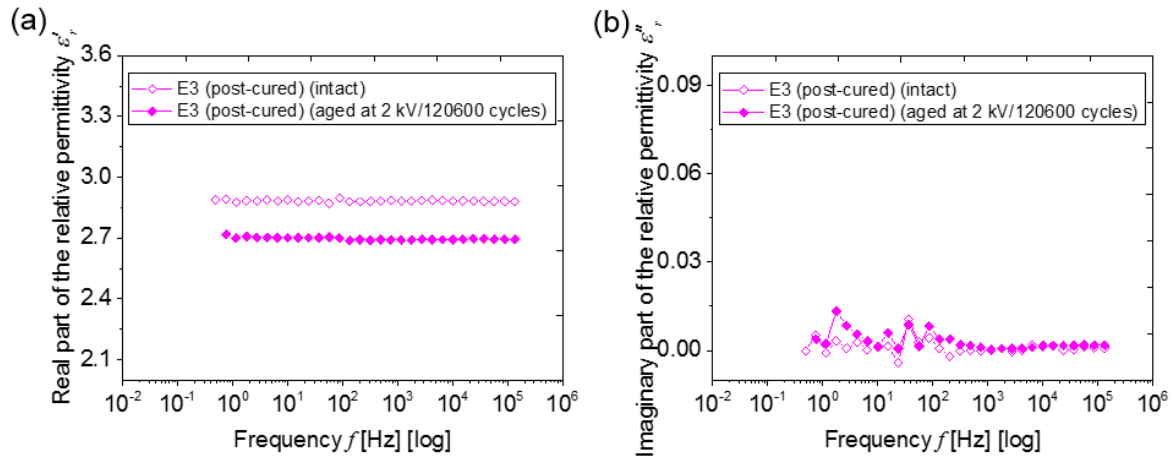
Figure A10. Frequency spectra of the real part of the relative permittivity (ε'_r) and the imaginary part of the relative permittivity (ε''_r) of the intact and electromechanically aged post-cured E3 specimen.

A7   Calculation of equivalent deformation

A comparison between the electromechanical ageing and mechanical ageing was performed by applying cyclic loading at a strain amplitude of 5%, which is equivalent to electromechanical deformation. Figure A11 shows the calculation procedure based on the *principle strain theory* of incompressible materials.[230, 232, 237] It is however worth noting that this calculated equivalent strain is an approximate value, since the actual stress distributions of a tensile load and of a compression load are still very different.
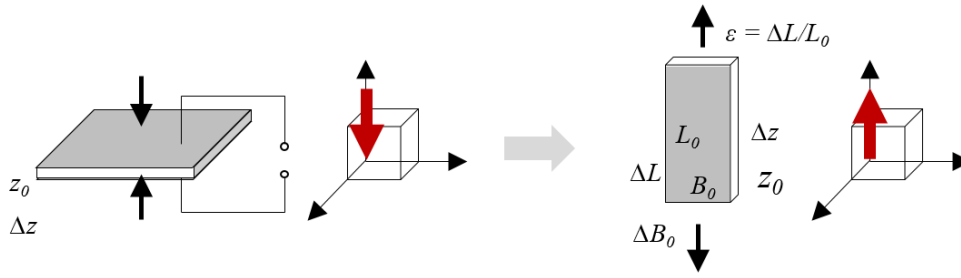
e.g., thin silicone film E1:

$\varepsilon_r = 3.2$
$\varepsilon_0 = 8.85 \times 10\text{-}12$ F/m
$Y = 0.1$ MPa
$d = 150$ µm
$V = 2$ kV

$$\Delta z = \varepsilon_r \varepsilon_0 \frac{V^2}{(z - \Delta z)^2}$$

$$\Delta z \approx 7.55 \text{ µm}$$

$$\frac{\Delta z}{z_0} \approx 5\%$$

$$I_3 = \lambda_1 \lambda_2 \lambda_3 = 1$$

$$\lambda_2 = \lambda_3 = \lambda_1^{(-1/2)}$$

$$\lambda_1 = 1 + \frac{\Delta z}{z_0} = 1 - 0.05 = 0.95$$

$$I_{1,compressive}$$
$$= \lambda_1^2 + \lambda_2^2 + \lambda_3^2 = \lambda_1^2 + \frac{2}{\lambda_1} \approx 3.008$$

$$\varepsilon = \Delta L / L_0$$

$$\lambda_1 = 1 + \frac{\Delta L}{L_0} = 1 + \varepsilon$$

$$I_3 = \lambda_1 \lambda_2 \lambda_3 = 1$$

$$\lambda_2 = \lambda_3 = \lambda_1^{(-1/2)}$$

$$I_{1,tensile}$$
$$= \lambda_1^2 + \lambda_2^2 + \lambda_3^2 = \lambda_1^2 + \frac{2}{\lambda_1}$$
$$= (1 + \varepsilon)^2 + \frac{2}{(1 + \varepsilon)}$$

$$I_{1,compressive} = I_{1,tensile}$$

$$(1 + \varepsilon)^2 + \frac{2}{(1+\varepsilon)} = 3.008$$

$$\varepsilon \approx 0.05225 \approx 5\%$$

Figure A11. Sketch of calculation of equivalent uniaxial tensile deformation from uniaxial compressive deformation.

A8 Properties of post-cured E3 during storage tests

After thermal post-curing (120°C/overnight), it was analyzed whether the properties of post-cured E3 remained stable for 23 days at room temperature. Post-cured E3 thin films, which were stored up to 48 h (2 day), 120 h (5 days), 168 h (7 days), and 552 h (23 days), were characterized with respect to variations in cross-linking density, relative permittivity, and dielectric breakdown strength. As shown in Figure A12, these properties appeared constant during storage over 3 weeks at room temperature. Compared to non-treated E3, results for the post-cured E3 showed that thermal post-

curing led to a minor increase in cross-linking density, together with a slight increase in elastic modulus. Differences in terms of relative permittivity and dielectric breakdown strengths, however, were insignificant.
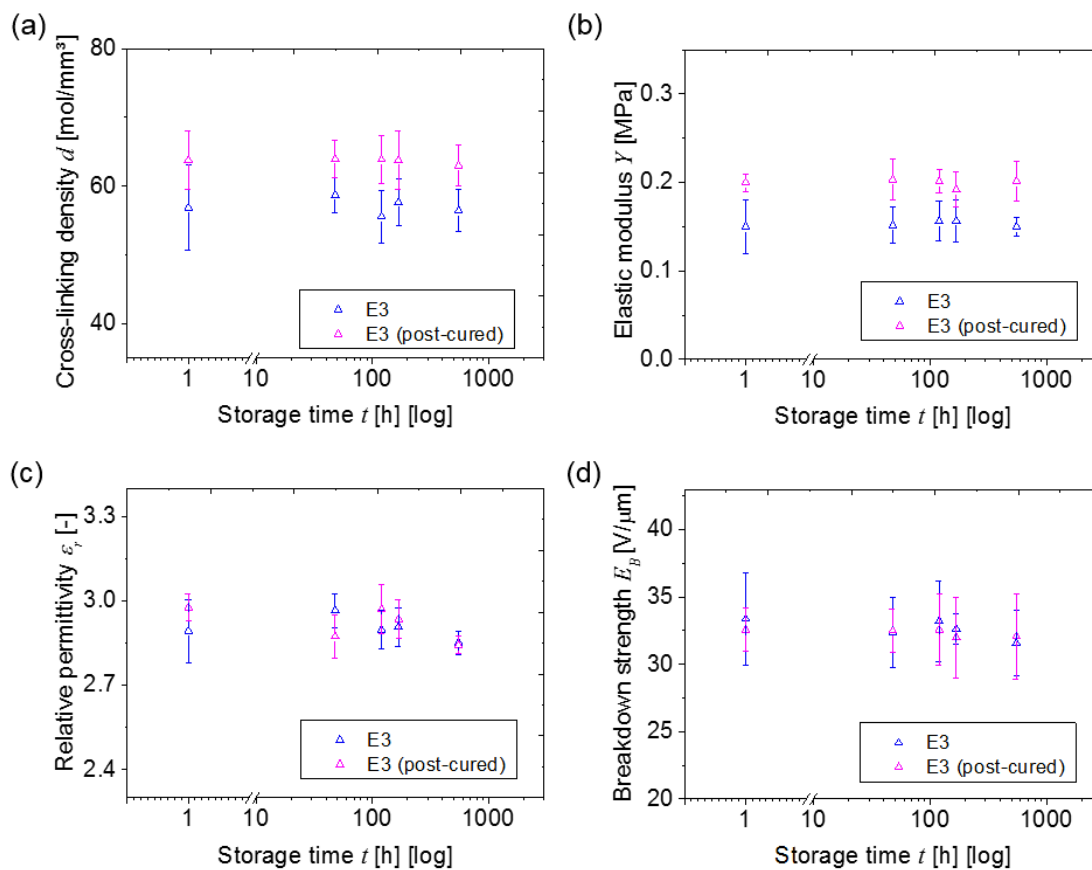

Figure A12. Comparison of material properties between E3 and post-cured E3 (a) cross-linking density (b) elastic modulus (c) relative permittivity (d) breakdown strength.

List of Publications

Journal Publications

[1]   M. Zhang, I. Denes, M. R. Buchmeiser, "An investigation of structure-property relationships of silicone-based dielectric electro-active polymer by varying stoichiometric imbalance of the network", *Macromol. Mater. Eng.* ***2016****, 301,* 337.

[2]   M. Zhang, I. Denes, M. R. Buchmeiser, "Interplay between mechanical fatigue and network structure and their effects on mechanical and electrical properties of thin silicone films with varying stoichiometric imbalance", *Macromol. Chem. Phys.* ***2016****, 217,* 1558.

[3]   M. Zhang, I. Denes, Y. Xue, M. R. Buchmeiser, "Ageing of Silicone-Based Dielectric Elastomers Prepared with Varying Stoichiometric Imbalance: Changes in Network Structure, Mechanical, and Electrical Properties", *Macromol. Chem. Phys.* ***2016****, 217,* 1729.

Conferences Publications

[1]   M. Zhang, I. Denes, M. R. Buchmeiser, "An approach to investigate the effect of mechanical fatigue on the electrical properties of thin silicone layers", in Proceedings of Actuator 2014, 14th International Conference on New Actuators, Bremen, 23-25 June **2014**.

[2]   M. Zhang, I. Denes, M. R. Buchmeiser, "The effect of mechanical fatigue on the electrical properties of dielectric elastomer thin layers", presented at ESNAM 2014, European Network of artificial muscle (ESNAM), London, 25-26 November **2014**.

[3]   M. Zhang, I. Denes, M. R. Buchmeiser, "Effect of network structure on mechanical and electrical properties of silicone-based dielectric elastomer", in Proceedings of EuroEAP 2015, 5th International conference on Electromechanically Active Polymer (EAP) transducers & artificial muscles, Tallinn, 9-10 June **2015**.

Curriculum Vitae

Personal Information

Last Name	Zhang
First Name	Mengjia
Date of Birth	12 January 1988
E-Mail	mengjia.zhang@yahoo.de

Education

03.2013 - 12.2016	Ph.D., Polymer Chemistry, University of Stuttgart, Germany
03.2011 - 02.2013	M.Sc., Applied Chemistry, Reutlingen University, Germany, GPA 3.5
03.2009 - 02.2011	B.Sc., Applied Chemistry, Reutlingen University, Germany, GPA 3.6
09.2008 - 01.2009	German, Tongji University, Shanghai, China
09.2006 - 07.2008	B.Eng., Chemical Engineering, Donghua University, Shanghai, China, GPA 3.9

Working Experience

Since 07.2016	Reliability Engineering in Sensor Development, Robert Bosch GmbH, Reutlingen
03.2013 - 06.2016	Ph.D. Candidate, Robert Bosch GmbH, Renningen Reliability of Dielectric Elastomers
08.2012 - 01.2013	Master Thesis, Robert Bosch GmbH, Gerlingen-Schillerhöhe Electrical and Electrochemical Characterization of Ageing Effects in Lithium-Ion Battery
01.2012 - 06.2012	Working Student, Bosch Sensortec GmbH, Reutlingen Sensor Characterization/Validation
06.2011 - 09.2011	Working Student, Robert Bosch GmbH, Reutlingen Corrosion Protection, Failure Analysis
10.2010 - 02.2011	Working Student, Robert Bosch GmbH, Reutlingen Corrosion Protection, Electrochemistry, Impedance Spectroscopy
03.2010 - 09.2010	Internship and Bachelor Thesis, Robert Bosch GmbH, Schwieberdingen Internship: Reliability of Polymer Materials Bachelor Thesis: Reliability Design of Snap-fit Components Made of PA66-GF30 in Early-Phase Development

Stuttgart, 06 October 2016